THE STRUCTURAL PROPERTIES OF GLASSFIBRE REINFORCED PLASTICS

QUTAIBA JAMAL AL-KHAYATT

A THESIS SUBMITTED FOR THE DEGREE OF
DOCTOR OF PHILOSOPHY

DEPARTMENT OF CIVIL ENGINEERING
UNIVERSITY OF ASTON IN BIRMINGHAM

DECEMBER 1974

S Y N O P S I S.

The research work described in this thesis is concerned with the development of glassfibre reinforced plastics for structural uses in Civil Engineering construction.

The first stage was primarily concerned with the design of GRP lamintes with structural properties and method of manufacture suitable for use with relatively large structural components. A cold setting, pressure moulding technique was developed which proved to be efficient in reducing the void content in the composite and minimising the exothermic effect due to curing. The effect of fibre content and fibre arrangement on strength and stiffness of the composite was studied and the maximum amount of fibre content that could be reached by the adopted type of moulding technique was determined.

The second stage of the project was concerned with the introduction of steel-wire "sheets" into the GRP composites, to take advantage of the high modulus of steel wire to improve the GRP stiffness and to reduce deformation.

The experimental observations agreed reasonably well with theoretical predictions in both first and second stages of the work.

The third stage was concerned with studying the stability of GRP flat rectangular plates subjected to uniaxial compression or pure shear, to simulate compression flanges or shear webs respectively. The investigation was concentrated on the effect of fibre arrangement in the plate on buckling load. The effect of the introduction of steel-wire sheets on the plate stability in compression was also investigated. The boundary conditions were chosen to be close to those usually assumed in built-up box-sections for both compression flanges and webs. The orthotropic plate and the mid-plane symmetric theories were used successfully in predicting the buckling load

theoretically. In determining the buckling load experimentally, two methods were used. The Southwell plot method and electrical strain gauge method. The latter proved to be more reliable in predicting the buckling load than the former, especially for plates under uniaxial compression. Sample design charts for GRP plates that yield and buckle simultaneously under compression are also presented in the thesis.

The final stage of the work dealt with the design and test of GRP beams. The investigation began by finding the optimum cross-section for a GRP beam. The cross-section which was developed was a thin walled corrugated section which showed higher stiffness than other cross-sections for the same cross-sectional area (i.e. box, I, and rectangular sections). A cold setting, hand layings technique was used in manufacturing these beams which were of nine types depending on the type of glass reinforcement employed and the arrangement of layers in the beam.The simple bending theory was used in the beam design and proved to be satisfactory in predicting the stresses and deflections. A factor of safety of 4 was chosen for design purposes and considered to be suitable for long term use under static load. Because of its relatively low modulus, GRP beams allowable deflection was limited to $^{1}/_{120}$th of the span which was found to be adequate for design purposes.

A general discussion of the behaviour of GRP composites and their place relative to the more conventional structural material was also presented in the the thesis.

ACKNOWLEDGEMENTS

The author wishes to express his gratitude to his supervisor Professor M.Holmes,B.Sc.,Ph.D.,D.Sc.,C.Eng., F.I.C.E.,F.I.Struct.E.,F.I.Mun.E., the Head of the Department of Civil Engineering of the University of Aston in Birmingham, for his generous help, guidance and encouragement throughout this research project.

The author also wishes to express his appreciation to:The Ministry of Industry (National Electricity Administration) of the Republic of Iraq for their financial support during the course of this work.

Messrs.J.Huddart, J.Quinn and T.Seddon of Pilkington Bros.,St.Helens, Lancashire, England, for their invaluable efforts in fabricating the GRP beam specimens.

Mr.A.E.Galliers of National-Standard Co.,Ltd., Kidderminster, Worcestershire, England, for his free supply of all the steel-wire sheets used in this project.

Mr.W.Parsons, the Departmental Superintendent of the Civil Engineering Department at the University of Aston, together with all the technicians and the secretarial staff of the same department, for their willing and useful advice during all the stages of this project.

Mrs.M.Hasleton, for her excellent typing of the script. Miss P.Sage for reproducing the drawings with such good care.

His parents and wife, for their patience, help and encouragement.

C O N T E N T S.

CHAPTER 3 (contd)

CHAPTER 3 (contd)

Page No.

CHAPTER 5 (contd) Page No.

N O T A T I O N.

A	–	Area of GRP beam cross-section.
A_{ij}	–	In-plane stiffness matrix.
A'_{ij}	–	In-plane compliance matrix.
a	–	Plate length.
B_{ij}	–	Stiffness coupling matrix.
B.M.	–	Bending moment.
b	–	Lower width of GRP beam, See Figs(6.1 and 7).
b_T	–	Total width of GRP beam, See Figs.(6.1 and 2).
b'	–	Plate width.
C	–	Contiguity factor.
C_{ij}	–	Stiffness matrix in the principal directions.
$\overline{C}_{ij}$	–	Transformed stiffness matrix in the off-axis directions.
D	–	Lower depth of GRP beam measured from the centre line of the tension flange to the line x-x, see Fig.(6.1).
D_{ij}	–	Flexural stiffness matrix or flexural rigidity.
D_T	–	Total depth of GRP beam, see Fig.(6.1).
D'	–	Lower depth of GRP beam measured from the bottom of the tension flange line x-x, and equal to $\left(D + \frac{t}{2}\right)$, see Fig.(6.1).
D'_{ij}	–	Flexural compliance matrix.
E_L, E_T	–	Elastic moduli in the principal longitudinal and transverse directions respectively.
E_f	–	Elastic modulus of glass fibres.
E_m	–	Elastic modulus of the resin matrix.
E_S	–	Elastic modulus of steel wires.
E_{FL}	–	Flexural modulus.
E_m	–	Elastic modulus of the voided matrix.
F	–	Shearing force.
F_L	–	Axial strength of unidirectional composite.

$F_{L(t)}$ – Axial tensile strength of unidirectional composites.

$F_{L(c)}$ – Axial compressive strength of unidirectional composite.

F_T – Transverse strength of unidirectional composites.

$F_{T(t)}$ – Transverse tensile strength of unidirectional composite.

$F_{T(c)}$ – Transverse compressive strength of unidirectional composite.

$F_{(FL)}$ – Flexural strength.

f – Allowable stress.

G_{LT} or G_{xy} – Longitudinal or principle shear modulus.

G_{12} – Off-axis shear modulus.

$\overline{G}_m$ – Voided matrix shear modulus.

h – Plate thickness or depth.

I – Moment of inertia.

I_{TL} – Moment of inertia of GRP beam cross-section about the neutral axis when this axis is below the line x-x, see Fig.(6.1).

I_{TU} – Moment of inertia of GRP beam cross-section about the neutral axis when this axis is above the line x-x, see Fig.(6.2).

k – Compressive buckling coefficient of isotropic material.

k_b – Buckling coefficient of GRP composite under uniaxial compression.

k_s – Buckling coefficient of GRP composite under pure shear.

L – Length of GRP beam.

$\left(\frac{L}{b'}\right)$ – Distance between successive buckling waves under pure shear, see Fig.(5.17).

M – Multidirectional ply ratio.

M_i – Distributed (and twisting) moments.

M_i^T – Thermal moment.

$\overline{M}_i$ – Effective moment = $M_i + M_i^T$.

m – $\cos\alpha$.

m' – Number of buckling half wavelength in the x or longitudinal direction under uniaxial compression.

N_i - Stress resultant, where i = 1,2, or 6.

N_i^T - Thermal force.

$\bar{N}_i$ - Effective stress resultant = $N_i + N_i^T$.

N_x, N_y - Normal stress resultant in the x or y direction respectively.

N_{xy} - Shearing stress resultant.

$N_{x(cr)}$ - Critical compressive buckling load.

$N_{xy(cr)}$ - Critical buckling load in pure shear.

n - $\sin\alpha$.

n' - Number of buckling half wavelength in the y or transverse direction under uniaxial compression.

P - Applied load.

p - Ratio of normal stresses = σ_2/σ_1.

q - Ratio of shear stress = τ_{12}/σ_1.

r - Radius of GRP beam compression flange, or ratio of normal strength $\frac{F_L}{F_T}$.

$\bar{r}$ - Distance from the top of GRP beam cross-section to the line x-x, see Fig.(6.1).

S - Shear strength of unidirectional composite (assumed equal to interlaminar shear strength).

S_{ij} - Stiffness compliance matrix (inverse of C_{ij}).

s - Shearing strength ratio = $\frac{F_L}{S}$.

T_{ij} - Tensor.

$\bar{T}$ - Temperature.

t - Thickness or depth.

V_f - Glass fibre volume fraction in the composites.

V_m - Resin matrix volume fraction in the composite.

V_R - Overall volume fraction of reinforcement in the composite = $V_s + V_f$.

V_s - Steel-wires volume fraction in the composite.

V_v - Voids volume fraction in the composite.

$\bar{V}_f$ – Voided fibre volume fraction.

$\bar{V}_R$ – Voided volume fraction of reinforcement in composite.

v – Plate characterisc value = $\sqrt{\frac{D_1 D_2}{D_3}}$.

W – Externally applied load.

y_N – Neutral axis position from the top of the GRP beam cross-section.

$\bar{y}$ – Distance from the neutral axis position to the line x-x, see Figs.(6.1 and 2).

Z – Section modulus.

α – Fibre orientation or lamination angle.

γ – Shear strain component.

δ – Deflection.

ε_{ij} – Strain component.

ε_i^o – Inplane strain component.

κ – Curvature.

ν – Poisson's ratio.

ν_f – Poisson's ratio of glass fibres.

ν_{LT} or ν_{xy} – Longitudinal Poisson's ratio of GRP composite in the principle direction.

ν_m – Poisson's ratio of resin matrix.

ν_{TL} or ν_{yx} – Transverse Poisson's ratio of GRP composite in the principle direction.

ν_{1a} – Poisson's ratio of GRP composite in a direction other than the principle direction.

σ – Stress component.

σ_{cr} – Critical local buckling stress under uniaxial compression.

σ_f – Tensile stress of glass fibre in the composite.

σ_s – Ultimate tensile stress of steel wire at failure.

σ_1 – Longitudinal stress component.

σ_2 – Transverse stress component.

σ_m' – Tensile stress in resin matrix at the composite failure strain.

τ	-	Shearing stress component.
τ_{LT} or τ_{xy}	-	Shearing stress component in the principle direction.
ϕ	-	Plate aspect ratio $\frac{a}{b}$,.
ψ	-	Tangent of the angle (β) that the buckling wave in pure shear makes with the verticle at the centre of the plate, see Fig.(5.17).

Subscripts.

f	-	Glass fibre.
m	-	resin matrix
V	-	Voids.
L,X	-	Longitudinal associated with the principle direction.
T,Y	-	Transverse associated with the principle direction.
(t)	-	Tension.
(C)	-	Compression.
(FL)	-	Flexure.
1	-	Longitudinal in a direction other than the principle.
2	-	Transverse in a direction other than the principle.
6	-	Shear.

C H A P T E R 1

INTRODUCTION

1.1) Introduction:

Glass reinforced plastics have been steadily gaining acceptance as a construction material for reasons such as, its smooth surface finish, good permanent colouring, low electrical and heat conductivity, good corrosion resistance and finally its translucency. These properties have resulted in the glass reinforced plastics being widely used as a construction material for many non-structural applications.

The high specific strength (strength/density ratio) of this material makes it of interest to structural designers and researchers to study the possibility of employing glass reinforced plastics for structural application.

Its disadvantages for structural application include its relatively low modulus, its creep behaviour and its fire resistance properties and its relatively high cost. These factors have militated against its rapid adoption as a structural material.

1.2) Aims of the present work:

The ultimate aims of this work are to find a suitable moulding technique and feasible design criteria for some of the basic structural uses to which the material might be applied. Consideration has been given to the effect of fibre content and orientation of the individual layer and to the stacking sequence of all layers on mechanical properties of the material.

1.3) Basic Assumptions:-

The glass reinforced plastic material is generally assumed to have the following properties:-

1.3) contd.

(i) To be a laminated homogeneous transversely isotropic material.

(ii) The laminate is symmetric about the middle horizontal plane.

(iii) In the composite under consideration, the thickness is considered to be very small compared to other dimensions.

(iv) The strain is considered to be of equal magnitude in the constituents of the composite.

(v) The material is considered to obey Hooke's Law.

1.4) Theory Applied:

The method of continuum analysis has been adopted in this project for the sake of material characterization of strength and stiffness.

The yield criterion which has been considered to be acceptable for the design of glass reinforced plastic composites is the generalized Von-Mises (Distortional Energy) yield criterion for transversely isotropic materials in a state of plain stress.

In studying the buckling load of glass fibre composite plates under uniaxial compression or pure shear, the specially orthotropic and mid-plane symmetric theories have been adopted.

Finally, simple bending theory was used in the design of glass reinforced beams with the following considerations:-

(i) The material of the beam specimens is homogeneous transversely isotropic and has nearly the same value of longitudinal moduli in tension and compression.

1.4) contd.

(ii) The beam is initially straight and all longitudinal filaments bend into circular arcs with a common centre of curvature.

(iii) Transverse cross-sections remain plane and perpendicular to the neutral surface after bending.

(iv) The radius of curvature is large compared with the dimension of the cross-section.

(v) The stress is pure longitudinal and the stress concentration effect under point loads is neglected.

1.5) Components investigated:

In addition to the general characterization of glass fibre and steel wire - glass fibre reinforced composites, the following structural components have been investigated,

(i) Glass fibre reinforced flat rectangular plates subjected to uniaxial compression or pure shear.

(ii) Glass fibres reinforced simply supported beams.

C H A P T E R 2

GENERAL BACKGROUND

2.1) Glass Fibre Reinforced Plastics.

2.1.1) Introduction.

Glass fibre reinforced plastics are composite made by reinforcing a thermosetting resin with glass fibres. Many other composites are known, ranging from wood, which is lignin reinforced with cellulose fibres, and reinforced concrete, to laminates made by reinforcing a resin with sheets of paper or fabric (ref.2-1).(In the remainder of this thesis the term glassfibre reinforced plastic will be abbreviated to GRP).

GRP was developed into commerical viability about 20 years ago. At the present time the consumption of this type of material in the industrial world is increasing rapidly and the applications cover building construction, marine units, chemical plants, rail and road transport, cladding and sheeting and aerospace applications. In spite of these wide applications of GRP many properties still remain undetermined for the design engineer, especially the structural properties of GRP for load bearing applications.

Structural GRP composites have higher strength to weight ratios than most other conventional engineering materials. They are also attractive in appearance and can contribute substantially to the architectural beauty of the structure. They can easily be made translucent and are easily pigmented to give any desired colours to the structure. Further, GRP, as many other plastics, has exceedingly good corrosion resistance, which is far superior to that of many conventional structural materials and they are very amenable to prefabrication. This property, together with their light weight, makes GRP composites very

2.1.1) contd.

useful materials in systems of industrial building, (ref.2-2).

2.1.2) Strength:

The ultimate strength of GRP may be varied according to the type of reinforcement used and the amount of fibre volume fraction in each particular direction of the composite. In the later case high strengths are only found in the direction of high fibre volume fraction which reflects the anisotropic behaviour of the composite. GRP shows different tensile and compressive strengths and because most GRP composites are considered as laminated composites this creates the possibility of interlaminar shear failure; a phenomenon peculiar to fibre reinforced laminated composites. The interlaminar shear strength may be an order of magnitude lower than the tensile or compressive strength and it is in fact a significant weakness of the material. Table (2-1) shows a comparison of mechanical properties of two types of widely used GRP laminates and other structural materials.

From Table (2-1), it can be seen that steel is a close competitor to GRP but even this material compares poorly with both forms of GRP composites on a specific strength basis.

2.1.3) Modulus of Elasticity.

The modulus of GRP materials is much lower than that of structural steel. The ramifications of low modulus are twofold. Firstly, the deformation of GRP structures will be larger than similar structures made of conventional materials. However, since deflections are related to stiffnes the cross-sectional geometry can be tailored to compensate for the low

Property	Specific Gravity	Tensile Strength	Tensile Modulus	Compressive Strength	Impact Strength	Specific Strength	Specific Modulus
Unit	-	MN/m^2	GN/m^2	MN/m^2	KJ/m^2	MN/m^2	GN/m^2
Random GRP	1.4	100	7	150	75	70	5
Unidirectional GRP	2.0	800	30	350	250	400	15
Mild Steel	7.8	400	200	250	50	50	26
Light Alloys	2.8	450	70	80	25	160	25
Plywood (exterior grade)	0.8	58	8	28.5	-	72.5	10
Concrete	2.3	-	-	6.9	-	3	-

TABLE (2.1) Mechanical properties of GRP Laminates compared with other structural materials.

2.1.3) contd.

modulus and the best structural forms for GRP are shells, folded plates, stressed skin systems and thin walled corrugated sections. The second aspect of the low modulus is that buckling may become the governing design criteria whenever compressive loading is present. Again this can be overcome by using a suitable structural form such as ribbed, sandwich, curved or corrugated forms of constructions (ref.2-3). Table (2.1) shows a comparison between the moduli of GRP and other engineering materials.

2.1.4) Effect of Water.

Water is well accepted as a major cause in the reduction of strength of glass fibres in a composite. It is also considered as a cause of destruction of the bond between the matrix and reinforcement and both swelling and plasticisation of the resin. GRP composites may be produced as water resistant if their constituents are treated for this purpose. For example, a silane or silicone finish to the glass fibres and resins of low water absorption lead to composites with improved water resistance. The question of water attack is more fully discussed in refs.(2-4,5,6,7).

2.1.5) Creep.

GRP material is visco-elastic, i.e. its extension under stress is a function of time. Creep of GRP depends upon the stability of the fibres and upon the extent to which the matrix itself is subject to direct loading. Thus in composites reinforced with unidirectional fibres less creep strain occurs than in other fibre configuration. On the

2.1.5) contd.

other hand, creep under interlaminar shear stresses and creep in short-fibre (chopped strand) composites will be large unless the matrix itself is relatively creep resistant. Creep also occurs in laminates that are wound or pressed with fibres at some angle $\pm \theta$ to the stress axis.

The creep behaviour of short-fibre composites is governed by the matrix rather than the fibres. Under long term load there will be three processes occuring in a short-fibre composite. Shear stresses at the fibre ends will be relaxed causing load redistribution; stress relaxation will occur in the matrix and load will be transferred into the fibres; and finally, creep of the fibres themselves may occur, see ref.(2-8).

In general the difference in creep behaviour between the various types of laminates can be related principally to glass content. Another factor is irregularity or lack of reinforcing continuity in the load direction as is the case for chopped strand mat laminates.

Insufficient work has been carried out for the designer to be able to predict the creep behaviour of GRP confidently. This is particularly true with respect to creep under stresses other than tensile. However, ref.(2.9) suggests that results of short term creep tests can be usefully extrapolated over longer periods. Finally, ref.(2-11) notes that the principle factors affecting creep from the design point of view are:

1) Material construction (i.e. mat or fabric).

2) Stress level.

3) Environment.

4) Temperature.

2.1.5) contd.

A general review on creep of fibre reinforced composites could be found in refs.(2-3,10).

2.1.6) Fatigue.

When engineering materials are subjected to repeated loading they may fail under a load much lower than the short-term ultimate load. This phenomenon has been a problem to engineers since the early part of the nineteenth Century and is called "fatigue". Originally attention was concentrated only on metals, subsequently this phenomenon was recognised in virtually all engineering materials including concrete, asphalt mixes and plastics. Glass reinforced plastic of all kinds have been found to be susceptible to fatigue failure under repeated loading.

Only some aspects of the mechanism of fatigue damage in GRP are understood. Refs.(2-12,13 and 14) give a considerable amount of data on the fatigue characteristics of chopped strand mat and woven fabric polyester laminates. For these types of laminates the mechanism of fatigue failure is reasonably well understood. The first stage of failure is tensile debonding within strands which are perpendicular to the applied load. The subsequent stages are joining of debonds, resin cracking and final failure. Ref.(2-15) states that the stages in the cyclic life of a GRP laminate depends on the material and the manner of loading. In axially stressed, unidirectionally reinforced laminates an initial debonding process is also evident due to the difference in deformation between the resin and glass. Further processes are matrix cracking and even disintegration where the fibres remain relatively undamaged.

2.1.6) contd.

In ref.(2-16), the fatigue ratio (fatigue strength/ ultimate strength) at 10^7 cycles for twenty-two tests were reported. The tests were for a wide range of glass content, loading conditions, laminate construction and resin type. The fatigue ratios range from 0.13 to 0.39 with only two values below 0.20 and an average value of 0.25. These results indicate that a factor of safety of 5 on ultimate stress would be conservative for the majority of tests.

The effects of glass-content on fatigue are reported in ref.(2-12) and show that the glass content had only a small effect on long-term fatigue strength.

The conclusions regarding the effect of termpature on fatigue are at variance. At cryogenic temperature, ref.(2-17) reports that the fatigue strength was equivalent to or an improvement on the room temperature fatigue strength. This was not substantiated by ref.(2-18) which finds that the fatigue strength at -20°C was reduced to that of the room temperature strength. In addition the fatigue strength was found to decrease at elevated temperatures. Ref.(2-19) in a very limited investigation, shows that the weeping strain (i.e. the strain at which fluid can seep into and through the laminate), decreased beyond 40°C for loading conditions in excess of 100,000 cycles. This work was for one resin system and for filament wound pipe and has not been substantiated for any other conditions.

More information on fatigue in GRP may be found in ref.(2-20).

2.1.7) Long Term Properties.

This section will be devoted to general remarks

2.1.7) contd.

concerning fatigue, creep and strength-retention characteristics and may be considered as a continuation to Sections (2.1.5,6) above.

Figs.(2.1,2 and 3) were extracted from (ref.2-1, P.46) and represent a series of tests on different glass reinforcement under a repating load of up to 10^8 cycles and five years continuous loading.

Examination of the curves indicates that:-

1) Both tensile and flexural fatigue strength with both random reinforcement and bi-directional reinforcement tend to level off at between 20-25 per cent of their short-term ultimate strength of 10^7 cycles. Fig.(2-1).

2) At a tensile loading of 50 per cent of the short-term ultimate strength, the total creep after 10^4 hrs. is in the order of 0.005 in/in. Even though GRP exhibits extremely low strain to failure it is seen that the laminate creep over extended periods will be negligible when the working stress levels are in the order of 10% of the short-term ultimate, Fig.(2-2).

3) The tensile strength retention of laminate continuously loaded to a level of 50 per cent of the short-term ultimate strength will sustain this load for 10^4 hrs. As with the creep characteristics, at a working stress level approximately 10 per cent of the short-term ultimate it is expected that strength retention would be entirely adequate, Fig.(2-3).

A general but interesting observation from the above long-term data is that random chopped strand glass mat reinforced laminates are shown to have fatigue strength retention, creep resistance and continuous loading strength

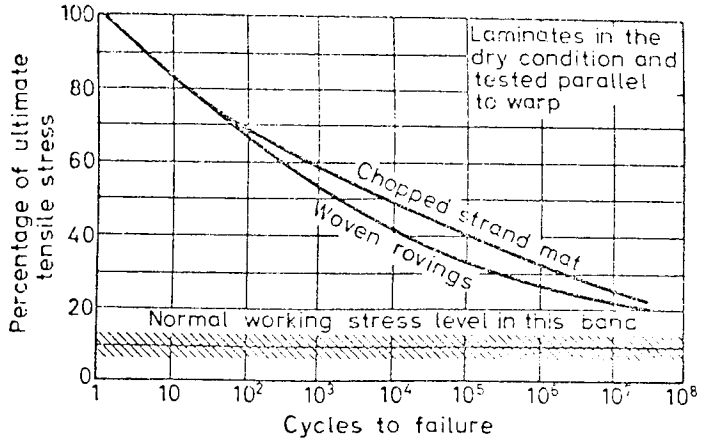

Fig . 2.1 Tensile fatigue strength of polyester glass fibre laminates. ref. 2.1.

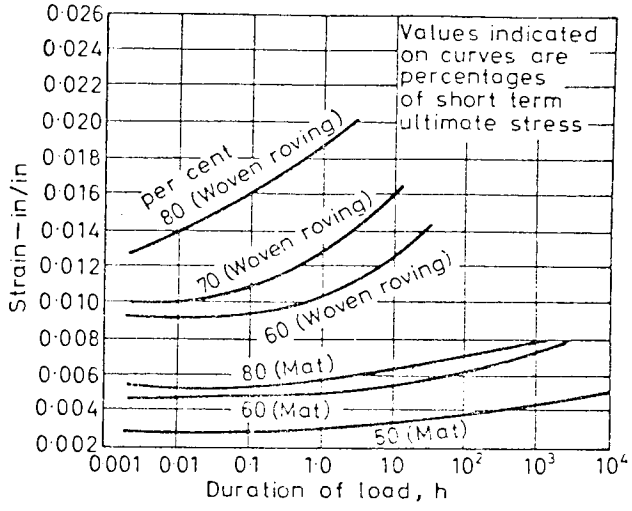

Fig. 2.2. Tensile creep of continuously loaded polyester glassfibre laminates. ref. 2.1.

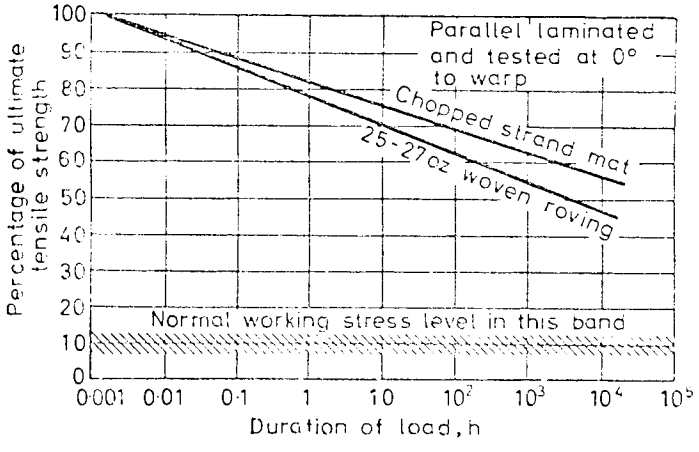

Fig. 2.3 Tensile strength retention of continuously loaded polyester glassfibre laminates ref 2.1

2.1.7) contd.

retention similar to laminates reinforced with continuous woven fibres.

2.1.8) Impact Strength.

There is a certain ambiguity in existing definitions of impact strength and its relation to the toughness of a material. In general, under impact loading many materials behave in a brittle fashion (i.e. with little or no plastic deformation before fracture). The easier property to measure in a rapid test such as a Charpy or Izod test is the energy absorbed from the pendulum. When this type of test is used, the energy absorbed to break the specimen is higher than that to damage the specimen to such an extent that for design purposes could be useless. This is because, in addition to the energy required to crack the resin, energy is also required to tear the glass fibres apart or out of the resin. In the case of glass fabric or mat reinforced polyester this can be considerably more than the energy required to crack the resin and make the structure permeable to water or other environments. So that care should therefore be exercised when using impact results from this test method as they may be misleading.

Further information may be obtained from ref.(2-10).

2.1.9) Ductility.

GRP is a brittle material and differs from mild steel by not undergoing plastic deformation before ultimate failure. Two disadvantages arise from this brittle type of behaviour. Firstly, in GRP stress redistribution and relief is not as effective as in ductile materials (e.g. mild steel) at

2.1.9) contd.

points of stress concentration. Hence structural joints must be designed with special care in GRP. Secondly, steel structures show considerable deformations prior to catastrophic failure which may serve as a warning of impending failure. Such warning would not be expected in GRP structures.

2.1.10) Durability.

GRP composites suffer a reduction in strength, modulus and appearance when exposed to the atmosphere, where ultra-violet light and water are the main causes of the degradation, ref.(2-21). Hence some resins with low water absorption and treated against ultra-violet light give composites a better weathering resistance.

Ref.(2-22) states that the decrease in tensile and interlaminar shear strength ranges between 10-20 per cent if the GRP unit is exposed to the atmosphere for a period of 3 years, although compressive strength shows an increase of 10 per cent.

Heat and atmospheric pollution can also significantly effect the properties of GRP composites.

2.1.11) Fire Resistance.

All organic materials burn if the temperature increases above the ignition temperature (about 250°C for GRP) for any length of time. Hence GRP is classed as combustible when used independelty and its use is restricted in buildings by the building regulations unless specially treated to increase its fire resistance.

2.1.12) Mouldability.

GRP, unlike most conventional materials, gives the designer a degree of freedom to design the sort of material he needs as well as the shape of the structural component desired. This freedom is subject to economic considerations and moulding techniques currently available. Of the many manufacturing techniques currently used in the plastics industry a selection is given below:-

1. Hand lay up and contact moulding
2. Spray up technique
3. Hot and cold press moulding
4. Polyester Dough moulding compounds
5. Continuous resin injection for glass fibre moulding
6. Continuous Pultrusions
7. Vacuum bag
8. Pressure bag
9. Continuous laminating
10. Filament winding
11. Fabrique winding

A detailed description on the above techniques may be found in ref.(2-23).

2.1.13) Glass-Resin Interface:

Unidirectional glass fibres cannot bear load in compression and shear unless they are embedded in a resin matrix that gives the fibres the necessary stiffness for resistance to such loading system. The glass and resin are mutually reinforcing, the strong, stiff glass carries most of the stress and the polymer matrix distributes the external load to all the fibres, while at the same time protecting them. This load sharing requires that stress be transferred

2.1.13) contd.

across the interface between glass and resin, the physical and chemical properties of which should be known. There is no sharp, well defined interface between glass and resin for the glass is coated with a heterogeneous mixture, itself resinous in nature, and this in turn is coated with the resin forming the matrix of the composite structure. The constitution and properties of the resin is different from both the coating and the glass. The whole interfacial region is about 10^{-2} μm thick or greater, see Fig.(2.4).

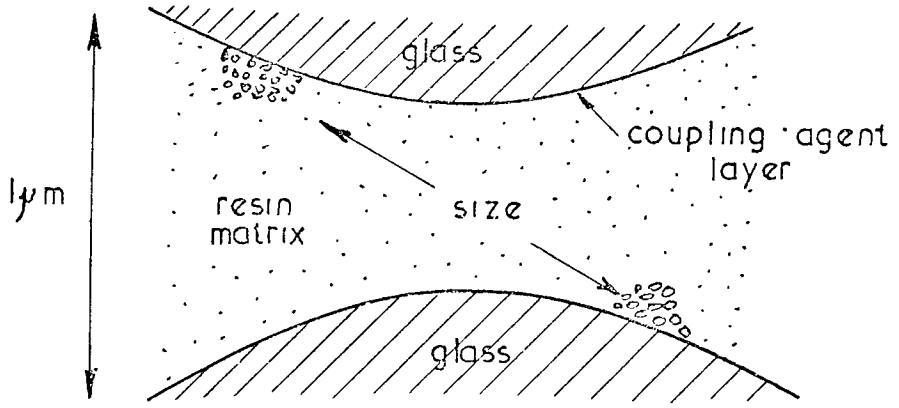

FIG.(2.4), Section of a composite normal to the fibre axis showing an area of the interfacial region.

A thorough characterization of fibre-resin interface may be found, ref.(2-24).

2.2) GRP Constituents.

So far the characteristics of GRP composites have been discussed. In this section, the discussion will be concentrated on the constituent materials which form the GRP composites. These materials are the glass fibres and the thermosetting plastic resins.

2.2.1) Glass fibres.

The reinforcement which is currently of most general use is glass fibre formed from inorganic oxides.

The most common glass fibres are made from so-called E-glass. Another more recent type of glass composition, S-glass is of higher modulus and higher price than E-glass. The properties of E and S glass fibres are given in Table (2.2)

Glass	Composition Percentage by weight					Young's Modulus	Strength+	Density
	SiO_2	Al_2O_3	CaO	MgO	B_2O_3	(GN/m^2)	(GN/m^2)	($10^3 kg/m^3$)
S	65	25	-	10	-	84.1	4.83	2.49
E	54	14	17.5	4.5	10	72.4	3.45	2.55

+ Average strength of undamaged 6 cm length fibre.

Table (2.2)

Properties of S glass and E glass fibres (ref.2-25).

Other types of glass fibres are available commercially for special purposes and are more expensive than the E glass fibres. These types are listed below.

1. Alkali-lime glass (A-glass): A coarse fibre usually used in some textile fibres.
2. C-Glass: This type of fibre was developed for applications requiring greater corrosion resistance to acids than that of E-glass.
3. D-Glass: This was developed for its low dialetric constant for use in randomes. It has a low density not exceeding 2.16 gm/cm^3.
4. M-Glass: Possesses a high elastic modulus and is used for many structural applications where the limiting

2.2.1) contd.

4. contd.

design factor is stiffness rather than strength. It's Young's modulus, 11.4 GN/m^2 (15.9×10^6 psi), is about 50% greater than that of the E-Glass.

5. Fused Silica: Is a unique glass, particularly in its resistance to softening at elevated temperature and in its low density (2.10-2.21 gm/cm^3) and high strength in fibre form which varies between 5.61 to 9.81 GN/m^2 (800,000-1,400.000 psi).

Further details of special purposes glass fibres may be found in ref.(2-26).

2.2.1(i) Production of Glass fibres.

The principle of manufacture is shown diagrammatically in Figs.(2.5 and 6). The equipment described in ref.(2-27) to produce a single filament of E glass is shown in Fig.(2.5). Molten E glass is contained in an electrically heated platinum bushing, a filament is drawn downward through a nozzle and wound on to a drum.

The principle of the Owens-Corning manufacturing process, ref.(2-28), is shown in Fig.(2.6). Glass in the form of marble or batch is introduced into the bushing. The base of the bushing contains a number of nozzels (of the order of 200) and a filament is drawn from each. A sizing is applied to the filaments just before they are gathered into a strand, after which a traversing mechanism winds the strand on to the forming cake. When the forming cake reaches the desired weight the winder is stopped and the cake removed and placed in an oven to be cured. The cured strand is then processed into roving. A roving may contain 1,12 or 20 strands

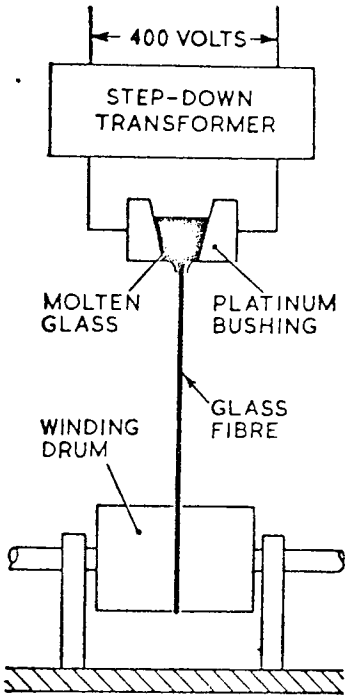

Fig.2.5. Diagrammatic representation of glass fibre drawing process (ref. 2.27)

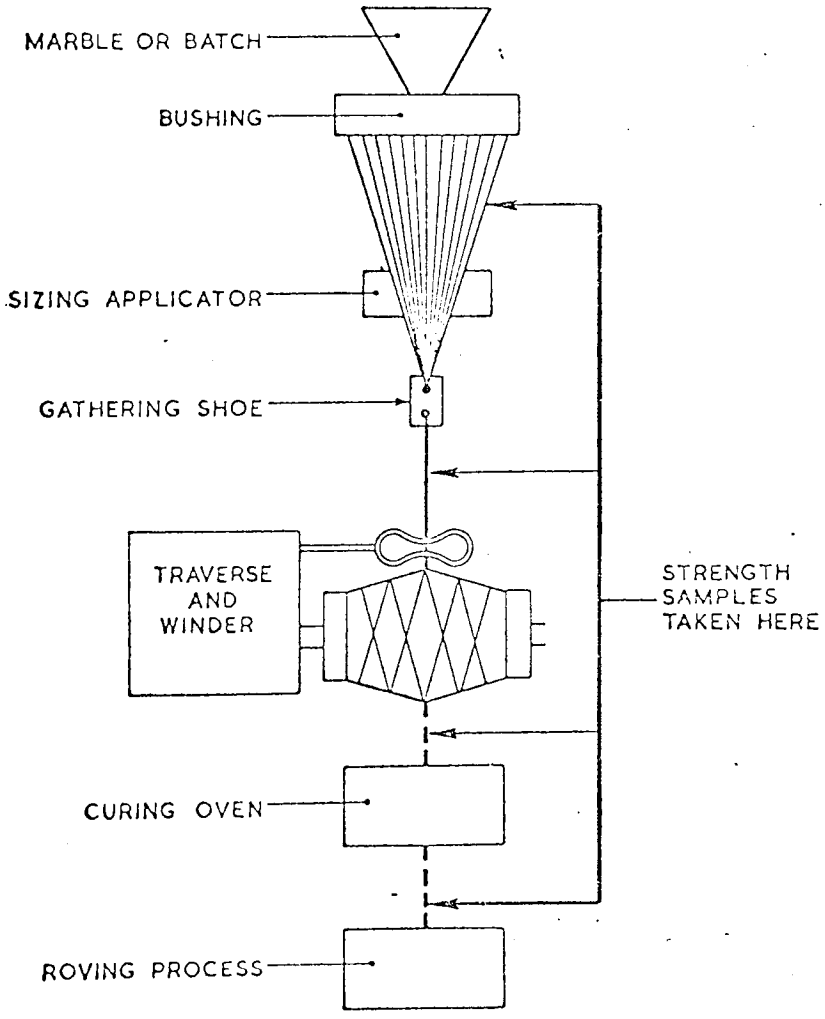

Fig. 2.6. Diagrammatic representation of glass fibre forming scheme (ref 2.28)

2.2.1(i) contd.

and is described as 1, 12 or 20-end roving.

Further details on glass fibre production are given in ref.(2-29).

2.2.1(ii) Forms of Reinforcements.

Glass fibre reinforcement may be produced in many forms depending on type of component to be manufactured, the moulding technique, and the design requirements.

The types of fibre reinforcement available commercially are:-

1. Yarns
2. Fabrique and tapes
3. Rovings
4. Woven roving fabriques, (unidirectional and bidirectional)
5. Chopped strands
6. Chopped strands mat

Full descriptions of these reinforcements may be found in ref.(2-29).

2.2.2) Resins:

In this section discussion will be limited to thermosetting resins. Thermosetting materials are those that undergo a chemical polymerization reaction (cure) when heated and reheating does not reverse the process. The most common resins used in GRP are polyester, epoxy, and phenolic. Phenolic resin, although it is the cheapest, requires high moulding pressure and is only used in certain applications using the pressure moulding manufacturing process. Polyester and expoxy resins have the following composition and properties.

1. Polyester Resins: unsaturated polyesters are made

2.2.2) contd.

1. contd.

by reacting together a dihydric alcohol and a dibasic acid, either or both of which contain a double bonded pair of carbon atoms. The main properties of this resin are shown in Table (2.3).

2. Epoxide Resin: linear polymers made by condensing epichlorhydrin with polyhydroxy compounds. The properties of this resin are also shown in Table (2.3).

	Cured Polyester	Cured Epoxy
Specific gravity	1.10 - 1.46	1.11 - 1.40
Tensile Strength (MN/m^2)	42 - 91	28 - 91
Tensile Modulus (GN/m^2)	2 - 4.5	2.4
Compressive Strength (MN/m^2)	89.6 - 251	103 - 172
Shrinkage	0.004 - 0.008	0.001 - 0.004
Heat resistance C°	60 - 204	46 - 288

Table (2.3) TYPICAL RESINS PROPERTIES

Other types of special purpose resin may also be used with glass fibres but are of a very high cost. These are:-

1. Melamin - good electrical and heat resistance
2. Silicon - highly heat resistant
3. Furane - good chemical resistant.

A more detailed account of resin systems may be found in ref.(2-23).

REFERENCES.

2-1) PARKYN,B., "Glass reinforced plastics", Iliffe Books, London, 1970.

2-2) BENJAMIN,B.S.,"Plastic as structural material", The Consultant Engineer, November 1965, pp.43-45.

2-3) COOK,D.J., "Factors influencing the design of glass reinforced plastic structure", Uniciv report No.R-101, University of New South Wales, Australia, December 1972.

2-4) BOLLER,K.H., 14th Annual Meeting of reinforced plastics Division of the Society of the plastics industry, February 1959, Paper 10.

2-5) BENJAMIN,B.S., "Structural design with plastics" Van Nostrand Reinhold, 1969, P52.

2-6) STEEL,D.J., Transaction Plastics Institute, Volume 33, 1965, P.161.

2-7) KABELKA,J., 5th International reinforced plastics Conference, November 1966, Paper 17.

2-8) MILEIKO,S.T., Journal of Materials Science, Volume 5, P.254, 1970.

2-9) McLOUGHLIN,T.R., Modern Plastics, Volume 45, February 1968.

2-10) HARRIS,B., "The Strength of fibre composites", Composites, July 1972, PP.152-1967.

2-11) BOTT,T.R., and BARKER,A.J., "Creep in reinforced plastics", British Plastics Federational Report on fatigue and creep in reinforced plastics, London 1967, PP.8-13.

2-12) SMITH,T.R., and OWEN,M.J., "Fatigue Properties of RP", Modern Plastics, April, 1969, PP.124-128.

2-13) OWEN,M.J., and SMITH,T.R., "Some fatigue peroperties of chopped strand mat/polyester laminates", Plastics and polymers, February 1968.

2-14) OWEN,M.J., et al. "Failure of glass reinforced plastics with special reference to fatigue" Plastics and Polymers, June 1969.

2-15) OWEN,M.J., "Dynamics fatigue of reinforced plastics" British Plastics Federation report on fatigue and creep in reinforced plastics, London, 1967, PP.13-18.

2-16) British Plastics Federation report on fatigue and creep in reinforced plastics, London, 1967, P.26.

2-17) BRINK,N.O., "Mechanical behaviour of reinforced plastics at cryogenic temperature", Journal, Society of Plastics Engineers, October 1964.

2-18) MATTING,A., and WAGENER,K., "Fatigue in glass-reinforced plastics", Kunststoffe, Volume 34, December 1964.

2-19) ISHAM,A.B., "Design of fibre glass reinforced plastics chemical storage tanks". Proc.21st Annual Conference, of Plastics Industry, February 1966, Section 16-E.

2-20) OWEN,M.J., Reference 1, Chapter 18, PP.251-267.

2-21) MATTHAN,J.,et al. "Ageing and weathering of glass fibre reinforced polyester resins", a review of the literature on the ageing and weathering of plastics, Part 4, RAPRA.

2-22) SCOTT,K.A., and MATTHN,J., Reference 1, Chapter 16, pp.220-231.

2-23) MORGAN,P. etc., "Glass reinforced plastics" Iliffe books Ltd., London, 1961.

2-24) NORMAN,R.H., et al., Reference 1, Chapter 15, PP.206-219.

2-25) McCRUM,N.G., "A review of the science of fibre reinforced plastics", H.M.Stationery Office, London, 1971, P.12.

2-26) BROUTMAN & KROCK, "Modern Composite Materials", 1964.

2-27) THOMAS,W.F., Physics Chem.Glasses, Vol.14, 1960.

2-28) PATRICK,A.J., and HOOD,J.H., Proc.20th Annual Conference, Society of Plastics Industry, February 1965, Section 9-D.

2-29) WARING,L.A.R., Reference 1, Chapter 10, pp.121-145.

CHAPTER 3

STRUCTURAL PROPERTIES OF GLASS FIBRE REINFORCED PLASTICS.

3.1) Introduction.

In the previous chapter, a general definition of GRP composites and their constituents was introduced.

This chapter is mainly concerned with the manufacturing technique for the GRP composites under investigation, and with the elastic and strength properties of the monolayer with respect to the principal and other directions.

The effect of fibre content and orientation, in addition to the effect of voids on the elastic and strength performance of unidirectional composites will be investigated, from which the strength and elastic properties of the multidirectional laminated system may be determined and a method of design of these composites can be obtained.

The stress-strain relationship in tension and compression for unidirectional, cross-ply, angle-ply and multidirectional GRP composites will be studied.

Finally, for the general characterization of the composites under investigation, the method of material testing will be discussed and the design of test specimens used in the material characterization will be presented.

3.2) Stiffness.

The very low stiffness of GRP lamintes has proved a serious obstacle to the development of efficient structual designs. General stress levels in GRP components should be severely constrained to be far below the ultimate tensile or compressive strength in order to avoid elastic buckling and excessive deformations.

Structural design in GRP is normally influenced more strongly by the elastic modulus of the monolayer than by the layer strength. Therefore careful evaluation of elastic constants should be treated as an important part of the design process.

3.2.1) Hooke's Law For Anisotropic Materials.

From elementary theory of elasticity, the generalized Hooke's Law for a continuous material is defined by

$$\sigma_i = C_{ij}\,\varepsilon_j \qquad (3.1)$$

$$i,j = 1,2.... 6$$

Equation (3.1) shows thirty six elastic constants are needed to relate stress and strain below the proportional limit of the material.

The stiffness matrix C_{ij} in equation (3.1) is of symmetric construction (i.e. $C_{ij} = C_{ji}$), and the most general form of the stiffness matrix of symmetric anisotropic materials is as follows:-

$$\begin{bmatrix} C_{11} & C_{12} & C_{13} & C_{14} & C_{15} & C_{16} \\ & C_{22} & C_{23} & C_{24} & C_{25} & C_{26} \\ & & C_{33} & C_{34} & C_{35} & C_{36} \\ & & & C_{44} & C_{45} & C_{46} \\ \text{Symmetric} & & & & C_{55} & C_{56} \\ & & & & & C_{66} \end{bmatrix} \qquad (3.2)$$

3.2.1) contd.

for a total of twenty one elastic constants.

If equation (3.1) is inverted it will yield the following

$$\varepsilon_i = S_{ij}\,\sigma_j \qquad (3.3)$$

where S_{ij} is the inverse of the stiffness matrix C_{ij}. Since the inverse of a symmetric matrix is also symmetric, then $S_{ij} = S_{ji}$ for a total of twenty one compliance elements.

In this program the material under consideration is assumed to be thin (i.e. the dimension in the verticle axis of symmetry is very small compared with the dimensions of the longitudinal and transverse axes). Therefore the analysis throughout the program will be of a two-dimensional nature in a state of generalized plane stress. Equation (3.3) in matrix form then becomes

$$\begin{bmatrix} \varepsilon_x \\ \varepsilon_y \\ \gamma_{xy} \end{bmatrix} = \begin{bmatrix} S_{11} & S_{12} & S_{16} \\ S_{12} & S_{22} & S_{26} \\ S_{16} & S_{26} & S_{66} \end{bmatrix} \begin{bmatrix} \sigma_x \\ \sigma_y \\ \tau_{xy} \end{bmatrix} \qquad (3.4)$$

In the above case six elastic constants are needed. If the material is assumed to be orthotropic, and the coordinate axes coincide with the principle axes, equation (3.4) reduces to

$$\begin{bmatrix} \varepsilon_L \\ \varepsilon_T \\ \gamma_{LT} \end{bmatrix} = \begin{bmatrix} S_{11} & S_{12} & 0 \\ S_{12} & S_{22} & 0 \\ 0 & 0 & S_{66} \end{bmatrix} \begin{bmatrix} \sigma_L \\ \sigma_T \\ \tau_{LT} \end{bmatrix} \qquad (3.5)$$

where L and T are related to the principal longitudinal and transverse axes respectively.

To determine the stress-strain relationships for the two dimensional orthotropic problem requires the inversion of equation (3.5) the result is

3.2.1) contd.

$$\begin{bmatrix} \sigma_L \\ \sigma_T \\ \tau_{LT} \end{bmatrix} = \begin{bmatrix} C_{11} & C_{12} & 0 \\ C_{12} & C_{22} & 0 \\ 0 & 0 & C_{66} \end{bmatrix} \begin{bmatrix} \varepsilon_L \\ \varepsilon_T \\ \gamma_{LT} \end{bmatrix} \qquad (3.6)$$

where

$$C_{11} = \frac{S_{22}}{S_{11}S_{22}-S_{12}^2}$$

$$C_{12} = \frac{S_{12}}{S_{11}S_{22}-S_{12}^2}$$

$$C_{22} = \frac{S_{11}}{S_{11}S_{22}-S_{12}^2}$$

and

$$C_{66} = \frac{1}{S_{66}}$$

It can be noticed that two dimensional orthotropy requires only four elastic constants.

3.2.2) Stress-Strain Relation for a Unidirectional Layer Referred to the Principal Axes.

Consider the two dimensional case of an orthotropic unidirectional composite monolayer in which the longitudinal direction is L and the transverse direction is T (Fig.3.1).

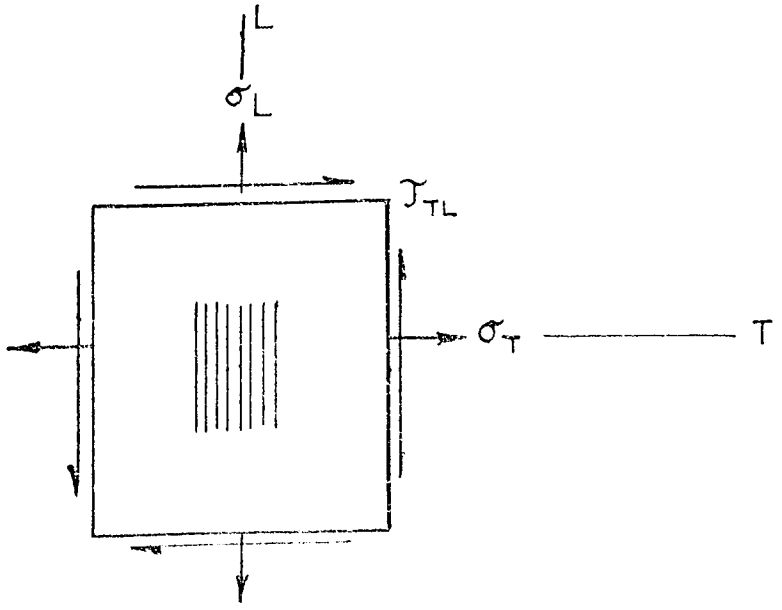

FIG.(3.1)

3.2.2) contd.

The elastic modulii to characterize this layer are E_L and E_T in the longitudinal and transverse directions respectively, G_{LT}, the shearing modulus associated with L and T directions, ν_{LT}, the longitudinal Poisson's ratio giving the transverse strain caused by a strain in the longitudinal direction and ν_{TL}, the transverse Poisson's ratio, giving the longitudinal strain caused by a strain in the transverse direction.

The relations of these five constants to the four independent elastic constants of equation (3.6) can be established by letting σ_L of equation (3.6) be the only non-zero stress. Then the equation becomes

$$\sigma_L = C_{11}\,\varepsilon_L + C_{12}\,\varepsilon_T$$
$$0 = C_{12}\,\varepsilon_L + C_{22}\,\varepsilon_T$$

which can be solved to yield

$$\varepsilon_L = \frac{\sigma_L\, C_{22}}{C_{11}C_{22} - C_{12}^2}$$

and (3.7)

$$\varepsilon_T = \frac{\sigma_L\, C_{12}}{C_{11}C_{22} - C_{12}^2}$$

The modulus E_L is defined as

$$E_L = \frac{\sigma_L}{\varepsilon_L}$$

and the substitution of the first of equation (3.7) yields

$$E_L = C_{11} - \frac{C_{12}^2}{C_{22}} \qquad (3.8)$$

The longitudinal Poisson's ratio is defined as

$$\nu_{LT} = - \frac{\varepsilon_T}{\varepsilon_L}$$

Equation (3.7) can be substituted in the above expression to obtain

$$\nu_{LT} = \frac{C_{12}}{C_{22}} \tag{3.9}$$

A repetition of this procedure with σ_T the only non-zero stress in equation (3.6) yields

$$E_T = \frac{\sigma_T}{\varepsilon_T} = C_{22} - \frac{C_{12}^2}{C_{11}} \tag{3.10}$$

and

$$\nu_{TL} = -\frac{\varepsilon_L}{\varepsilon_T} = \frac{C_{12}}{C_{11}} \tag{3.11}$$

Finally, if τ_{LT} is assumed to be the only non-zero stress in equation (3.6), then

$$G_{LT} = \frac{\tau_{LT}}{\gamma_{LT}} = C_{66} \tag{3.12}$$

which is the fifth elastic constant.

Since only four independent elastic constants were indicated by equation (3.6), some relationship must exist between the five constants mentioned above. Dividing equation (3.8) by equation (3.10) gives

$$\frac{E_L}{E_T} = \frac{C_{11}}{C_{22}} \tag{3.13}$$

also dividing equation (3.9) by equation (3.11) yields

$$\frac{\nu_{LT}}{\nu_{TL}} = \frac{C_{11}}{C_{22}} \tag{3.14}$$

From equations (3.13) and (3.14) we can obtain the relationship

$$\frac{E_L}{E_T} = \frac{\nu_{LT}}{\nu_{TL}} \tag{3.15}$$

Therefore any three of the four constants in equation (3.15) plus G_{LT} constitute an equivalent set of four independent elastic constants in the principal material directions.

It is usually easier to work with stiffness and compliance elements than the five elastic constants just discussed. The equivalent expressions are

3.2.2) contd.

$$C_{11} = \frac{E_L}{1 - \nu_{LT}\nu_{TL}}$$

$$C_{12} = \frac{\nu_{LT} E_T}{1 - \nu_{LT}\nu_{TL}} = \frac{\nu_{TL} E_L}{1 - \nu_{LT}\nu_{TL}} \qquad (3.16)$$

$$C_{22} = \frac{E_T}{1 - \nu_{LT}\nu_{TL}}$$

and

$$C_{66} = G_{LT}$$

for the stiffness element defined in equation (3.6).

For the compliance element defined in equation (3.5)

$$S_{11} = \frac{1}{E_L}$$

$$S_{12} = -\frac{\nu_{LT}}{E_L} = -\frac{\nu_{TL}}{E_T} \qquad (3.17)$$

$$S_{22} = \frac{1}{E_T}$$

and $$S_{66} = \frac{1}{G_{LT}}$$

3.2.3) <u>Micromechanical Methods of Predicting The Elastic Constants For a Unidirectional Layer Referred to The Principal Axes.</u>

The analytical methods used for composite materials are divided into two major categories, micro and macromichanics. These methods are different in the geometrical scale of reference. The micromechanic deals with the constituent properties of the monolayers, while macromechanics describes the combined characteristics of a number of layers. So in this section attention will be concentrated on the determination of elastic constants of composite by the means of micromechanical methods (i.e. as a function of its constituent properties, the fibres and the resin matrix).

3.2.3) contd.

It is important to empahsize that the availability of many types of composite materials has made it feasible to design a material for a given set of properties. This modern composite concept recognizes that the material design phase is an integral part of the structural design process.

Many models representative of the fibre-matrix microstructure have been constructed for the sake of analysis. For typical glass filament, prepreg tapes and rovings, the monolayer is made up of a large number of filament bundles. When these bundles are compressed, and if they are ideally "Packed" during the laminating process, individual filaments become arranged in either a square geometric array in the matrix Fig.(3.2A) or a hexagonal array Fig.(3.2B).

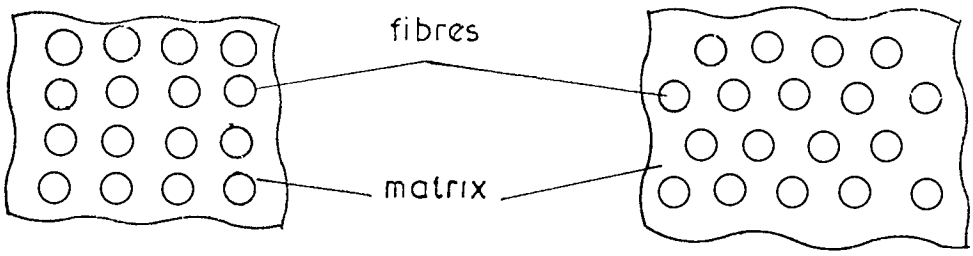

A-A square array of fibres in a matrix element

B-A hexagonal array of fibres in a matrix element

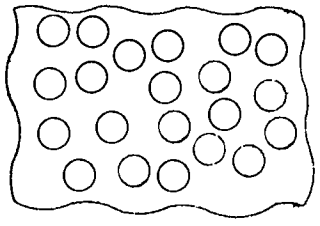

C-A random array of fibres in a matrix element

FIG.(3.2)

3.2.3) contd.

In most cases, however, small diameter fibre systems (such as glass) do not pack ideally, and a random cross-sectional array is obtained as shown in Fig.(3.2C). Strict fabrication process control is required to obtain the desirable geometric arrays in the first two systems.

Many studies on the composite media have been undertaken in recent years, in these studies the composite media were assumed to be locally hetrogeneous and grossly homogeneous with the following combinations, (ref.3.2).

1) Local and gross isotropy.

2) Local anistropy and gross isotropy.

3) Local isotropy and gross anistropy.

The number of independent elastic constants increases from two, for the grossly istropic case, to four, five or six for the unidirectional composite. The exact number depends on the type of symmetry of the composite, as dictated by the assumed packing arrangement of the fibres in the composite.

Symmetry	Number of Independent Constants	Fibre Packing
Orthotropy (2-Dimensional)	4	Random
Transverse Isotropy	5	Hexagonal or Random
Tetragonal	6	Square

TABLE (3.1) (Extracted from ref.3.2)

Considering the unidirectional layer as the basic unit of the fibre reinforced composite or the laminated composite, it means dealing with a parallel set of fibres embodied in an otherwise homogeneous

3.2.3) contd.

matrix material. The unidirectional layer constituents are consider to be of isotropic nature, while the layer itself, if its coordinates coincide with the principal axes, is of orthotropic behaviour having nine independent constants. ref.(3.1, P.9).

If the filaments are arranged in a random fashion as illustrated in Fig.(3.2C), then it is reasonable to consider this transverse plane as an isotropic plane and the composite could be considered as a transversely istropic composite with five independent elastic constants. This situation also applies to that occurring when the fibres are arranged in a regular hexagonal array. (See Table 3.1 and Fig.3.2B).

The terms orthotropic or transversely isotropic mentioned in the above discussion, describe special symmetry of material whose properties vary with direction. The type of symmetry defines the number of independent properties required to describe the material.

For any of these geometries, interest is centred on finding the effective elastic constants which represent the average values of the phase variables. In the principal direction the stiffness matrix of the composite can be considered as a function of the following parameters,

$$C_{ij} = f(E_f, \nu_f, V_f, E_m, \nu_m, V_m, V_v, C) \qquad (3.18)$$

As mentioned in Section (3.2.2), the elastic constants that characterize the stiffness matrix C_{ij} of a unidirectional monolayer are five. The methods used to predict these elastic constants may be divided into,

a) boundary methods utilizing variational principles. (ref.3.3).

3.2.3) contd.

b) elasticity approaches involving computerized solutions, (ref.3.4,5).

c) simplified models. (ref.3.6)

While the results based on variational principles are more rigorous mathematically, the precision for real composite is far outweighed by the influence of complex processing variables, (e.g. fibre damage and degradation, non-uniform curing residual stresses, cracks,...etc.). The same observation applies to the elasticity solutions. Solutions based on simplified models are correlated with experimental results and result in relatively simple results of greater applicability.

A review of the theories used to predict the elastic constants is now presented.

i) Prediction of Longitudinal Elastic Modulus (E_L):

The law of mixture given by the following equation is used as an acceptable approximation for the longitudinal modulus

$$E_L = V_f E_f + V_m E_m \qquad (3.19)$$

TSAI(3-2) modifies the above expression to

$$E_L = k(V_f E_f + V_m E_m) \qquad (3.20)$$

where k is a misalignment factor to account for non-parallel or non-straight fibres. This factor ranges from about 0.9 to 1. By this limitation of the factor k the modification is therefore not very significant.

EKVALL(3-7) also modifies the law of mixture by using a mechanics of material approach for a lamina consisting of glass roving or strands, taking into account the triaxial stress condition in the matrix due to the restraint provided by the filament materials, this equation is

3.2.3) contd.

i) contd.

$$E_L = V_f E_f + V_m E_m'$$

where

$$E_m' = \frac{E_m}{(1-2\nu_m^2)} \qquad (3.21)$$

Again in the light of variations in experimental behaviour this modification is not so significant, for valuesof ν_m of approximately 0.30 a factor of 0.82 is obtained. The law of mixture (equation 3.19) is generally taken as an acceptable approximation for the longitudinal modulus

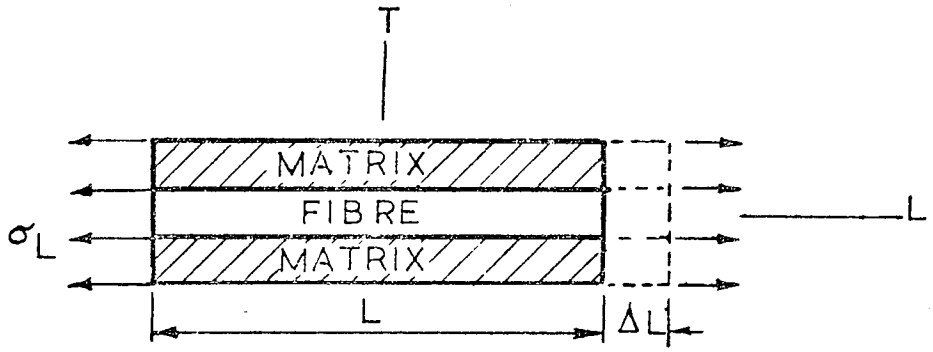

FIG.(3.3)

ii) Prediction of Longitudinal Poisson's Ratio (ν_{LT}):

The longitudinal Poisson's ratio can be derived from Fig.(3.3) as

$$\varepsilon_T = -\nu_{LT}\,\varepsilon_L$$

and the total deformation in the transverse direction is

$$\Delta_T = t\nu_{LT}\varepsilon_L = \Delta_{fT} + \Delta_{mT}$$
$$= tV_f\nu_f\varepsilon_L + tV_m\nu_m\varepsilon_L$$

$$\therefore \quad \nu_{LT} = V_f\,\nu_f + V_m\,\nu_m \qquad (3.22)$$

Equation (3.22) is similar to the law of mixtures for the longitudinal modulus given by equation (3.19). Equation (3.22) agrees with the assumption of EKVALL

3.2.3) contd.

ii) contd.

for laminates of one-filament diameter thickness. It also agrees with his expression for lamina consisting of glass roving or strands, ref.(3.7).

Rosen et.al.(3.3,8), find by using the variational boundary method, that the bounds on ν_{LT} coincide for a random array of hollow circular filament surrounded by matrix materials. Their expression is

$$\nu_{LT} = \frac{V_f E_f L_1 + V_m E_m L_2 \nu_m}{F_f E_f L_3 + V_m E_m L_2} \qquad (3.23)$$

where

$$L_1 = 2\nu_f(1-\nu_m^2)V_f + V_m(1+\nu_m)\nu_m$$

$$L_2 = V_f(1-\nu_f-2\nu_f^2)$$

and

$$L_3 = 2(1-\nu_m^2)V_f + (1+\nu_m)V_m$$

For solid filaments, they cannot obtain the bounds directly for an hexagonal array because of the more complicated nature of the problem.

Whitney (3.9) uses a model analogous to that of Hashin and Rosen, but is much less rigorous mathematically. In the analysis he assumes that the fibres are circular in cross section and are continuous through the composite. He also assumes that the fibres are packed in such a manner as to make the plane of the composite cross-section isotropic (i.e. random packing). His expression for the longitudinal Poisson's ratio is

$$\nu_{LT} = \nu_m - \frac{2(\nu_m-\nu_f)(1-\nu_m^2)E_f V_f}{E_m(1-V_f)L' + [LV_f + (1+\nu_m)]E_f} \qquad (3.24)$$

where

$$L' = 1-\nu_f - 2\nu_f^2$$

$$L = 1-\nu_m - 2\nu_m^2$$

3.2.3) contd.

ii) contd.

Using the technique for cylindrical inclusions and incorporating the concept of a contiguity factor C, TSAI(3-2) obtains

$$\nu_{LT} = (1-C)\ \frac{K_f V_f (2K_m+G_m)V_f + K_m \nu_m (2K_f+G_m)V_m}{K_f(2K_m+G_m) - G_m(K_f-K_m)V_m}$$

$$+ C\ \frac{K_m \nu_m (2K_f+G_f)\nu_m + K_f(2K_m+G_f)V_f \nu_f}{K_f(2K_m+G_f) + G_f(K_m-K_f)V_f} \qquad (3.25)$$

where

$$K_f = E_f/2(1-\nu_f)\ ,$$

$$K_m = E_m/2(1-\nu_m)\ ;$$

$$G_f = E_f/2(1+\nu_f)\ ;$$

$$G_m = E_m/2(1+\nu_m)\ ;$$

The value of factor C varies linearly between C = 0 (for isolated fibres) and C = 1 (for fibres in contact).

It is interesting to note that the law of mixtures of equation (3.22) for ν_{LT} is in a reasonable agreement with equation (3.25) as will be shown later in this chapter.

Once the longitudinal Poisson's ratio ν_{LT} has been found, the transverse ratio ν_{TL} can be obtained from equation (3.15), provided E_L and E_T are known.

iii) Prediction of Transverse Modulus (E_T):

The mechanical interaction between the fibres and matrix materials becomes more complex when transverse loads are involved. For example, Rosen et al.(3-3,8), consider hollow circular filaments surrounded by matrix materials to represent cylindrical inclusions arranged in either random or hexagonal array. The problem they considered is

3.2.3) contd.

iii) contd.

three dimensional with transverse isotropy for the hexagonal and random arrays. The relationship they derived for the transverse modulus is given as

$$E_T = \frac{4G_T K_T}{K_T + \psi G_T} \tag{3.26}$$

where

$$\psi = 1 + \frac{4K_T \nu_{TL}^2}{E_L}$$

and K_T and G_T are the transverse bulk and shearing modulii respectively given by the following expressions,

$$K_T = \frac{K_m K_f + \bar{K} G_m}{V_m K_f + V_f K_m + G_m} \tag{3.27}$$

where K_m, K_m and G_m can be found from equation (3.25) and

$$\bar{K} = K_f V_f + K_m V_m,$$

and

$$G_T = G_m \frac{(\alpha + \beta_m V_f)(1+\rho V_f^3) - 3V_f V_m^2 \beta_m^2}{(\alpha - V_f)(1+\rho V_f^3) - 3V_f V_m^2 \beta_m^2} \tag{3.28}$$

where

$$\alpha = \frac{\gamma + \beta_m}{\gamma - 1} \quad ; \quad \beta = \frac{1}{3 - 4\nu},$$

$$\rho = \frac{\beta_m - \gamma\beta_f}{1 + \gamma\beta_f} \quad ; \quad \gamma = \frac{G_f}{G_m}$$

Equation (3.26) is rather formidable. For example, the bounds on G_T require the solution of a system of eight simultaneous equations representing the boundary conditions on representative volume elements.

Shaffer (3-10) uses a model consisting of parallel rods of different areas and moduli of elasticity, fixed

3.2.3) contd.

iii) contd.

to rigid end plates in order to simulate the fibres and matix in the composite body. His solution for a hexagonal array packing which is applicable for a fibre volume fraction less than 68% is:-

$$E_T = E_m \left[\frac{1-(1 - \frac{E_m}{E_f})(0.8247 \sqrt{\frac{A_f}{A}} - \frac{A_f}{A})}{1-0.8247 \sqrt{\frac{A_f}{A}} (1 - \frac{E_m}{E_f})} \right] \qquad (3.29)$$

where

$\frac{A_f}{A}$ represents the fibre volume faction V_f.

For V_f above 68 per cent equation (3.29) reduces to the following

$$E_T = \frac{E_m}{1 - \frac{A_f}{A}(1 - \frac{E_m}{E_f})} \qquad (3.30)$$

A simple mechanics of materials approach can be used by assuming that both fibre and matrix are under the same transverse stress σ_T, giving

$$E_T = \frac{E_f E_m}{E_m V_f + E_F V_m} \qquad (3.30a)$$

which is equal to the lower bound of the longitudinal modulus. Equation (3.30a) is not a close approximation for E_T, because under the action of transverse stress it is not likely that the constituent materials will experience either the same transverse stress or the same longitudinal Poisson's effect deformation. The final result is that one of the constituents (most likely the matrix) tries to shorten more than the other

3.2.3) contd.

iii) contd.

in the longitudinal direction and shearing stresses are developed on the interface between the two materials.

Ekvall(3-6), uses, for lamina thicknesses of one-filament diameter and square or rectangular filaments, the simple mechanics of material approach,but attempts to eliminate the unequal longitudinal Poisson's deformation, by applying additional longitüdinal stress such that

$$\sigma_{mL} A_m + \sigma_{fL} A_f = 0$$

This results in a biaxial state of stress, and results in the following value for transverse modulus:-

$$\frac{1}{E_T} = \frac{V_m}{E_m} + \frac{V_f}{E_f} - \frac{V_f}{E_f} \frac{[(E_f \nu_m / E_m) - \nu_f]^2}{[(V_f E_f / V_m E_m) + 1]} \qquad (3.31)$$

Still using the mechanics of materials approach, but modified for stress concentration effects caused by the fibres, Ekvall obtains

$$E_T = E_f \int_0^{\pi/2} \frac{\sin\theta \, d\theta}{(E_f/E_m)(1-\nu_m^2) + R \sin\theta \left[1 - (E_f/E_m)(1-\nu_m^2)\right]} \qquad (3.32)$$

for the transverse modulus of a lamina of thickness one-filament diameter using round filament. In equation (3.32) R is the ratio of filament diameter to filament spacing given by

$$R = \frac{4F_f}{\pi(V_f + V_m)} = \frac{4V_f}{\pi} = \frac{4(1-V_m)}{\pi}$$

For glass roving or strands Ekvall(3-7) derives

$$E_T = \frac{E_f E_m'}{V_f E_m' + V_m E_f (1-\nu_m^2)} \qquad (3.33)$$

to allow for the triaxial effect mentioned in sub-section (i)

3.2.3) contd.

iii) contd.

in the prediction of the longitudinal modulus. E'_m is defined by equation (3.21).

Again using a similar technique, together with the contiguity factor interpolation scheme, Tsai(3-2) derives the relationship

$$E_T = 2\left[1-\nu_f+(\nu_f-\nu_m)V_m\right]\left[(1-C)\frac{K_f(2k_m+G_m)-G_m(K_f-K_m)V_m}{(2K_m+G_m)+2(K_m-K_f)V_m}\right.$$

$$\left. + C\,\frac{K_f(2K_m+G_f)+G_f(K_m-K_f)V_m}{(2K_m+G_f)-2(K_m-K_f)V_m}\right] \qquad (3.34)$$

where the various terms are defined in equation (3.25).

iv) Prediction of Longitudinal Shear Modulus (G_{LT}):

Using the mechanics of materials approach and assuming equal shearing stresses on the constituent materials Ekvall(3-6) derives,

$$G_{LT} = \frac{G_f G_m}{V_m G_f + V_f G_m} \qquad (3.35)$$

for a lamina of one filament thickness with square or rectangular cross-section.

For the same thickness but with circular section filaments he derives,

$$G_{LT} = \frac{G_f G_m}{R\phi G_m + (1-R)G_f} \qquad (3.36)$$

where R is defined in (3.32), and ϕ is a material parameter given by

3.2.3) contd.

iv) contd.

$$\phi = \int_0^{\pi/2} \frac{\sin\theta \, d\theta}{(G_m/G_f)+\sin\theta\left[1-(G_m/G_f)\right]}$$

Equation (3.36) is also Ekvall's expression for the shearing modulus of a lamina with glass roving or strands(3-7).

Rosen et al.(3-3,8) use the variation method to obtain two bounds of G_{LT}.

$$G_{LT} \text{ (upper bound)} = G_m(m_G V_1 + V_2)$$
$$G_{LT} \text{ (lower bound)} = \frac{G_m}{V_1/m_G + V_2} \qquad (3.37)$$

for an hexagonal array of solid filaments. V_1 and V_2, the fractional volume of the composite cylinders forming the hexagonal pattern and the remaining fractional volume respectively, are given by:-

$$V_1 = \frac{\pi}{2\sqrt{3}}$$

$$V_2 = 1-V_1$$

and

$$M_G = \frac{\eta(1+\beta^2)+(1-\beta^2)}{\eta(1-\beta^2)+(1-\beta^2)}$$

where

$$\eta = \frac{G_f}{G_m}$$

and

$$\beta = \frac{V_f}{V_1}$$

If the filaments are randomly distributed the bounds will coincide and be given by:-

3.2.3) contd.

iv) contd.

$$G_{LT} = G_m \frac{\eta(1+V_f) + V_m}{\eta(V_m) + 1 + V_f} \tag{3.38}$$

While Whitney(3-9) predicts the shear modulus by the following expression

$$G_{LT} = \frac{[(G_f+G_m)+(G_f-G_m)V_f]G_f}{[(G_f+G_m)-(G_f-G_m)V_f]} \tag{3.39}$$

Finally, Tsai(3-2) gives the expression,

$$G_{LT} = (1-C)G_m \frac{2G_f-(G_f-G_m)V_m}{2G_m+(G_f-G_m)V_m} + C\,G_f \frac{(G_f+G_m)-(G_f-G_m)V_m}{(G_f+G_m)+(G_f-G_m)V_m} \tag{3.40}$$

for the shearing modulus, where the value of C is defined in equation (3.25).

v) Selection of the Appropriate Theory:

The foregoing theories all suffer the objection that the mathematical models on which they are based do not very accurately relate to the observed experimental behaviour. Possible causes of the disagreement include,

a) Laminated composites are generally fabricated at elevated temperatures which generate a residual thermal strain in the resin that probably affects the overall properties.

b) The filament spacing along the composite length is non-uniform and this together with the presence of vaids tends to cause discrepancies with theory.

c) While the experimental data normally give the surface properties, a typical laminated composite specimen may be non-uniform through its thickness.

3.2.3) contd.

v) contd.

d) The behaviour of the bulk resin is probably different from that of the resin within the lamina.

To account for the above mentioned effects, particularly for transverse and shear loading, Tsai(3-2) has suggested, utilizing contiguity and misalignment factors which are derived from extensive experimental data. In addition, his model assumes a random fibre packing which is very near to the real fibre arrangement in a composite, while other investigators assume either hexagonal or square array packing which need special and difficult techniques for fabrication.

Tsai recognises that at high fibre content fibres will be contiguous (touching), and not necessarily separated by matrix as assumed by other investigators. So (Tsai) incorporates a filament contiguity factor in his theoretical works especially in the prediction of the transverse and shear moduli.

The problem of filament contiguity can be resolved by taking two extreme cases

a) All filaments are isolated (C = 0).

b) All filaments are contiguous (C = 1).

The actual packing of the filament is represented by a linear combination of the two extreme cases.

After assessing the merits of the various theoretical models described above and their correlation with experimental results, it was decided to use the equations given below to predict the properties of the laminates used in this investigation. These laminates were manufactured from unidirectional layers using a cold curing pressure mould with variable fibre volume fraction.

3.2.3) contd.

a) E_L, will be predicted by equation (3.19) (Low of mixture)

b) ν_{LT}, will be predicted by both equation (3.22) (Low of mixture) and equation (3.25) (Tsai approach).

c) E_T, will be predicted by equation (3.34) (Tsai approach)

d) G_{LT}, will be predicted by equation (3.40) (Tsai approach)

e) ν_{TL} will be predicted by equation (3.15).

3.2.4) Stress-Strain Relationship For a Unidirectional Layer Referred to Arbitrary Axes:

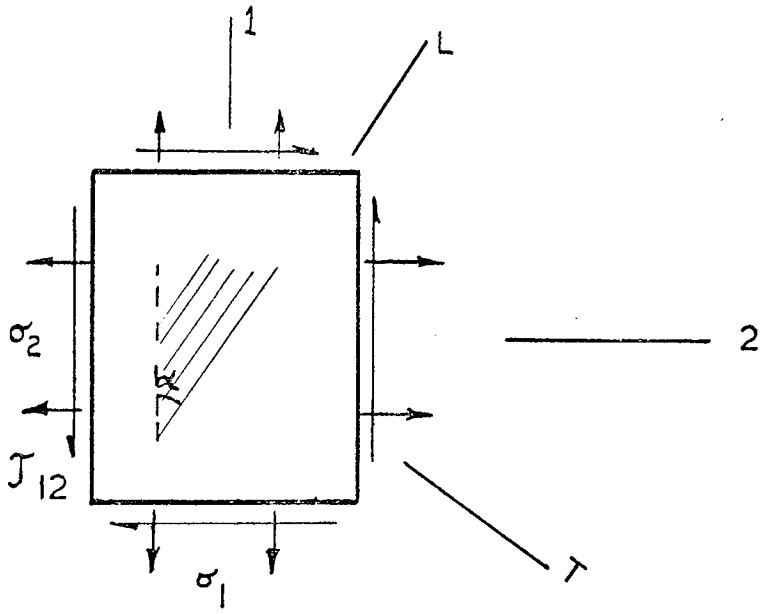

FIGURE (3.4)

Consider a unidirectional layer subjected to in plane stresses σ_1 and σ_2 acting at α and $(90-\alpha)$ respectively to the principal material direction L, as shown in Fig.(3.4). The properties in the 1-2 directions in terms of those in the L-T directions can be determined by transformation of stresses and strains. These quantities transform according to the second order tensor transformation,

$$T_{ij} = a_{ik}\, a_{j\ell}\, T_{k\ell} \qquad (3.41)$$

for the two dimensional case shown in Fig.(3.4) the table of pertinent direction cosines is

3.2.4) contd.

	1	2
L	$a_{11} = \cos\alpha$	$a_{12} = \sin\alpha$
T	$a_{21} = -\sin\alpha$	$a_{22} = \cos\alpha$

TABLE (3.2)

Then the stresses on 1-2 axes can be transformed to the principle L-T axes by

$$\begin{bmatrix} \sigma_L \\ \sigma_T \\ \tau_{LT} \end{bmatrix} = [T] \begin{bmatrix} \sigma_1 \\ \sigma_2 \\ \tau_{12} \end{bmatrix} \qquad (3.42)$$

and the strains by

$$\begin{bmatrix} \varepsilon_L \\ \varepsilon_T \\ \frac{1}{2}\gamma_{LT} \end{bmatrix} = [T] \begin{bmatrix} \varepsilon_1 \\ \varepsilon_2 \\ \frac{1}{2}\gamma_{12} \end{bmatrix} \qquad (3.43)$$

where

$$T = \begin{bmatrix} \cos^2\alpha & \sin^2\alpha & 2\sin\alpha\cos\alpha \\ \sin^2\alpha & \cos^2\alpha & -2\sin\alpha\cos\alpha \\ -\sin\alpha\cos\alpha & \sin\alpha\cos\alpha & \cos^2\alpha - \sin^2\alpha \end{bmatrix} \qquad (3.44)$$

The angle α is positive in the case where the load axes 1-2 are rotated clockwise with respect to the principal axes L-T, as shown in Fig.(3.4).

When tensorial rather than engineering strain elements are used, equation (3.6) can be written,

$$\begin{bmatrix} \sigma_L \\ \sigma_T \\ \tau_{LT} \end{bmatrix} = \begin{bmatrix} C_{11} & C_{12} & 0 \\ C_{12} & C_{22} & 0 \\ 0 & 0 & 2C_{66} \end{bmatrix} \begin{bmatrix} \varepsilon_L \\ \varepsilon_T \\ \frac{1}{2}\gamma_{LT} \end{bmatrix} \qquad (3.45)$$

The unknown transformed stiffness matrix $[\bar{C}]$ for the same tensorial form is given by

$$\begin{bmatrix} \sigma_1 \\ \sigma_2 \\ \tau_{12} \end{bmatrix} = \begin{bmatrix} \bar{C}_{11} & \bar{C}_{12} & 2\bar{C}_{16} \\ \bar{C}_{12} & \bar{C}_{22} & 2\bar{C}_{26} \\ \bar{C}_{16} & \bar{C}_{26} & 2\bar{C}_{66} \end{bmatrix} \begin{bmatrix} \varepsilon_1 \\ \varepsilon_2 \\ \frac{1}{2}\gamma_{12} \end{bmatrix} \qquad (3.46)$$

3.2.4) contd.

substituting equations (3.42) and (3.43) in equation (3.45) yields,

$$[T]\begin{bmatrix}\sigma_1\\ \sigma_2\\ \tau_{12}\end{bmatrix} = [C][T]\begin{bmatrix}\varepsilon_1\\ \varepsilon_2\\ \frac{1}{2}\gamma_{12}\end{bmatrix}$$

or

$$\begin{bmatrix}\sigma_1\\ \sigma_2\\ \tau_{12}\end{bmatrix} = [T]^{-1}[C][T]\begin{bmatrix}\varepsilon_1\\ \varepsilon_2\\ \frac{1}{2}\gamma_{12}\end{bmatrix} \qquad (3.47)$$

A comparison of equation (3.46) and (3.47) shows that

$$[\bar{C}] = [T]^{-1}[C][T] \qquad (3.48)$$

Performing the above matrix multiplication yields the following,

$$\begin{aligned}
\bar{C}_{11} &= C_{11}\cos^4\alpha + 2(C_{12}+2C_{66})\sin^2\cos^2\alpha + C_{22}\sin^4\alpha\\
\bar{C}_{12} &= (C_{11}+C_{22}-4C_{66})\sin^2\cos^2\alpha + C_{12}(\sin^4\alpha+\cos^4\alpha)\\
\bar{C}_{16} &= (C_{11}-C_{12}-2C_{66})\sin\alpha\cos^2\alpha + (C_{12}-C_{22}+2C_{66})\sin^3\alpha\cos\alpha\\
\bar{C}_{22} &= C_{11}\sin^4\alpha+2(C_{12}+2C_{66})\sin^2\alpha\cos^2\alpha + C_{22}\cos^4\alpha\\
\bar{C}_{26} &= (C_{11}-C_{12}-2C_{66})\sin^3\alpha\cos\alpha + (C_{12}-C_{22}+2C_{66})\sin\alpha\cos^3\alpha\\
\bar{C}_{66} &= (C_{11}+C_{22}-2C_{12}-2C_{66})\sin^2\alpha\cos^2\alpha+C_{66}(\sin^4\alpha+\cos^4\alpha)
\end{aligned} \qquad (3.49)$$

Thus the stress-strain relationship for a unidirectional layer referred to arbitrary axes 1-2 is given by equation (3.46), where the stiffness elements are defined by equations (3.48) or (3.49). Values of C_{ij} are given by equation (3.16).

The transformed stress and strain equations could be obtained by expanding the inverse of equations (3.42) and (3.43) to obtain the values,

3.2.4) contd.

$$\sigma_1 = \sigma_L \cos^2\alpha + \sigma_T \sin^2\alpha - 2\tau_{LT} \sin\alpha \cos\alpha$$

$$\sigma_2 = \sigma_L \sin^2\alpha + \sigma_T \cos^2\alpha + 2\tau_{LT} \sin\alpha \cos\alpha \qquad (3.50)$$

$$\tau_{12} = \sigma_L \sin\alpha\cos\alpha - \sigma_T \sin\alpha\cos\alpha + \tau_{LT}(\cos^2\alpha - \sin^2\alpha)$$

for transformed stresses, and

$$\varepsilon_1 = \varepsilon_L \cos^2\alpha + \varepsilon_T \sin^2\alpha - \gamma_{LT} \sin\alpha\cos\alpha$$

$$\varepsilon_2 = \varepsilon_L \sin^2\alpha + \varepsilon_T \cos^2\alpha + \gamma_{LT} \sin\alpha\cos\alpha \qquad (3.51)$$

$$\gamma_{12} = 2\varepsilon_L \sin\alpha\cos\alpha + 2\varepsilon_T \sin\alpha\cos\alpha + \gamma_{LT}(\cos^2\alpha - \sin^2\alpha)$$

for transformed strains. The transformed stress-strain relationship can be expressed by the following. (See ref. 3-1):-

$$\sigma_1 = \bar{C}_{11}\,\varepsilon_1 + \bar{C}_{12}\,\varepsilon_2 + \bar{C}_{16}\,\gamma_{12}$$

$$\sigma_2 = \bar{C}_{12}\,\varepsilon_1 + \bar{C}_{22}\,\varepsilon_2 + \bar{C}_{26}\,\gamma_{12} \qquad (3.52)$$

$$\tau_{12} = \bar{C}_{16}\,\varepsilon_1 + \bar{C}_{26}\,\varepsilon_2 + \bar{C}_{66}\,\gamma_{12}$$

In these expressions

$$\bar{C}_{11} = \frac{1}{\Delta}\left(\frac{1}{E_2} - \lambda_2^2 G_{12}\right)$$

$$\bar{C}_{12} = \frac{1}{\Delta}\left(\frac{\nu_{12}}{E_1} + \lambda_1\lambda_2 G_{12}\right)$$

$$\bar{C}_{16} = \frac{G_{12}}{\Delta}\left[\left(\frac{\nu_{12}}{E_2} + \lambda_1\lambda_2 G_{12}\right)\lambda_2 + \left(\frac{1}{E_2} - \lambda_2^2 G_{12}\right)\lambda_1\right]$$

$$\bar{C}_{22} = \frac{1}{\Delta}\left(\frac{1}{E_1} - \lambda_1^2 G_{12}\right)$$

$$\bar{C}_{26} = \frac{G_{12}}{\Delta}\left[\left(\frac{1}{E_1} - \lambda_1^2 G_{12}\right)\lambda_2 + \left(\frac{\nu_{12}}{E_1} + \lambda_1\lambda_2 G_{12}\right)\lambda_1\right]$$

$$\bar{C}_{66} = \frac{G_{12}}{\Delta}\left(\frac{1-\nu_{12}\nu_{21}}{E_1 E_2}\right)$$

where

$$\Delta = \left(\frac{1}{E_1} - \lambda_1^2 G_{12}\right)\left(\frac{1}{E_2} - \lambda_2^2 G_{12}\right) - \left(\frac{\nu_{12}}{E_1} + \lambda_1\lambda_2 G_{12}\right)^2$$

These properties are related to those along the principal axes by the following.

3.2.4) contd.

$$\frac{1}{E_1} = \frac{\cos^4\alpha}{E_L} + \left(\frac{1}{G_{LT}} - \frac{2\nu_{LT}}{E_L}\right)\sin^2\alpha\cos^2\alpha + \frac{\sin^4\alpha}{E_T}$$

$$\frac{1}{E_2} = \frac{\sin^4\alpha}{E_L} + \left(\frac{1}{G_{LT}} - \frac{2\nu_{LT}}{E_L}\right)\sin^2\alpha\cos^2\alpha + \frac{\cos^4\alpha}{E_T}$$

$$\frac{1}{G_{12}} = \frac{\cos^2 2\alpha}{G_{LT}} + \left(\frac{1+\nu_{LT}}{E_L} + \frac{1+\nu_{TL}}{E_T}\right)\sin^2 2\alpha \qquad (3.53)$$

$$\frac{\nu_{12}}{E_1} = \frac{\nu_{21}}{E_2} = \frac{\nu_{LT}}{E_L} - \frac{1}{4}\left(\frac{1+\nu_{LT}}{E_L} + \frac{1+\nu_{TL}}{E_T} - \frac{1}{G_{LT}}\right)\sin^2 2\alpha$$

$$\lambda_1 = -\left[\frac{\sin^2\alpha}{E_T} - \frac{\cos^2\alpha}{E_L} + \frac{1}{2}\left(\frac{1}{G_{LT}} - 2\frac{\nu_{LT}}{E_L}\right)\cos 2\alpha\right]\sin 2\alpha$$

$$\lambda_2 = -\left[\frac{\cos^2\alpha}{E_T} - \frac{\sin^2\alpha}{E_L} - \frac{1}{2}\left(\frac{1}{G_{LT}} - 2\frac{\nu_{LT}}{E_L}\right)\cos 2\alpha\right]\sin 2\alpha$$

3.3) Strength.

It is necessary to know the strength properties of the unidirectional monolayer, in order to understand its effect on the strength characteristics of the multidirectionally oriented laminated composite. The applications of any of the available failure criteria for the multidirectionally oriented composite subjected to a general state of stress requires the principal stress (or strain) levels of the monolayer to be known.

Since the unidirectional layer is a composition of parallel glass fibres imbedded in a resin matrix, the matrix has an important effect on the strength of the composite. In addition, the elastic properties of the resin matrix are different in tension and compression and the fructure mode of the fibre-resin system is different in tension and compression, therefore, the monolayer itself will exhibit different principal strengths in tension and compression. These principal strengths are the longitudinal and transverse tension and compression, and the longitudinal shear.

Unlike the elastic properties, principal strengths cannot

3.3) contd.

be accurately predicted from theoretical models, with the possible exception of the longitudinal tensile strength which can be predicted within limits acceptable for normal design purposes. The rest can only be predicted by semi-empirical nal expressions. The material parameters which affect the five principle strengths of a unidirectional monolayer are:-

a) Fibre strength characteristics.

b) Fibre modulus.

c) Matrix stress-strain characteristics under direct and shear loading.

d) Fibre and void volume fraction.

The manner in which the principal strengths vary with these parameters will be presented later.

3.3.1) Theories of Material Design.

In order to design a material of the nature of anisotropic G.R.P. it is necessary to know how the elastic and strength properties are affected by variations in the amount and arrangement of the constituent materials.

Two methods often used by analyzing the material properties of GRP composites are:-

(i) Netting Analysis:

This method of analysis assumes that the resin matrix has no load carrying ability and serves only to hold the reinforcing fibres in position, it assumes that only the fibres bear load.

In practice, this method of analysis is inaccurate and even the adjustment of empirical factors does not lead to satisfactory results. The main objection to this method is that strength evaluation can only be achieved in the

3.3.1) contd.

(i) contd.

direction of the fibres and not in any other direction. Bishop(3-11) modifies this method to extend its ability to predict the directional properties of fibre reinforced composite. A detailed explanation of his theory can be found in ref.(3-11) and the final mathematical model is also presented in the same reference.

(ii) Continuum Analysis:

This method of analysis assumes the resin matrix influences the mechanical properties of the composite, by considering that the stiffness and strength of the resin matrix has a significant effect on the overall properties of the composite. The characterization of GRP composites will be achieved by the aid of this theory throughout this thesis.

3.3.2) Strength of Unidirectional Monolayer.

(i) Tensile Strength: (Longitudinal).

Since the strength of continuous fibre composites depend on the failure stress and strain of all the fibres making up the composite, the determination of strength must consider possible statistical effects. Such an expression, developed by Rosen(3-12), for the prediction of longitudinal tensile strength of a unidirectional monolayer is

$$F_{L(t)} = V_f(\alpha\beta\delta e)^{-1/\beta} \qquad (3.54)$$

where V_f is the fibre volume fraction, α and β are constants defining the "Link strength" of the filaments, δ is the ineffective fibre length, and e the base of natural logarithms.

Rosen's analysis characterizes the tensile strength

3.3.2) contd.

(i) contd.

of the monolayer in terms of the statistical strength characteristics in the resin matrix around the broken ends of fibres and is based on the fact that the strength of bare fibres varies inversely with their length because of the random existance of flows on the surface of the filaments.

Statistical effects are not, however, too significant in well aligned G.R.P. composits and the rule of mixture is sufficiently accurate for most purposes. The value for longitudinal strength given by the rule of mixture (ref.3-13) is:-

$$F_{L(t)} = \sigma_f V_f + \sigma'_m(1-V_f) \qquad (3.55)$$

where σ_f is the fibre breaking strength, σ'_m is the stress carried by the matrix when the composite is stressed to its ultimate tensile stress.

Equation (3.55) is not valid at small fibre strains, or where there are substantial differences in the Poisson's ratio of the constituents.

(ii) Compressive Strength: (Longitudinal).

Many researchers have demonstrated the high compressive strength that can be achieved by unidirectional fibre composites under uniaxial loading (see ref.3-14). It is suggested thatthe mode of failure is a micro-buckling of the fibres in a fashion analogous to the buckling of a column on an elastic foundation.

Analysis of this instability mode are shown in refs.(3-14) and (3-15). The analysis assumes a layered two dimensional medium in which the fibres are considered to

3.3.2) contd.

(ii) contd.

buckle in a sinusoidal pattern. When the adjacent fibres buckle 180° out of phase, the overall strain of the matrix is EXTENTIONAL STRAIN, but when they buckle in phase, the major strain of the matrix is SHEAR STRAIN. These two modes are denoted as the extensional and shear modes respectively. See Fig.(3.5).

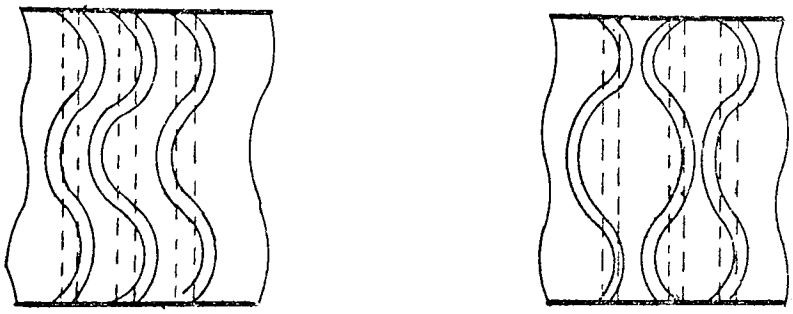

(A) Shear Mode (B) Extensional Mode

FIGURE (3.5)

The compressive strength expression for the shear mode is given by the following

$$F_{L(c)} = \frac{G_m}{1 - V_f} \tag{3.56}$$

and the associated strain is given by

$$\varepsilon_{(cr)} = \frac{1}{V_f(1-V_f)} \left(\frac{G_m}{E_f}\right) \tag{3.57}$$

The expression for the extensional mode is:-

$$F_{L(c)} = V_f \left[\frac{2E_f E_m V_f}{3(1 - V_f)}\right]^{\frac{1}{2}} \tag{3.58}$$

and the critical strain of the composite

3.3.2) contd.

(ii) contd.

$$\varepsilon_{(cr)} = \left[\frac{2V_f}{3(1-V_f)}\right]^{\frac{1}{2}} \left(\frac{E_m}{E_f}\right)^{\frac{1}{2}} \qquad (3.59)$$

Fig.(3.6) shows a graphical representation of equations(3.56) and (3.58) for GRP as a function of fibre volume fraction. The figure shows that the extensional mode only governs the behaviour of a composite for small fibre volume fractions not exceeding 20%.

The failure strains defined by equations (3.57), (3.59) are plotted in Fig.(3.7) which shows that for many composites the calculated failure strain levels exceed the proportional limit strain of the matrix. For strains in excess of the proportional limit, the matrix may be treated as an elastic-perfectly-plastic material and the secant modulus used to define the matrix stiffness. For the more dominant shear mode, the following expression can be used in the plastic range to replace the elastic equation (3.56)

$$F_{L(c)} = \left[\frac{V_f E_f \sigma_y}{3(1-V_f)}\right]^{\frac{1}{2}} \qquad (3.60)$$

where σ_y is the matrix yield stress level. A plot of equation (3.60) is shown in Fig.3.6 labelled "inelastic".

Boit(3-16) treats the internal instability of a layered medium with the following result:-

$$F_{L(c)} = \frac{G_m}{(1-V_f)} \left[\frac{1+n\frac{V_m}{V_f}}{1+n^2+\frac{n(V_m-V_f)^2}{2V_m V_f}}\right]^{\frac{1}{2}} \qquad (3.61)$$

where $n = \frac{G_m}{G_f}$

when the fibre/matrix modulus ratio is large n approaches

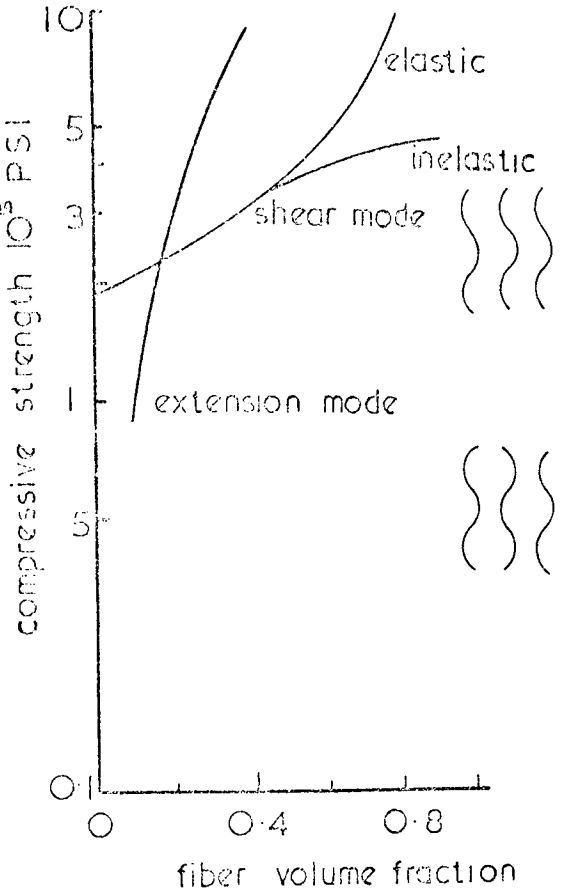

Fig. 3.6

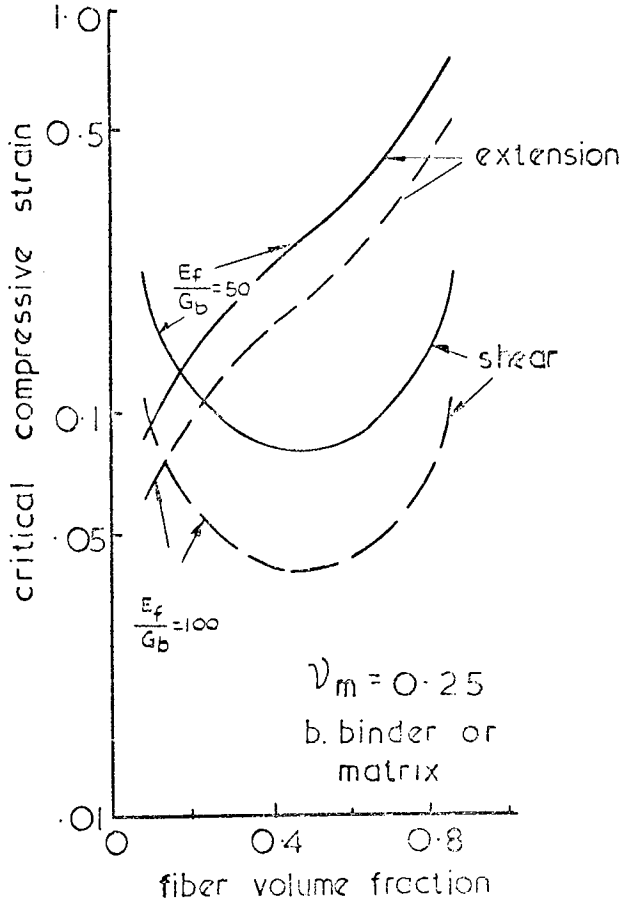

Fig. 3.7.

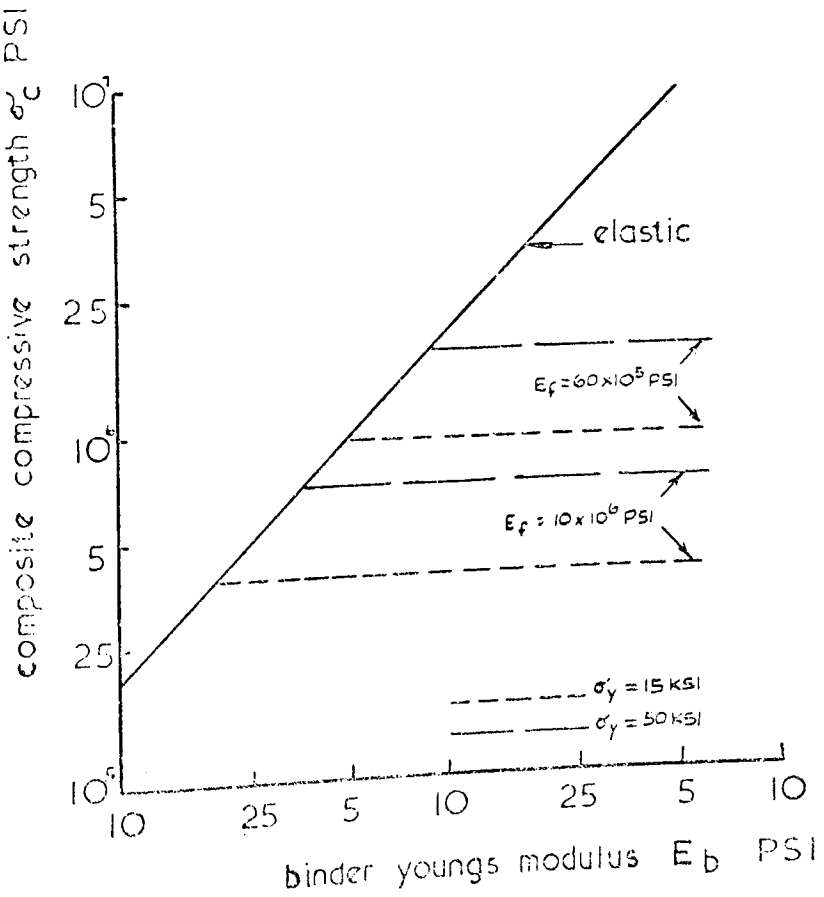

Fig 3.8

(ii) contd.

zero and equation (3.61) reduces to equation (3.56).

The results of these studies, including the elastic-plastic matrix, is summarized in Fig.(3.8), which shows a plot of the compressive strength of the composite (at a constant fibre volume fraction) as a function of the matrix elastic modulus. In the elastic range, the dominant parameter is matrix elastic modulus, but for the inelastic range, there are strength cut-offs which depend on both fibre modulus and matrix strength. For example, the compressive strength of a GRP composite cannot be improved by increasing the matrix modulus unless the matrix strength is increased. For higher modulus fibres such as boron or carbon fibures in an epoxy matrix, improvement in composite strength cannot be achieved by increasing matrix strength until the matrix stiffness is also increased.

The details presented in Fig.(3.8) show that the nature of changes made in the matrix properties to improve the compressive strength of the composite of a certain type of fibre depends upon the base of reference. In some cases performance is limited by a matrix yield stress at a given fibre modulus, whereas for other cases a gain in compressive strength could be achieved by improving the matrix modulus. This approach could be used as a guide for reasonable changes in matrix properties to yield improved composite strength.

The prediction of longitudinal compressive strength has always greatly exceeded the observed experimental results. This may be due to the following reasons presented in ref.(3-17).

a) Imperfect unidirectional arrangement in the basic monolayer, which leads to lateral eccentricities in the fibres.

3.3.2) contd.

(ii) contd.

b) Lateral displacement of fibres along their lengths due to the movement of matrix during curing, and the direct effect of the laminating cure pressure.

c) Periodic lateral deformation in the filaments caused by thermal residual stresses generated by cool-down from the laminating temperature level.

d) The presence of voids in the matrix phase which decrease the matrix shear stiffness and lowers the effective filament-to-matrix bond strength.

Experimentally compressive strengths are from 50%-25% of theoretically predicted values, and observed failure mode are due to fibre instability and/or crack extension failure (see ref.3-18).

(iii) Transverse Tension And Compressive Strengths:

Prediction of these two strengths is complicated because they are sensitive to inclusions of voids and foreign matter leading to complex failure modes. To date there is no exact analytical model that can be trusted to predict these strength although Dow & Rose(3-19) and Shu & Rosen(3-20) have studied this problem using plastic limit analysis of plasticity in order to predict upper and lower bounds of strength. Unfortunately the gap between these two bounds is too wide to lead to results of practical use.

Hashin(3-21) has concluded from his experimental observations that the strength properties of the matrix are a dominant parameter in assessing the transverse strength of the unidirectional layer. He also concluded that the transverse strength of fibre reinforced material with stiff

3.3.2) contd.

(iii) . contd.

fibres is of the order of magnitude of matrix strength. A similar approach has been used by Dimnock & Abrahams(3-22) and (3-23).

(iv) Interlaminar Strength:

Interlaminar failure is a phenomenon peculiar to reinforced platics. This occurs because the fibre-resin adhesion and matrix shear strength in such material are usually much lower than in metallic composite.

The interlaminar planes that exist in fibre-reinforced plastics between laminations of mats or layers of filament wound tape or roving are in fact weak planes in the material. Failure of fibre reinforced plates or beams subjected to flexural load often occurs by interlaminar shear failure due to high interlaminar stresses created at the beam neutral axis. In fact, beams with low span/depth ratios are often used as a test method to determine the interlaminar shear strength, since the shear stresses at the neutral axis exceed the interlaminar shear strength before the outer fibre stresses exceed the tensile or compressive strength of the material.

Interlaminar planes are essentially resin-rich boundaries between laminates and are often subjected to the accumulation of voids that have serious effects on the interlaminar strength.

The interlaminar shear strength is influenced mainly by the resin matrix strength, the matrix-fibre interface strength, and any voids that may be present in the interlaminar areas.

The interlaminar shear strength is considered to be

3.3.2) contd.

(iv) contd.

the most critical parameter in fibre reinforced composites, as it is often a mode of failure for plates or beams subjected to flexural loading and also appears to be a common mode of failure in axial compression. Because of this the topic of interlaminar shear has received considerable attention from researchers.

Interlaminar shear strength is difficult to determine accurately and there is much disagreement as to the best means of measurement. It is often measured by a short beam- three point bending test, because of the ease and cheapness of this test method. But a suitable span/depth ratio of the specimen should be chosen to achieve a pure shear failure as will be discussed in detail later in this chapter.

(v) Flexural Strength:

The flexural strength of unidirectional laminates always exceed the compressive strength of the material and normally has a value approaching the tensile strength. The reason why flexural strength exceeds the uniaxial compressive strength, is given by a theory that has been applied to wood, which shows similar behaviour. The stress gradient in bending compression allows only a few extreme fibres to be stressed highly, whilst the inner, lowly stressed fibres, restrain the highly stressed outer fibres from the premature and massive buckling that occur in direct compression. Thus the flexural stresses can increase to a value approaching the tensile strength before flexural failure occurs.

In measuring flexural strength, rectangular beam specimens are normally tested under three point loading

3.3.2) contd.

(v) contd.

and the strength calculated from the simple bending theory.

Because of the general planar anisotropy, longitudinal deflection will be accompanied by transverse deflection and warping of the beam, which become critical if the width/depth ratio is high. In addition, the loading system will introduce torques, secondary bending moment and shear forces, which interact with the primary bending moment. As a result, the simple bending theory may not give the flexural strength very precisely. To achieve better agreement with theory the beam should be symmetric with respect to the vertical longitudinal middle plane.

Hashin(3-24) concludes that the equation of isotropic beam theory can be adopted when the material is orthotropic through the thickness and is reasonably accurate for the general anisotropic case provided the span/depth ratio for a three point loaded beam is greater than 20. Even for the orthotropic case it is better to maintain the span/depth ratio above this limit to compensate for any local anistropic effect.

In conclusion it may be stated that the actual mode of failure depends on the relative magnitude of tensile, compressive and interlaminar shear strengths, width/depth ratio, span/depth ratio, and loading condition.

Further discussion on the effect of material anisotropy can be found later in this chapter.

3.3.3) Theories of Failure:

In spite of considerable research effort in the field of fibre reinforced composites, a completely satisfactory

3.3.3) contd.

theory of failure is still lacking, since the factors that control fracture at the micro-mechanical level are very complex.

A number of failure criteria have been suggested which can be conveniently divided into two groups ref.(3-25). Those in the first group are based on extensions of isotropic theories and require only the use of two or three principle strengths and the interlaminar shear strength. Those in the second group require additional data from the results of complex strength tests. A statement of these failure criteria is given below:-

GROUP ONE:

Maximum Stress (Stowell & Lu);

$$\sigma_L = F_L \; ; \; \sigma_T = F_T \; ; \; \tau_{LT} = S \qquad (3.62)$$

Maximum Strain

$$\sigma_L = F_L + \nu_{LT}\sigma_T \; ; \; \sigma_T = F_T + \nu_{LT}(E_T/E_L)\sigma_L$$

$$\tau_{LT} = S \qquad (3.63)$$

Hill

$$\left[\frac{\sigma_L}{F_L}\right]^2 - \left[\frac{1}{F_L^2} + \frac{1}{F_T^2} - \frac{1}{S^2}\right]\sigma_L\sigma_T + \left[\frac{\sigma_T}{F_T}\right]^2 + \left[\frac{\tau_{LT}}{S}\right]^2 = 1 \qquad (3.64)$$

Norris interaction

$$\left[\frac{\sigma_L}{F_L}\right]^2 + \left[\frac{\sigma_T}{F_T}\right]^2 + \left[\frac{\tau_{LT}}{S}\right]^2 = 1 \qquad (3.65)$$

Azzi and Tsai

$$\left[\frac{\sigma_L}{F_L}\right]^2 - \frac{\sigma_L\sigma_T}{F_L^2} + \left[\frac{\sigma_T}{F_T}\right]^2 + \left[\frac{\tau_{LT}}{S}\right]^2 = 1 \qquad (3.66)$$

3.3.3) contd.

Norris failure

$$\left[\frac{\sigma_L}{F_L}\right]^2 - \frac{\sigma_L\sigma_T}{F_L F_T} + \left[\frac{\sigma_T}{F_T}\right]^2 + \left[\frac{\tau_{LT}}{S}\right]^2 = 1 \; ;$$

$$\left[\frac{\sigma_L}{F_L}\right]^2 = 1 \quad ; \quad \left[\frac{\sigma_T}{F_T}\right]^2 = 1 \tag{3.67}$$

GROUP TWO:

Hoffman

$$\frac{\sigma_L^2 - \sigma_L\sigma_T}{F_{L(c)}F_{L(t)}} + \frac{\sigma_T^2}{F_{T(c)}F_{T(t)}} + \left[\frac{F_{L(c)} - F_{L(t)}}{F_{L(c)}\,F_{L(t)}}\right]\sigma_L + \left[\frac{F_{T(c)} - F_{T(t)}}{F_{T(c)}\,F_{T(t)}}\right]\sigma_T + \left[\frac{\tau_{LT}}{S}\right]^2 = 1 \tag{3.68}$$

Modified Marin (Franklin).

$$\frac{\sigma_L - K_2\sigma_L\sigma_T}{F_{L(c)}F_{L(t)}} + \frac{\sigma_T^2}{F_{T(c)}F_{T(t)}} + \left[\frac{F_{L(c)} - F_{L(t)}}{F_{L(c)}\,F_{L(t)}}\right]\sigma_L + \left[\frac{F_{T(c)} - F_{T(t)}}{F_{T(c)}\,F_{T(t)}}\right]\sigma_T + \left[\frac{\tau_{LT}}{S}\right]^2 = 1 \tag{3.69}$$

Gol'denblat and Kopnov.

$$\frac{1}{2}\left[\frac{1}{F_{L(t)}} - \frac{1}{F_{L(c)}}\right]\sigma_L + \frac{1}{2}\left[\frac{1}{F_{T(t)}} - \frac{1}{F_{T(c)}}\right]\sigma_T + \left\{\frac{1}{4}\left[\frac{1}{F_{L(t)}} + \frac{1}{F_{L(c)}}\right]^2\sigma_L^2 + \frac{1}{4}\left[\frac{1}{F_{T(t)}} + \frac{1}{F_{T(c)}}\right]^2\sigma_T^2 + 2H_{12}\sigma_L\sigma_T + \left[\frac{\tau_{LT}}{S}\right]^2\right\}^{\frac{1}{2}} \tag{3.70}$$

3.3.3) contd.

Tsai and Wu

$$\left[\frac{1}{F_{L(t)}} - \frac{1}{F_{L(c)}}\right]\sigma_L + \left[\frac{1}{F_{T(t)}} - \frac{1}{F_{T(c)}}\right]\sigma_T + \frac{\sigma_L^2}{F_{L(t)}F_{L(c)}} + \frac{\sigma_T^2}{F_{T(t)}F_{T(c)}} + 2H_{12}\sigma_L\sigma_T + \left[\frac{\tau_{LT}}{S}\right]^2 = 1 \quad (3.71)$$

where K_2 and H_{12} are constants in failure theories.

The maximum stress theory is recommended for filamentary composites and has been applied to metallic composites ref.(3-26).

The maximum strain theory has been applied to beron-epoxy and boron-glass-epoxy composites.

The distortional-energy criterion was first applied by Norris(3-27) and then developed by Tsai(3-28).

Hoffman(3-29), extended Tsai's analysis taking into account the differing strengths in tension and compression (Bauschinger effect).

Ashkenazi(3-30) developed an "interaction formula" but does not consider the s trength in pure shear as a basic material property and applies his results to materials such as plywood. Marin(3-31) also developed a failure criteria for anisotropic materials but it is a special case of Hill's theory written in terms of the principal stresses. The main difference is that, while Hill employed the yield stress in shear with respect to the principal axes of anisotropy, Marin used the yield stress in shear measured with a material element oriented at 45 degrees to the principal axes of anisotropy. Marin also adopted the transformation properties to the theory to permit a generalization of the analysis for a material subjected to combined stresses at any orientation.

3.3.3) contd.

Tsai and Wu(3-32) have developed their failure criterion for application to anisotropic materials, taking account of the difference in strength for positive and negative stresses, different material symmetries, multi-dimensional space, and multi-axial stresses.

For GRP application, the modified plane stress distortional energy criterion by Tsai (equation 3.66) is generally accepted as the best failure criterion, ref.(3.33). This criterion remains applicable when the material properties are different in tension and compression provided that the allowable stresses F_L and F_T are modified according to the sign of σ_L and σ_T. The four possibilities are given in Table (3.3).

Stress Quadrant	σ_L	σ_T	F_L	F_T
1	+	+	Tension	Tension
2	-	+	Compression	Tension
3	-	-	Compression	Compression
4	+	-	Tension	Compression

TABLE (3.3)

This theory is applicable to laminated as well as unidirectional fibrous composites, employing simple material properties derived from unidirectional specimens alone. This permits the theory to be applied to any combination of uni-directional layers. This theory is general and can be used to find ultimate strength and strain in any direction for any given orientation of fibre and any number of layers.

This criterion has been adopted in this thesis as the failure criterion for GRP laminated composits.

3.3.4) Strength of Quasi-Homogeneous Anisotropic Layers:

In order to determine the strength of laminated multidirectional anisotropic composite materials, the evaluation must be based on a reliable method of analysis of the strength of unidirectional or quasi-homogeneous composites.

The theory starts by considering a material whose anisotropy possesses three mutually orthogonal planes of anisotropy and then finds the function of combined stress components acting on that anisotropic medium that causes failure.

Hill(3-34) generalized the von-Mises isotropic yield criterion by introducing parameters of anisotropy to describe anisotropic materials. The yield criterion was assumed to be quadratic in the stress components and took the following form

$$2f(\sigma_{ij}) = F(\sigma_T-\sigma_V)^2 + G(\sigma_V-\sigma_L)^2 + H(\sigma_L-\sigma_T)^2 + L\,\tau_{LT}^2 + 2M\,\tau_{VL}^2 + 2N\,\tau_{TL}^2 = 1 \qquad (3.72)$$

where F,G,H,L,M,N, are material coefficients characteristics of the state of anisotropy, and L,T,V are the axes of anisotropic symmetry.

The failure criteria takes this form only when the axes of symmetry coincide with principle axes, otherwise, the stress components should be transformed.

Since the materials of interest are thin if compared with their lateral dimensions, the only non-zero stress components are σ_L, σ_T and τ_{LT}, and a state of plain stress is assumed to exist (See section 3.2.1).

For transversely isotropic, quasi-homogeneous materials, the principle strengths F_T and F_V are of equal magnitude (See section 3.2.3) and the failure criterion becomes

3.3.4) contd.

$$\left(\frac{\sigma_L}{F_L}\right)^2 - \frac{1}{r}\left(\frac{\sigma_L \sigma_T}{F_L F_T}\right) + \left(\frac{\sigma_T}{F_L}\right)^2 + \left(\frac{\tau_{LT}}{S}\right)^2 = 1 \qquad (3.73)$$

where F_T is the principle strength in the direction of the fibre, F_T is the principle strength in the direction transverse to the fibres, and S is the shearing strength on the plane of anisotropic symmetry.

If the externally applied stresses follow axes of symmetry different from that of the material, then the yield condition in equation (3.73) will not be applicable until the off-axis stress component has been transformed to the material axes of symmetry.

By putting $m = \cos\alpha$; $n = \sin\alpha$; $\sigma_6 = \tau_{12}$ in equation (3.44) and substituting in equation (3.42):-

$$\begin{bmatrix} \sigma_L \\ \sigma_T \\ \tau_{LT} \end{bmatrix} = \begin{bmatrix} m^2 & n^2 & 2mn \\ n^2 & m^2 & -2mn \\ -mn & mn & m^2-n^2 \end{bmatrix} \begin{bmatrix} \sigma_1 \\ \sigma_2 \\ \sigma_6 \end{bmatrix} \qquad (3.74)$$

Tsai(3-35) introduces the following stress ratios for convenient use in the analysis:-

$$p = \frac{\sigma_2}{\sigma_1} \quad ; \quad q = \frac{\tau_{12}}{\sigma_1} = \frac{\sigma_6}{\sigma_1}$$
$$r = \frac{F_L}{F_T} \quad ; \quad s = \frac{F_L}{S} \qquad (3.75)$$

Thus employing the notation of equation (3.75) and introducing equation (3.74), the failure criterion becomes

3.3.4) contd.

$$\left[1 - p+p^2r^2 +q^2s^2 \right]m^4 + 2q\left[3-p-2pr^2+(p-1)s^2\right]m^3n$$
$$+ \left[8q^2+2(p+2q^2)r^2+(p-1)^2(s^2-1)-2q^2s^2\right]m^2n^2$$
$$+ 2q\left[3p - 1 - 2r^2 - (p-1)s^2\right]mn^3$$
$$+ \left[p^2-p+r^2+q^2s^2 \right]n^4 \qquad (3.76)$$
$$= \left(\frac{F_L}{\sigma_1}\right)^2 = \left(\frac{rF_T}{\sigma_1}\right)^2 = \left(\frac{sS}{\sigma_1}\right)^2$$

The above discussion may be summarized as follows:
For a given anisotropic body characterized by F_L ,F_T (or r) and S (or s) in reference coordinates 1-2, with a given orientation of the material axes of symmetry α and subjected to combined stress σ_1, σ_2 (or p), and τ_{12} (or q), the magnitude of the applied stresses at failure can be determined by solving equations (3.76) for σ_1. Alternatively, equation (3.76) may be regarded as the strength of a quasi-homogeneous anisotropic material subjected to combined stresses as a function of the orientation of the symmetry axes α. This analysis has been shown to agree well with experimental results for glass fibre reinforced epoxy resin ref.(3-36). Equation (3.76) may be regarded as the transformation equation for the strength of a quasi-homogeneous anisotropic material subjected to combined stresses; i.e. giving the strength characteristics as a function of the orientation of the symmetry axes, α.

a) For uniaxial stress, P = q = 0 and the failure condition is

$$m^4 + (s^2-1)m^2n^2 + r^2n^4 = \left(F_L/\sigma_1\right)^2$$

or

$$\sigma_1 = F_L\Big/\left[m^4+(s^2-1)m^2n^2+r^2n^4\right]^{\frac{1}{2}} \qquad (3.76a)$$

3.3.4) contd.

b) The case for pure shear can be derived by letting $\sigma_1 = \sigma_2 = 0$ in equation (3.74), and then by substituting into equation (3.73), (equation 3.76 cannot be used directly for this case since σ_1 is equal to zero.) one obtains

$$4m^2n^2(r^2+2)/[s^2+(m^2-n^2)^2] = (S/\sigma_6)^2 \qquad (3.76b)$$

or

$$\sigma_6 = S/[4m^2n^2(r^2+2)/s^2+(m^2+n^2)^2]^{\frac{1}{2}}$$

3.3.5) Strength of Laminated Systems:

In this section the laminated theory of strength developed by Tsai(3-28) will be discussed.

This theory depends on the assumption that the strength of a laminated composite depends on the thermo-mechanical properties of the lamination, which includes the thickness and orientation of each layer, the stacking sequence, the oriented ply ratio, the lamination temperature, helical angle, ... etc. In the laminating process, two interaction sources are introduced.

Firstly, there is a mechanical interaction created by the transverse non-homogenity of the laminated composite. As a result, non-uniform stress will be distributed across the composite according to the relative stiffness of the laminated layers. A further mechanical interaction is introduced by the anisotropy of the constituent layers in the cross-coupling represented by the "16" and "26" components of the stiffness matrix C_{ij}.

Secondly, a thermal interaction can be developed due to the differential thermal expansion (or contraction) between constituent layers. This occurs if the composite is

3.3.5) contd.

laminated at temperatures elevated relative to the service temperature of the laminated unit. This tends to create initial stresses in the composite.

The theory also considers that both mechanical and thermal interactions will not affect the linearity of the composite stress-strain relationship. Any discontinuties in the slope of the stress-strain relationship come from the failure of the constituent layers during the progress of loading and the ultimate strength of the composite is reached when all the constituent layers have failed.

In the analysis, it is assumed that each constituent layer of the laminated composite is quasi-homogeneous and orthotropic and is in a state of plane stress. The three dimensional generalized Hooke's law for any constituent layer is:-

$$\varepsilon_i = S_{ij}\,\sigma_i + \alpha_i\,\overline{T} \qquad (3.77)$$

$$i,j = 1,2,\ldots,6$$

This equation shows that the total strain is the sum of mechanical strain (first term) and thermal strain (second term).

Inversion of equation (3.77) gives:-

$$\sigma_i = c_{ij}(\varepsilon_i - \alpha_i\,\overline{T}) \qquad (3.78)$$

Integrating equation (3.78) across the thickness of the laminated composite yields the following (see ref.3-35).

$$\overline{N}_i = N_i + N_i^{\overline{T}} = A_{ij}\,\varepsilon_j^o + B_{ij}\chi_j \qquad (3.79)$$

$$\overline{M}_i = M_i + M_i^{\overline{T}} = B_{ij}\,\varepsilon_j^o + D_{ij}\chi_j \qquad (3.80)$$

where

$$(N_i, M_i) = \int_{-h/2}^{h/2} \sigma_i(1,z)\,dz \qquad (3.81)$$

3.3.5) contd.

$$\text{and } (N_i^{\overline{T}}, M_i^{\overline{T}}) = \int_{-h/2}^{h/2} C_{ij}\alpha_j \overline{T}\,(1,z)dz \qquad (3.83)$$

$$\text{and } (A_{ij}, B_{ij}, D_{ij}) = \int_{-h/2}^{h/2} C_{ij}(1, z, z^2)dz \qquad (3.83)$$

Equations (3.79) and (3.80) are the basic constitutive equations for a laminated anisotropic composite, taking into account equivalent thermal loadings. These equations can be presented in a matrix form by:-

$$\begin{bmatrix} \overline{N} \\ \overline{M} \end{bmatrix} = \begin{bmatrix} A & B \\ B & D \end{bmatrix} \begin{bmatrix} \varepsilon^o \\ \chi \end{bmatrix} \qquad (3.84)$$

The inverted form of equation (3.84).

$$\begin{bmatrix} \varepsilon^o \\ \chi \end{bmatrix} = \begin{bmatrix} A' & B' \\ B' & D' \end{bmatrix} \begin{bmatrix} \overline{N} \\ \overline{M} \end{bmatrix} \qquad (3.85)$$

The final form of the stress component of the kth layer is given by:-

$$\sigma_i^{(K)} = C_{ij}^{(K)} \left[(A'_{jk} + zB'_{jk})\overline{N}_k + (B'_{ij} + zD'_{jk})\overline{M}_k - \alpha_j^{(K)}\overline{T} \right] \qquad (3.86)$$

Equation (3.86) is the most general expression for stresses as a function of stress resulstant, moments and temperature. A complete derivation of this equation can be found in ref.(3-28).

3.4) Effect of Voids on Mechanical Properties:

One of the important fabrication induced variables which has pronounced effect on the performance of structural reinforced composites and which needs to be considered in the design of composite materials is the problem of voids.

Although the void content of filamentary composites is controllable to a certain degree, the complete elimination

3.4) contd.

of voids in practical full-scale structures employing composite materials does not appear to be feasible at present time. Consequently, if composites are to be successfully employed as structural materials, an insight on the effect of voids on structural performance is desirable.

Among the composite properties which are strongly influenced by voids are interlaminar shear strength, compressive strength, fatigue life, and, to a lesser degree, the moduli of elasticity.

3.4.1) Effect of Voids on Elastic Properties:

Greszczuk(3-61) states that the matrix modulus (E_m) is reduced by the presence of voids to $\overline{E}_m$, where:-

$$\overline{E}_m = \left[E_m \left(1 - \frac{V_v}{1 - \overline{V}_f} \right) \right] \qquad \text{(V-1)}$$

and

$$\overline{V}_f = (1 - V_v) V_f \qquad \text{(V-2)}$$

and V_v is the voids volume fraction.

From equations (V-1) and (V-2) it can be seen that all the elastic constants will be affected by the presence of voids because they are functions of the fibre volume fraction and/or the matrix modulus. This issue will be considered further in the discussion of the experimental results.

3.4.2) Effect of Voids on Compressive Strength:

Since the compressive strength is a function of the shear modulus of the matrix (G_m) and the fibre volume fraction (V_f), and since both these quantites are reduced

3.4.2) contd.

by the presence of voids to $\overline{G}_m$ and $\overline{V}_f$, their compressive strength will be significantly affected by the presence of voids. Due to the presence of voids equation (3.56) becomes:-

$$F_{L(c)} = \frac{\overline{G}_m}{1-\overline{V}_f} \qquad (V-3)$$

where

$$\overline{G}_m = \frac{\overline{E}_m}{2(1+\nu_m)} \qquad (V-4)$$

The value of $\overline{E}_m$ can be obtained from equation (V-1).

3.4.3) Effect of Voids on Interlaminar Shear Strength:

In Ref(3-61) the effect of voids on the interlaminar shear strength is investigated by considering two cases. The first case, considers the voids to be spherical in shape and arranged in a cubic array. The average applied shearing stress which causes failure is given by:-

$$\tau = \left[1 - \frac{\pi}{4}\left(\frac{6V_v}{\pi(1-\overline{V}_f)}\right)^{\frac{2}{3}}\right] \tau_{max} \qquad (V-5)$$

where τ_{max} represents the shear strength of a void-free composite, and the ratio τ/τ_{max} represents the interlaminar shear strength reduction of a composite resulting from the presence of voids.

The second case, considers the voids to be cylindrical and arranged in a rectangular array. In this case the shear strength is:-

$$\tau = \left[1 - \left(\frac{4V_v}{\pi(1-\overline{V}_f)}\right)^{\frac{1}{2}}\right] \tau_{max} \qquad (V-6)$$

Again the term in brackets represents the reduction in interlaminar shear strength resulting from the presence of voids.

3.5) Determination of Strength And Stiffness of Multidirectional Laminated Systems.

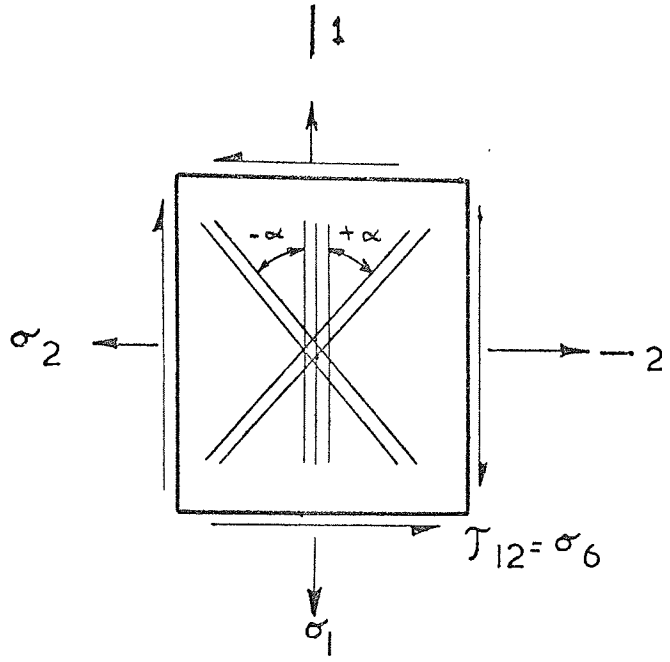

FIGURE (3.9)

The term multidirectional laminated system in this thesis is used to define a composite in which the constituent lamina are stacked in three directions. This three directional system which is generated from a combination of unidirectional laminates oriented at 0, $+\alpha$, and $-\alpha$ relative to the 1-stress direction with a symmetrical arrangement about the middle plane of the composite body, (Fig.3.9).

The reason for adopting this multidirectional system in the design of GRP composites for structural use is to take the advantage of the anisotropic behaviour of the unidirectional monolayers to achieve an optimum strength-stiffness performance under any desired stressing system applied to the laminated composite.

3.5.1) Basic Assumptions And Main Equations:

The basic and most general equation that can be used to predict the stress components of laminated composites is equation (3.86). Some simplifications of equation (3.86) have been effected to correspond to the boundary conditions arising from the type of fabrication and fibre arrangement of the composite used in this project, are discussed below.

a) Since the moulding technique adopted in this project is by means of a cold set pressure mould, then the problem of the residual thermal stresses will be nearly eliminated because of the absence of elevated temperature during the curing period or the laminating process.

b) In order to have enough time to release air bubbles from the interlaminar planes during moulding, the amount of catalyst added in the resin was kept to a minimum and never exceeded 0.1%. This procedure reduced exothermic action during the curing period to a minimum. Hence thermal stresses and air voids were minimised.

c) The stacking sequence of the reinforcing layers were arranged to be symmetric about the middle plane and hence the stiffness coupling matrix [B] and its compliance [B'] may be eliminated from equation (3.86).

d) The stressing of the test specimens was kept uniform and symmetric about the centre of thickness and hence the bending moments $\bar{M}_k$ may be eliminated from the general equation (3.86).

In consideration of (a),(b),(c) and (d) equation (3.86) can be simplified to:-

$$\sigma_i^{(K)} = C_{ij}^{(K)} \; A'_{jk} \; \bar{N}_k \qquad (3.87)$$

3.5.1) contd.

where

$$N_k^T = 0 \text{ (ambient temperature, curing or lamination)}$$

and

$$\bar{N}_k = N_k + N_k^T$$

Then

$$\bar{N}_k = N_k \tag{3.88}$$

Substituting equation (3.88) into equation (3.87):-

$$\sigma_i^{(K)} = C_{ij}^{(K)} \; A'_{jk} \; N_k \tag{3.89}$$

where (K) = 1,2,...n relates to the layer number

and

k = 1,2,6 relates to the stress component.

The unidirectional layer oriented at 0° ($\alpha = 0$) will be given a superscript (1) and labled (outer layers) because the 0° layers will always occur as the outer layers, while the angular oriented layers ($\alpha \neq 0$) will be given a superscript (2) and labled (inner layers).

$$\text{Let } M = \frac{h^{(1)}}{h^{(2)}} \tag{3.90}$$

where $h^{(1)}$ is the thickness of the outer layers

and $h^{(2)}$ is the thickness of the inner layers

The expansion of equation (3.89) for different stress components is shown below.

CASE 1 : Axial Load (N_1)

(a) For outer layers:

$$\sigma_1^{(1)} = \left[C_{11}^{(1)} \; A'_{11} + C_{12}^{(1)} \; A'_{21} + C_{16}^{(1)} \; A'_{61}\right] N_1$$

$$\sigma_2^{(1)} = \left[C_{12}^{(1)} \; A'_{11} + C_{22}^{(1)} \; A'_{21} + C_{26}^{(1)} \; A'_{61}\right] N_1$$

$$\sigma_6^{(1)} = \left[C_{16}^{(1)} \; A'_{11} + C_{26}^{(1)} \; A'_{21} + C_{66}^{(1)} \; A'_{61}\right] N_1 \tag{3.91}$$

3.5.1) contd.

(b) For inner layers:

$$\sigma_1^{(2)} = \left[C_{11}^{(2)} A_{11}^{'} + C_{12}^{(2)} A_{21}^{'} + C_{16}^{(2)} A_{61}^{'} \right] N_1$$

$$\sigma_2^{(2)} = \left[C_{12}^{(2)} A_{11}^{'} + C_{22}^{(2)} A_{21}^{'} + C_{26}^{(2)} A_{61}^{'} \right] N_1$$

$$\sigma_6^{(2)} = \left[C_{16}^{(2)} A_{11}^{'} + C_{26}^{(2)} A_{21}^{'} + C_{66}^{(2)} A_{61}^{'} \right] N_1$$

CASE 2 : Transverse Load (N_2)

(a) For outer Layers:

$$\sigma_1^{(1)} = \left[C_{11}^{(1)} A_{12}^{'} + C_{12}^{(1)} A_{22}^{'} + C_{16}^{(1)} A_{62}^{'} \right] N_2$$

$$\sigma_2^{(1)} = \left[C_{12}^{(1)} A_{12}^{'} + C_{22}^{(1)} A_{22}^{'} + C_{26}^{(1)} A_{62}^{'} \right] N_2$$

$$\sigma_6^{(1)} = \left[C_{16}^{(1)} A_{12}^{'} + C_{26}^{(1)} A_{22}^{'} + C_{66}^{(1)} A_{62}^{'} \right] N_2$$

(3.92)

(b) For inner Layers:

$$\sigma_1^{(2)} = \left[C_{11}^{(2)} A_{12}^{'} + C_{12}^{(2)} A_{22}^{'} + C_{25}^{(2)} A_{62}^{'} \right] N_2$$

$$\sigma_2^{(2)} = \left[C_{12}^{(2)} A_{12}^{'} + C_{22}^{(2)} A_{22}^{'} + C_{26}^{(2)} A_{62}^{'} \right] N_2$$

$$\sigma_6^{(2)} = \left[C_{16}^{(2)} A_{12}^{'} + C_{26}^{(2)} A_{22}^{'} + C_{66}^{(2)} A_{62}^{'} \right] N_2$$

CASE 3 : Shear Load (N_6)

(a) For outer Layers:

$$\sigma_1^{(1)} = \left[C_{11}^{(1)} A_{16}^{'} + C_{12}^{(1)} A_{26}^{'} + C_{16}^{(1)} A_{66}^{'} \right] N_6$$

$$\sigma_2^{(1)} = \left[C_{12}^{(1)} A_{16}^{'} + C_{22}^{(1)} A_{26}^{'} + C_{26}^{(1)} A_{66}^{'} \right] N_6$$

$$\sigma_6^{(1)} = \left[C_{16}^{(1)} A_{16}^{'} + C_{26}^{(1)} A_{26}^{'} + C_{66}^{(1)} A_{66}^{'} \right] N_6$$

(3.93)

3.5.1) contd.

(b) For inner Layers:

$$\sigma_1^{(2)} = \left[C_{11}^{(2)} A'_{16} + C_{12}^{(2)} A'_{26} + C_{16}^{(2)} A'_{66} \right] N_6$$

$$\sigma_2^{(2)} = \left[C_{12}^{(2)} A'_{16} + C_{22}^{(2)} A'_{26} + C_{26}^{(2)} A'_{66} \right] N_6$$

$$\sigma_6^{(2)} = \left[C_{16}^{(2)} A'_{16} + C_{26}^{(2)} A'_{26} + C_{66}^{(2)} A'_{66} \right] N_6$$

where $C_{ij}^{(1)}$ can be found from equations (3.16)

and $C_{ij}^{(2)}$ can be found from equations (3.49) by putting

$C_{ij}^{(2)} = \overline{C}_{ij}$ in these equations.

$$A'_{ij} = A^*_{ij} - B^*_{ij} D^{*-1}_{ij} H^*_{ij}$$

$$A^*_{ij} = A^{-1}_{ij} \qquad (3.94)$$ (See ref.3-28)

$$B^* = - A^{-1} B$$

$$H^* = B A^{-1}$$

As mentioned before, because of symmetric lay up about the middle plane, the coupling matrix [B] will vanish from equations (3.94) which becomes

$$A'_{ij} = A^{-1}_{ij} \qquad (3.95)$$

Expanding equation (3.95):-

$$\begin{aligned}
A'_{11} &= \frac{1}{A}(A_{23}A_{66} - A_{26}^2) \\
A'_{12} &= \frac{1}{A}(A_{26}A_{16} - A_{12}A_{66}) \\
A'_{16} &= \frac{1}{A}(A_{12}A_{16} - A_{22}A_{16}) \\
A'_{22} &= \frac{1}{A}(A_{11}A_{66} - A_{16}^2) \\
A'_{26} &= \frac{1}{A}(A_{12}A_{16} - A_{11}A_{26}) \\
A'_{66} &= \frac{1}{A}(A_{11}A_{22} - A_{12}^2)
\end{aligned} \qquad (3.96)$$

where

3.5.1) contd.

$$\overline{A} = A_{11}(A_{22}A_{66}-A_{26}^2) - A_{12}(A_{12}A_{66}-A_{16}A_{26}) + A_{16}(A_{12}A_{26}-A_{22}A_{16})$$

The in-plane stiffness matrix of the composite (A_{ij}) can be predicted from the following equations

$$\begin{aligned}
A_{11} &= t\left[\left(\frac{M}{M+1}\right)C_{11}^{(1)} + \left(\frac{1}{M+1}\right)C_{11}^{(2)}\right] \\
A_{12} &= t\left[\left(\frac{M}{M+1}\right)C_{12}^{(1)} + \left(\frac{1}{M+1}\right)C_{12}^{(2)}\right] = t\,C_{12} \\
A_{22} &= t\left[\left(\frac{M}{M+1}\right)C_{22}^{(1)} + \left(\frac{1}{M+1}\right)C_{22}^{(2)}\right] \\
A_{66} &= t\left[\left(\frac{M}{M+1}\right)C_{66}^{(1)} + \left(\frac{1}{M+1}\right)C_{66}^{(2)}\right] = t\,C_{66} \\
(A_{16},A_{26}) &= \frac{1}{M+1}\left(C_{16}^{(2)}, C_{26}^{(2)}\right)
\end{aligned} \qquad (3.97)$$

where M is defined in equation (3.90).

3.5.2) Behaviour Under Load:

(i) Uniaxial Tension.

The strength analysis of a laminated multidirectional composite is achieved by substituting the stress components of the Kth layer. Calculated from equation (3.89) into the general yield condition. Equation (3.76).

From equation (3.76), the maximum σ_1, in combination with the particular p and q that each constitute layer can sustain, can be determined. When this maximum is reached, failure in the particular layer or layers is considered to have occurred. After this failure, the remaining layers, which have not failed, will have to carry additional stresses. This redistribution of stress is accompanied by partial or complete mechanical uncoupling of the layers. The net result is that a new effective stiffness, as reflected in new values

3.5.2) contd.

(i) contd.

of the $[A'_{ij}]$ matrix of equation (3.89), will cause a change in the distribution of stresses in each of the constituent layers still intact. The effective stress-strain relationship of the composite is changed and a "knee" or discontinuity occurs in the stress-strain relationship. New values of the $[A'_{ij}]$ matrix, which are computed from the revised $[A_{ij}]$ matrix, now must be used in equation (3.89) for the computation of stresses. These new stresses are substituted into the yield condition of equation (3.76) to determine the next layers to fail. This process is repeated until all the layers have failed.

When M = 0 in equation (3.97) i.e. when the 0° layers are not included, failure occurs in a single stage as the positively and negatively oriented layers fail simultaneously.

(ii) Uniaxial Compression:

The behaviour of multidirectional laminated composites under uniaxial compression is completely different to that under uniaxial tension.

Since the compressive strength of the unidirectional monolayer is completely controlled by the matrix and since the matrix acts as a support to the unidirectional fibres under compressive stress, the failure of any of the constituent layers will cause failure of the whole composite. This may be explained as follows, whenever failure occurs in any part of the composite by any compressive mode such as delamination (fibre instability, or failure of the interface) or shear failure (yielding and failure of the resin matrix), a resin matrix failure is involved and therefore the load bearing capacity of all constituent

3.5.2) contd.

(ii) contd.

layers reduces to zero. Hence uniaxial compression failure occurs in a single stage.

3.5.3) Numerical Example:

In this section a numerical example is given of the calculation of the strength, modulus, and stress-strain relationship for a multidirectional laminated composite under uniaxial tension or compression. Consider a six-layer GRP laminated composite of the following configuration 0,+45,-45, -45, +45, 0, subjected to uniaxial tension or uniaxial compression.

The mechanical properties of the unidirectional monolayer are:-

$$\left.\begin{aligned} V_f &= 0.46 \\ \overline{V}_f &= 0.45 \\ V_v &= 0.03 \end{aligned}\right\} \text{assumed} \qquad \left\{\begin{aligned} E_f &= 73.58\ \text{KN/mm}^2 \\ \nu_f &= 0.22 \\ E_m &= 4.10\ \text{KN/mm}^2 \\ \nu_m &= 0.33 \end{aligned}\right.$$

$$\left.\begin{aligned} E_L &= 34.80\ \text{KN/mm}^2 \\ E_T &= 6.30\ \text{KN/mm}^2 \\ \nu_{LT} &= 0.25 \\ \nu_{TL} &= 0.045 \\ G_{LT} &= 2.70\ \text{KN/mm}^2 \end{aligned}\right\} \text{calculated}$$

	Tension	Compression
F_L KN/mm^2	0.68	0.41
F_T =	0.051	0.090
S =	0.052	0.052

Assume that all the glass fibre layers are of the same weight and of the same thickness, then from equation (3.90)

3.5.3) contd.

$$M = 0.5$$

using equations (3.16) yields,

$$\begin{aligned} C_{11}^{(1)} &= 35.15 \text{ KN/mm}^2 \\ C_{12}^{(1)} &= 1.59 \text{ KN/mm}^2 \\ C_{22}^{(1)} &= 6.36 \text{ KN/mm}^2 \\ C_{66}^{(1)} &= 2.70 \text{ KN/mm}^2 \end{aligned} \qquad \text{(E-1)}$$

and from equations (3.49)

$$\begin{aligned} C_{11}^{(2)} &= 13.87 \text{ KN/mm}^2 \\ C_{12}^{(2)} &= 8.47 \text{ KN/mm}^2 \\ C_{22}^{(2)} &= 13.87 \text{ KN/mm}^2 \\ C_{66}^{(2)} &= 9.58 \text{ KN/mm}^2 \end{aligned} \qquad \text{(E-2)}$$

and because of the symmetrical lay-ups, the inplane shear deformation is eliminated and $C_{16}^{(1)} = C_{26}^{(1)} = C_{16}^{(2)} = C_{26}^{(2)} = 0$. From equation (3.97) the following can be obtained,

$$\begin{aligned} A_{11} &= 20.89 \text{ KN/mm} \\ A_{22} &= 11.59 \text{ KN/mm} \\ A_{12} &= 6.19 \text{ KN/mm} \end{aligned} \qquad \text{(E-3)}$$

and from equation (3.96) A'_{ij} can be determined

$$\begin{aligned} A'_{11} &= 0.057 \text{ mm/KN} \\ A'_{22} &= 0.105 \text{ mm/KN} \\ A'_{12} &= -0.031 \text{ mm/KN} \end{aligned} \qquad \text{(E-4)}$$

(i) Condition of Uniaxial Tension:

a) For 0° unidirectional layers (outer layers); substituting the values of $C_{ij}^{(1)}$ obtained from eqn.(E-1) and the values of A'_{ij} obtained from eqn.(E-4) into the first part of equations (3.91) yields the following

3.5.3) contd.

(i) contd.

a) contd.

$$\sigma_1^{(1)} = 1.95 \quad N_1$$

$$\sigma_2^{(1)} = -0.09 \quad N_1 \qquad \text{(E-5)}$$

$$\sigma_6^{(1)} = 0$$

By substituting equations (E-5) into the general yield condition equation (3.76) for $\alpha = 0$ and the strength ratios $r = 13.33$ and $s = 13.07$ (See eqn.3.75):-

$$\underline{N_1 = 0.30 \text{ KN/mm}^2}$$

b) For $\pm$ 45° unidirectional layers (inner layers) substituting the values of $C_{ij}^{(2)}$ obtained from eqn.(E-2) and the values of A'_{ij} obtained from eqn.(E-4) into the second part of equations (3.91) yields the following;

$$\sigma_1^{(2)} = 0.47 \quad N_1$$

$$\sigma_2^{(2)} = 0.02 \quad N_1 \qquad \text{(E-6)}$$

$$\sigma_6^{(2)} = 0$$

By substituting equations (E-6) in to the general yield condition equation (3.76) for $\alpha = +45°$ or $-45°$ (which in fact gives the same results because of the symmetric lay-up about the middle plane and the even number of oriented layers which alwyas occurs in this type of laminated composite) and using the strength ratios $r = 13.33$ and $s = 13.07$:-

$$N_1 = \underline{0.155 \text{ KN/mm}^2}$$

Comparing the preceding values of N_1, it can be seen that the inner layers fail before the outer layers, and after failure of the inner layers the stiffness reduces.

3.5.3) contd.

b) contd.

The effective stiffness of the composite before failure of the inner layers is simply the reciprocal of A'_{11}

$$\therefore E_1 = \frac{1}{A'_{11}} = \underline{17.54 \text{ KN/mm}}$$

Thus, the in-plane strain at failure of the inner layers is:-

$$\varepsilon_1 = \frac{0.155}{17.54} = \underline{0.88\%}$$

After failure of the $\pm$ 45° layers the only stiffness in the composite will be that of the unidirectional layer at 0°. The $[A_{ij}]$ matrices of the composite now becomes:-

$$\begin{aligned} A_{11} &= 11.60 \text{ KN/mm} \\ A_{12} &= 0.52 \text{ KN/mm} \\ A_{22} &= 2.10 \text{ KN/mm} \end{aligned} \qquad \text{(E-7)}$$

and the new $[A'_{ij}]$ matrices is:-

$$\begin{aligned} A'_{11} &= 0.087 \text{ mm/KN} \\ A'_{12} &= -0.02 \text{ mm/KN} \\ A'_{22} &= 0.48 \text{ mm/KN} \end{aligned} \qquad \text{(E-8)}$$

and

$$\begin{aligned} \sigma_1^{(1)} &= 3.03 \, N_1 \\ \sigma_2^{(1)} &= 0.01 \, N_1 \sim 0 \end{aligned} \qquad \text{(E-9)}$$

Thus the effective stiffnes after failure of the inner layers is:-

$$E_2 = \frac{1}{A'_{11}} = \frac{1}{0.087} = \underline{11.49 \text{ KN/mm}}$$

The ultimate tensile strength can be calculated in the following manner.

The stress in the outer layers immediately before

3.5.3) contd.

b) contd.

the failure of the inner layers is computed from the first of equation (E-6) using $N_1 = 0.155$ KN/mm giving $\sigma_1^{(1)} = 0.073$ KN/mm^2.

Since the maximum value $\sigma_1^{(1)}$ can reach after complete uncoupling is equal to the axial tensile strength, 0.68 KN/mm^2. The outer layers can be stressed by an additional amount equal to

$$0.68 - 0.073 = 0.61 \text{ KN/mm}^2$$

Using equation (E-9), this additional stress beyond inner layer failure represents a stress resultant of $0.61/3.03 = 0.201$ KN/mm. Thus the ultimate stress resultant is:-

$$N_1 = 0.155 + 0.201 = \underline{0.356 \text{ KN/mm}^2}$$

The strain of the composite between inner layer failure and complete failure is:-

$$\varepsilon_2 = \frac{0.201}{11.49} = \underline{1.70\%}$$

Hence the total strain to failure is $0.88 + 1.70 = \underline{2.58\%}$

(ii) Condition of Uniaxial Compression:

Following similar steps to those used for uniaxial tension except that the value of the strength ratios r and s becomefrom eqn.(3.76) 4.56 and 7.88 respectively:-

a) The maximum stress resultant at failure for the outer layers (0° unidirectional),

$$N_1 = \underline{0.21 \text{ KN/mm}^2}$$

b) The maximum stress resulstant at failure for the inner layers ($\mp$ 45° unidirectional),

$$N_1 = \underline{0.195 \text{ KN/mm}^2}$$

3.5.3) contd.

b) contd.

Hence under uniaxial compression failure occurs at a stress resultant N_1 = 0.195 KN/mm. (See discussion in Section 3.5.2(ii))

The modulus of the composite up to failure (no discontinuity appearing in the stress-strain relation) is:-

$$E_1 = \underline{17.54\ KN/mm^2},$$

i.e. theoretically the same as the modulus for tension.

The ultimate strain at failure is

$$\varepsilon_1 = \frac{0.195}{17.54} = \underline{1.1\%}$$

A graphical representation of the above results for tension and compression is shown in Figs.(3.44) and (3.45) respectively.

3.6) Details of the experimental Program:

3.6.1) Introduction:

Before fibre reinforced composites can be seriously used as structural materials it is essential that reliable experimental data are collected for their mechanical properties.

For these anisotropic non-homogeneous materials, preparation, testing and analysis are usually costly and time consuming. So there is an urgent need to develop or modify existing test methods towards greater simplicity and economy. This is being investigated by ASTM(3-37,38,39), Ref.(3-40,41,42), British Standard Institute(3-43) and others (3-44,45,46,49).

In this section some of the basic problems involved in the testing of composite materials with particular reference to GRP will be summarized. The precuations and modifications necessary in extending the existing test methods will also be

3.6.1) contd.

discussed. The investigation is mainly based on tensile, compressive, flexural and interlaminar shear tests.

Before any experimental program is begun, several important questions must be asked including:-

a) The purposes for which the experimental information is required.

b) The existence or not of a theory for correlation with the experimental results.

c) Can significant environmental factors be adequately represented in the experimental program?

d) Is the material composition known? (i.e. it is important to know the reinforcement, matrix and void content of the composite, because these constituents play a vary important rôle in composite characterization).

3.6.2) Mechanical Behaviour Consideration in The Testing of Composites:

(i) Elastic Anistropy:

As mentioned above, fibre reinforced materials are generally anisotropic. In the general anisotropic case with more than nine elastic constants, normal stress or shear stress can produced both normal strains and shear strains. Similar coupling between bending moments and axial forces may occur due to unsymmetric lamination of the unidirectional layers of a laminate. The result of such coupling of stress in a test specimen is the development of complex stress and s train fields within them. Hence the basic concept of simple and uniform states of stress on which most test specimens are designed will no longer be valid and formulae derived for isotropic materials must be used with care.

3.6.2) contd.

(ii) Strength anisotropy:

GRP composites exhibit different tensile and compressive strengths in both the principle material axes and for off-axis loading. Also there may be weak planes through which the composite can fail in shear or tension before the expected high strength in another mode is reached. Thus the composite may fail prematurely in a different mode from that which was intended. Any strength calculated without recognising this change in failure mode may be considerably in error.

(iii) Low modulus/strength ratio:

The modulus/strength ratio of GRP is low compared to that of other materials including steel. Therefore GRP test specimens suffer large deformation before failure. Beam specimens, for example deflects 6 to 8 times more than mild steel beams of similar dimensions. The formula derived using the linear theory of structural analysis may not then correctly predict the flexural strength and modulus of the material. This will be discussed later in this chapter.

(iv) Ratio of Shear/Tensile Stiffness:

The ratio of the shear modulus and Young's modulus of fibre reinforced composites such as carbon fibre reinforced plastics (CFRP) and asbestos fibre reinforced plastices are generally low compared to that of metals. Consequently, in composite beam specimens, the shear deflection forms a considerable part of the total deflection. Under these conditions, the assumption that plane sections remain plane and perpendicular to the neutral plane is invalid. Young's modulus calculated from the measured deflection will also be incorrect. Although GRP composites

3.6.2) contd.

(iv) contd.

have a higher shear/tensile stiffness ratio than carbon or asbestos mentioned above, the effects mentioned are still significant with GRP.

It has also been observed that the composite strength varies with the specimen size, number of plies and the stacking sequence.(3-48,49).

Unless test specimens are proportioned, prepared and loaded correctly keeping the above points in mind, the results may not be reliable.

3.6.3) Materials for Specimens:

(i) Type of Glassfibres:

The fibreglass reinforcement used in preparing the specimens in this project was E-Glass unidirectional cloth type Y-996 supplied by Fothergill & Harvey Ltd.

(ii) Type of Resin and Catalyst:

The resin used in the project was preaccelerated Beetle Polyester Resin 837 supplied by BIP. For curing, this type of resin requires the addition of a suitable amount of Methyl Ethyl Ketone Peroxide to effect rapid gelation at room temperature. The amount of catalyst added to the resin with the moulding technique used was limited to 0.1 per cent in order to increase the gelation time.

3.6.4) Description of Moulds and Moulding Technique:

The moulds used in preparing the GRP sheets were metal moulds from which sheets could be produced of dimensions 1150 × 250 × 4 mm, 440 × 100 × 4 mm and 75 × 75 × 12 mm. (See Fig.(3.77)).

3.6.4) contd.

The moulds were manufactured with very smooth surfaces and before moulding took place a layer of mould release wax followed by BIP separating agent type LL894 were applied. After the separating agent had dried the following moulding procedure was adopted.

a) A layer of catalized resin was applied to the mould base to achieve a smooth surface on the moulded sheet.

b) A layer of glassfibre cloth was placed in the mould and a sufficient amount of resin was poured onto it. 25 gms of resin per 1 cm^2 of fibreglass cloth was found to be sufficient for the type of moulding adopted.

c) Special purpose rollers and plywood tampers were then used to achieve uniform fibre-resin wetting and to get rid of air bubbles trapped between the fibres and the resin surfaces.

d) Repeat (a), (b) and (c) until the desired number of glass fibre layers had been placed. Then the plunger of the mould was brought down under load onto stops to achieve a nominal 12 mm or 4 mm thick finished sheet.

e) The mould was left for 24 hours at room temperature for curing before release of the sheet from the mould.

Five different GRP sheets were moulded in this manner which contained 4,5,6,7 and 8 layers of glass mat and produced 27,39,46,57 and 64% fibre content respectively.

3.6.5) Tensile test:

(i) The Test Specimens:

A properly conducted uniaxial tensile test can yield valuable information on the behaviour of the

3.6.5) contd.

(i) contd.

material. Generally specimens are oriented so that the material orthotropy axes coincide with the specimen axes.

Anisotropic specimen may also be used to determine the shear modulus ref.(3-50), fibre orientation effects (3-51), and the failure criterion under complex state of stress (3-36).

When the fibres are non-symmetrically oriented with reference to the specimen axis, or the specimen is not loaded along the axis of material orthotropy, the specimen is in effect a general anisotropic test coupon and a non-uniform state of stress is generated due to the development of shear strain within the body of the specimen. A uniform state of stress may be achieved in these coupons if the conventional clamps are dispensed with and the specimen is loaded through pins and wires(3-52). If the specimen is orthotropically tested the coupling between shear and normal stresses and strains vanishes (i.e. $C_{16} = C_{26} = 0$) and the effect of anisotropy can be greatly reduced and the conventional clamping device can be used.

Local anisotropy may occur near the free boundaries of some orthotropic specimens such as angle-ply and random mat composites, due to the generation of inter-laminar shear stresses in these regions even under uniform uniaxial tension (ref.3-53). The use of cylindrical tension coupons eliminate this form of anisotropy, (ref. 3-52).

3.6.5) contd.

(i) contd.

A tensile failure away from the grips and within the gauged zone is a desired mode of failure in tensile strength tests. However, the specimens may fail around the grips, or the curved necks, as a result of fibre damage and/or weak interlaminar shear strengths. Damage to the fibre by the grips often can be prevented by bonding on end tabs of some suitable materials like aluminium.

An adequate tab length can be predicted by an expression derived by Nair et al.(ref.3-47), in order to prevent a shear failure of the specimen in the tab area. The length ℓ_t is given by the following:-

$$\ell_t = \frac{1}{2}\left(\frac{w_g}{w_t}\right)\frac{F_{L(t)}}{S}\, t_g \qquad (3.98)$$

where

w_g, w_t: the width of specimen at the gauge and tab regions respectively.

t_g: Thickness of the gauge zone.

Equation (3.98) shows that it is possible to eliminate shear failure by changing the tab length, reducing the thickness (t_g) or by necking down the specimen at the gauze zone or both as suggested in (ref.3-47).

Ewins(3-42) discussed the problem of achieving tensile failure within the gauge length limit by waisting the specimen in either their width or thickness to ensure that the shear strength was nowhere exceeded, while allowing the ultimate tensile stress to be achieved at the minimum section. To accomplish this the following

3.6.5) contd.

(i) contd.

relationship was used:-

$$\frac{dy}{dx} = \frac{S}{F_{L(t)}} \left(\frac{y^2 - y_o^2}{y_o^2} \right)^{\frac{1}{2}} \qquad (3.99)$$

where y_o = the minimum half thickness (or half width)

y = the local half thickness (or half width) at a distance x from the point of minimum thickness or width.

The following conclusions may be drawn from the above discussion:-

a) Although it may be practical with filamentary composites, a reduced thickness specimen will not be reliable for use with a laminated composite. In laminated composites each individual layers within the composite are not exactly straight along the specimen length, but take a wavy pattern as shown in Fig.(3.10), which makes the amount of interlaminar resin variable along the specimen length, hence any reduction in the thickness will affect the fibre volume fraction of the reduced area and a false evluation of strength will be obtained.

b) Double reduction in width and thickness is unattractive because two separate machining operation would be required with a corresponding increase in cost. In addition the risk of fibre damage will be greater in this type of specimen.

c) If equation (3.99) is applied to reduce the width of the GRP specimen the overall dimensions of the specimen will be much larger than conventional specimen dimensions and hence it will be uneconomical.

The profile equation of the specimen after

3.6.5) contd.

(i) contd.

c) contd.

integrating equation (3.99) is,

$$x = \frac{F_{L(t)}}{S} \; y_o \; \ell in \left(y + \sqrt{y^2 - y_o^2}\right) \qquad (3.100)$$

Equation (3.99) is adequate for thickness reduction

FIGURE (3.10)

(ii) Details of Test Specimens Used in The Program To Predict The Longitudinal Properties:

a) Necked Specimen:

A modification to the tensile specimen described in Dastin(3-54) and in ASTM D638 was effected by making the reduction in the width more gradual in order to minimise the effect of stress concentrations on the waisted part of the specimen. This was done by increasing the radius of fillet from 75 mm to 110 mm.

To prevent fibre breakage under the grips, soft aluminium alloy pads were bonded on to the GRP specimen to provide a good gripping surface for the test machine wedge-grips and to eliminate potential fibre breakage, The adhesive used was Araldide AY111 added to an equal part of hardner AH111.

The tab length of the specimen was 41 mm which is well within the limit of equation (3.98). See Figure (3.11A).

3.6.5) contd.

(ii) contd.

b) Uniform Cross-Section Specimen:

A uniform cross-section specimen was also used in this program to determine the tensile properties of GRP. The specimen is shown in Fig.(3.11B).

The advantage of this specimen is that it can be used to determine the tensile strength, modulus, the stress-strain behaviour mostly up to failure, and the Poisson's ratio at different stress levels. This type of specimen reduces the shear stresses relative to a waisted specimen, an important factor for a material with lower shear strength compared to its tensile and compressive strength. In addition these specimens are more easily and cheaply prepared than waisted specimens.

The chosen specimen width of 19 mm. was a compromise between two conflicting requirements. Firstly, the width should be reasonably large to prevent shear failure and to allow for the measurement of transverse strains so that the Poisson's ratio can be determined. Secondly, the width should be minimized to reduce the effect of in-plane bending strains arising from test machine misalignment and the development of non-uniform shearing stains particularly where off-axis tensile properties for unidirectional GRP are being determined. Soft aluminium alloy pads were again used.

(iii) Transverse Tensile Properties:

In the plane normal to the fibre direction, unidirectional GRP can be considered as isotropic. So that, compared to longitudinal tension, stress concentration

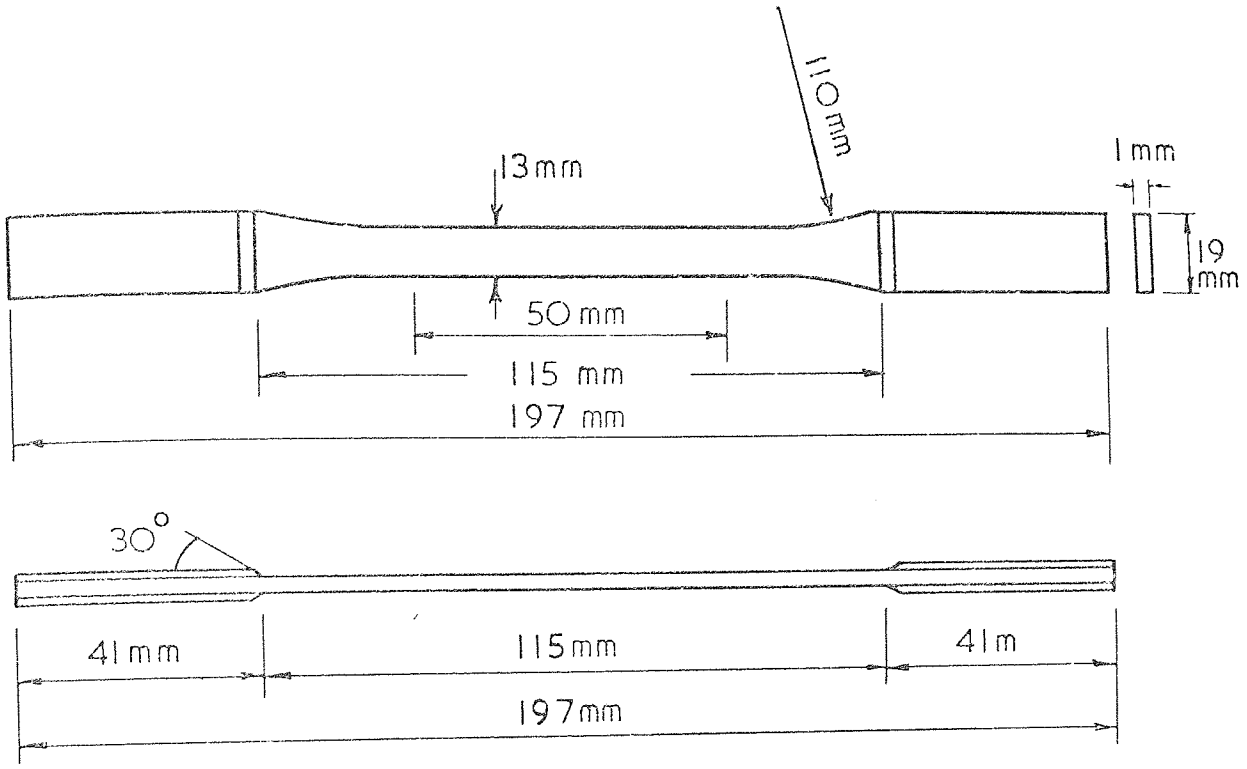

A. Necked specimen

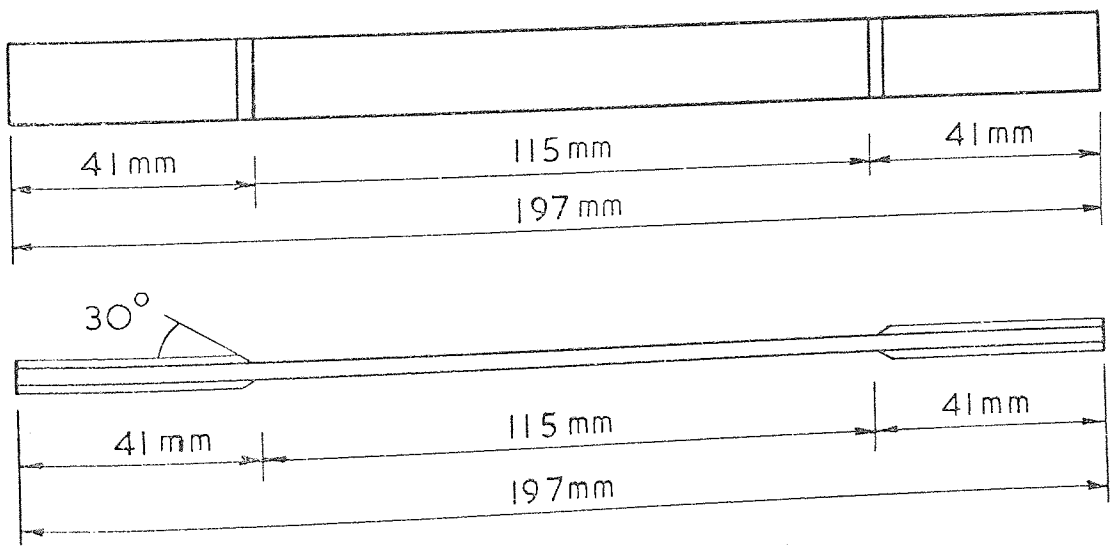

B. Un - necked specimen

Fig. 3.11. Tensile specimens

3.6.5) contd.

(iii) contd.

tends to be relatively small. Furthermore, the transverse tensile/shear strength ratio (about 1:1) is very much lower than the longitudinal/shear strength ratio (about 15:1), hence the limitation on taper or wasiting will not be significant. In addition the transverse stiffness/transverse strength ratio is about the same as for the longitudinal direction so that the bending stress created from any machine misalignment will be of the same order as in the longitudinal direction. Hence the same dimensions for unwaisted specimen can be used for this direction as those used in the longitudinal direction.

The same specimen can be used for the tensile characterization of off-axis unidirection and multi-directional GRP composites.

(iv) Specimens Preparation and Test Procedure:

a) Longitudinal Tensile Tests:

The specimens discussed in (iia) and (b) above were intended for use up to failure and to give tensile strength, modulus, Poisson's ratio and stress-strain behaviour simultaneously. The necked specimens were used to determine tensile strength, whilst the uniform cross-section specimens were used for the determination of strength, elastic constants and stress-strain relationship. Two electrical resistance strain gauges supplied by "Technic Measure" were fixed in the longitudinal and transverse directions.

Both types of specimen were tested in a DENISON testing machine using wedge grips which had been adjusted to produce, as nearly as possible, a pure

3.6.5) contd.

(iv) contd.

a) contd.

tensile load in the gauge length. The loading rates adopted produced failure of the necked specimens in 30-90 seconds and of the constant cross-section specimens in 120-240 seconds. Five specimens of each of the five different fibre volume contents were tested.

b) Transverse Tensile Tests:

The constant cross-section specimens were used for the transverse tests, and the same test conditions were used as those employed for the longitudinal tests except that the loading rate produced failure in 10-45 seconds on strength tests and 45-75 seconds in other tests.

Five specimens of each of the five different fibre contents were tested. The results of the tensile tests are shown in Table 3.4.

3.6.6) Compressive Test:

(i) The Test Specimens:

Compressive testing is much more complex than tensile testing both in terms of experiment technique and interpretation of results. A true compressive failure involves more than one type of microfailure and may include shear failure of the matrix, microbuckling of the fibres within the matrix and longitudinal delamination and then buckling of the resulting "columns".

A number of unwanted failure modes may occur due to unsymmetrical deformation of the specimen e.g. overall elastic buckling, interlaminar shear failure. End crushing and brooming, have also been observed.

3.6.6) contd.

(i) contd.

For high strength-low stiffness composites, waisting the section may not fully eliminate end brooming, and gross buckling may also take place. Loading the specimen through the lateral forces rather than the end cross sections (3-55) has been tried with some success in these cases. Purslow(3-41) suggests that to ensure failure occurs remote from the end fittings, waisting of the specimen cross-section should be carried out, especially for those composites with very high longitudinal compressive strength to shear strength ratio. The waisting reduces the stresses generated in the specimen and prevents shear failures. The waisting of the specimen should be according to the following relationship

$$y = \frac{d}{2} \exp \left| \frac{S}{F_{L(c)}} \quad \frac{2X}{d} \right| \qquad (3.101)$$

where d is the maximum thickness at the centre of the waisted section, 2y is the specimen thickness at a distance X from the centre.

Furthermore he suggests that for shear strength/compressive strength ratios less than 1:30, the waisted length of the specimen ℓ should be:-

$$\ell = 17.5d \qquad (3.102)$$

Ewins(3-42) also recommends waisting the specimen through its thickness but according to equation (3.98) for tensile specimens, replacing tensile by compressive strength in the equation.

British Standard(3-43) suggests two types of specimen i.e. cylindrical and cubical specimens in methods 303A and

3.6.6) contd.

(i) contd.

303C. ASTM(3-39) suggests rectangular flat specimens with specified slenderness ratio to eliminate buckling, also recommend a supporting jig for compressive specimens of thickness less than 3.2 mm.

(ii) Design And Detail of Test Specimens:

Three types of specimen were used in this test program.

a) Prismatic Specimens:

These were made longer than the specimen recommended in method B.S.2787, 1970 303B., and were of dimension 12.7 × 12.7 × 25.4 mm. The length of the specimens were increased to enable a longer electrical strain gauge to be attached in order to obtain a more accurate stress-strain relationship and a clearer mode of failure Fig.(3.12A).

b) Thin Sheet Specimens:

1) Waisted Specimens: These specimens were designed for the determination of compressive strength only. (Fig.3.12B). Since the compressive/shear strength ratio is not as high as that in CFRP, the waisting of the specimen was made across the width, not as recommended in(3-40,41,42) across the thickness.

The waisted width to the original width ratio was fixed at 1:2 utilising a semi-circular shape, to keep the failure area away from the specimen ends and to reduce the magnitude of the stress concentrations. The length of the waisted part was 17 mm long which is approximately equal to that used in ref.(3-41) for CFRP specimens and is acceptable from the stand-point of stability. Aluminium end blocks were fixed

3.6.6) contd.

(ii) contd.

b) contd.

1) contd.

to the specimen to prevent end crushing during loading. Failures were found to occur near the mid-length of the specimens.

2) Straight Edged specimens:

These specimens were designed according to ASTM D695, Pt.27, 1973: for GRP sheets of thickness greater than 3.2 mm. To overcome the stability problem, a slenderness ratio of 15:1 was adopted for this type of specimen. Aluminium end blocks were bonded to both ends of the specimens to prevent end crushing or brushing and to transmit load by shear from the test machine to the specimen, as suggested in (3-40,41,42). See Fig.(3.12C).

The advantages of the parallel sided specimen are,

i) Its unwaisted width provides adequate space for fixing electrical strain gauges in the longitudinal and transverse directions in order to measure the stress-strain relationship, Young's modulus and Poisson's ratio.

ii) It is easier and more economical to produce accurately.

iii) Full strength and stiffness characteristics can be obtained from the one specimen.

The strengths and modes of failure were approximately the same as those found from the waisted specimens.

3.6.6) contd.

(ii) contd.

For the reasons described in Section [3.6.5(iii)] the straight edged specimens can also be used to determine the transverse compressive properties of GRP composites.

Off-axis compressive strength testing with straight edged specimens is more complex than tensile testing, because of the generation of shearing stresses due to the fibre inclination from the principle direction. The waisted specimen is more reliable in this case than the straight edged one because the decrease in width of 50% tends to reduce the shearing stresses to an acceptable magnitude.

Details of the specimens are shown in Fig.(3.12D).

The elastic modulus, Poisson's ratio, and stress-strain relationship were obtained from straight edged specimens and were found to be at some variance with theoretical predictions.

All compressive tests results are shown in Table (3.5).

(iii) Preparation of Specimens and Test Procedure.

All specimens described in (ii)(a and b) were tested between parallel platens in a Denison testing machine. The load was applied at a rate that caused failure within 30--90 seconds from the start of the test. This loading rate applied only for the determination of strength.

For the determination of the modulus, Poisson's ratio and stress-strain relationship electrical resistance strain gauges were fixed on the prismatic and straight edged specimens in the same manner as for the tensile test specimens. In this case the load was applied at a rate

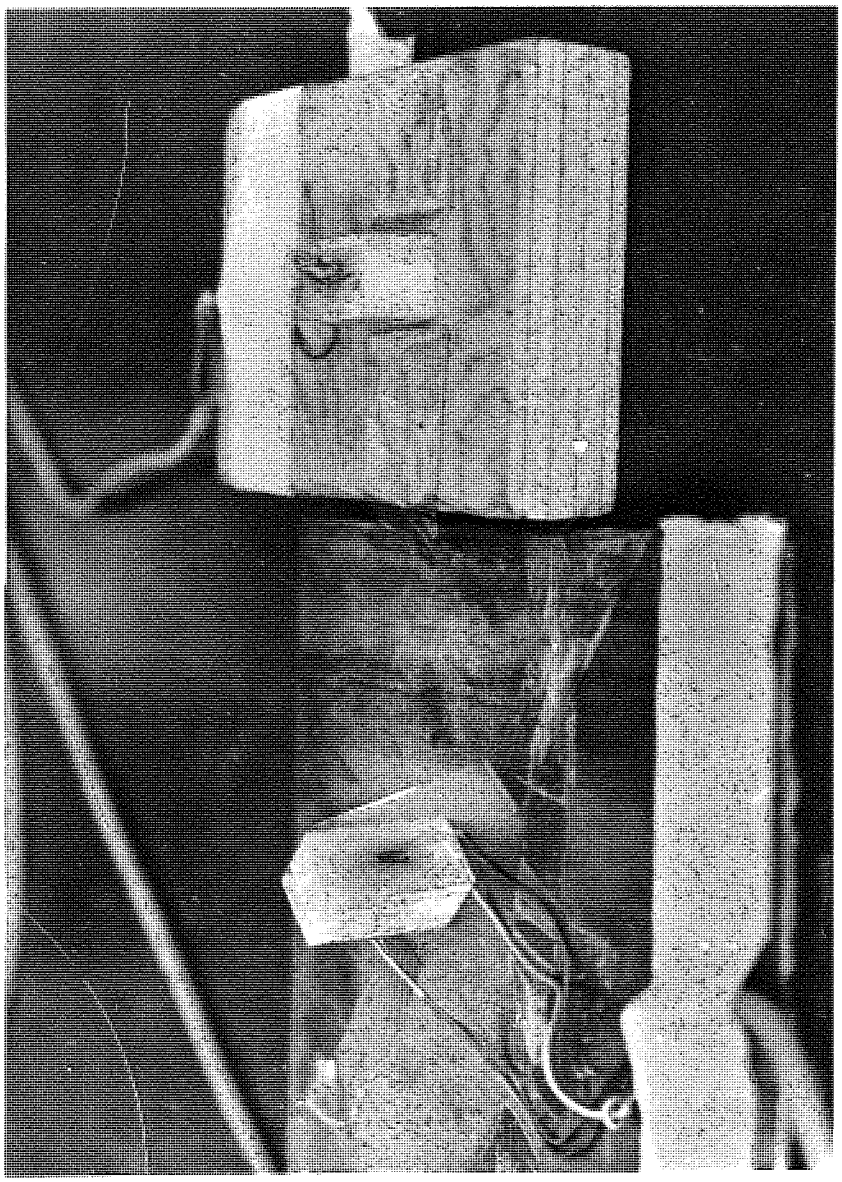

Fig. 3.12 a. Prismatic test specimen

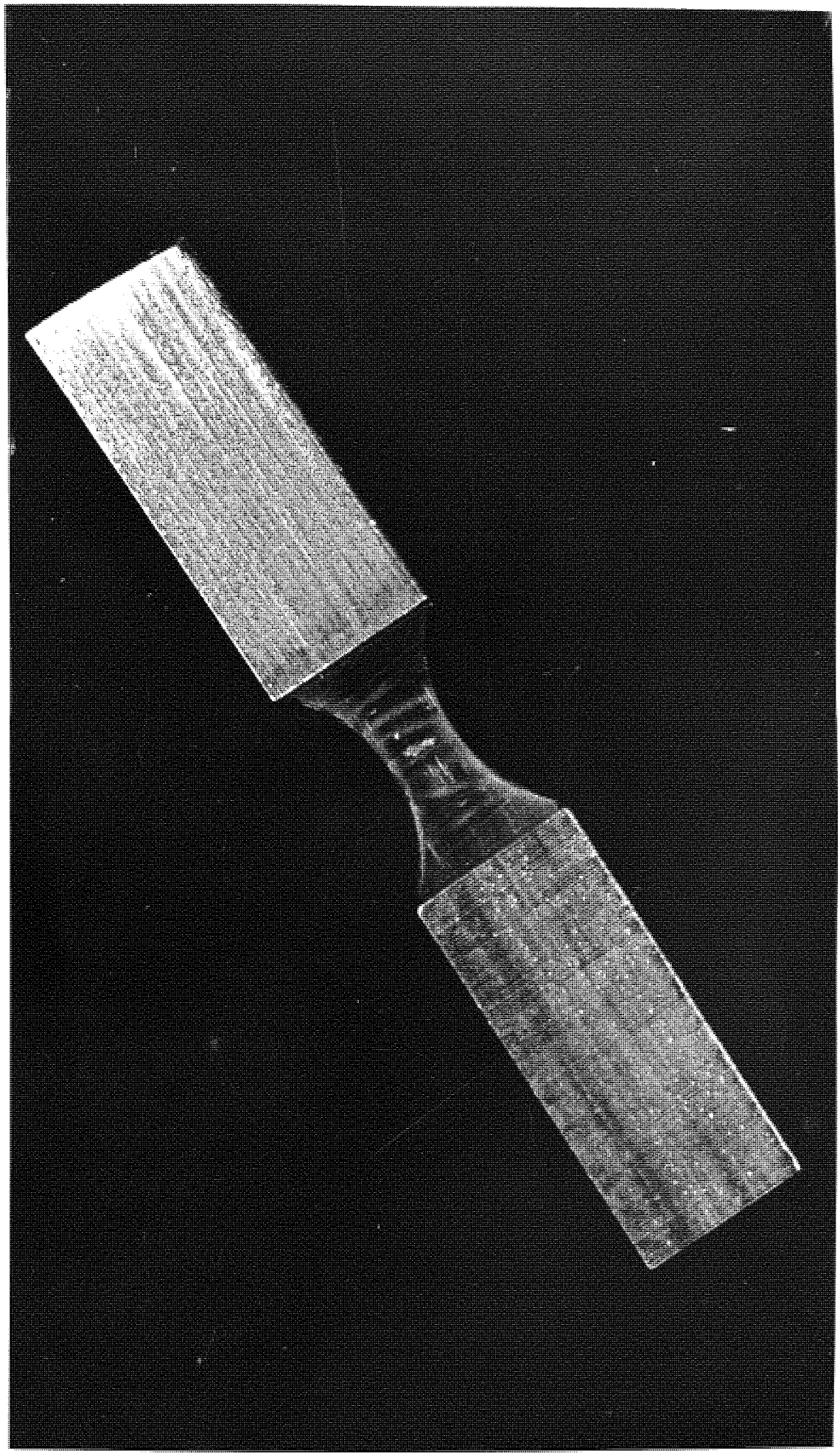

Fig. 3.12.b Waisted compression specimen

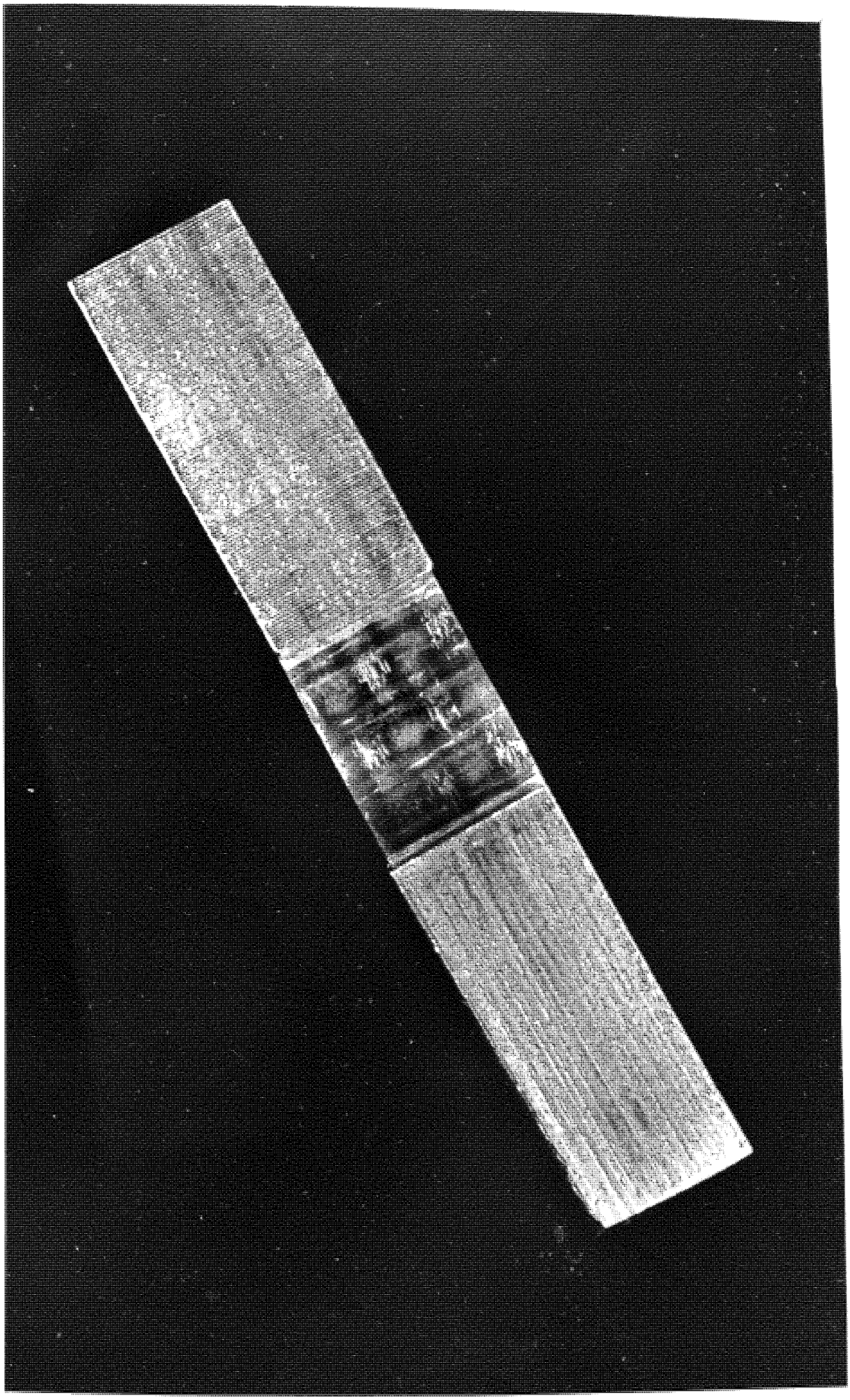

Fig. 3 12.c Straight edge compression specimen

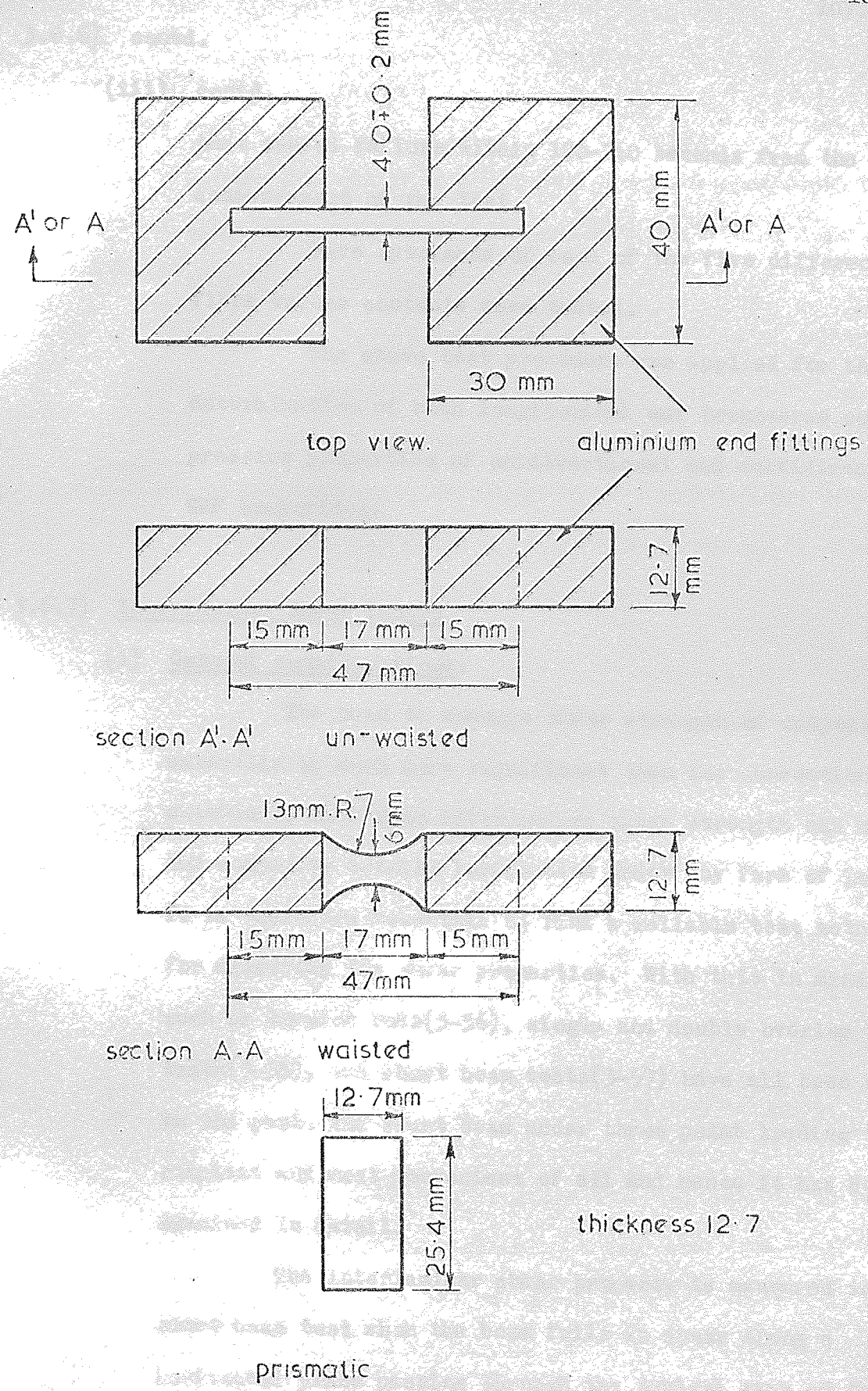

Fig. 3.12d. Details of compression specimens

3.6.6) contd.

(iii) contd.

that caused failure within 120-240 seconds from the commencement of the test.

Five specimens of each of the five different fibre volume contents were tested.

The above test procedure was applied for the determination of both longitudinal and transverse compressive properties of unidirectional and multidirectional GRP composites.

3.6.7) Interlaminar Shear Tests:

(i) General considerations:

The need to measure shear strength of composite materials is much more significant than for conventional materials, as a weak interlaminar shear strength can make the composite totally ineffective under any form of loading. It is therefore essential to find a reliable test method for measuring the shear properties. With this in mind tests such as torsion rods(3-56), single and double overlap tests(3-55), and short beam tests(3-57) have all been studied in the past. The short beam under three point loading is the simplest and most convenient of all and hence it has been examined in detail.

The interlaminar shear property is measured in a short beam test when the beam fails in shear along a horizontal plane passing through the neutral axis of the beam.

Sattar and Kellogg(3-58) determined the interlaminar shear strength of composits from short beam specimens using the geometry of span/depth ratio and width/depth ratio,

3.6.7) contd.

(i) contd.

noting that there is a limitation on the span/depth ratio above which the short beam specimen fails in a mode other than the shear mode.

In Ref.(3-58) mention is also made of the distortional energy theory for anistropic materials under plane stress (equation 3.73) in order to examine the interaction of flexural and shear stresses in the specimen.

For the short beam specimen under three point loading, equation (3.73) reduces to

$$\left(\frac{\sigma_L}{F_L}\right)^2 + \left(\frac{\tau_{LT}}{S}\right)^2 = c \qquad (3.102)$$

at failure $c \geq 1$

In equation (3.102), σ_L, F_L are considered to be the flexural stress and strength respectively, and τ_{LT}, S are the shear stress and strength respectively, also

$$\sigma_{L(max)} = \frac{3}{2}\left(\frac{P}{A}\right) \cdot \frac{L}{t} \text{ at the extreme fibres} \qquad (3.103)$$

and

$$\tau_{LT(max)} = \frac{3}{4}\left(\frac{P}{A}\right) \quad \text{at the netural plane} \qquad (3.104)$$

The shear stress distribtion is assumed to be of a parabolic nature reaching a maximum value of $3P/4A$ at mid-span on the neutral plane ($V = 0$), where P is defined as the total load at failure and A is the cross-sectional area, (See Fig.3.13). This shear stress is independent of span length. A bending stress distribution of $\frac{Mv}{I}$ also exists in the specimen reaching the maximum value defined by eqn.(3.103) at the extreme fibres at mid span.

3.6.7) contd.

(i) contd.

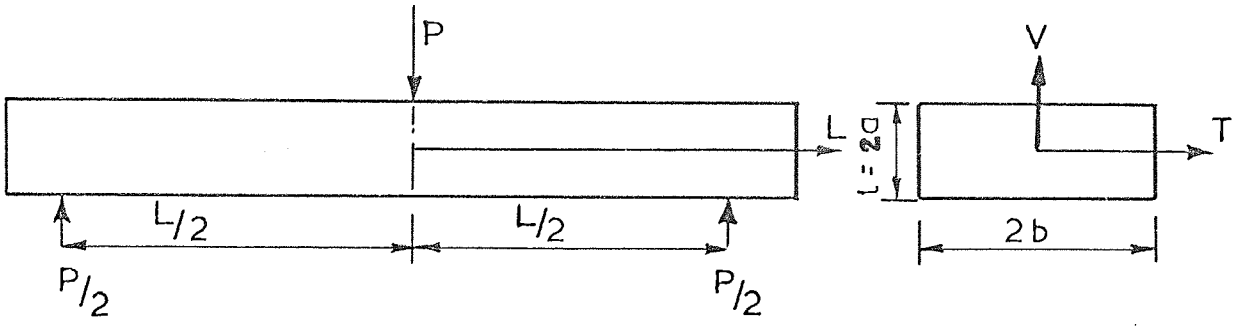

FIGURE (3.13) Short Beam Specimen.

Figure (3.14) shows a plot of the summation in equation (3.102) versus depth ($0 \leq v \leq a$) at the mid span location for flexural/shear strength ratio of 15 which is about average for GRP composites, and for various values of span/depth ratio. For convenience, the shear strength is assumed at $\frac{3}{4}(P/A)$, thus demanding a failure for each span/depth ratio chosen.

Figure (3.15) shows a plot of the main values of flexural/shear strengths ratio (F_L/S) required to ensure shear failure at a given span/depth ratio. This graph illustrates the I.L.S. failure zone and flexural failure zone with respect to span/depth ratio. The graph also contains two margins representing a transition zone between the I.L.S. failure mode and the flexural failure mode. This zone represents flexural stresses lying between 90% and 110% of the flexural strength. To ensure that specimens lie outside this transition zone and fail purely due to I.L.S. a margin representing 80% of the flexural strength is also defined on the graph. Using this criterion a span depth ratio of four was chosen for the GRP composite under consideration

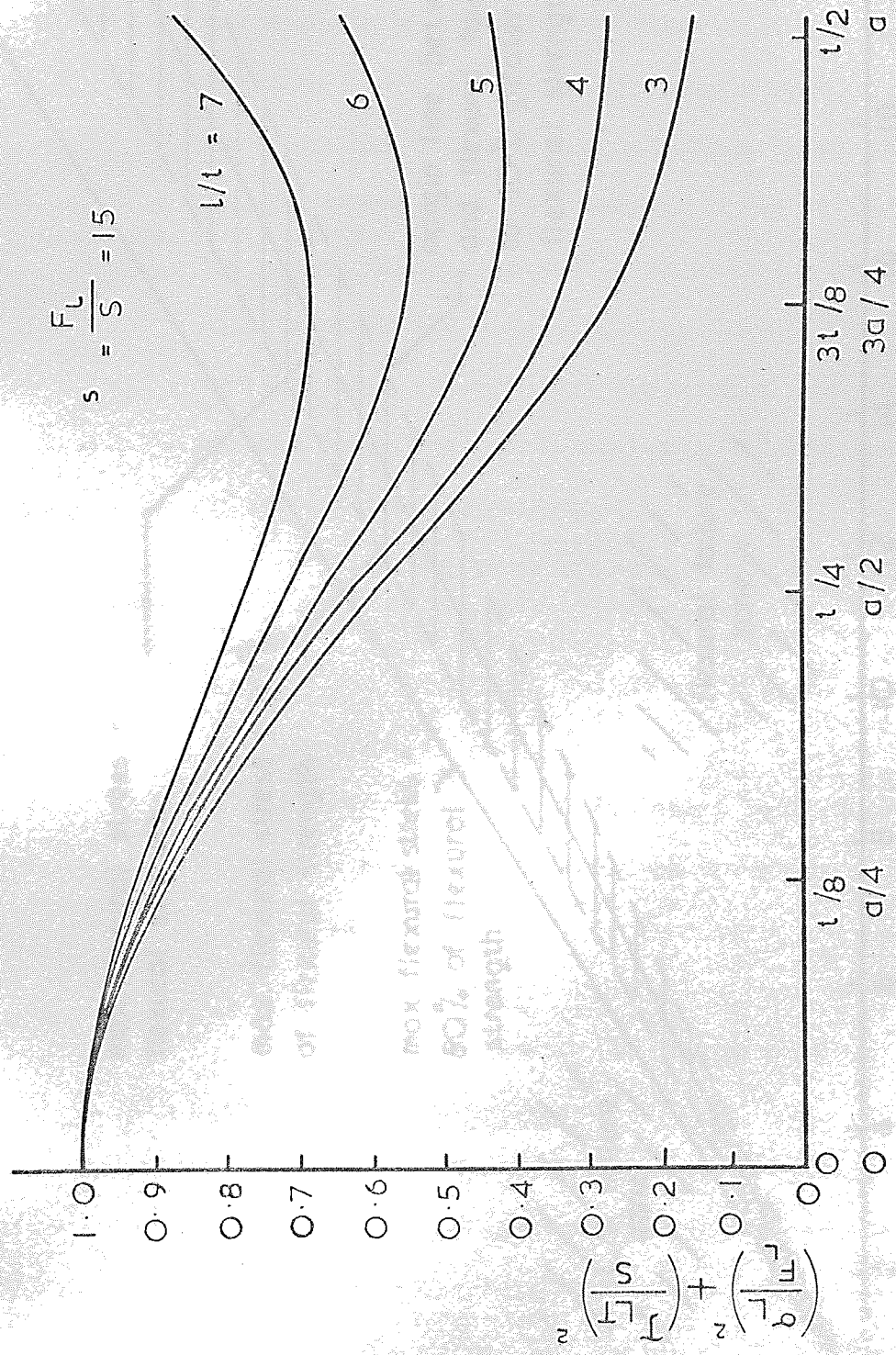

Fig. 3.14 Distortional energy versus depth. Failure occurs at maximum value, flexural strength = 15 times shear strength.

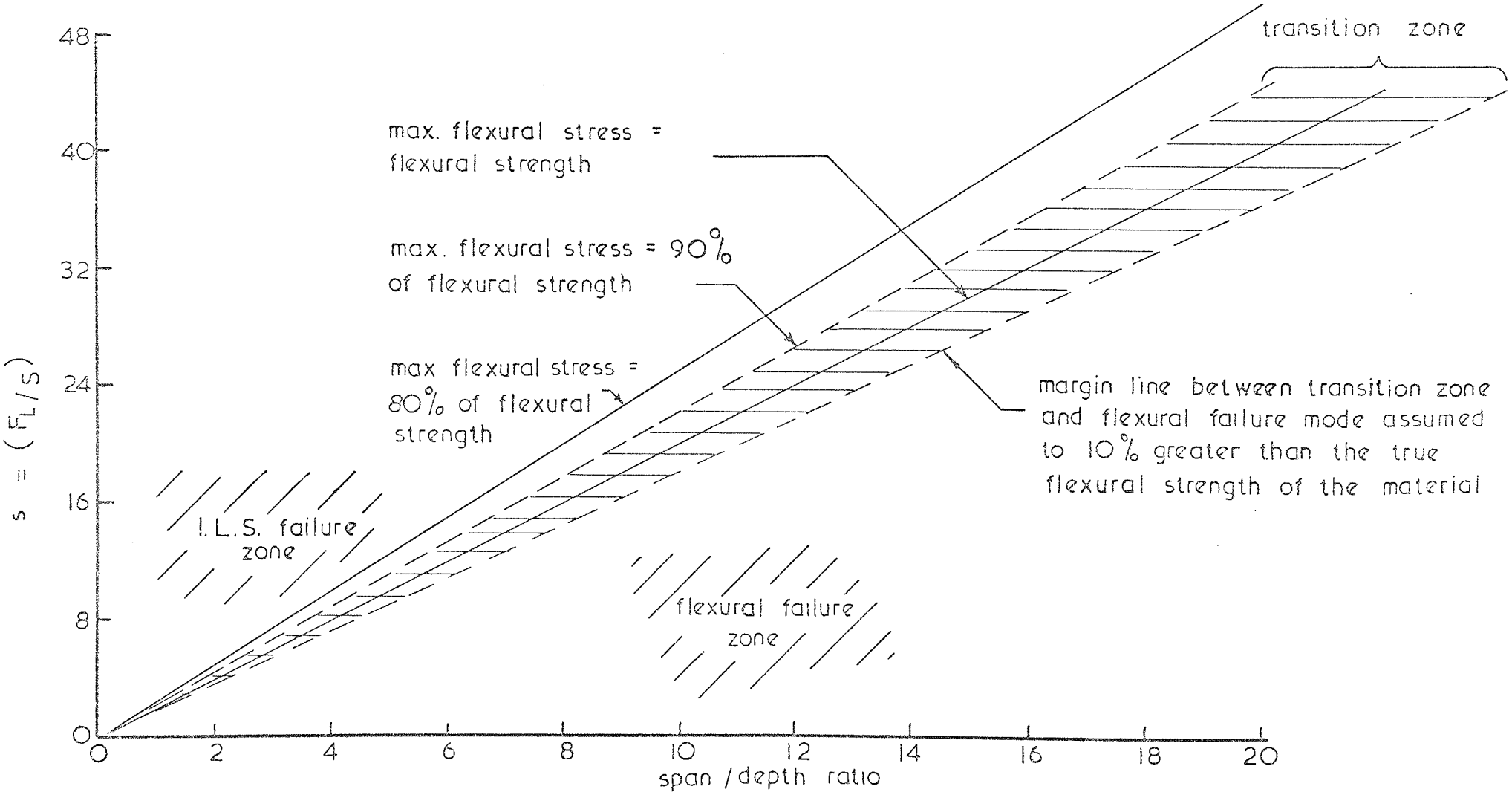

Fig. 3.15 Ratio of flexural strength to shear strength versus span to depth ratio

3.6.7) contd.

(i) contd.

which had an average flexural/shear strength ratio of approximately 14.

In Ref.(3.58) it was shown that specimen width has a significant effect on experimentally measured shear strength if calculated by the simple bending theory. For isotropic and oriented composites the shear stress varies through the width with a maximum value at the free-surfaces. The actual shear strength is therefore higher than the value calculated by the simple bending theory. The ratio $\bar{k}$ of the maximum shear strength and the nominal shear strength is plotted in Figure (3.16) against width/depth ratio for oriented fibre composites.

From the above discussion the following conclusion may be drawn:-

a) Improper span/depth ratios can lead to flexural rather than shear failure.

b) Width/depth ratios of the short beam shear specimen have a significant effect on the shear stress in the specimen.

c) The shear stress distribution across the width of the beam should be considered as non-uniform.

(ii) Detail of Test Specimens:

In accordance with the above discussion and Figure (3.15), the span/depth ratio adopted for the specimens was 4, this figure being consistent with a flexural/shear strength ratio of 14. The thickness of the specimen was 4 mm. and its overall dimensions were 24 × 10 × 4 mm.

(iii) Description of Test Loading System.

The I.L.S. test consisted of a simply supported

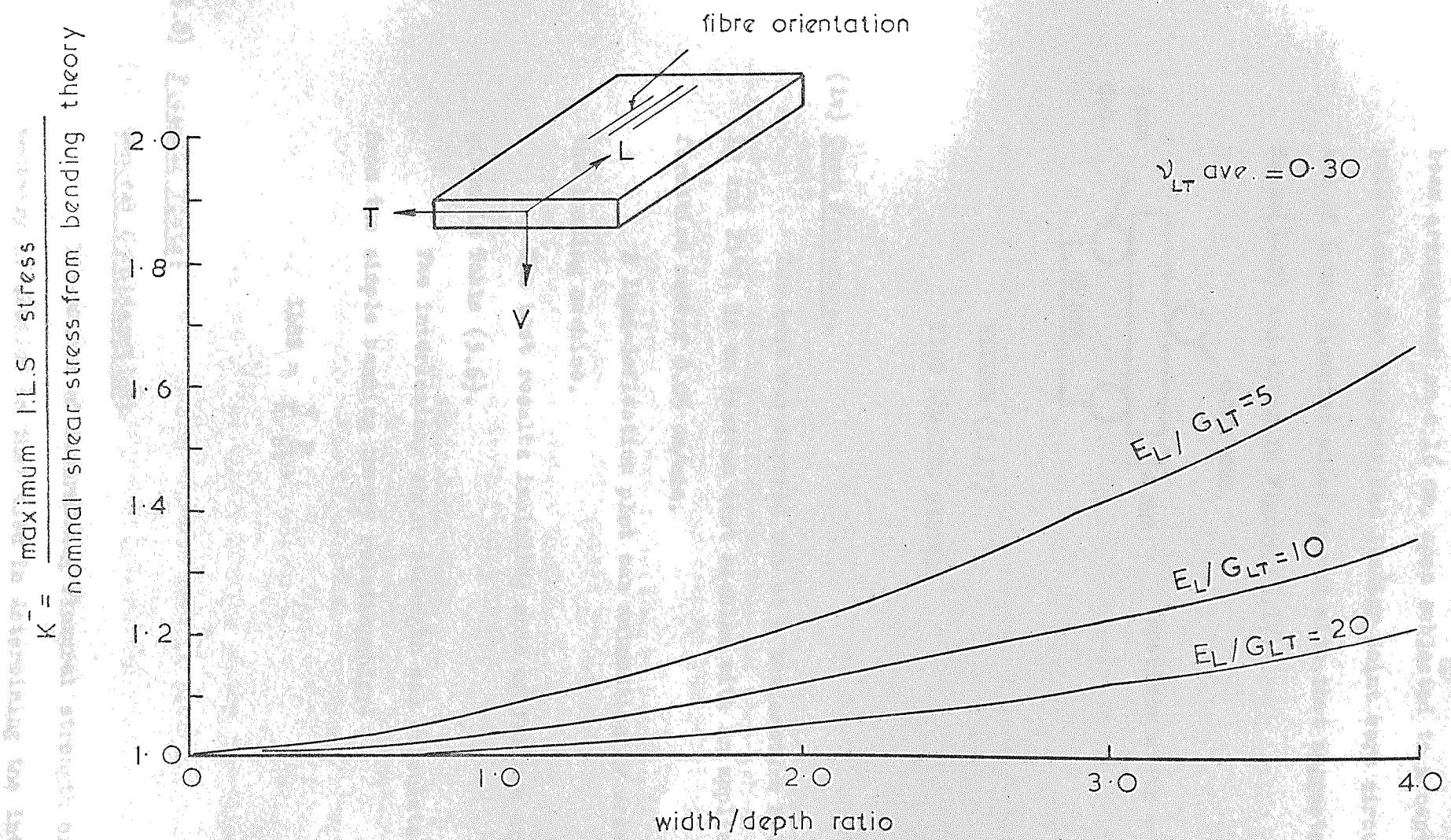

Fig. 3.16 ref 3.47

3.6.7) contd.

(iii) contd.

beam arrangement on a 16 mm. span subjected to a central point load. The supports and loading point were circular and of 6 mm. diameter which agreed with that suggested by Ewins(3-42) and shown in Figure (3.17).

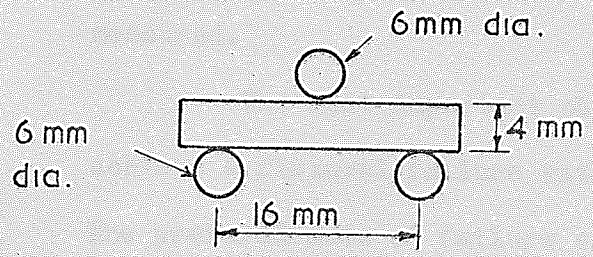

specimen width = 10 mm.

FIGURE (3.17)

ILSS LOADING SYSTEM.

(iv) Test Procedure.

The test was carried out at a temperature between 19 and 21°C. in an Instron test machine with an applied deformation rate of 0.05 cm/min.

A load-deflection plot was automatically drawn by the loading machine.

The test results including mode of failure are given in Table (3.6).

The interlaminar shear strength was calculated from the simple bending theory relationship:-

$$\text{ILSS} = \frac{3}{4}\,\frac{P}{bt}\,.$$

3.6.8) Flexural Tests:

(i) General Consideration:

The method of determining flexural strength experimentally is similar to that used in determining the interlaminar shear strength, i.e. a rectangular section specimen

3.6.8) contd.

(i) contd.

tested under three point bending. Although a four point loading system is preferable in so far as it gives a zone of constant bending moment, the three point loading system is simpler to apply and the deflections more easily measured.

The most important objective of this test is to achieve a flexural failure rather than a shear failure. The prefered mode of failure can be obtained by using test specimen with suitable span/depth ratios which in this case depend on the flexural/shear strength ratio, see Figure (3.15).

The effect of the low modulus/strength ratio results in large deflections and hence some error arises in using simple bending theory. For deflections greater than 10% of the span, the error in the modulus and strength calculated from simple bending theory also exceeds 10% Ref.(3-59).

The ratio of shear deflection to bending deflection is plotted in Figure (3.18) against span/depth ratio for various Young's modulus/shear modulus ratios. This figure shows that large span/depth ratios have to be chosen to reduce the significance of shear deflection.

The above considerations show that the choice of a suitable span-depth ratio is of primary concern for achieving the correct failure mode and accuracy.

The use of the simple bending theory for interpretation of experimental results must be carefully exercised. Figure (3.19) gives correction factors for simple bending theory strength and modulus determinations for various deflection/span ratios.

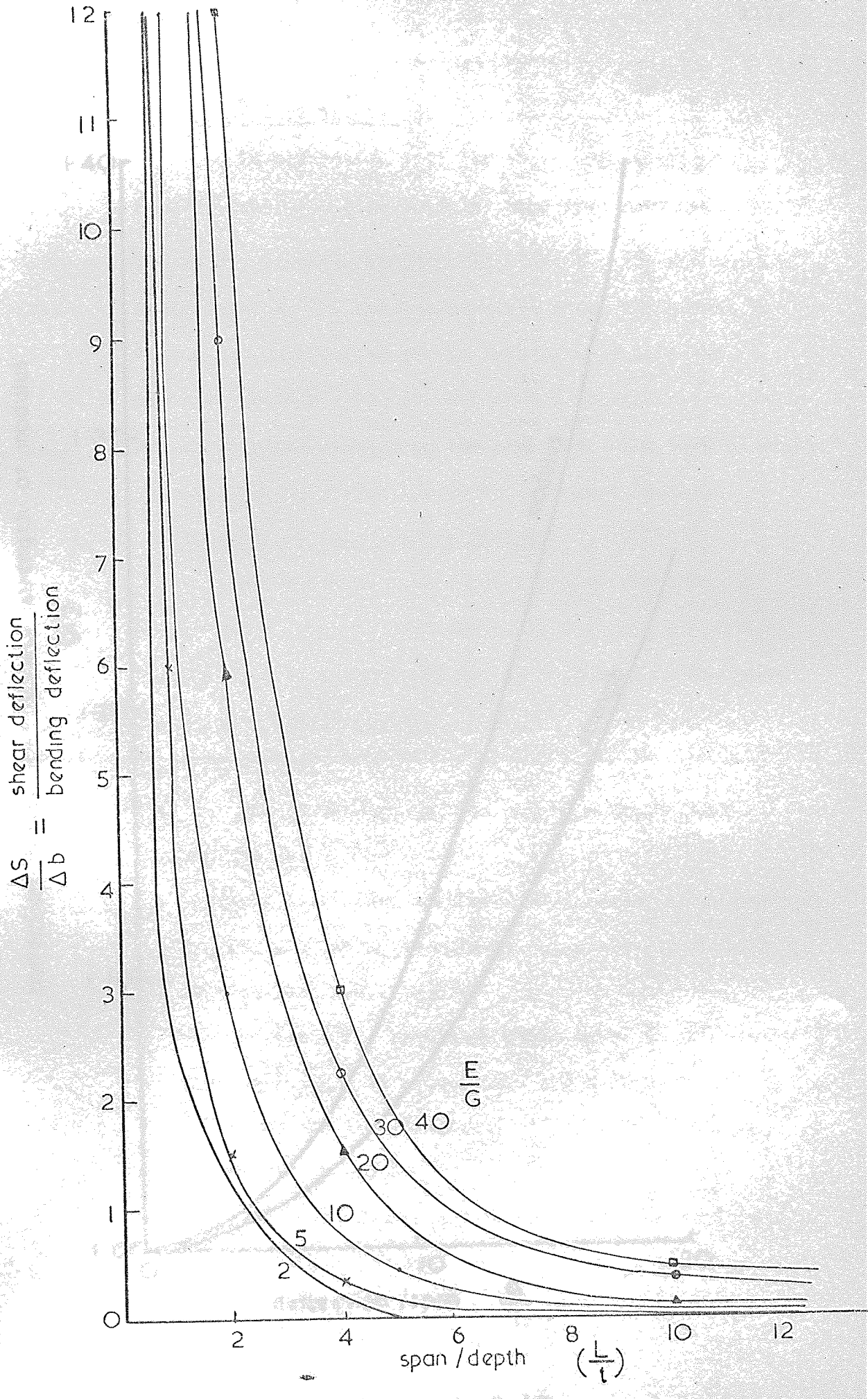
$\frac{\Delta S}{\Delta b}$ = $\frac{\text{shear deflection}}{\text{bending deflection}}$
12
11
10
9
8
7
6
5
4
3
2
1
0
2
4
6
8
10
12
span / depth $(\frac{L}{t})$
$\frac{E}{G}$
40
30
20
10
5
2

Fig 3.18

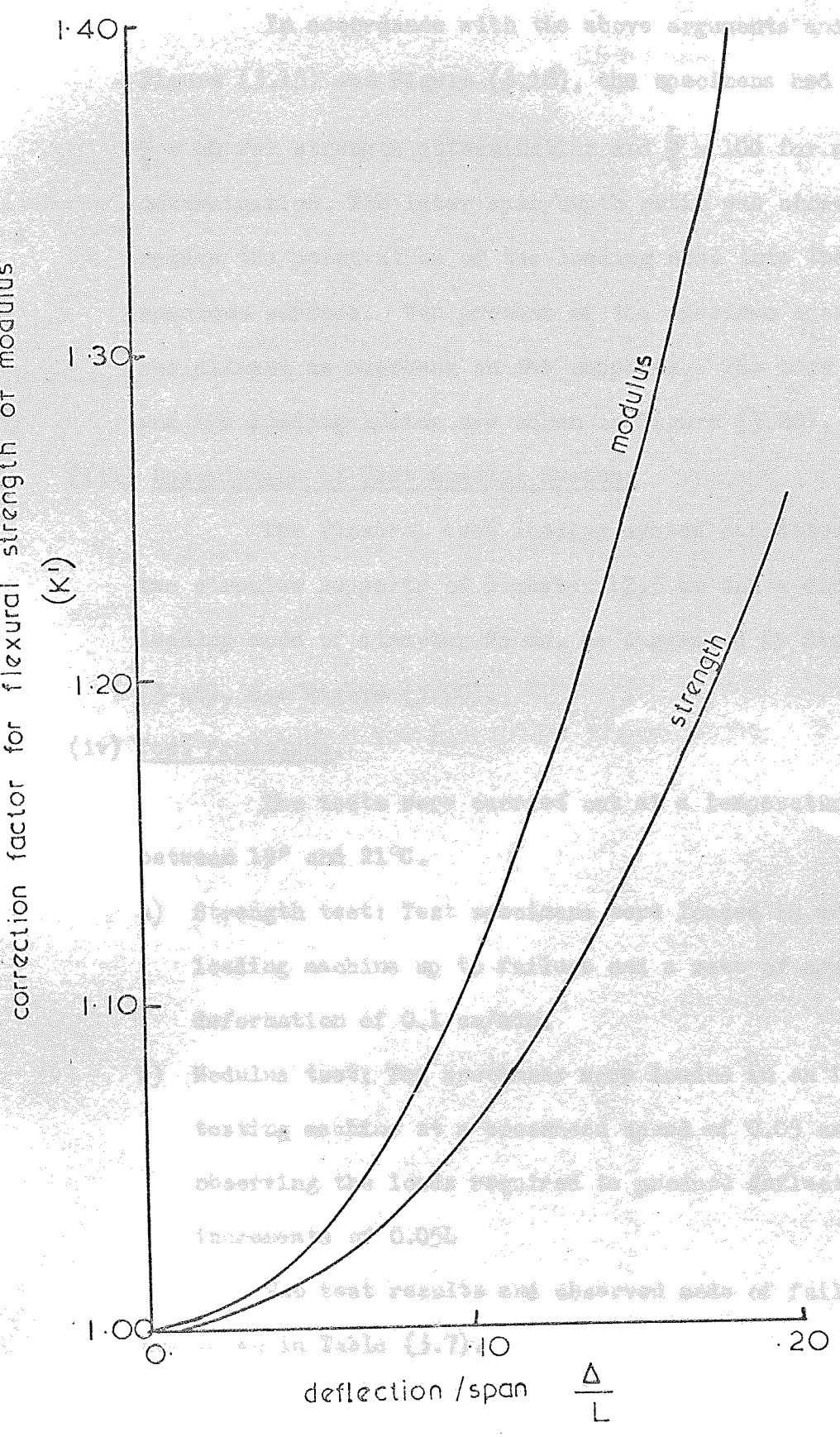

Fig. 3.19. Data from ref 3.60

3.6.8) contd.

(ii) Details of Test Specimens:

In accordance with the above arguments and Figure (3.15) and Figure (3.18), the specimens had $\frac{L}{t} = 40$ for strength determination and $\frac{L}{t} = 100$ for modulus determination. The later span/depth ratio was chosen to reduce the penetration of the loading nose into the specimen surface. Ten percent of the specimen span length was allowed as overhang on the supports. The test specimens and the loading system are shown in Figure (3.20).

(iii) Description of Test Loading System:

The flexural test loading system consisted of two circular supports of diameter 12.5 mm and a circular loading nose of diameter 25 mm. as suggested by Sturgeon (3-40), see Figure (3.20).

(iv) Test Procedure.

The tests were carried out at a temperature between 19° and 21°C.

a) Strength test: Test specimens were loaded in an Instron loading machine up to failure and a rate of applied deformation of 0.1 cm/min.

b) Modulus test: The specimens were loaded in an Instron testing machine at a crosshead speed of 0.05 cm/min, observing the loads required to produce deflection increments of 0.05L

The test results and observed mode of failure are shown in Table (3.7).

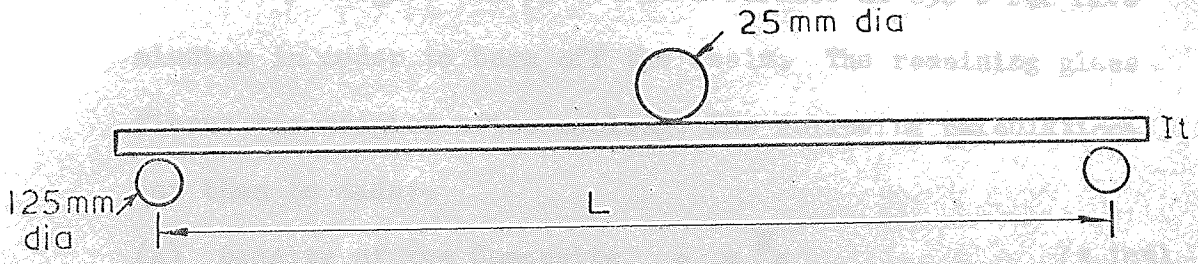

b. specimen width = 10 mm

for flexural strength determination $\frac{L}{D} = 40$

where flexural strength $= \frac{3}{2} \frac{PL}{bt^2}$ (simple bending theory)

for flexural modulus determination $\frac{L}{D} = 100$

where flexural modulus $= \frac{L}{4bt^3} \frac{P}{\delta}$

and δ is the observed deflection for applied load

modulus test specimen has been shown in fig. 3.11c.

Fig. 3.20

3.6.9) Determination of Fibre and Void Content of The Composites:

A rectangular piece of composite of known dimensions was accurately weighed and placed in a furnace at 650°C for five minutes in order to burn off the resin. The remaining glass fibres was weighed after cooling. The following calculations can then be made:-

(a) Density of the Composite $$\rho_c = \frac{W_c}{V_c} \qquad (3.105)$$

(b) Fibre Content by weight $$W_f = \frac{W_F}{W_c} \qquad (3.106)$$

(c) Fibre Volume fraction $$V_f = \frac{W_f/\rho_f}{V_c} \qquad (3.107)$$

(d) Void Volume fraction $$V_v = \frac{V_c - \left(\frac{W_f}{\rho_f} - \frac{W_R}{\rho_R}\right)}{V_c} \qquad (3.108)$$

where W_c = weight of GRP composite

V_c = volume of GRP composite

W_f = weight of glass fibre in the composite

W_R = weight of resin in the composite

ρ_R = density of resin, equal to 1.19 gm/cm^3

ρ_R = density of fibres, equal to 2.54 gm/cm^3

3.7) Discussion of Experimental Results:

3.7.1) Stress-Strain Relationship.

The stress-strain relationship of polyester resin in tension or compression was observed to be initially linear, becoming non-linear before failure as shown in Figures 3.21 and 3.22.

The stress-strain relationships for tension and compression are shown in Figures 3.23 to 3.45

The stress-strain relationship for unidirectional GRP laminated composites stressed in the fibre direction in

3.7.1) contd.

tension consisted of two straight lines of differing slope, whilst that for compression consisted of a single straight line. Some small non-linearity was observed at stresses approaching ultimate in both cases. The knee in the tensile stress/strain relationship is due to "crimping" of the fibres, on straightening under stress, transverse micro-cracking of the matrix results with a consequent siffness change.

Stress-strain curves for unidirectional GRP composites stressed at 90° to the filament direction in tension and compression are generally similar to the stress-strain curves for the resin matrix. In this direction the resin is the contiguous phase, and the stress-strain curve for the composite reflects the behaviour of the resin. Tensile failure of the composite occurs at stresses lower than that of resin tensile failure, because of stress or strain concentration at the filament resin interfaces.

Stress-strain curves of unidirectional GRP composites stressed at intermediate angles in tension and compression are transitional between those obtained for stressing along the fibres and across the fibres. The nearer the angle is to zero the closer the behaviour is to "along fibre stressing" and vice-versa.

Stress-strain curves for multidirectional laminated GRP composites are linear in tension and compression, a knee again occurring between the two straight portions for tension. The knee is due to failure of the angle orientated layers before the longitudinally orientated layers as discussed in section (3.5.2), the position of knee is variable depending on the value of M (e.g.3.90).

3.7.2) Tensile Properties:

Although the presence of voids has less effect on tensile properties than on other properties such as those in compression or interlaminar shear, the experimental results for tension were lower than the theoretical pedictions for both strength and stiffness. The probable reasons for this are the presence of stress concentration and misalignment of of fibres during fabrication. Notwithstanding this, the experimental results for unidirectional composite stressed in the fibre direction, are in reasonable agreement with the theory based on the law of mixture represented by equations (3.19), (3.55) and (3.22) for the prediction of E_L, $F_{L(t)}$, ν_{LT} respectively. The Tsai approach also shows a good agreement in predicting ν_{LT} i.e. equation (3.25) with C = 0.

The transverse tensile modulus may be predicted by equation (3.34), with the value of C = 1 or 0, the former value representing an upper bound of this property when the fibres are in contact, and the latter a lower bound when the fibres are completely surrounded by the resin matrix. The experimental results of the transverse modulus are well between the two bounds and are closer to the lower bound which may be used later for theoretical predictions for design purposes.

For unidirectional laminates, the theoretical transverse tensile strength was calculated to be equal to the tensile strength of the resin matrix. The experimental results however were well below this theory for the reason given in section (3.7.1).

The off-axis tensile properties of unidirectional GRP composites are in reasonable agreement with the Tsai approach discussed in section (3.3.4) and with equation (3.76a)

3.7.2) contd.

for strength prediction, and equation (3.53) for moduli prediction.

Experimentally the multidirectional laminated composites show good agreement with the theory discussed in section (3.5).

Photographs of the tensile modes of failure for different type of GRP composites and polyester resin are shown in Figures (3.69), (3.70) and (3.71).

Test results obtained from necked and unnecked specimens were in close agreement with each other, Figures (3.46 to 49,51,53 and 58), and the strength and stiffness of unidirectional GRP composites varied linearly with glass content over the whole range studied in the project, Figures (3.46,51).

3.7.3) Compressive Properties:

The prediction of elastic properties in compression was obtained from the same source as the tensile elastic properties. The general level of agreement between theory and experiment in compression was similar to that in tension.

The compressive strength for unidirectional laminates stressed in the fibre direction is highly affected by the presence of voids in the composite as previously described. Hence equation V.3 (section 3.4) was used to predict the longitudinal compressive strength. (N.B. equation 3.56 gives the same result as equation 3.61 for the composite materials used here). A further correction was applied by multiplying the value obtained from equation V.3 by 0.25 to allow for lateral displacement of fibres during curing shrinkage. This reduction factor is in agreement with ref.(3-18).

3.7.3) contd.

Again, for unidirectional laminates stressed in the fibre direction, the waisted and unwaisted specimens test results are lower than the theoretical prediction but they are in an acceptable range to the theoretical limits. The compression results of the prismatic specimens were in most cases less than that obtained from the other two types of specimens. This difference is probably due to geometrical irregularities that make the specimen surfaces not parallel to a certain accuracy, in addition to the direct transmition of load from the testing machine to the specimen which causes superficial cracks in the specimen body and hence, an early failure occurs mostly by delamination mode, as shown in Figure (3.74). Generally the specimens with the lowest fibre contents failed in a shear mode rather than a delamination mode. Figure 3.73 clearly shows the similarity between these shear modes and the shear mode for pure resin.

The test results show that the compressive strength increases with fibre volume fraction up to $V_f = 0.57$, for higher values of V_f the compressive strength decreases. Thus $V_f = 0.57$ represents the optimum resin content to provide an effective matrix.

For unidirectional lamintes, the theoretical transverse compressive strength was calculated to be equal to the compressive strength of the matrix and this theory agreed well with the experimental observations.

The composite longitudinal initial modulus varied linearly with glass content over the entire range investigated in this project.

For the off-axis properties, the approach used in the tension tests was adopted here, i.e. equation (3.76a)

3.7.3) contd.

for strength (where F_L becomes the compressive strength rather than the tensile strength) and (3.53) for modulus.

Experimental results for the multidirectional laminates were in good agreement with the theory discussed in section (3.5).

Photographs of the various compressive modes of failure are shown in Figures (3.72) and (3.73).

Test results obtained from the three types of specimens are shown in Figures (3.46 to 49 and 52 to 58).

3.7.4) Shear Properties.

Theoretically the interlaminar shear strength was calculated as equal to the shearing strength of the resin matrix. Experimental observations, in fact, showed that the interlaminar shear strength varied slightly with the range of fibre content used in this project, decreasing slightly with increasing fibre volume fraction.

Figure (3.67) shows the interlaminar shear strength calculated from the experimental results using the simple bending theory and the corrected results due to the width/depth ratio effect. The correction factor $\bar{k}$ was taken from Figure (3.16) for $E_L/G_{LT} = 10$ and $b/t = 2.5$. The experimental results are also shown in another form on Figure (3.67), i.e. the normalized unvoided experimental results calculated from equation (V-6) in section (3.4), where the void content in the composite was found to be approximately 3 per cent. (See Table 3.6).

A regression line was drawn through the voided corrected results, which are considered to be the true experimental representation for the ILSS, the equation of this

3.7.4) contd.

line is

$$\text{ILSS } (N/mm^2) = 52 - 0.08\ V_f \qquad (3.109)$$

If $V_f = 0$ in equation (3.109), then the value of ILSS is equal to 52 N/mm^2 which is considered to be the voided shearing strength of the matrix which is about 78 per cent of the unvoided shearing strength of the resin matrix, (approximately 67 N/mm^2).

The slight drop in ILSS with increasing fibre volume fraction is thought to result from stress concentrations introduced by voids.

Multidirectional composites showed a lower ILSS for both cross-ply and angle-ply compared to unidirectional GRP composites (see Figures 3.67 and 3.68). This may be related to the fibre arrangement within the composite, where the type of fibre nesting in the unidirectional composite can offer more mechanical bonding than the angle and cross-ply composite. Photographs of the different modes of failure are shown in Figure (3.75).

The shear modulus was found experimentally by the aid of three types of tensile modulus specimens (i.e. at orientations 0°, 90° and 45°) from which the longitudinal, transverse, and 45 deg. moduli respectively were determined. Using the results from these specimens in the first of equation (3.53) reduces to the following

$$\frac{1}{E_1} = \frac{1}{4}\left(\frac{1}{E_L} + \frac{1}{E_T} + \frac{1}{G_{LT}} - \frac{2\nu_{LT}}{E_L}\right) \qquad (3.110)$$

where G_{LT} is the only unknown in equation (3.110) and can thus be determined by

3.7.4) contd.

$$\frac{1}{G_{LT}} = \frac{4}{E_1} - \frac{1}{E_L} - \frac{1}{E_T} + \frac{2\nu_{LT}}{E_L} \qquad (3.111)$$

Experimental results for shear modulus agreed very well with the theoretical prediction of equation (3.40), see Figure (3.50).

3.7.5) Flexural Properties:

The experimental results for unidirection GRP composite in flexure indicate that the flexural strength and stiffness are dependent on the tensile strength and modulus, this finding agrees with the discussion in section (3.3.2v).

Due to the large deflections of the specimens a correction was made to the flexural strength and modulus derived from the simple bending theory. The correction was made with the aid of Figure (3.19) (See section 3.6.8).

A regression line was drawn through the corrected experimental results, giving the equation:-

$$F_{(FL)}\ N/mm^2 = 1{,}200\ V_f + 90 \qquad (3.112)$$

Equation (3.112) shows that for a value of fibre volume fraction equal to zero the flexural strength becomes equal to 90 N/mm^2 which is approximately the flexural strength of polyester resin (See Figure 3.59).

A similar regression line was also shown for the experimental result of flexural modulus, giving:-

$$E_{(FL)}\ N/mm^2 = 52{,}600\ V_f + 4000 \qquad (3.113)$$

Again for $V_f = 0$ the flexural modulus in equation (3.113) approaches the flexural modulus of the polyester resin, Figure (3.60).

3.7.5) contd.

The corrected test results given with the associated deflection are shown in Table (3.7).

Cross-ply, angle-ply and off-axis unidirectional results for flexural strength and modulus, give the same agreement with the tensile strength and modulus as those obtained from the unidirectional specimens. See Figures (3.61) to (3.66). Photographs of the different modes of failure are shown in Figure (3.76).

3.7.6) Voids Content:

The voids content in the composite were determined according to Section (3.6.9) and are shown in Table (3.8). As the variation in voids content was small, for simplicity a constant, mean value of 3% was taken for all specimens.

3.8) Conclusion.

The method of manufacture used throughout this program proved to be efficient in reducing the void content in the composite and minimizing the thermal effects.

For design purposes, it has been shown that the stress/strain relationship is linear. In addition the Tsai approach for predicting the elastic modulus was shown to be in good agreement with experimental results. The lower bound of this theory (i.e. C = 0) was consistently conservative, but not grossly so, and therefore is ideal for design purposes.

Tensile and compressive strengths showed a reasonable agreement with theory, in general agreement was less good for compressive strengths at high fibre volume fractions.

Interlaminar shearing strength showed little variation

3.8) contd.

with increasing fibre content, but it was highly affected, as was the compressive strength, by the void content in the composite.

Flexural properties were always found to approach the tensile properties of the composite and to vary directly with the fibre content.

Finally, it can be seen that, unlike the conventional structural materials, fibre reinforced materials because of their anisotropic behaviour can be controlled by suitable design and manufacture to provide a wide variety of desired structural properties.

OVERALL VOID VOLUME FRACTION

V_v = 0.03

			Theory		Experiment						
					Un-Necked Spec.		Necked Spec.	Poisson's Ratio			
No. of spec.	V_f	Fibre arrange-ment	Modulus N/mm^2	Strength N/mm^2	Modulus N/mm^2	Strength N/mm^2	Strength N/mm^2	Theory	Experiment	Standard Deviation (strength)	Overall mode of failure
5	0	-	4100	49	3214	-	51	0.330	0.360	7.5	Tension
5	0.27	Uni-0°	21500	401	19227	420	438	0.309	0.294	5.2	Splintering
5	0.39	Uni-0°	29900	564	24381	571	565	0.291	0.276	8.1	Splintering
5	0.46	Uni-0°	34800	658	27655	616	627	0.283	0.275	5.6	Splintering
5	0.57	Uni-0°	41900	792	32787	725	740	0.269	0.270	6.2	Splintering
5	0.64	Uni-0°	46800	887	41000	858	830	0.260	0.257	7.3	Splintering
5	0.27	Uni-30°	7720	102	8696	89	94	0.438	0.600	8.5	Tension
5	0.27	Uni-45°	5390	73	8000	60	62	0.406	0.320	9.1	Tension
5	0.27	Uni-60°	4700	57	4762	39	40	0.265	0.270	9.2	Tension
5	0.27	Uni-90°	4730	49	5500	30	32	0.071	0.070	7.5	Tension
5	0.27	Cross-ply 0,90,90,0	12990	319	15152	303	303	0.167	0.100	6.1	Splint & Tension
5	0.27	Angle-ply 45 x 45	5780	73	6250	77	77	0.53	0.370	7.7	Tension
5	0.46	0,45,-45 -45,45,0	17540	356	17790	327	-	0.485	0.320	8.1	Splint & Tension

Table (3 - 4) TENSILE PROPERTIES OF GRP COMPOSITES

* Results of Prismatic specimen

OVERALL VOIDS VOLUME FRACTION

V_v = 0.03

			Theory		Experiment						
					Un-necked Spec.		Necked spec.	Poisson's Ratio			
No. of spec	V_f	fibre arrange-ment	Modulus N/mm^2	Strength N/mm^2	Modulus N/mm^2	Strength N/mm^2	Strength N/mm^2	Theory	experiment	Standard Deviation (strength)	overall mode of failure
5	0	-	4100	91	3226*	94*	-	0.330	0.350	7.1	shear
5	0.27	Uni-0°	21500	310	16129	241	277	0.309	0.300	9.2	shear
5	0.39	Uni-0°	29900	449	23256	317	370	0.291	0.285	10.1	shear
5	0.46	Uni-0°	34800	506	26316	330	380	0.283	0.280	8.7	Delamination
5	0.57	Uni-0°	41900	619	32787	398	385	0.269	0.280	7.6	Delamination
5	0.64	Uni-0°	46800	733	40000	385	365	0.260	0.273	8.5	Delamination
5	0.27	Uni-30°	7720	110	9375	139	145	0.438	0.500	10.2	shear
5	0.27	Uni-45°	5390	90	7692	117	128	0.406	0.580	12.3	shear
5	0.27	Uni-60°	4700	85	5500	100	105	0.265	0.320	11.5	shear
5	0.27	Uni-90°	4730	91	6000	87	90	0.071	0.125	9.5	shear
5	0.27	cross-ply 0,90,90,0	12990	180	18950	194	219	0.167	0.190	8.2	Delamination
5	0.27	Angle-ply 45 x 45	5780	90	8070	110	98	0.53	0.430	8.8	shear
5	0.46	0,45,-45 -45,45,0	17540	195	16670	183	-	0.485	0.320	9.6	Delamination

Table (3-5) Compressive Properties of GRP Composite

$b/t = 2.5$

$E_L/G_{LT} = 10$

$\bar{K} = 1.17$ (From fig. 3-16)

$V_v = 0.03$

			Interlaminar Shear Strength (N/mm^2) (ILSS)						
	No. of spec.	V_f	Bending Theory (voided)	Corrected Bending Theory (Voided)	Corrected Bending Theory (Unvoided)	standard deviation	overall mode of failure	Shear modulus $N/mm^2 \times 10^{-3}$	
span/depth ratio	-	-	4:1	4:1	4:1	-	-	Ext.	Theory
	5	0.27	42.73	50.00	64.77	1.50	shear	3.3	1.8
	5	0.39	41.54	48.60	64.33	2.75	shear	2.6	2.3
	5	0.46	43.98	51.46	69.92	4.20	shear	2.8	2.7
	5	0.37	41.35	48.38	68.14	1.20	shear	3.6	3.4
	5	0.64	38.86	45.47	66.57	4.20	shear	4.0	4.1

Table (3-6) INTERLAMINAR SHEAR STRENGTH TEST RESULTS FOR UNIDIRECTIONAL GRP COMPOSITES

Overall Void Content

$V_v \doteq 0.03$

			Flexural Strength (N/mm^2)				Flexural Modulus (N/mm^2)				Standard Deviation		
	No. of spec.	V_f	$\frac{\Delta}{L}$	$*k'$	Bending Theory	Corrected Bending Theory	$\frac{\Delta}{L}$	$*k'$	Bending Theory	Corrected Bending Theory	Str.	Mod.	Mode of Failure
span/depth ratio	-	-	-	-	40:1	40:1	-	-	100:1	100:1	-	-	-
	5	0.27	0.158	1.156	337	390	0.063	1.040	16423	17080	17.5	95	Compression
	5	0.39	0.113	1.080	556	600	0.045	1.030	23175	23870	10.7	60	Compression
	5	0.46	0.109	1.060	637	675	0.043	1.020	26490	27020	15.3	102	Tension
	5	0.57	0.091	1.050	686	720	0.036	1.010	32366	32690	5.1	115	Tension
	5	0.64	0.071	1.030	815	840	0.028	1.008	40555	40880	12.8	86	Compression

Table (3 - 7)

Flexural Properties of Unidirectional GRP Composites

$*k'$: Correction factor

Density of fibres P_f = 2.54 gm/cm^3

Density of Resin P_m = 1.19 gm/cm^3

No.of Glass Layers	Fibre Content by Weight %	Fibre Content by Volume (V_f)%	Voids Content (V_v)%	Density of Composite (P_m)
4	44.4	27	3.21	1.50 gm/mm^3
5	58.0	39	2.82	1.69 "
6	66.5	46	3.10	1.77 "
7	71.3	57	2.95	1.58 "
8	78.4	64	3.31	2.00

Table (3.8) Voids Content and Densities

NOTE:- An overall void content equal to 0.03 was used throughout the investigation.

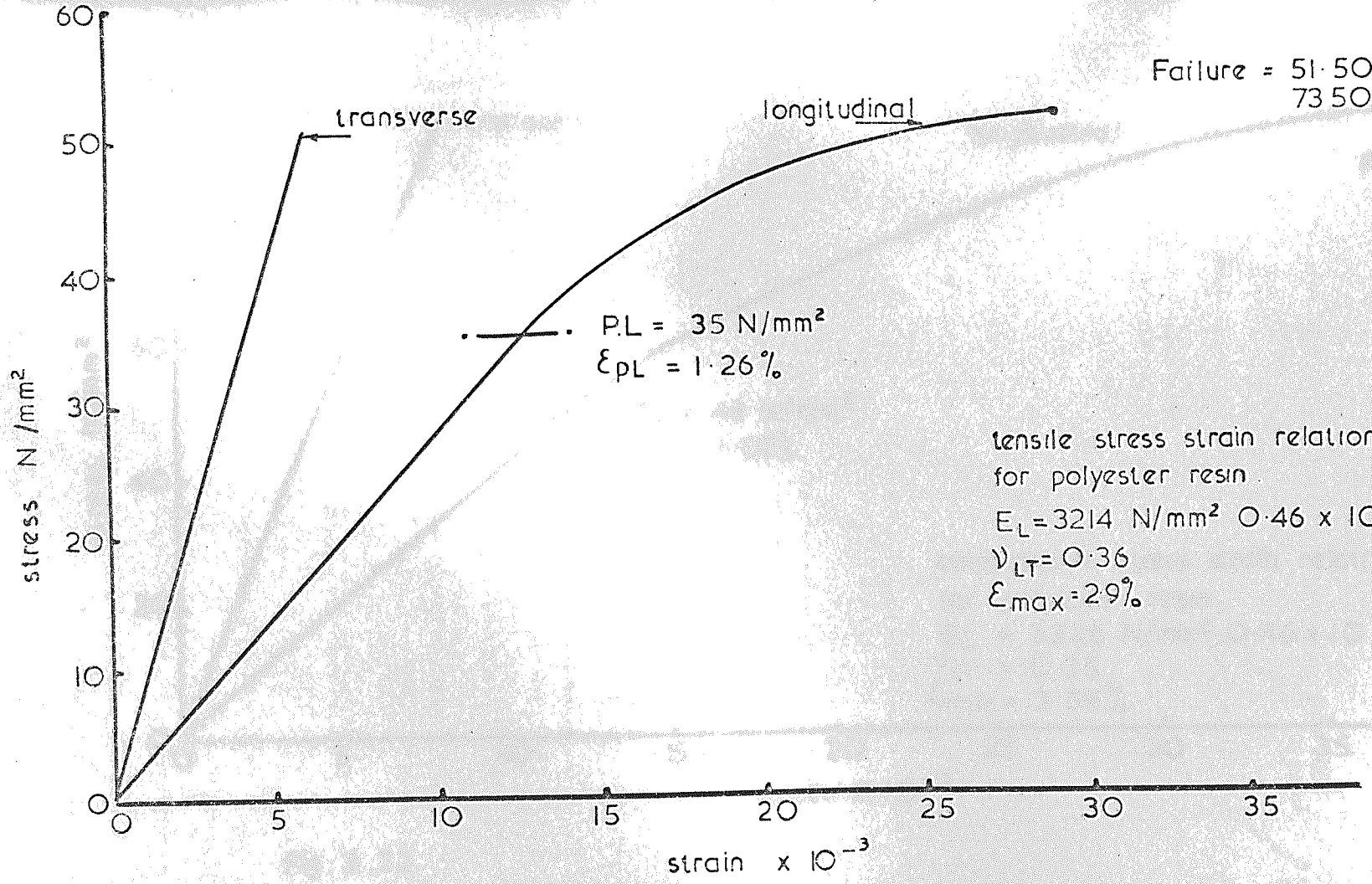
60
50
40
30
20
10
0
stress N/mm²
transverse
longitudinal
Failure = 51·50 N/mm
73·50 psi
P.L = 35 N/mm²
ε_pL = 1·26%
tensile stress strain relationship
for polyester resin
E_L = 3214 N/mm² 0·46 x 10⁶ psi
ν_LT = 0·36
ε_max = 2·9%
0
5
10
15
20
25
30
35
strain x 10⁻³

Fig. 3.21.

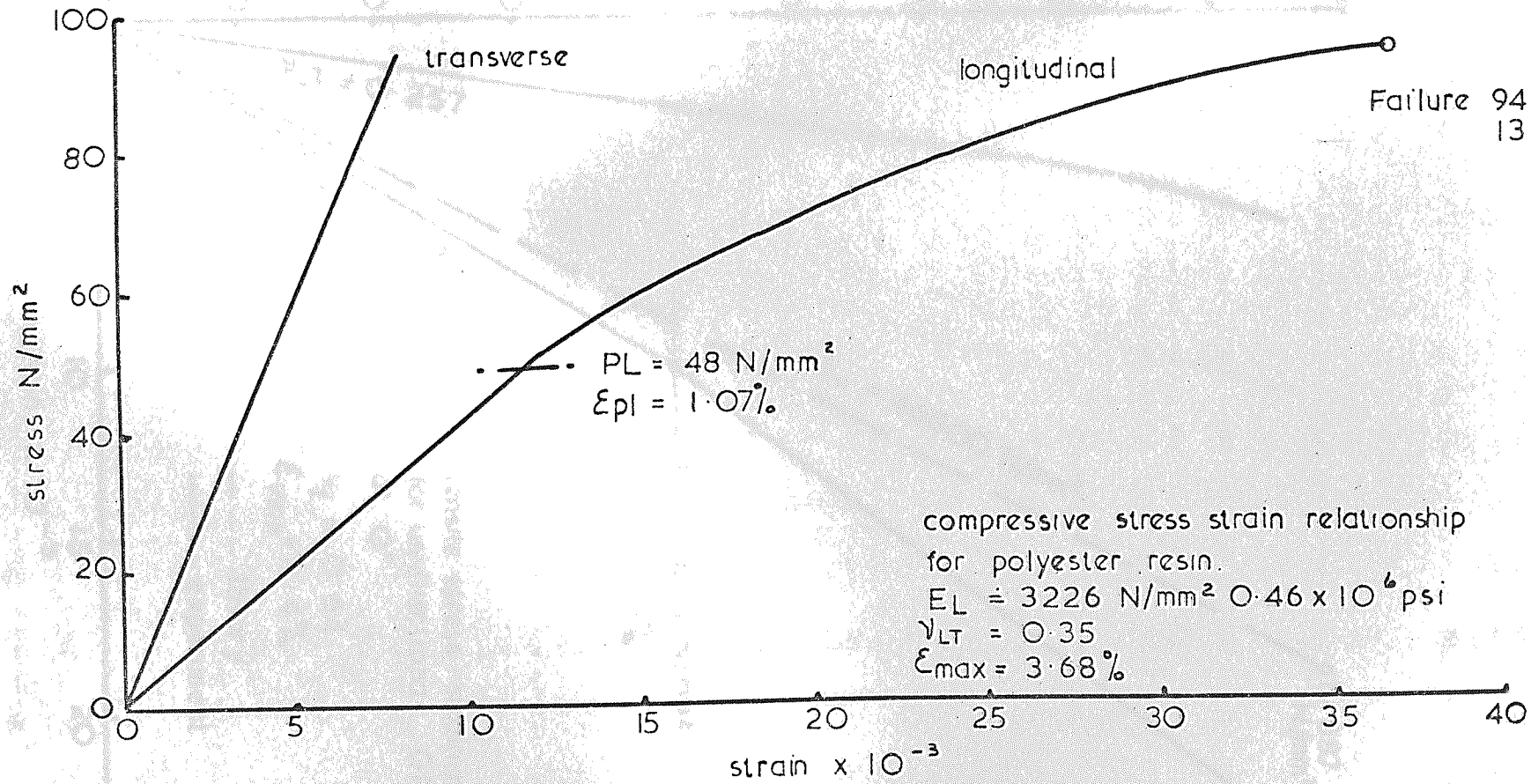
100
80
60
40
20
0
stress N/mm²
transverse
longitudinal
Failure 94.18 N/mm²
13440 psi
PL = 48 N/mm²
εpl = 1·07%
compressive stress strain relationship
for polyester resin.
EL = 3226 N/mm² 0·46 x 10⁶ psi
νLT = 0·35
εmax = 3·68%
0
5
10
15
20
25
30
35
40
strain x 10⁻³

Fig. 3.22.

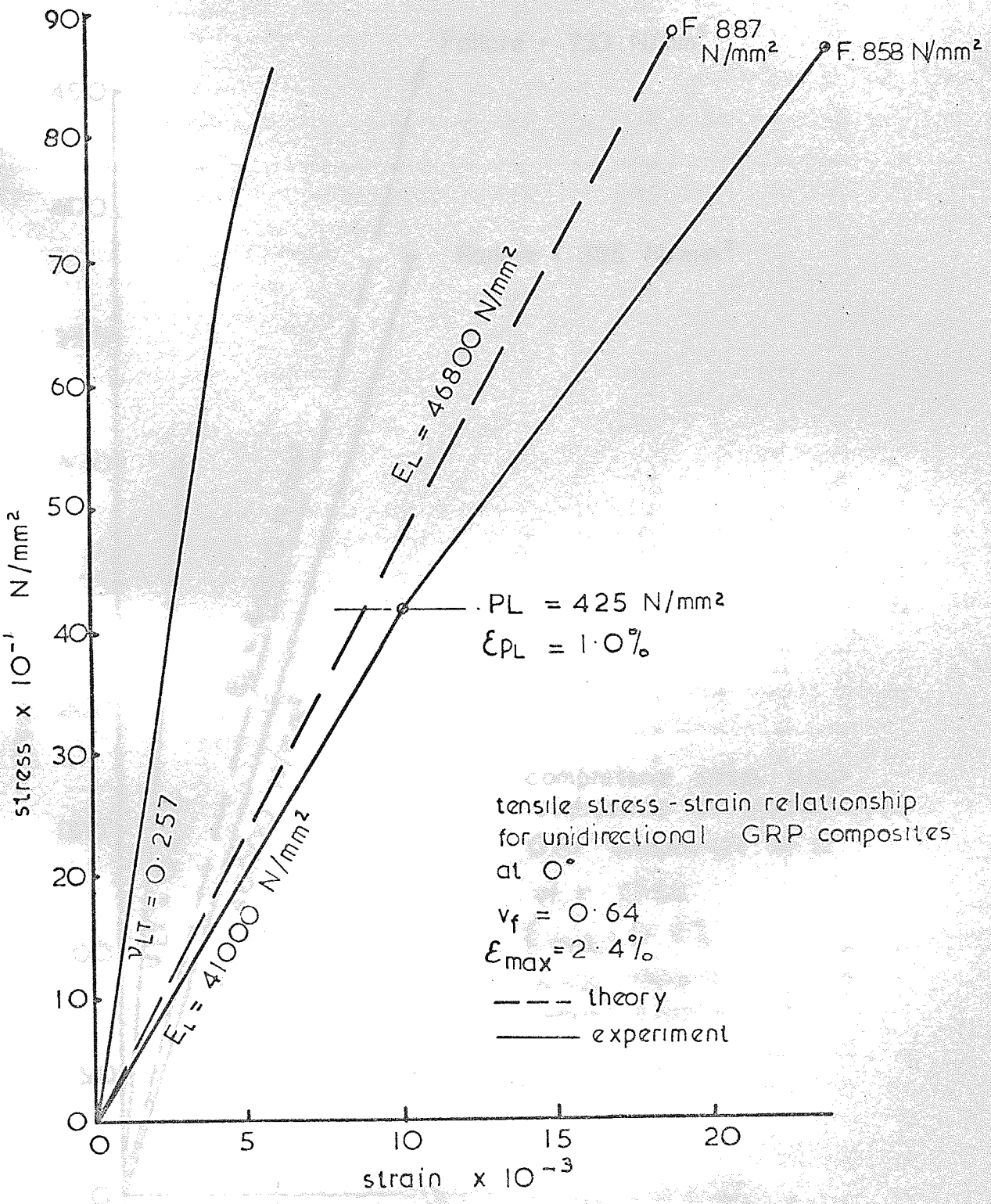
90
80
70
60
50
40
30
20
10
0
stress x 10⁻¹ N/mm²
0
5
10
15
20
strain x 10⁻³
F. 887 N/mm²
F. 858 N/mm²
E_L = 46800 N/mm²
E_L = 41000 N/mm²
ν_LT = 0·257
P_L = 425 N/mm²
ε_PL = 1·0%
tensile stress - strain relationship
for unidirectional GRP composites
at 0°
v_f = 0·64
ε_max = 2·4%
theory
experiment

Fig 3.23.

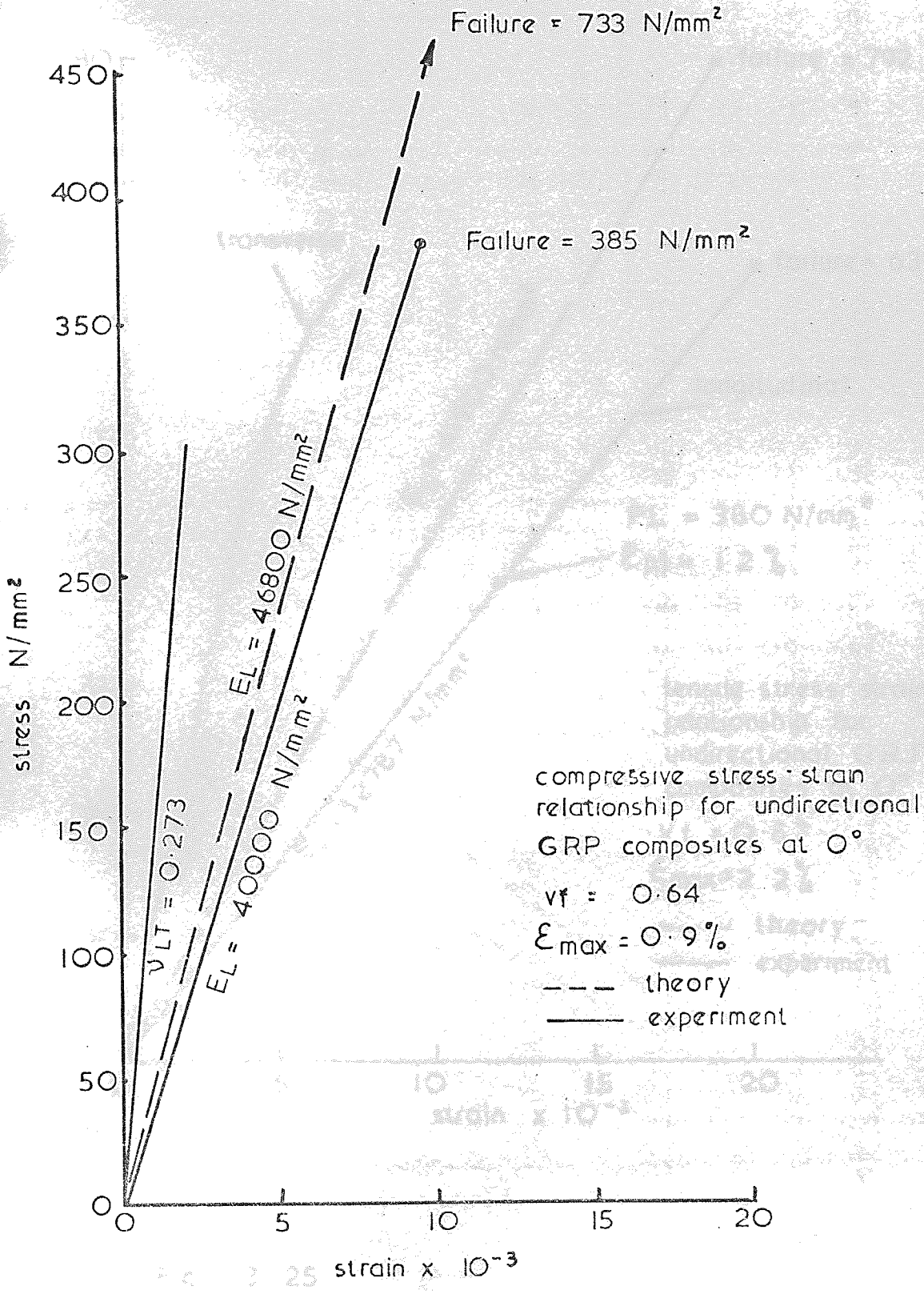
Failure = 733 N/mm²
Failure = 385 N/mm²
450
400
350
300
250
200
150
100
50
0
stress N/mm²
0
5
10
15
20
strain x 10⁻³
EL = 46800 N/mm²
EL = 40000 N/mm²
VLT = 0·273
compressive stress-strain relationship for undirectional GRP composites at 0°
Vf = 0·64
εmax = 0·9%
theory
experiment

Fig. 3.24

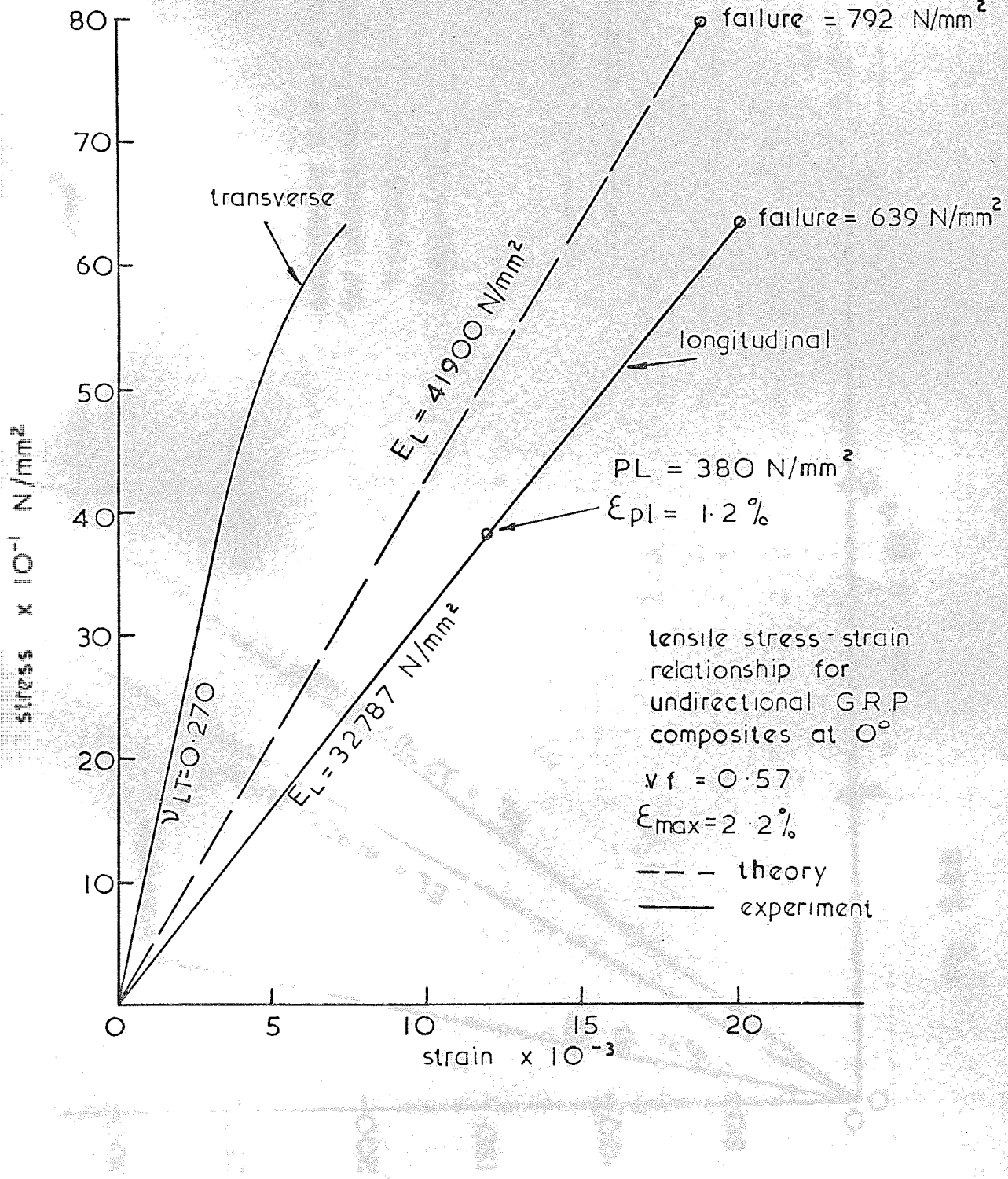
80
70
60
50
40
30
20
10
0
5
10
15
20
stress x 10^{-1} N/mm²
strain x 10^{-3}
failure = 792 N/mm²
failure = 639 N/mm²
transverse
longitudinal
E_L = 41900 N/mm²
E_L = 32787 N/mm²
ν_{LT} = 0·270
PL = 380 N/mm²
ε_{pl} = 1·2 %
tensile stress - strain relationship for undirectional G.R.P composites at 0°
v_f = 0·57
ε_{max} = 2·2 %
theory
experiment

Fig . 3. 25

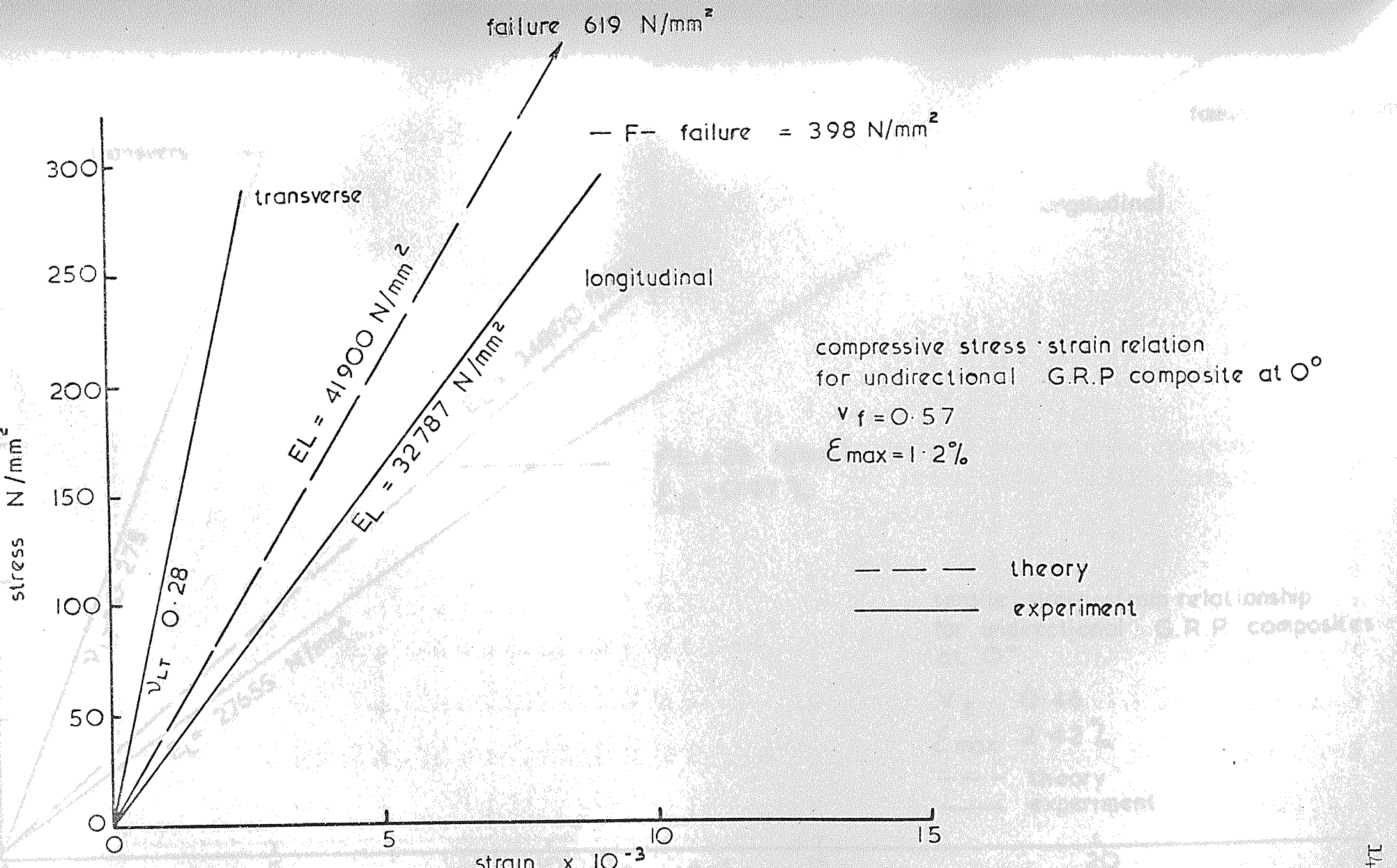
failure 619 N/mm²
— F— failure = 398 N/mm²
transverse
longitudinal
EL = 41900 N/mm²
EL = 32787 N/mm²
υLT 0·28
stress N/mm²
300
250
200
150
100
50
0
0
5
10
15
strain x 10⁻³
compressive stress · strain relation
for undirectional G.R.P composite at 0°
Vf = 0·57
εmax = 1·2%
— — — theory
———— experiment

Fig 3.26

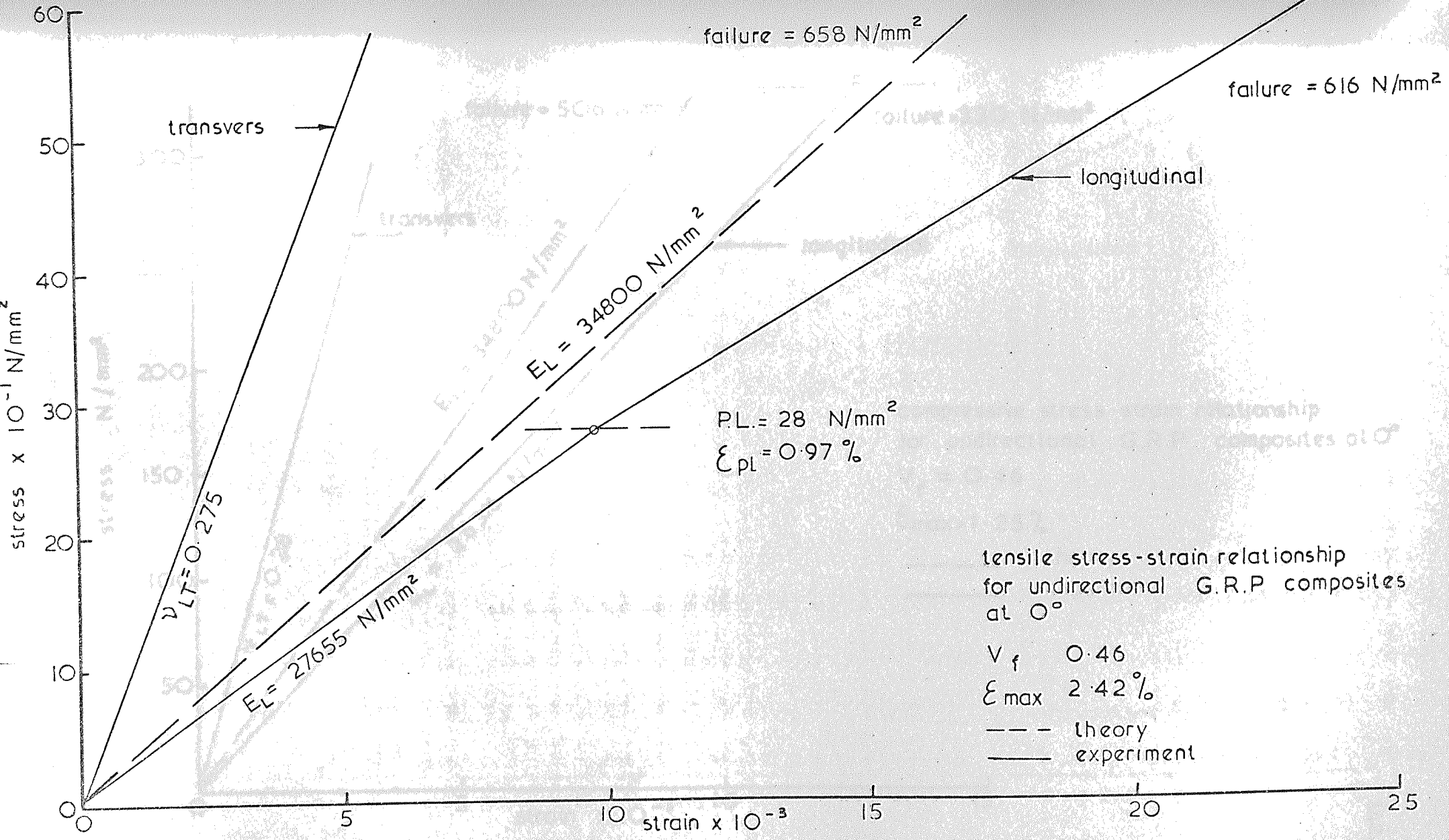
60
50
40
30
20
10
0
stress x 10^{-1} N/mm^2
transvers
failure = 658 N/mm^2
failure = 616 N/mm^2
F
longitudinal
E_L = 34800 N/mm^2
P.L.= 28 N/mm^2
ε_{pl} = 0·97 %
ν_{LT} = 0·275
E_L = 27655 N/mm^2
0
5
10
15
20
25
strain x 10^{-3}
tensile stress-strain relationship
for undirectional G.R.P composites
at 0°
V_f 0·46
ε_{max} 2·42 %
theory
experiment

Fig. 3.27.

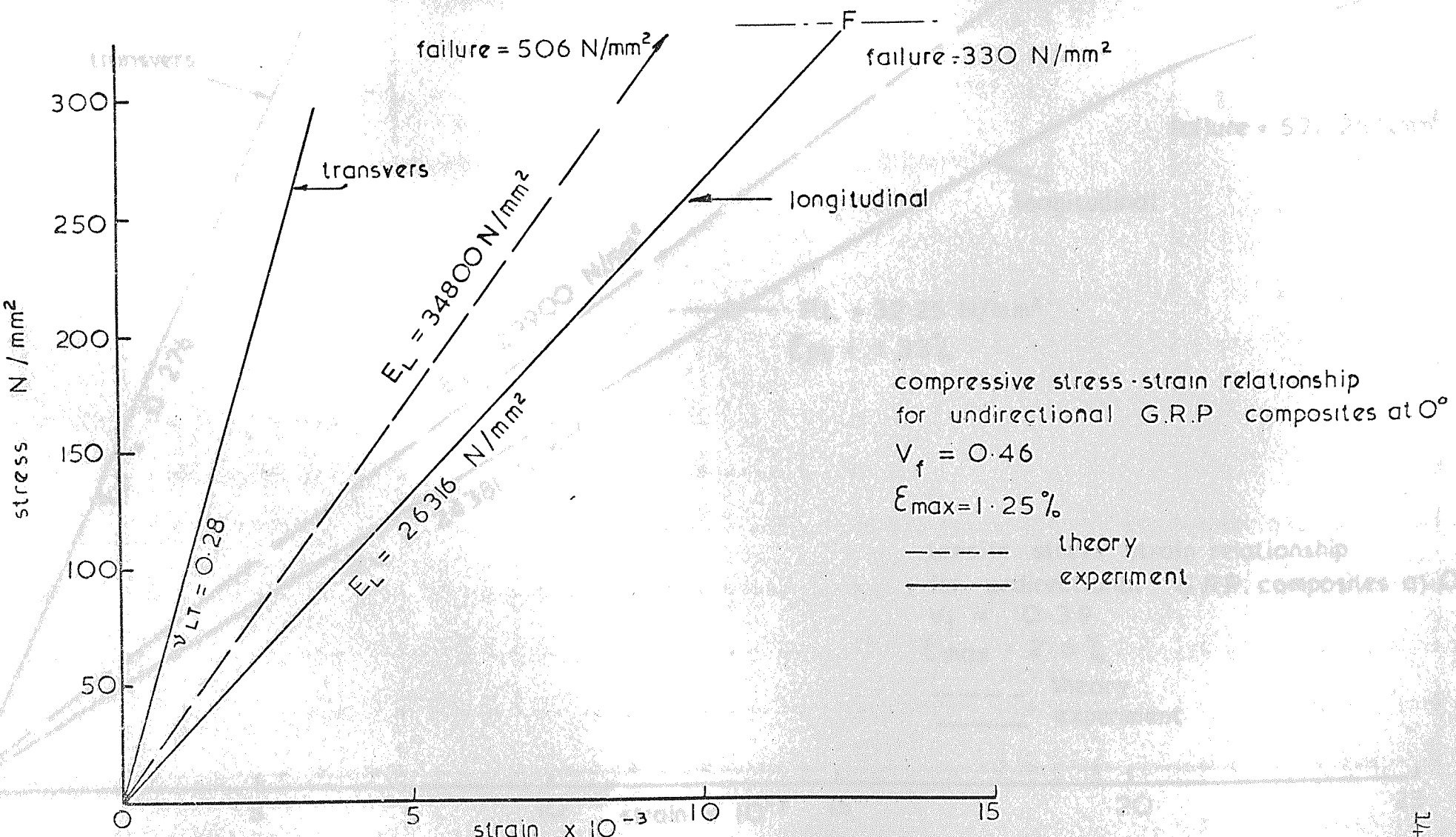
failure = 506 N/mm²
failure -330 N/mm²
F
transvers
longitudinal
E_L = 34800 N/mm²
E_L = 26316 N/mm²
ν_{LT} = 0.28
stress N/mm²
300
250
200
150
100
50
0
5
10
15
strain x 10^{-3}
compressive stress-strain relationship
for undirectional G.R.P composites at 0°
V_f = 0.46
ε_{max} = 1.25 %
theory
experiment

Fig. 3.28.

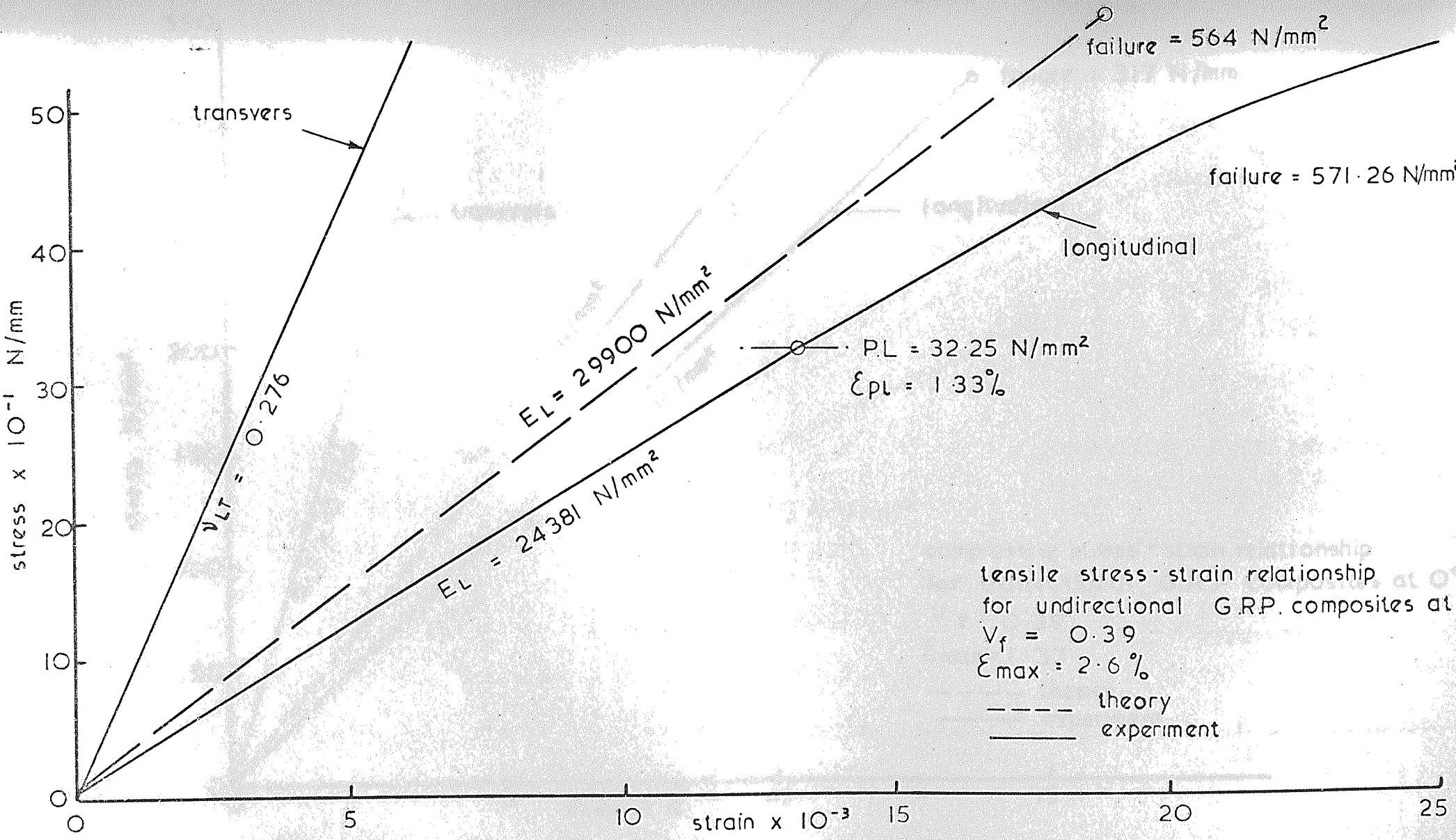
failure = 564 N/mm²
transvers
failure = 571·26 N/mm²
longitudinal
E_L = 29900 N/mm²
P.L = 32·25 N/mm²
ε_pl = 1·33%
ν_LT = 0·276
E_L = 24381 N/mm²
tensile stress · strain relationship
for undirectional G.R.P. composites at 0°
V_f = 0·39
ε_max = 2·6%
theory
experiment
stress x 10⁻¹ N/mm
strain x 10⁻³
0
10
20
30
40
50
5
15
25

Fig. 3.29.

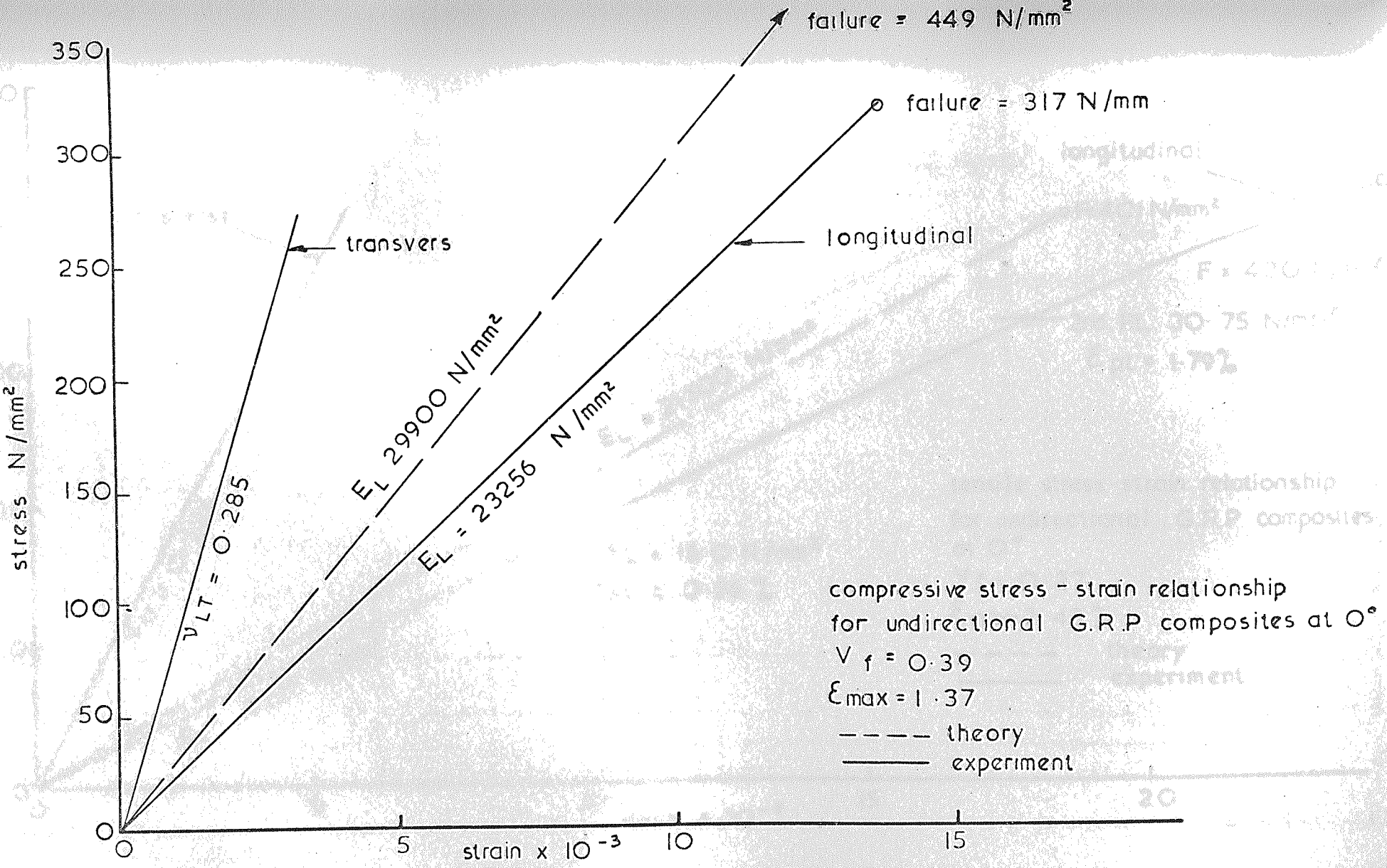
failure = 449 N/mm²
failure = 317 N/mm
transvers
longitudinal
E_L 29900 N/mm²
E_L = 23256 N/mm²
ν_{LT} = 0·285
stress N/mm²
350
300
250
200
150
100
50
0
0
5
10
15
strain x 10⁻³
compressive stress - strain relationship
for undirectional G.R.P composites at 0°
V_f = 0·39
ε_{max} = 1·37
theory
experiment

Fig. . 3.30

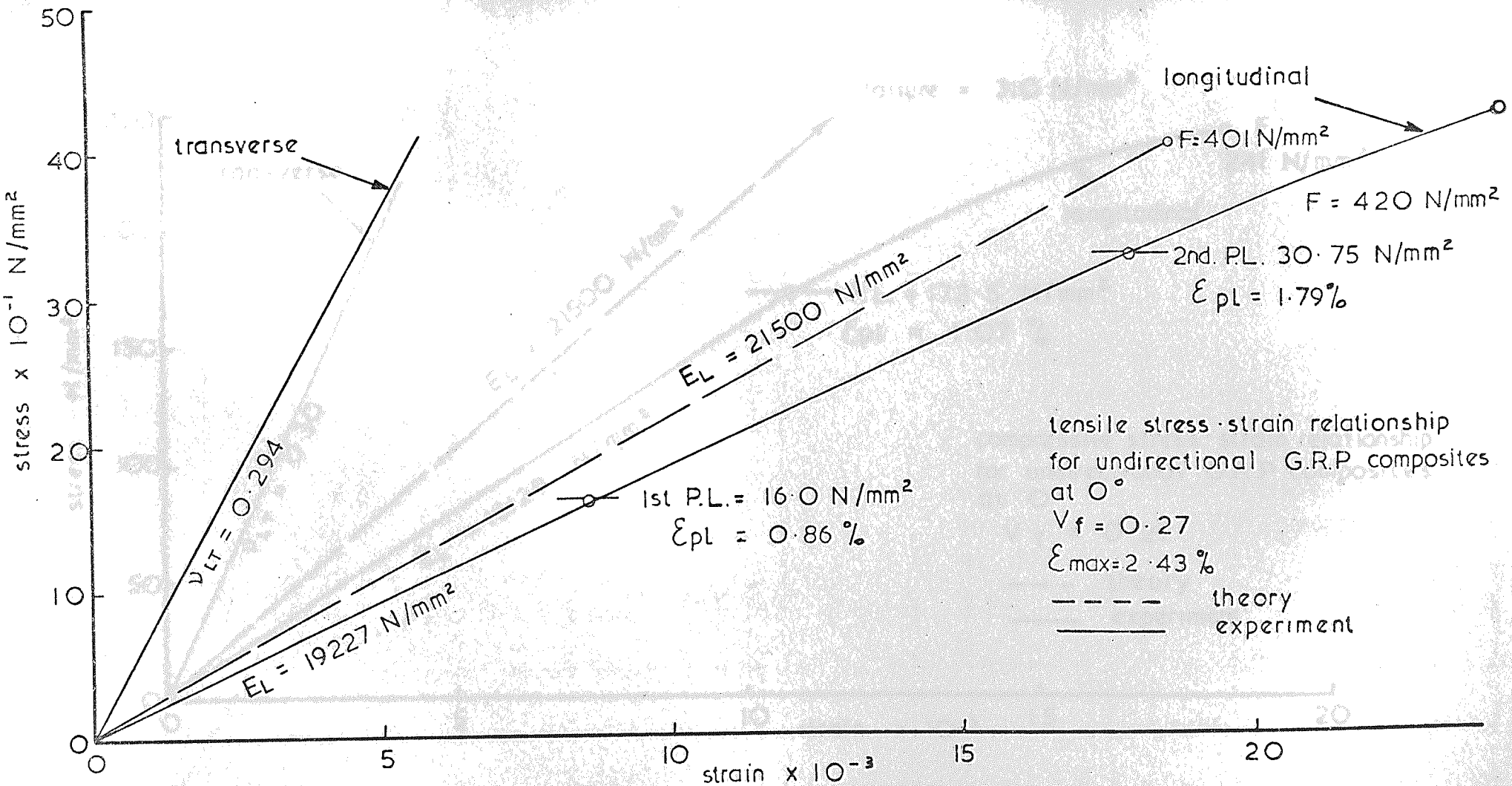
50
40
30
20
10
0
0
5
10
15
20
stress x 10^{-1} N/mm²
strain x 10^{-3}
transverse
$\nu_{LT} = 0.294$
$E_L = 21500$ N/mm²
$E_L = 19227$ N/mm²
longitudinal
F = 401 N/mm²
F = 420 N/mm²
2nd. P.L. 30·75 N/mm²
$\varepsilon_{pl} = 1.79\%$
1st P.L. = 16·0 N/mm²
$\varepsilon_{pl} = 0.86\%$
tensile stress-strain relationship
for undirectional G.R.P composites
at 0°
$V_f = 0.27$
$\varepsilon_{max} = 2.43\%$
theory
experiment

Fig. 3.31

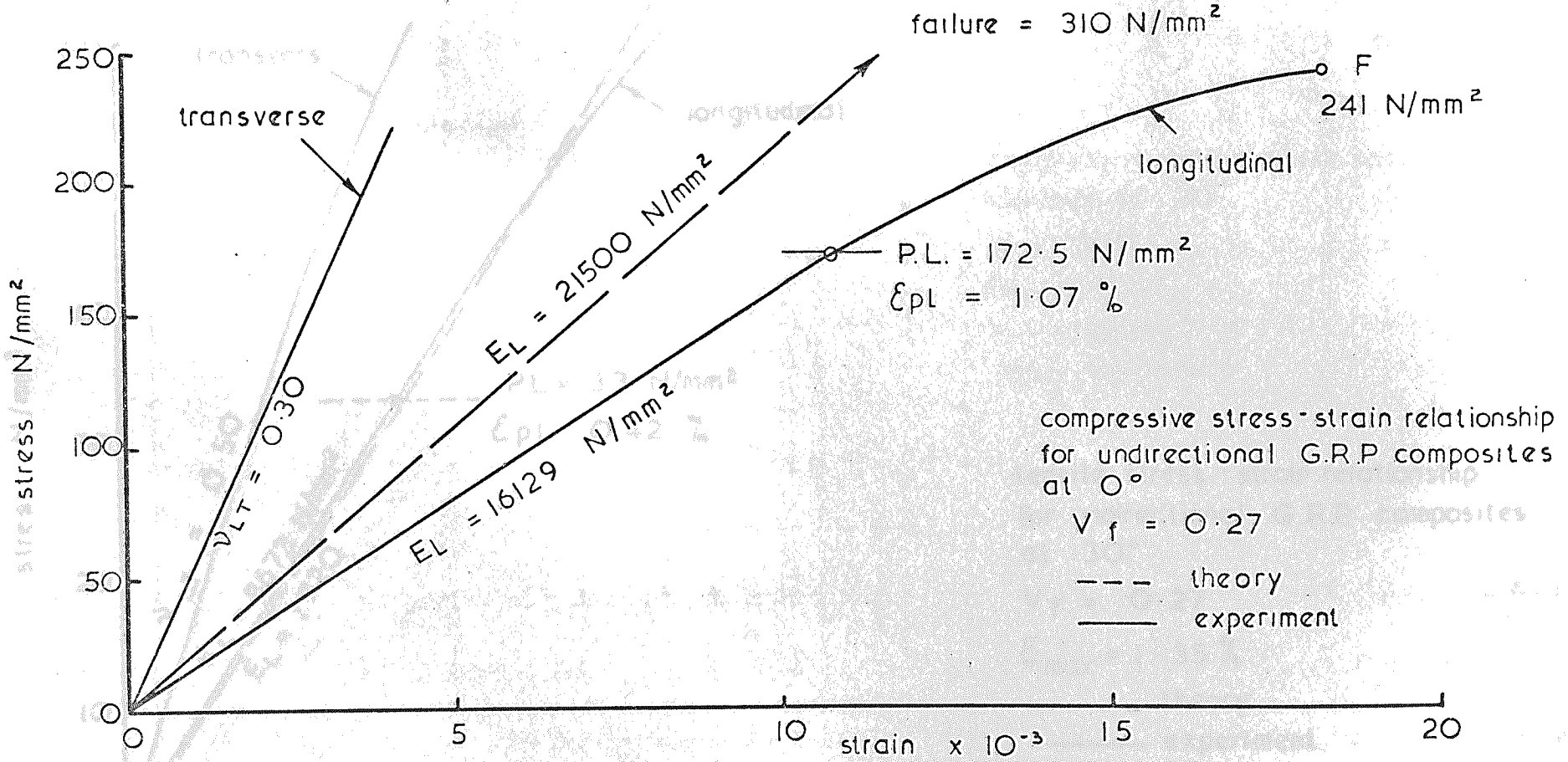
failure = 310 N/mm²
F
241 N/mm²
transverse
longitudinal
E_L = 21500 N/mm²
P.L. = 172·5 N/mm²
ε_pl = 1·07 %
ν_LT = 0·30
E_L = 16129 N/mm²
compressive stress-strain relationship
for undirectional G.R.P composites
at 0°
V_f = 0·27
--- theory
——— experiment
stress N/mm²
strain x 10⁻³
250
200
150
100
50
0
5
10
15
20

Fig. 3.32

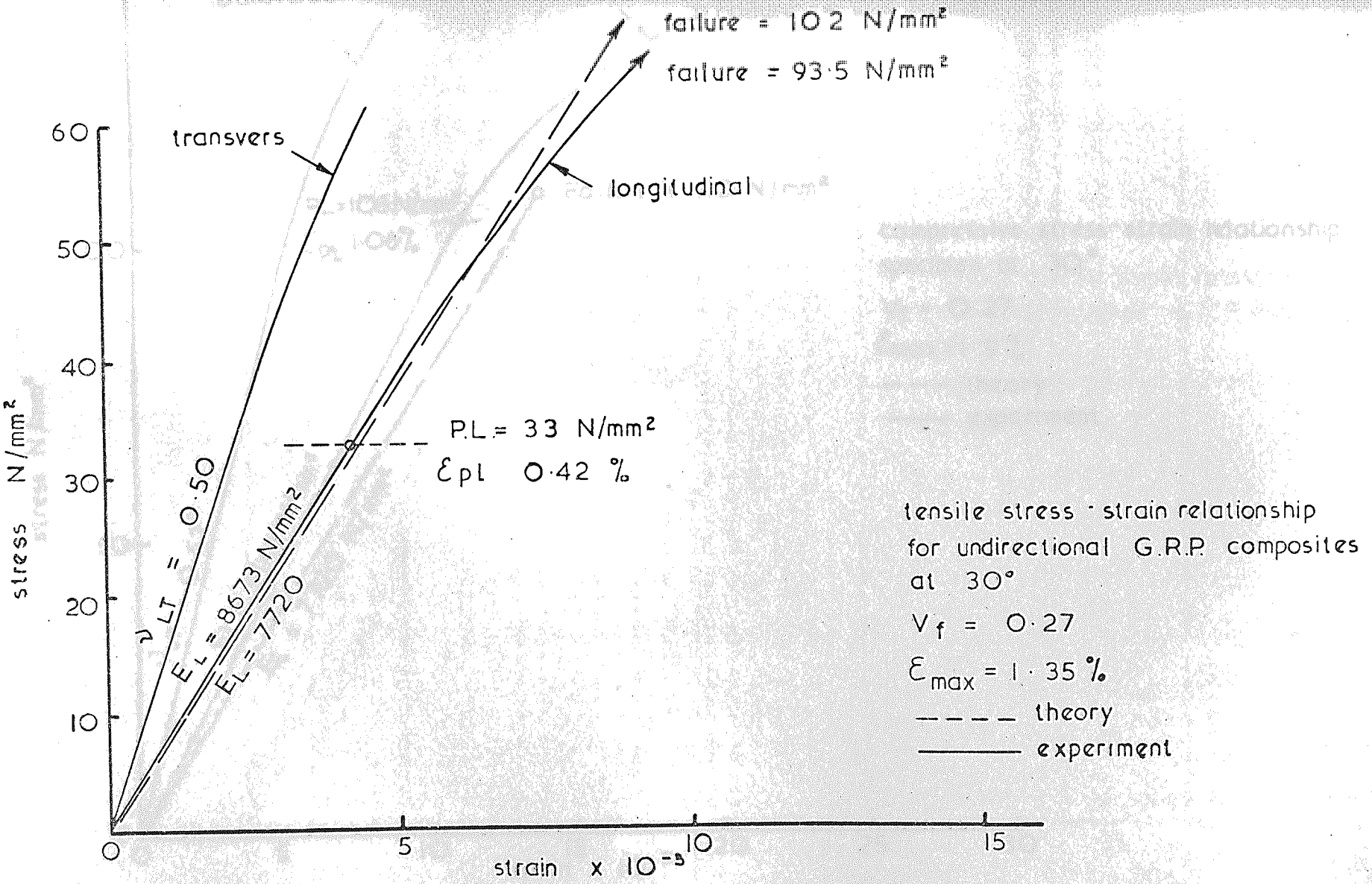

tensile stress - strain relationship
for undirectional G.R.P. composites
at 30°
V_f = 0·27
ε_{max} = 1·35 %
– – – – theory
——— experiment

Fig. 3.33

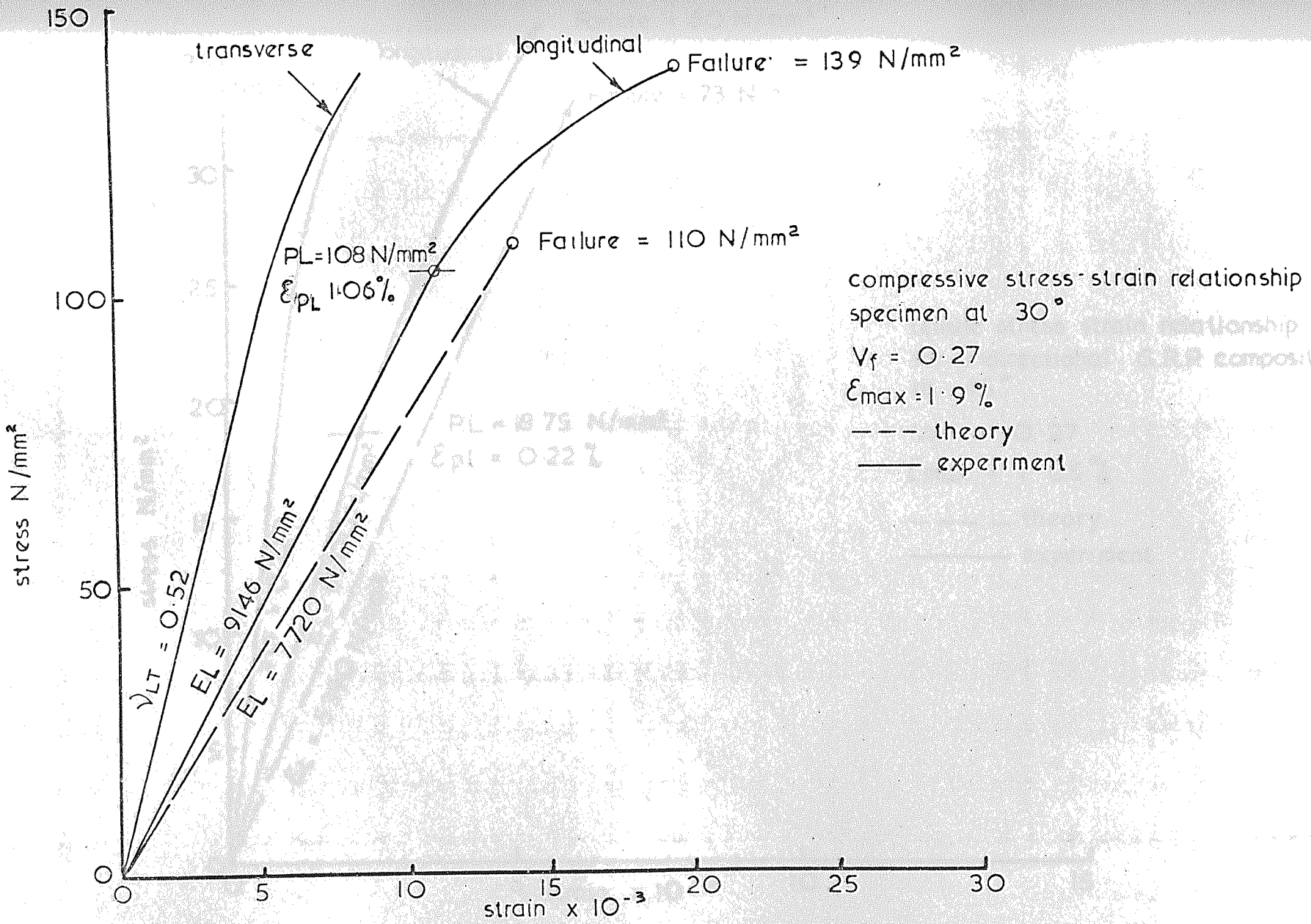
150
100
50
0
stress N/mm²
transverse
longitudinal
Failure = 139 N/mm²
Failure = 110 N/mm²
PL=108 N/mm²
ε_PL 1·06%
ν_LT = 0·52
EL = 9146 N/mm²
EL = 7720 N/mm²
compressive stress-strain relationship
specimen at 30°
V_f = 0·27
ε_max = 1·9 %
--- theory
—— experiment
0
5
10
15
20
25
30
strain x 10⁻³

Fig. 3.34

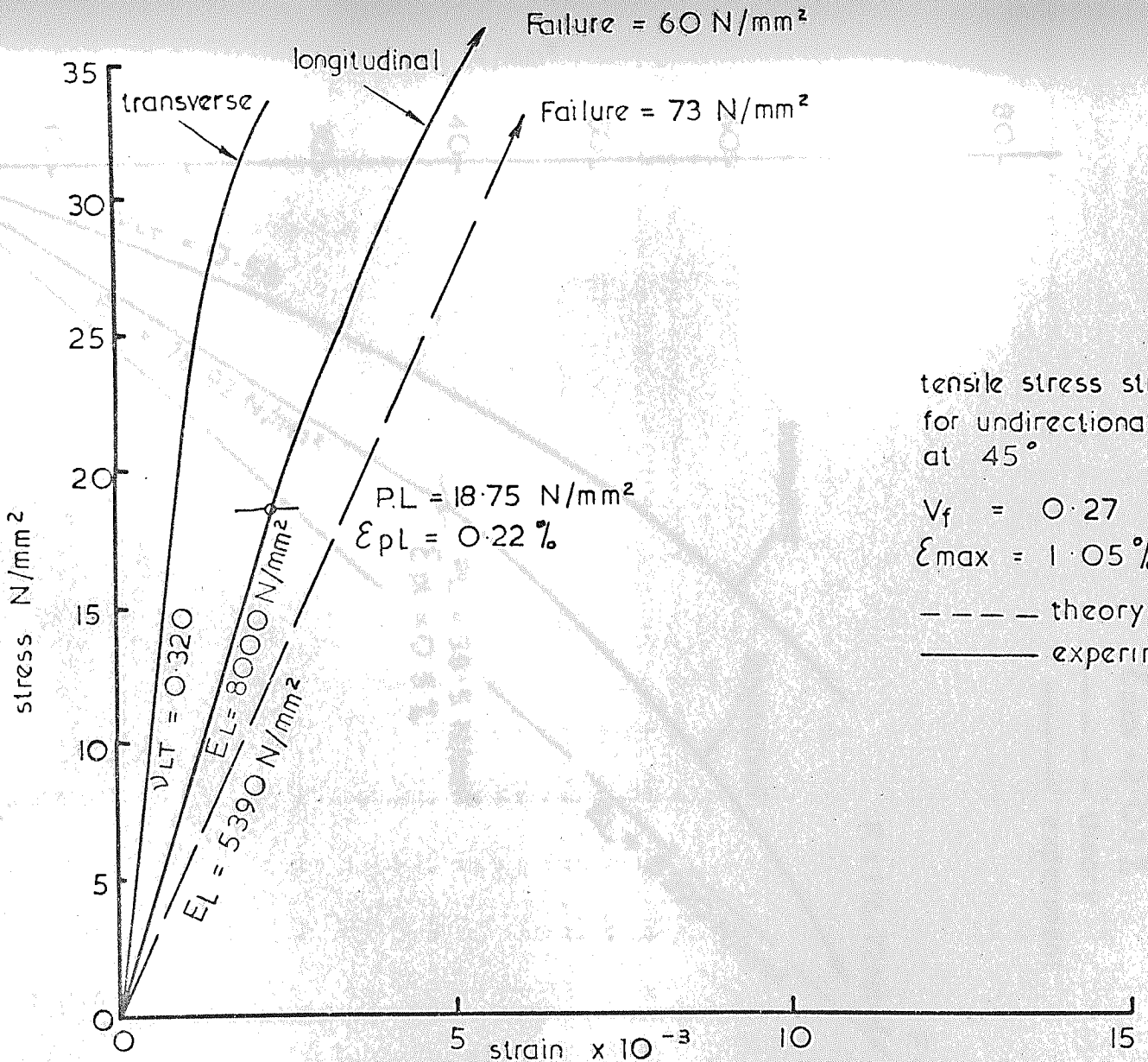

tensile stress strain relationship
for undirectional G.R.P. composites
at 45°

V_f = 0·27

ε_{max} = 1·05 %

– – – – theory

——— experiment

Fig. 3.35

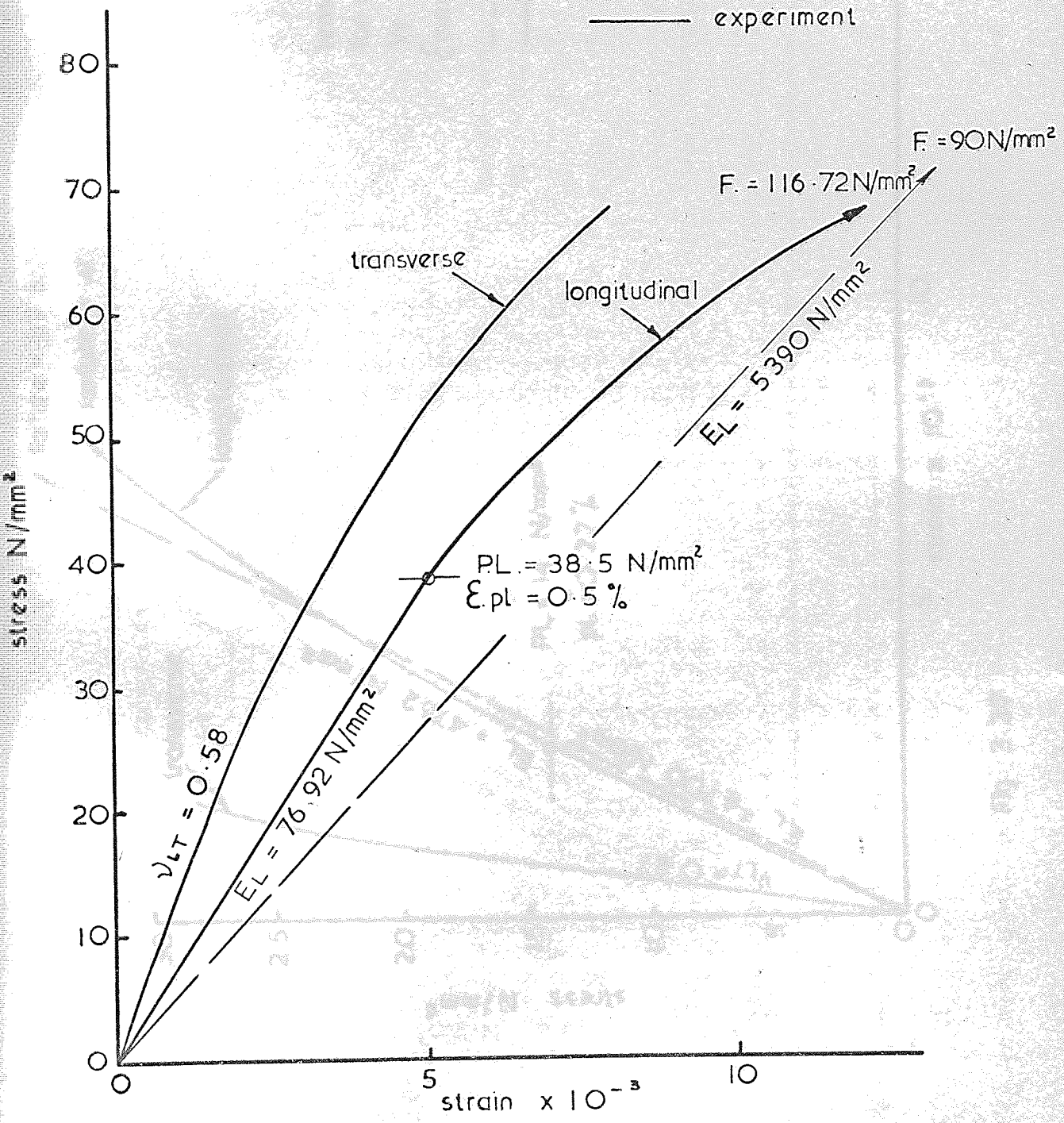
compressive stress - strain
relationship for undirectional
G.R.P. at 45°
V_f = 0·27
ε_{max} = 2·03 %
theory
experiment
F = 90N/mm²
F. = 116·72N/mm²
transverse
longitudinal
EL = 5390 N/mm²
P.L. = 38·5 N/mm²
ε.pl = 0·5 %
ν_{LT} = 0·58
EL = 76·92 N/mm²
stress N/mm²
strain x 10^{-3}
0
10
20
30
40
50
60
70
80
5
10

Fig. 3.36

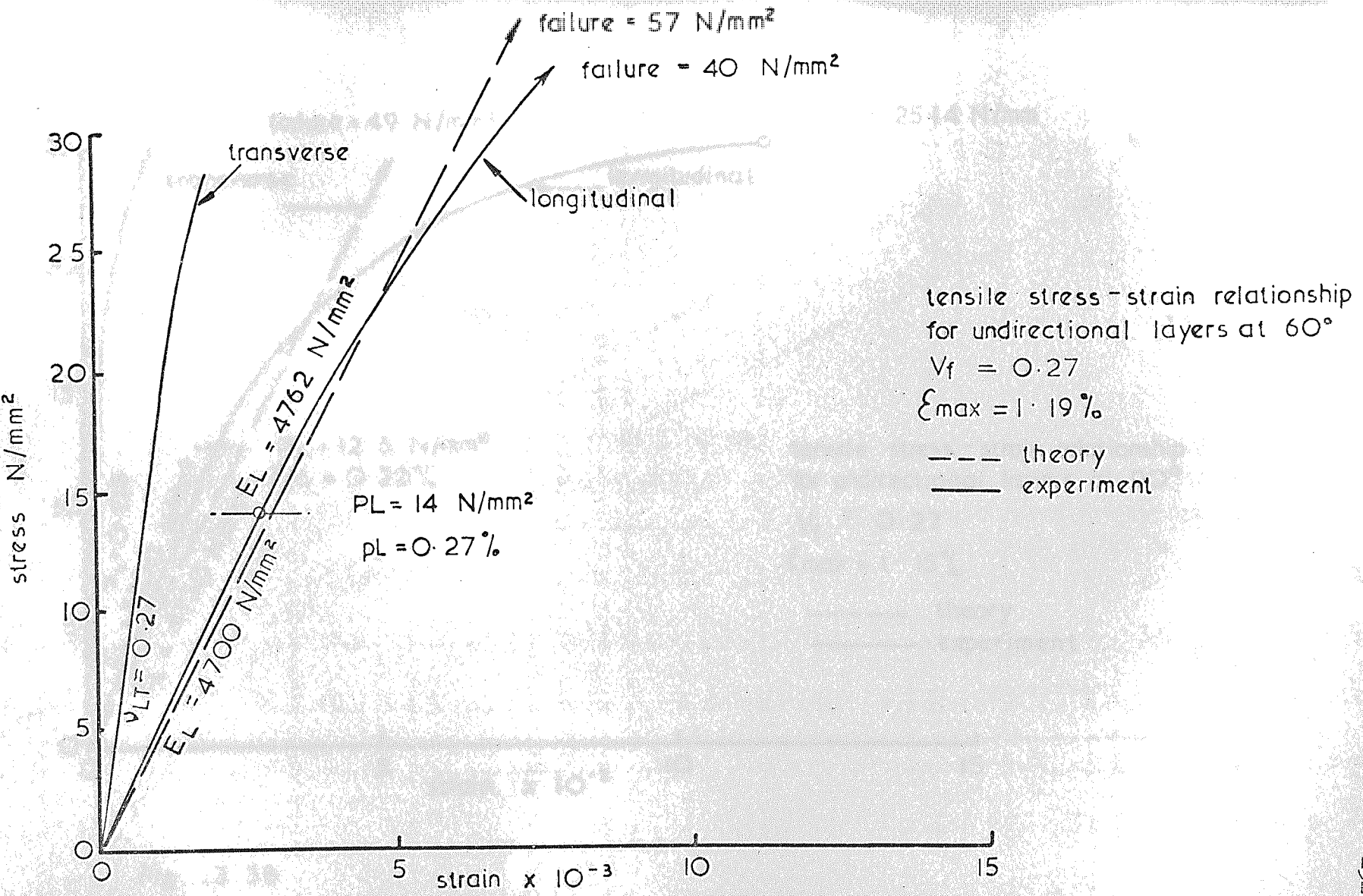

tensile stress - strain relationship
for undirectional layers at 60°
$V_f = 0.27$
$\varepsilon_{max} = 1.19\%$
— — — theory
——— experiment

Fig 3.37

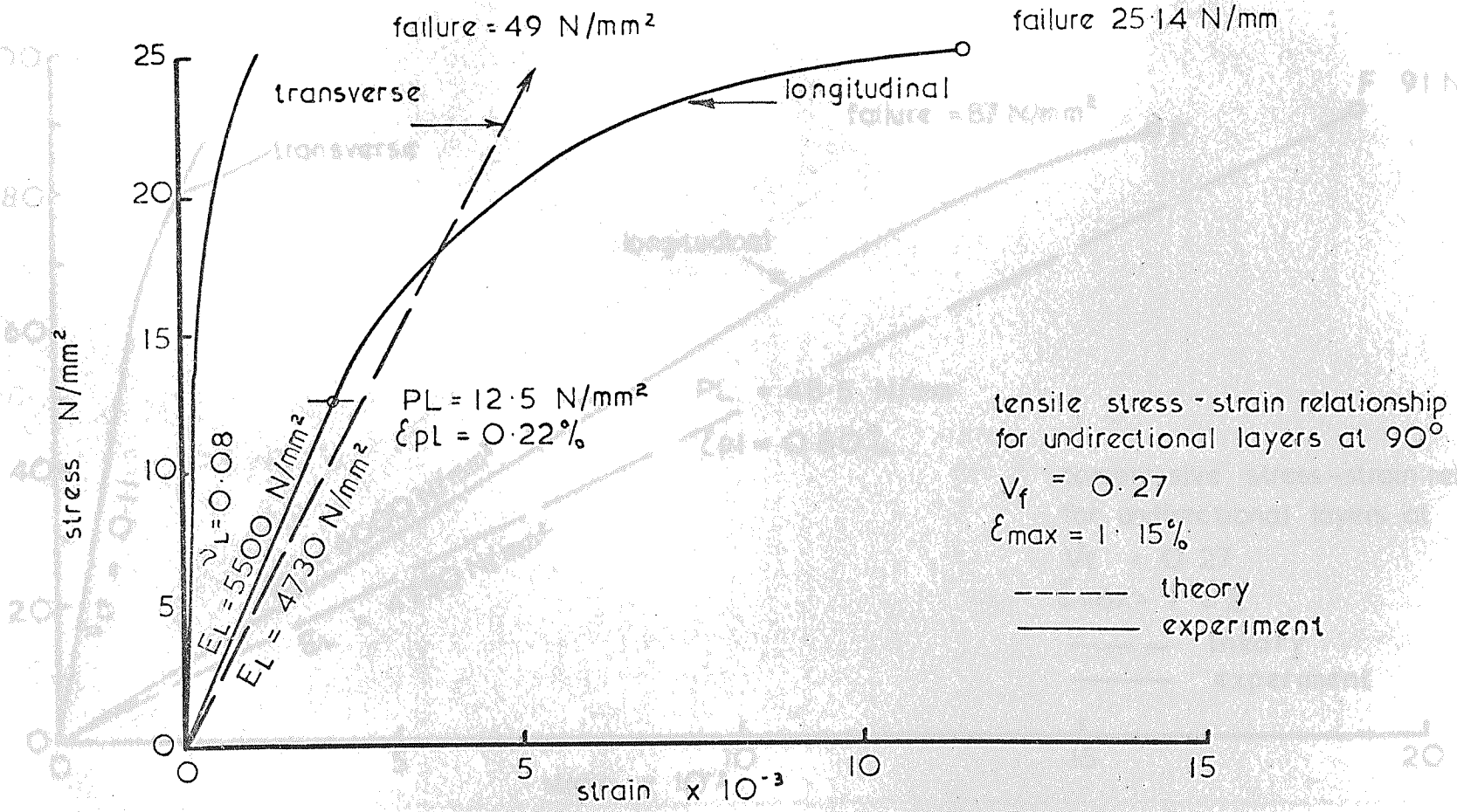
failure = 49 N/mm²
failure 25·14 N/mm
transverse
longitudinal
25
20
15
10
5
0
stress N/mm²
PL = 12·5 N/mm²
εpl = 0·22%
νL = 0·08
EL = 5500 N/mm²
EL = 4730 N/mm²
0
5
10
15
strain x 10⁻³
tensile stress - strain relationship
for undirectional layers at 90°
Vf = 0·27
εmax = 1·15%
theory
experiment

Fig. .3.38

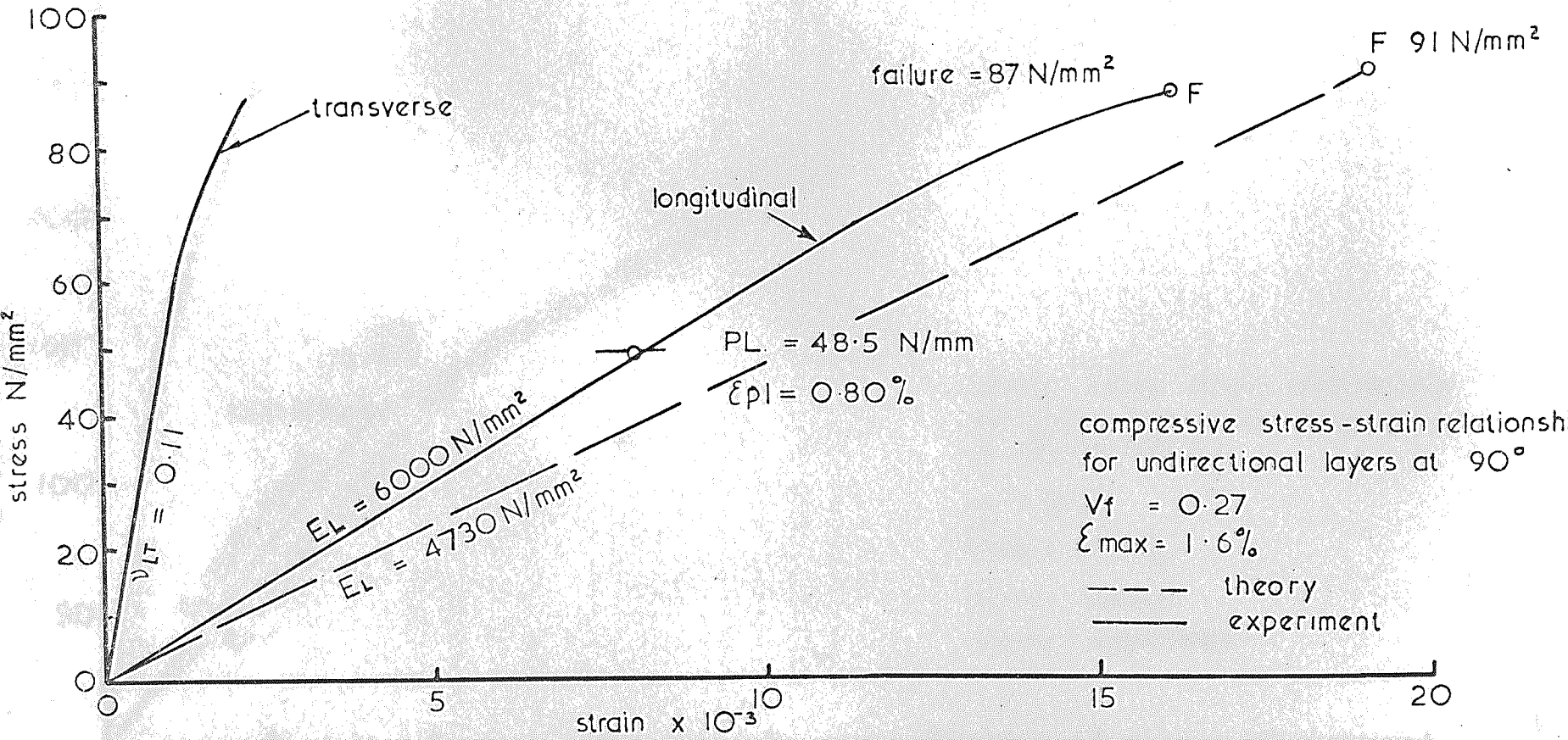
100
80
60
40
20
0
stress N/mm²
transverse
longitudinal
failure = 87 N/mm²
F
F 91 N/mm²
PL. = 48·5 N/mm
εpl = 0·80%
E_L = 6000 N/mm²
E_L = 4730 N/mm²
ν_LT = 0·11
compressive stress-strain relationship
for undirectional layers at 90°
Vf = 0·27
ε max = 1·6%
theory
experiment
0
5
10
15
20
strain x 10⁻³

Fig. 3.39.

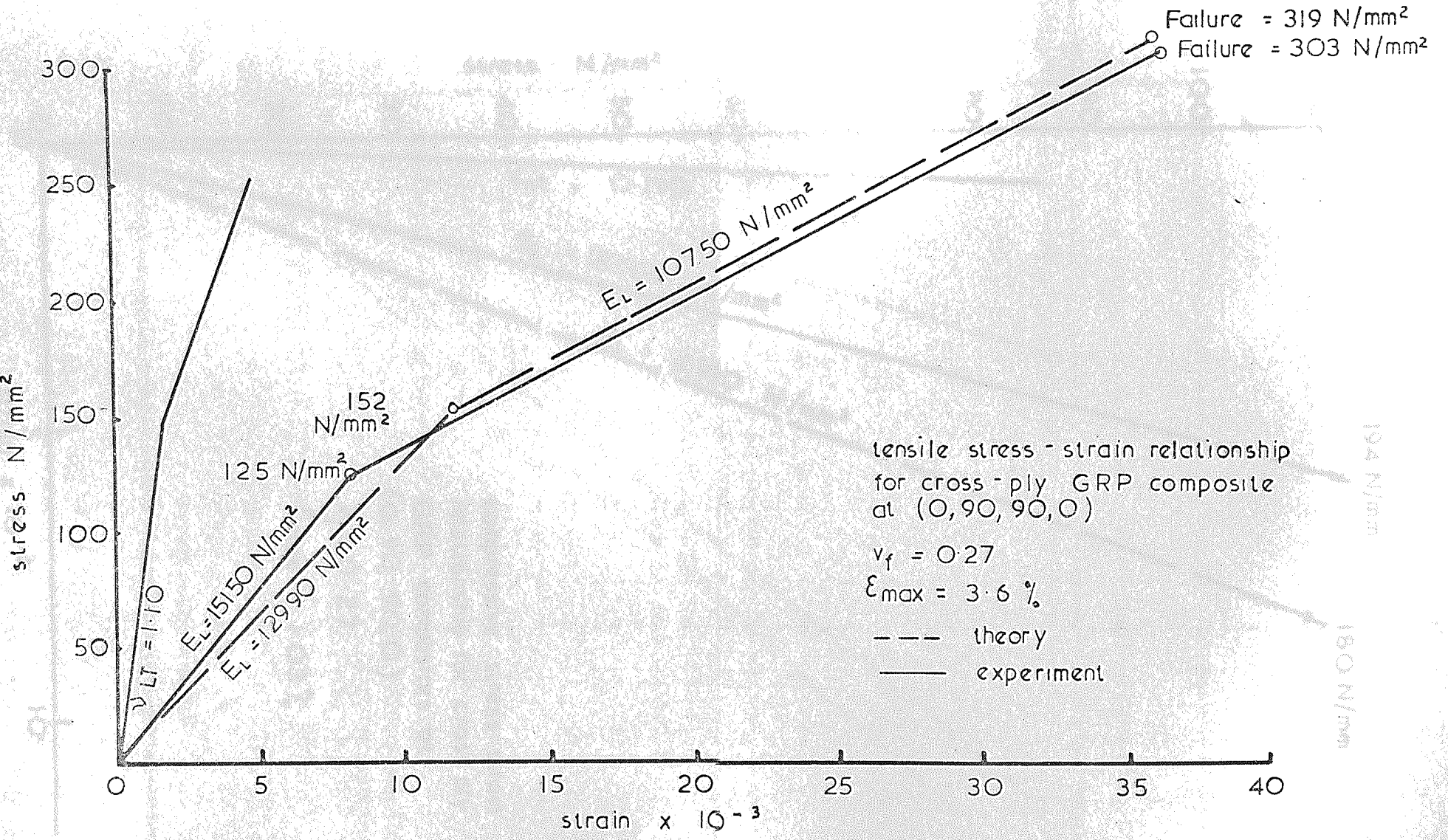
Failure = 319 N/mm²
Failure = 303 N/mm²
300
250
200
150
100
50
stress N/mm²
E_L = 10750 N/mm²
152 N/mm²
125 N/mm²
E_L = 15150 N/mm²
E_L = 12990 N/mm²
ν_{LT} = 1·10
tensile stress - strain relationship for cross - ply GRP composite at (0, 90, 90, 0)
v_f = 0·27
ε_{max} = 3·6 %
theory
experiment
0
5
10
15
20
25
30
35
40
strain x 10^{-3}

Fig. 3.40

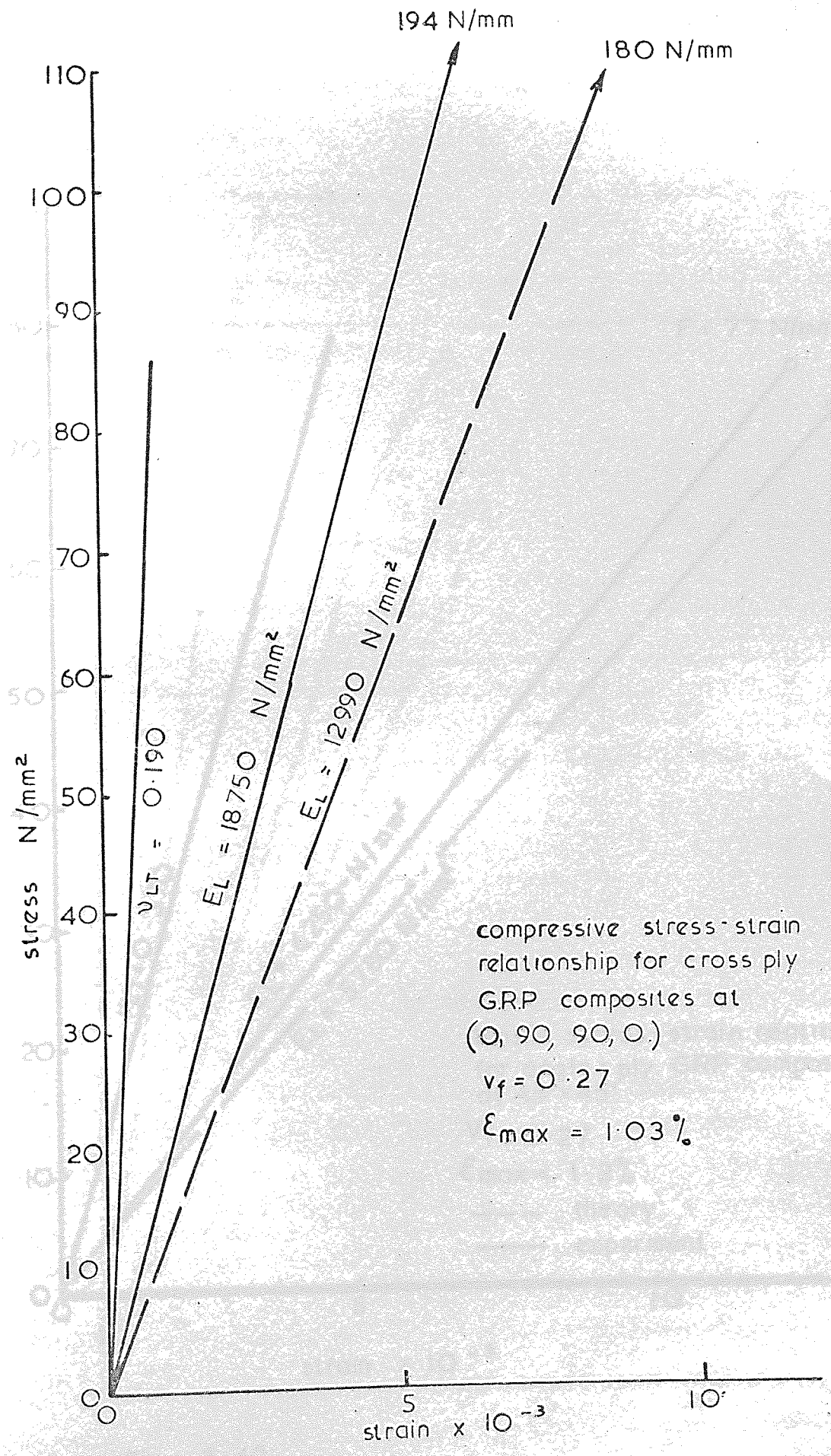
194 N/mm
180 N/mm
110
100
90
80
70
60
50
40
30
20
10
0
stress N/mm²
ν_{LT} = 0·190
E_L = 18750 N/mm²
E_L = 12990 N/mm²
compressive stress-strain relationship for cross ply G.R.P composites at (0, 90, 90, 0)
v_f = 0·27
ε_{max} = 1·03 %
0
5
10
strain x 10^{-3}

Fig 3.41

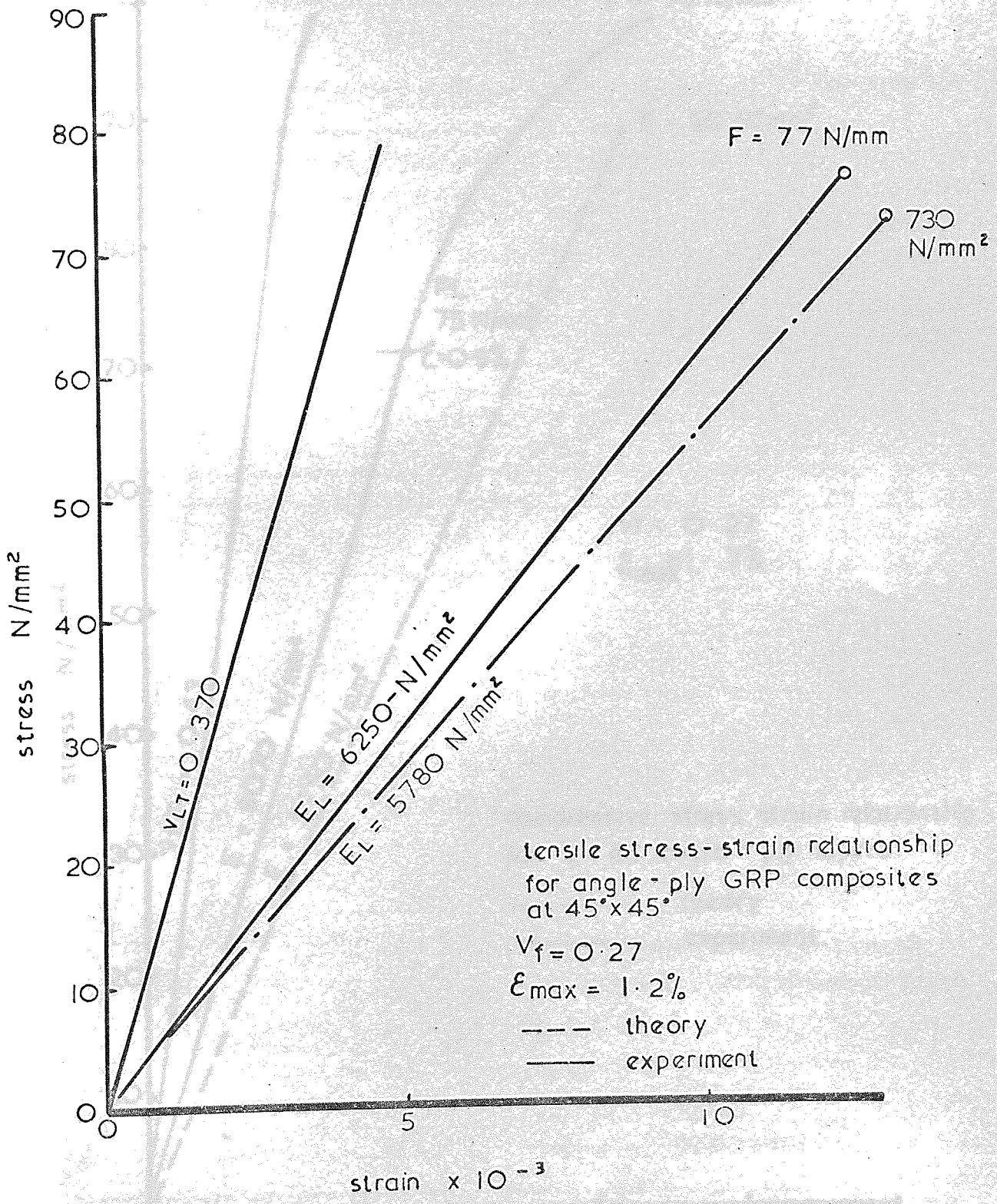
90
80
70
60
50
40
30
20
10
0
0
5
10
stress N/mm²
strain x 10⁻³
F = 77 N/mm
730 N/mm²
ν_LT = 0·370
E_L = 6250 N/mm²
E_L = 5780 N/mm²
tensile stress-strain relationship for angle-ply GRP composites at 45°x45°
V_f = 0·27
ε_max = 1·2%
theory
experiment

Fig. 3.42

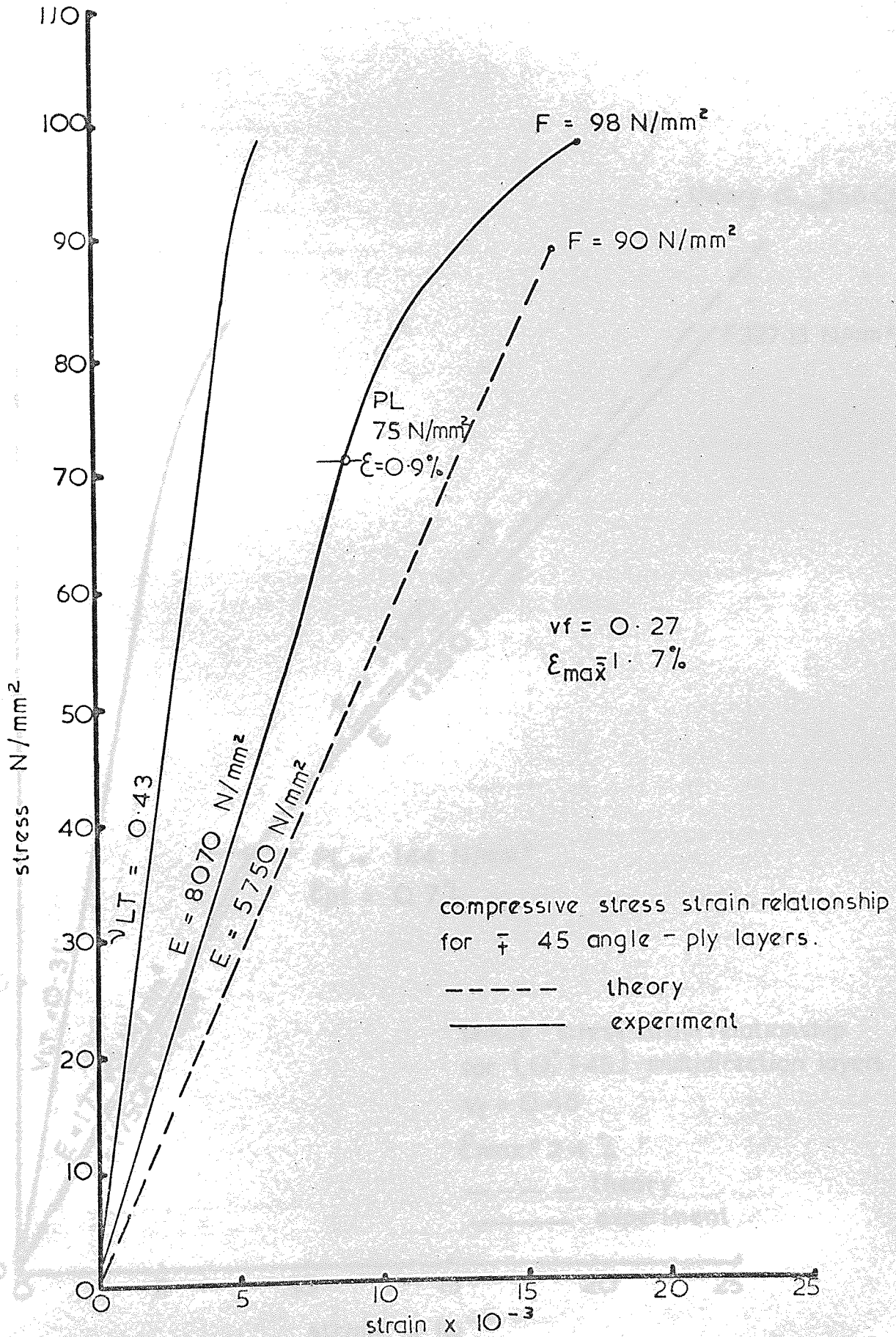
110
100
90
80
70
60
50
40
30
20
10
0
stress N/mm²
0
5
10
15
20
25
strain x 10⁻³
F = 98 N/mm²
F = 90 N/mm²
PL
75 N/mm²
ε=0·9%
νLT = 0·43
E = 8070 N/mm²
E = 5750 N/mm²
vf = 0·27
εmax = 1·7%
compressive stress strain relationship
for ∓ 45 angle - ply layers.
theory
experiment

Fig 3.43

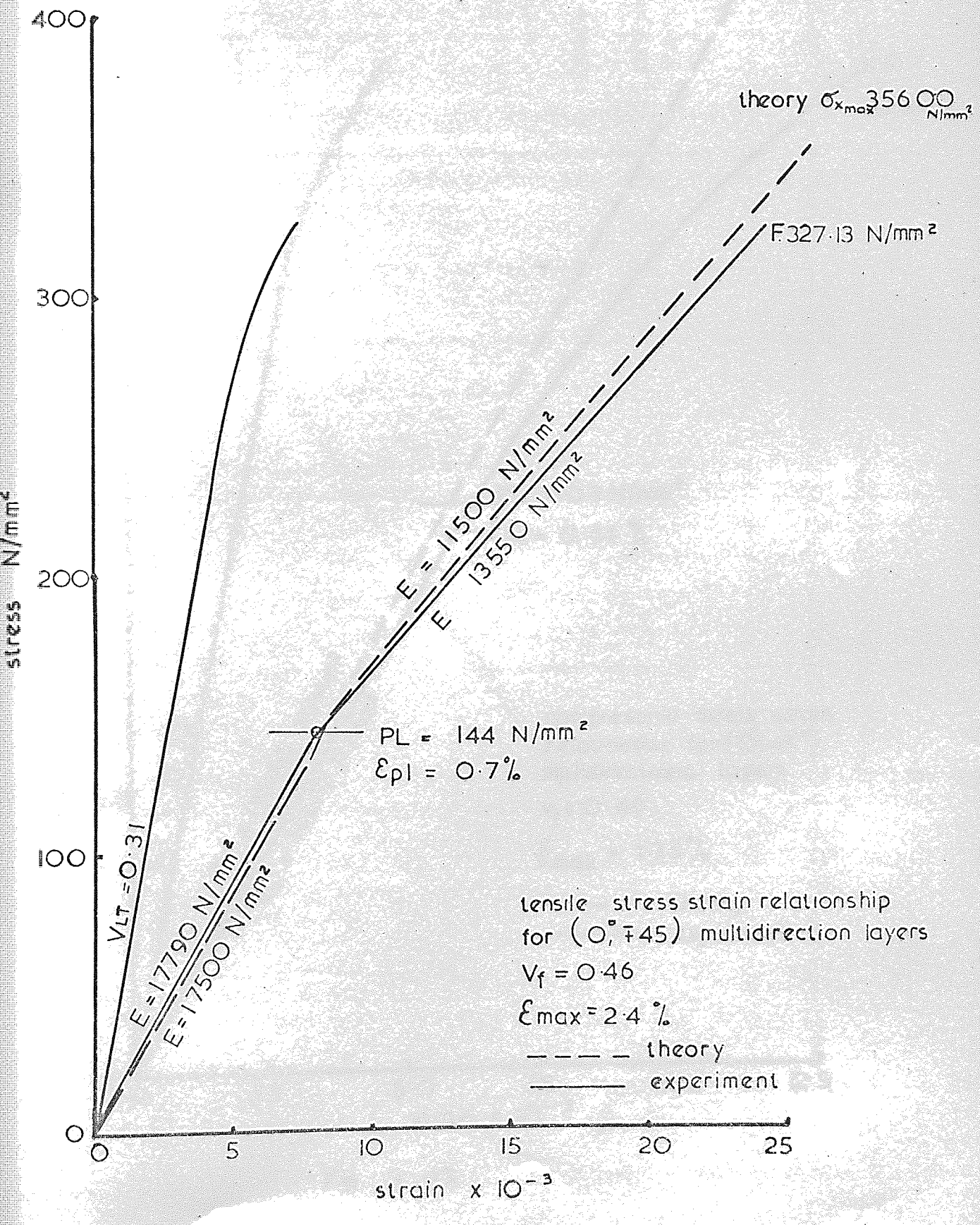
400
300
200
100
0
stress N/mm²
0
5
10
15
20
25
strain x 10⁻³
theory σx max 35600 N/mm²
F 327·13 N/mm²
E = 11500 N/mm²
E 13550 N/mm²
PL = 144 N/mm²
εpl = 0·7%
VLT = 0·31
E = 17790 N/mm²
E = 17500 N/mm²
tensile stress strain relationship
for (0°, ∓45) multidirection layers
Vf = 0·46
εmax = 2·4 %
theory
experiment

Fig. 3. 44

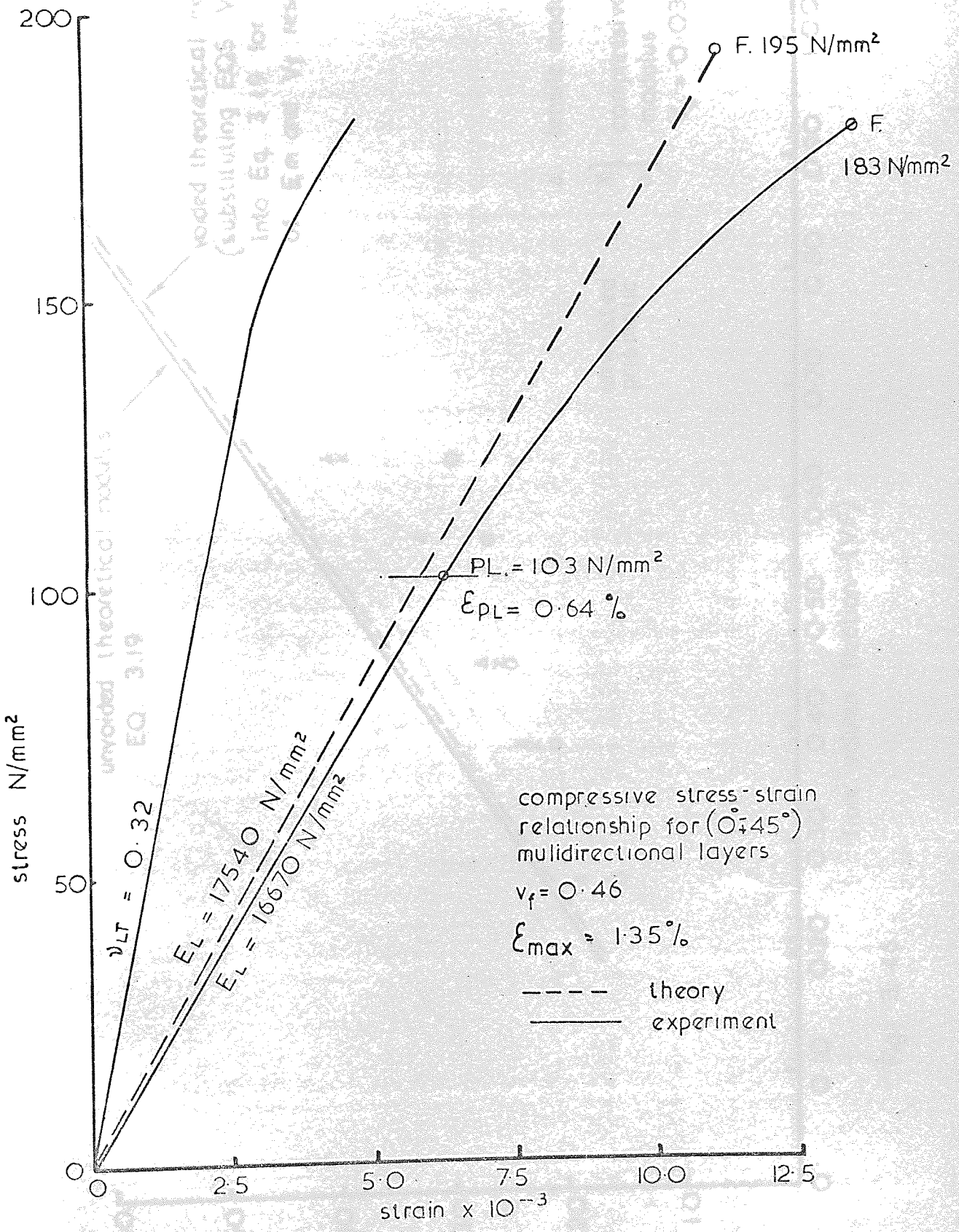
200
150
100
50
0
stress N/mm²
F. 195 N/mm²
F.
183 N/mm²
PL. = 103 N/mm²
ε_{PL} = 0·64 %
ν_{LT} = 0·32
E_L = 17540 N/mm²
E_L = 16670 N/mm²
compressive stress-strain
relationship for (0°∓45°)
mulidirectional layers
v_f = 0·46
ε_{max} = 1·35 %
theory
experiment
0
2·5
5·0
7·5
10·0
12·5
strain x 10^{-3}

Fig. 3.45

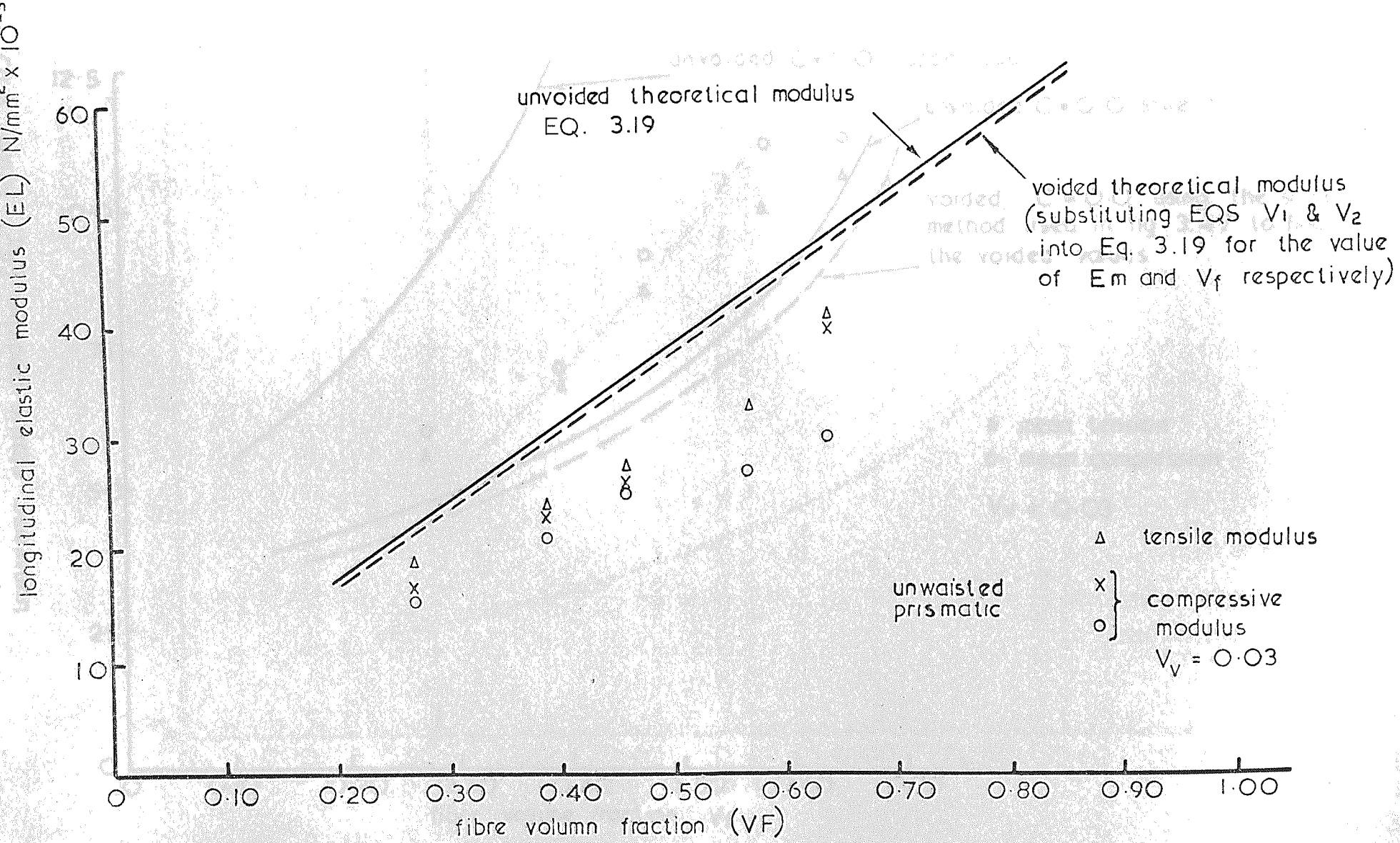
longitudinal elastic modulus (EL) N/mm² x 10⁻³
60
50
40
30
20
10
0
0·10
0·20
0·30
0·40
0·50
0·60
0·70
0·80
0·90
1·00
fibre volumn fraction (VF)
unvoided theoretical modulus
EQ. 3.19
voided theoretical modulus
(substituting EQS V1 & V2
into Eq. 3.19 for the value
of Em and Vf respectively)
Δ tensile modulus
unwaisted
prismatic
X
O
compressive
modulus
Vv = 0·03

Fig. 3.46

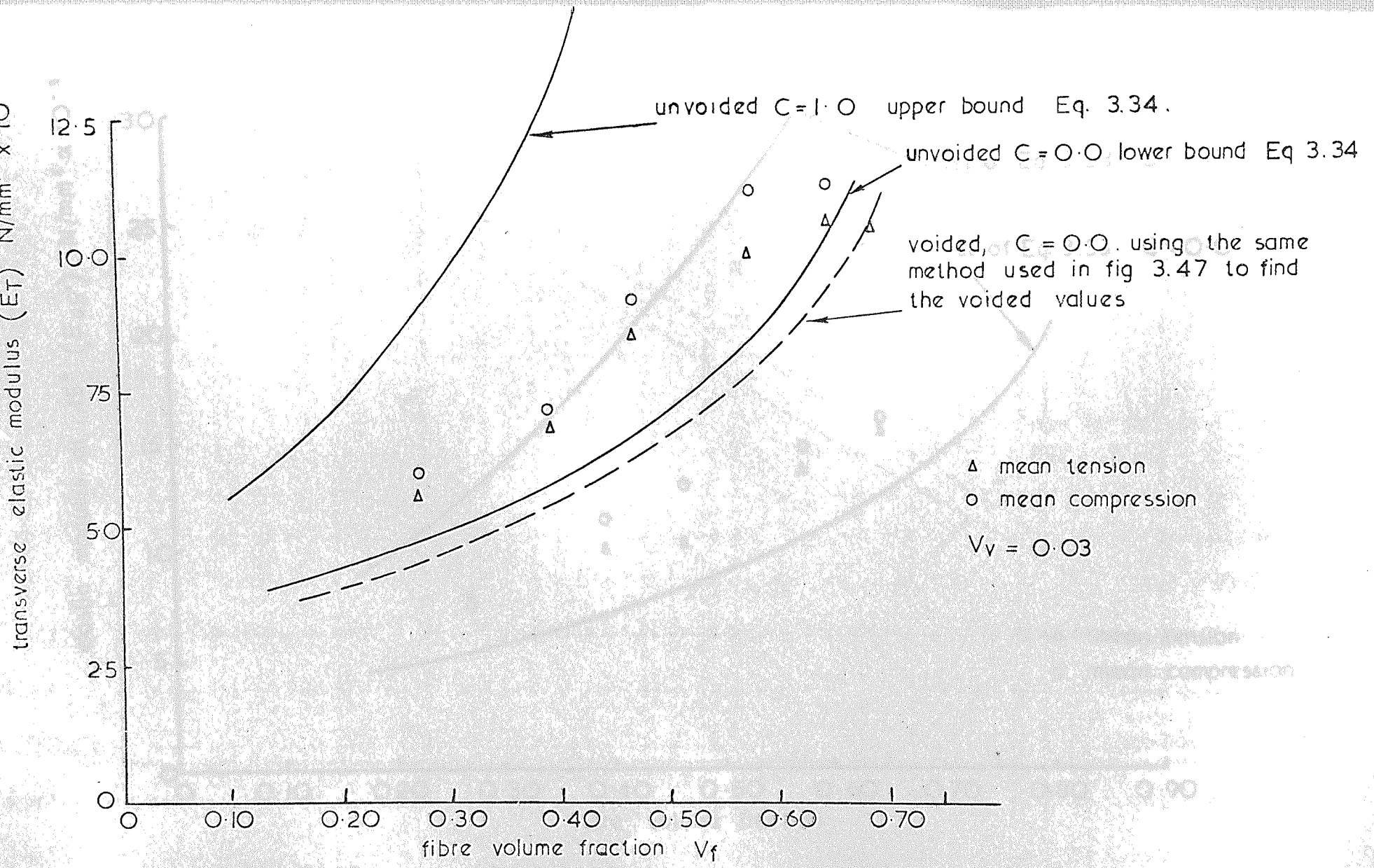
transverse elastic modulus (E_T) N/mm² x 10^{-3}
12·5
10·0
7·5
5·0
2·5
0
0·10
0·20
0·30
0·40
0·50
0·60
0·70
fibre volume fraction V_f
unvoided C = 1·0 upper bound Eq. 3.34.
unvoided C = 0·0 lower bound Eq 3.34
voided, C = 0·0. using the same method used in fig 3.47 to find the voided values
Δ mean tension
o mean compression
V_V = 0·03

Fig. 3.47

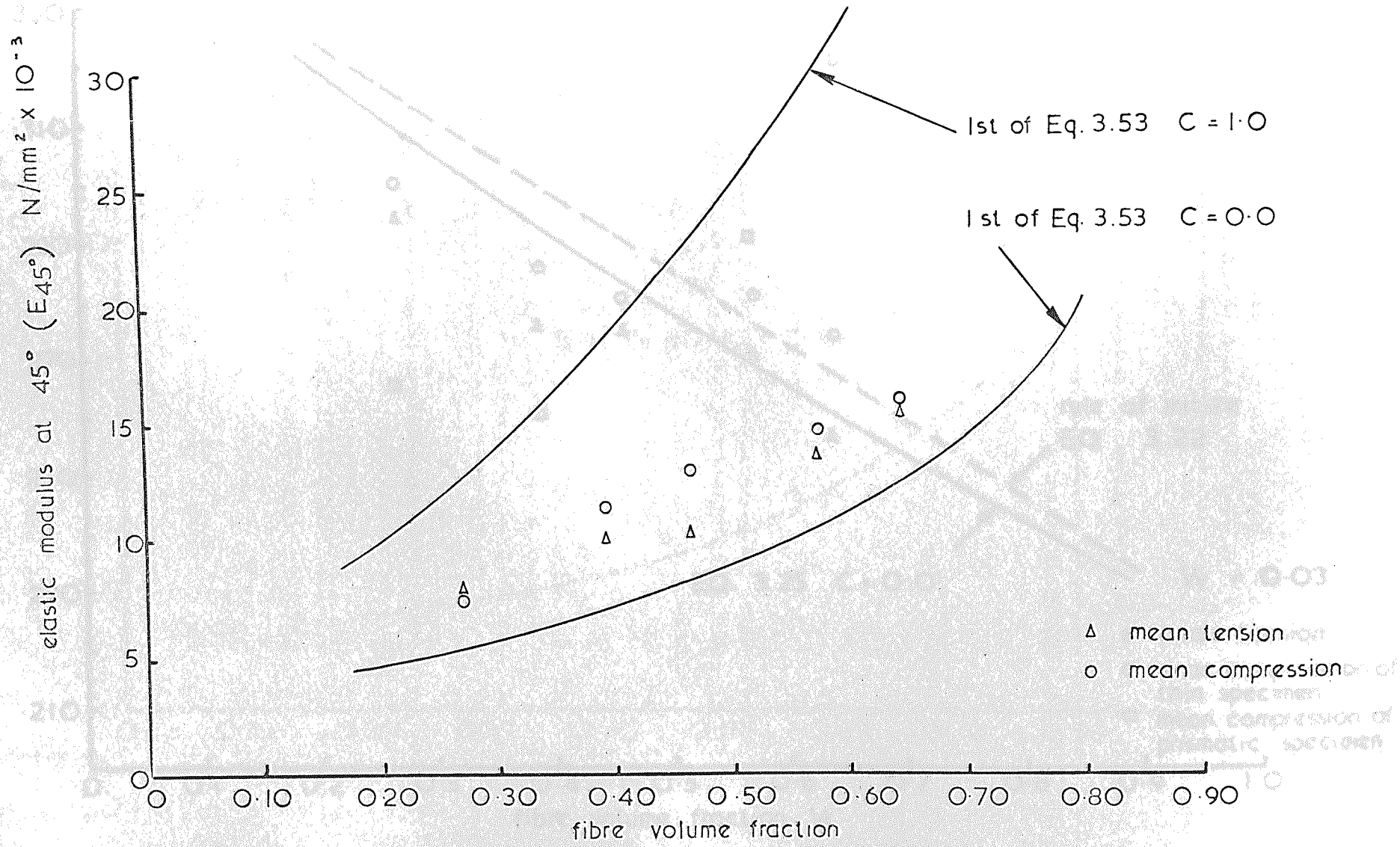
elastic modulus at 45° (E45°) N/mm² x 10⁻³
30
25
20
15
10
5
0
0
0·10
0·20
0·30
0·40
0·50
0·60
0·70
0·80
0·90
fibre volume fraction
1st of Eq. 3.53 C = 1·0
1st of Eq. 3.53 C = 0·0
mean tension
mean compression

Fig 3.48

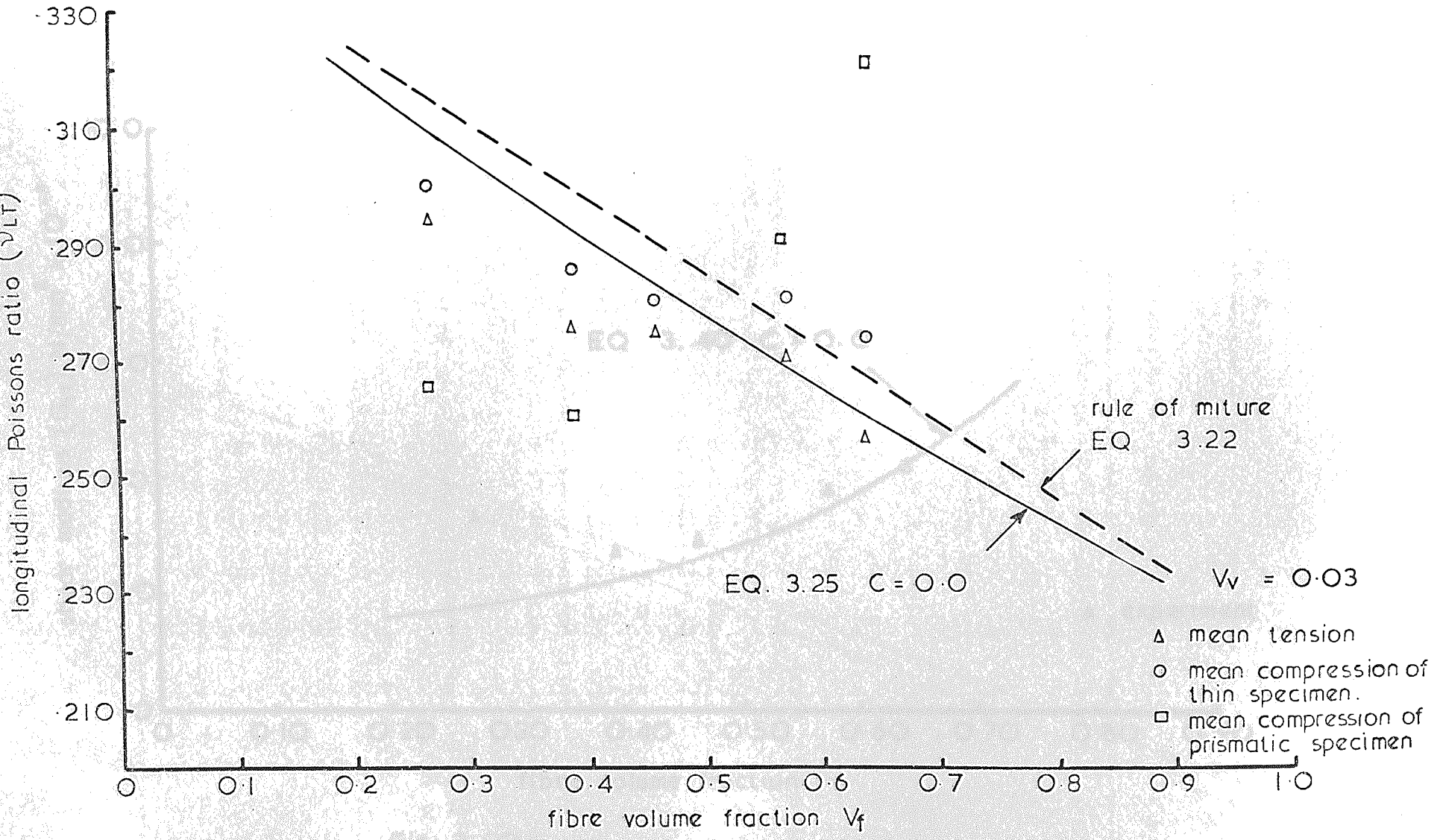
·330
·310
·290
·270
·250
·230
·210
longitudinal Poissons ratio (ν_{LT})
0
0·1
0·2
0·3
0·4
0·5
0·6
0·7
0·8
0·9
1·0
fibre volume fraction V_f
rule of miture
EQ 3.22
EQ. 3.25 C = 0·0
V_v = 0·03
mean tension
mean compression of thin specimen.
mean compression of prismatic specimen

Fig. 3.49.

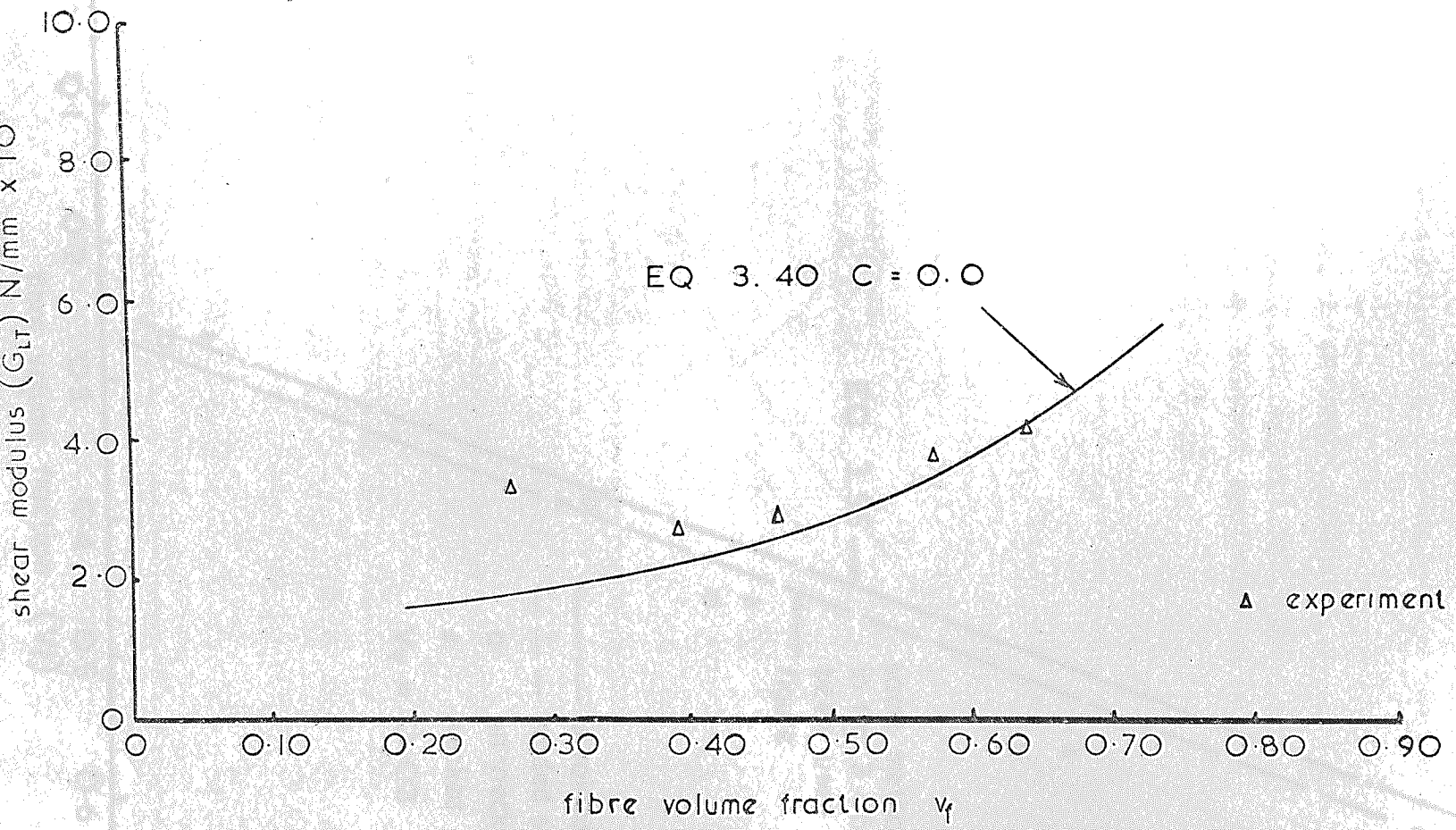
10·0
8·0
6·0
4·0
2·0
0
shear modulus (G_{LT}) N/mm^2 x 10^{-3}
EQ 3.40 C = 0.0
Δ experiment
0
0·10
0·20
0·30
0·40
0·50
0·60
0·70
0·80
0·90
fibre volume fraction V_f

Fig. 3.50

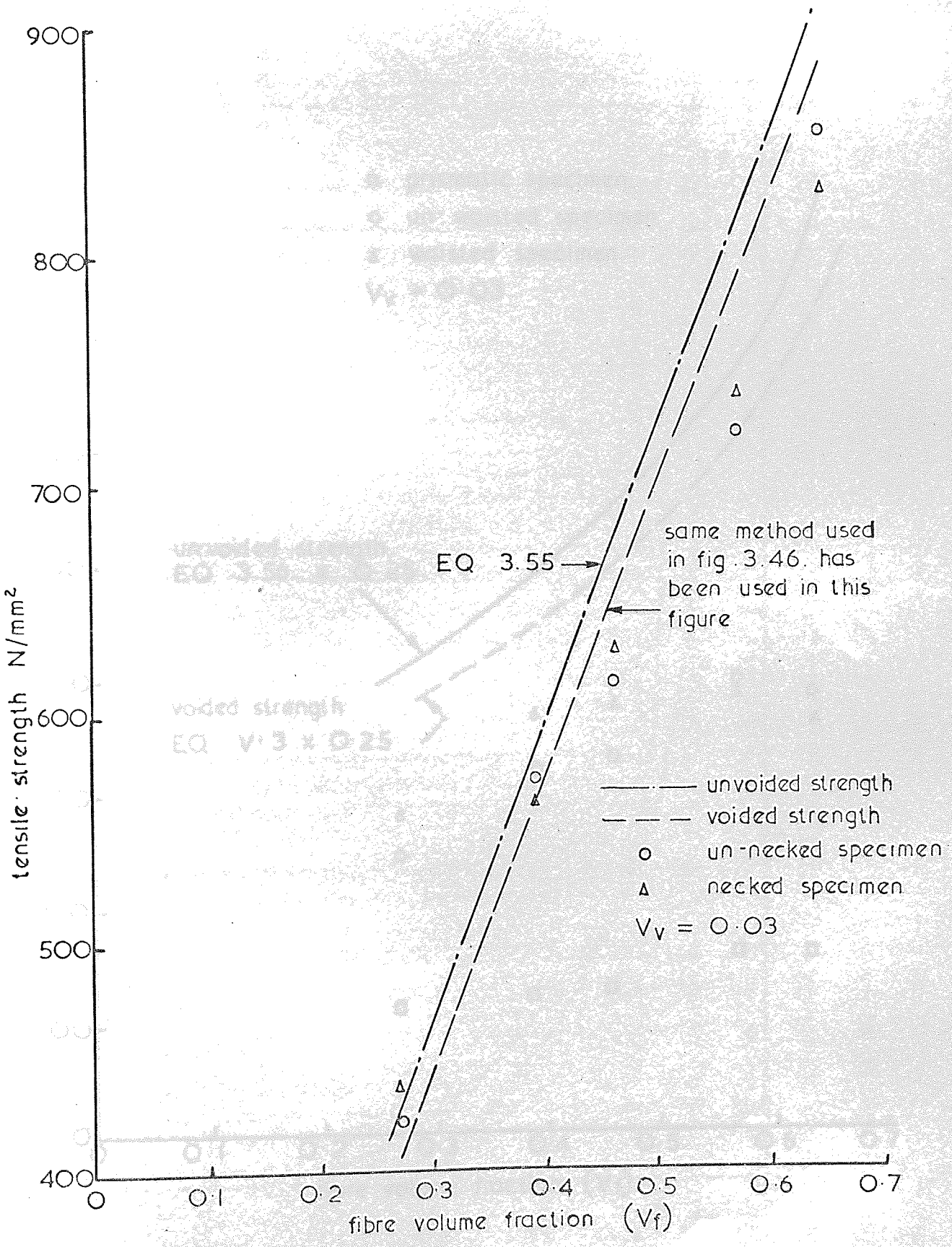
900
800
700
600
500
400
tensile strength N/mm²
0
0·1
0·2
0·3
0·4
0·5
0·6
0·7
fibre volume fraction (Vf)
EQ 3.55
same method used in fig. 3.46. has been used in this figure
unvoided strength
voided strength
un-necked specimen
necked specimen
Vv = 0·03

Fig. 3.51

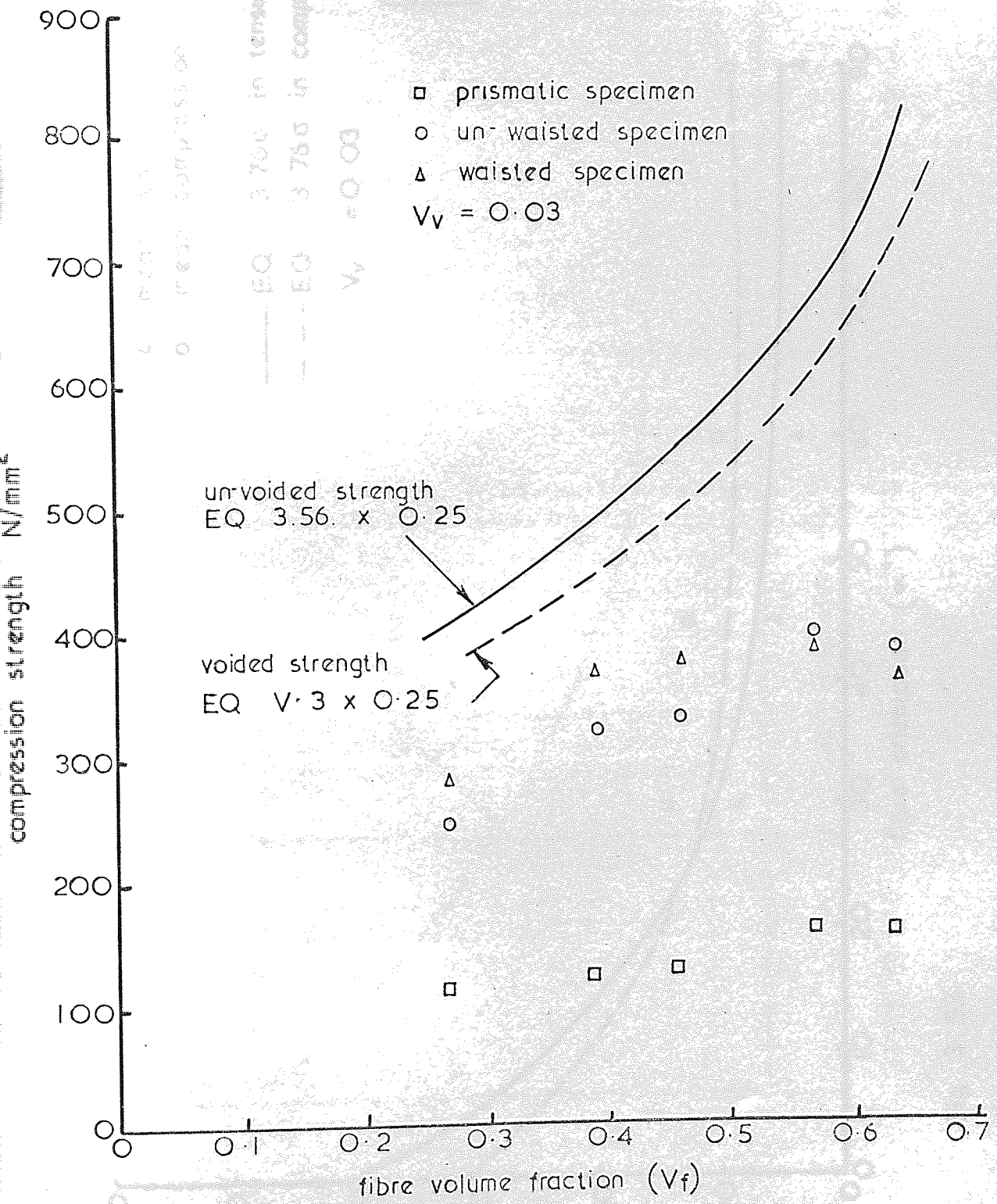
900
800
700
600
500
400
300
200
100
0
compression strength N/mm²
prismatic specimen
un-waisted specimen
waisted specimen
Vv = 0·03
un-voided strength
EQ 3.56 x 0·25
voided strength
EQ V·3 x 0·25
0·1
0·2
0·3
0·4
0·5
0·6
0·7
fibre volume fraction (Vf)

Fig. 3.52

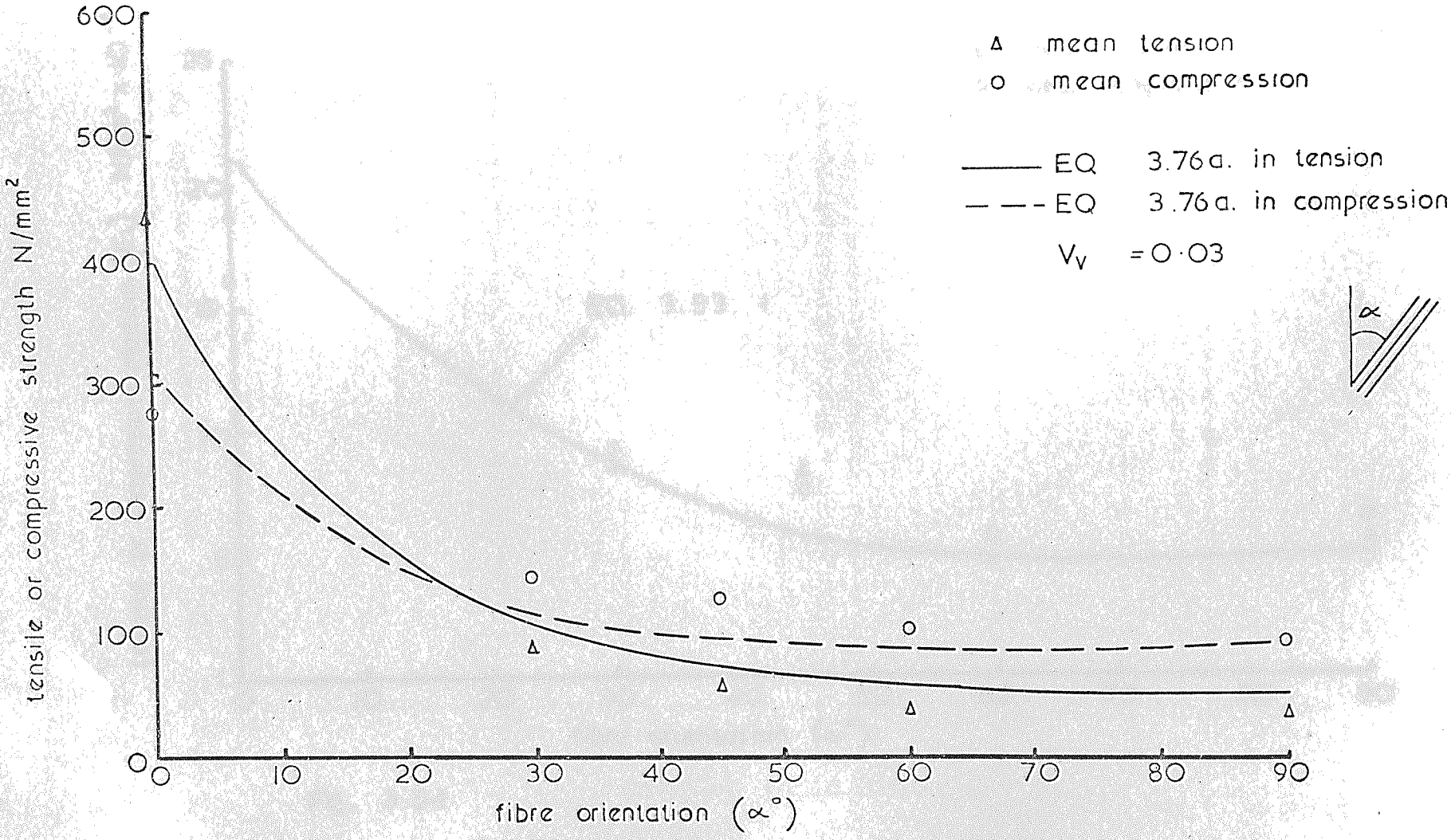
600
500
400
300
200
100
0
0
10
20
30
40
50
60
70
80
90
tensile or compressive strength N/mm²
fibre orientation (α°)
Δ mean tension
o mean compression
EQ 3.76a. in tension
EQ 3.76a. in compression
V_V = 0·03
α

Fig. 3.53

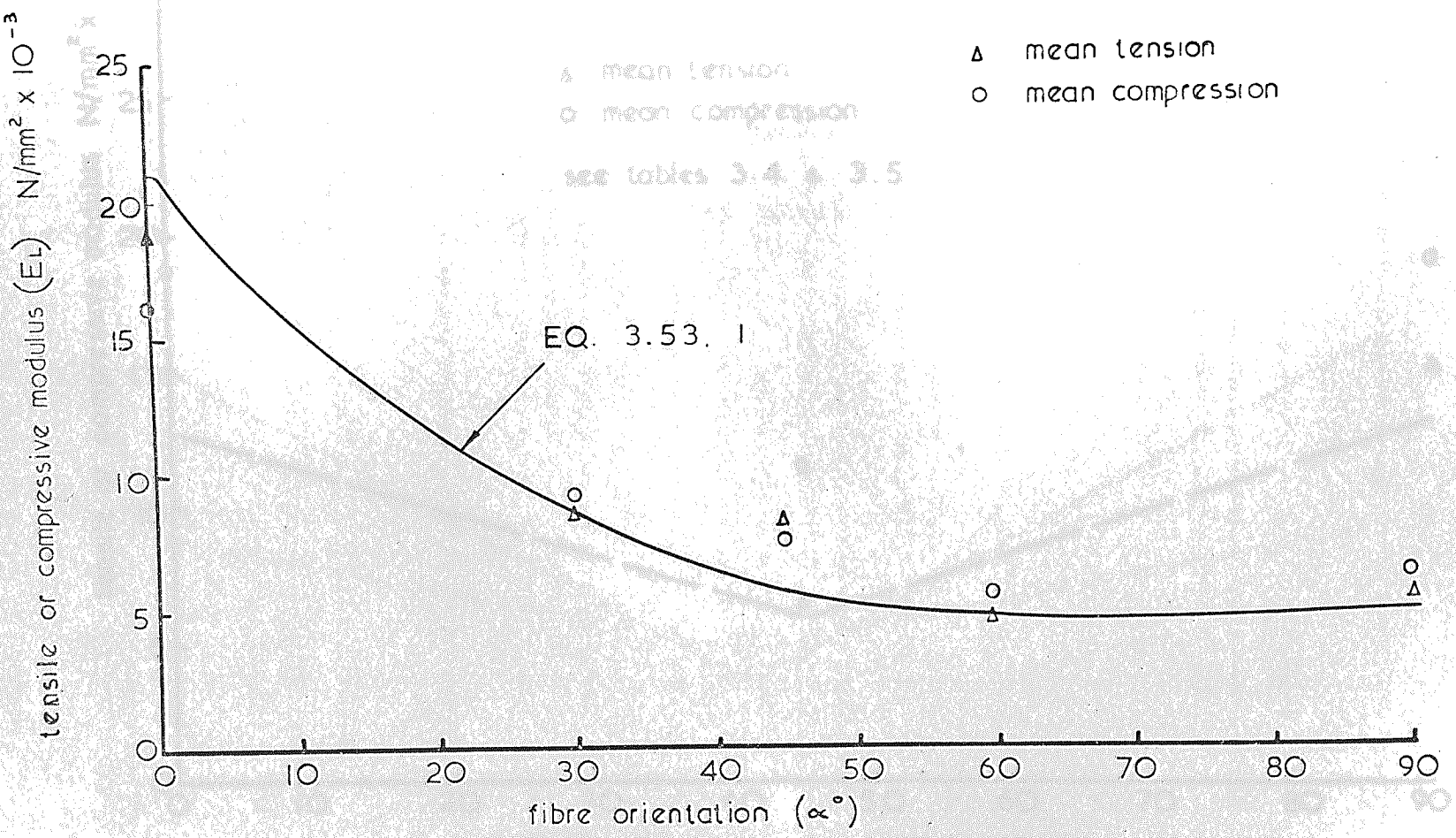
tensile or compressive modulus (EL) N/mm² x 10⁻³
25
20
15
10
5
0
0
10
20
30
40
50
60
70
80
90
fibre orientation (∝°)
EQ. 3.53. 1
Δ mean tension
○ mean compression

Fig. 3.54

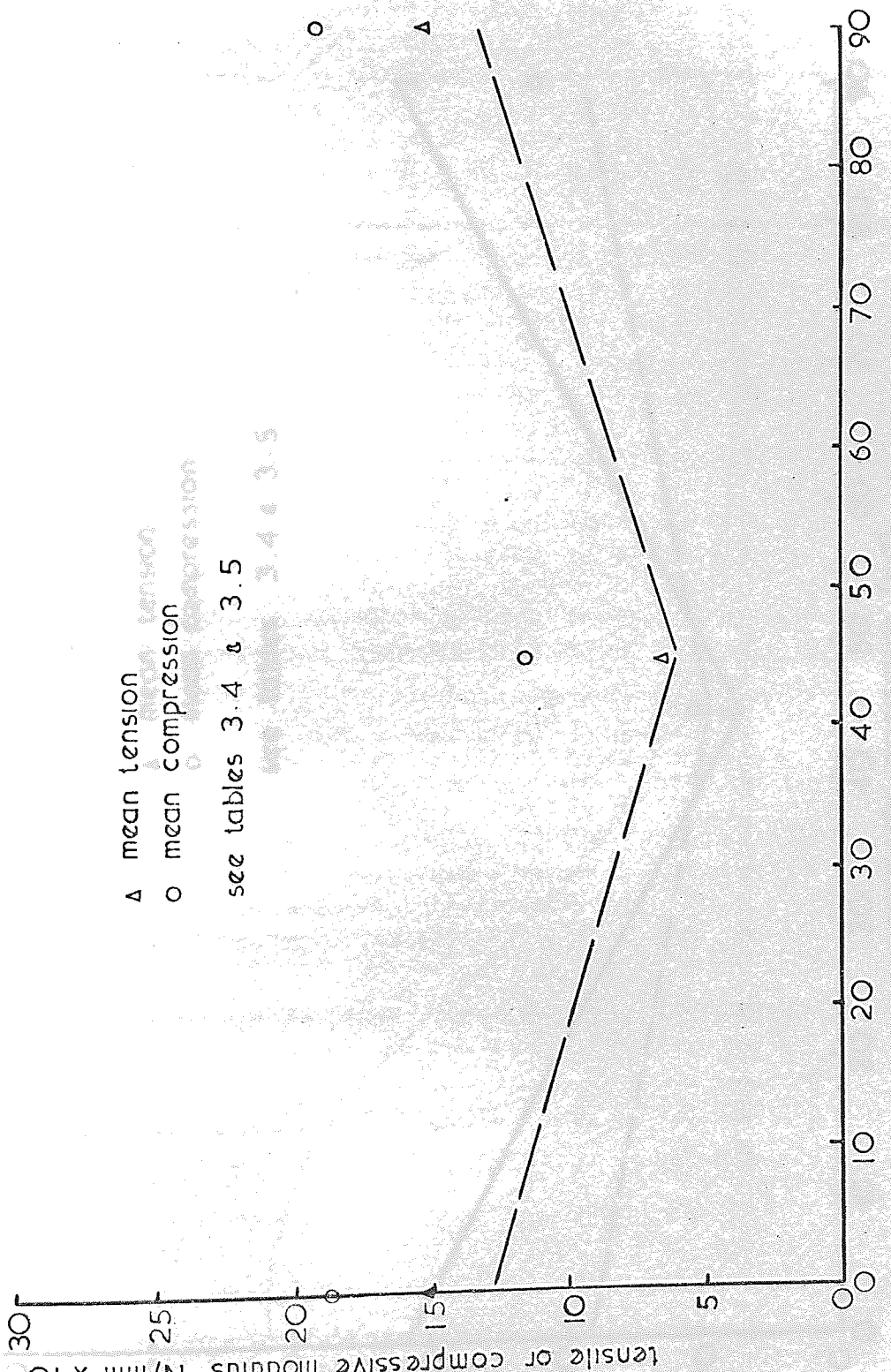
Δ mean tension
o mean compression
see tables 3.4 & 3.5
tensile or compressive modulus N/mm² x 10³
cross-ply orientation (α°)
0
10
20
30
40
50
60
70
80
90
5
10
15
20
25
30

Fig. 3.55

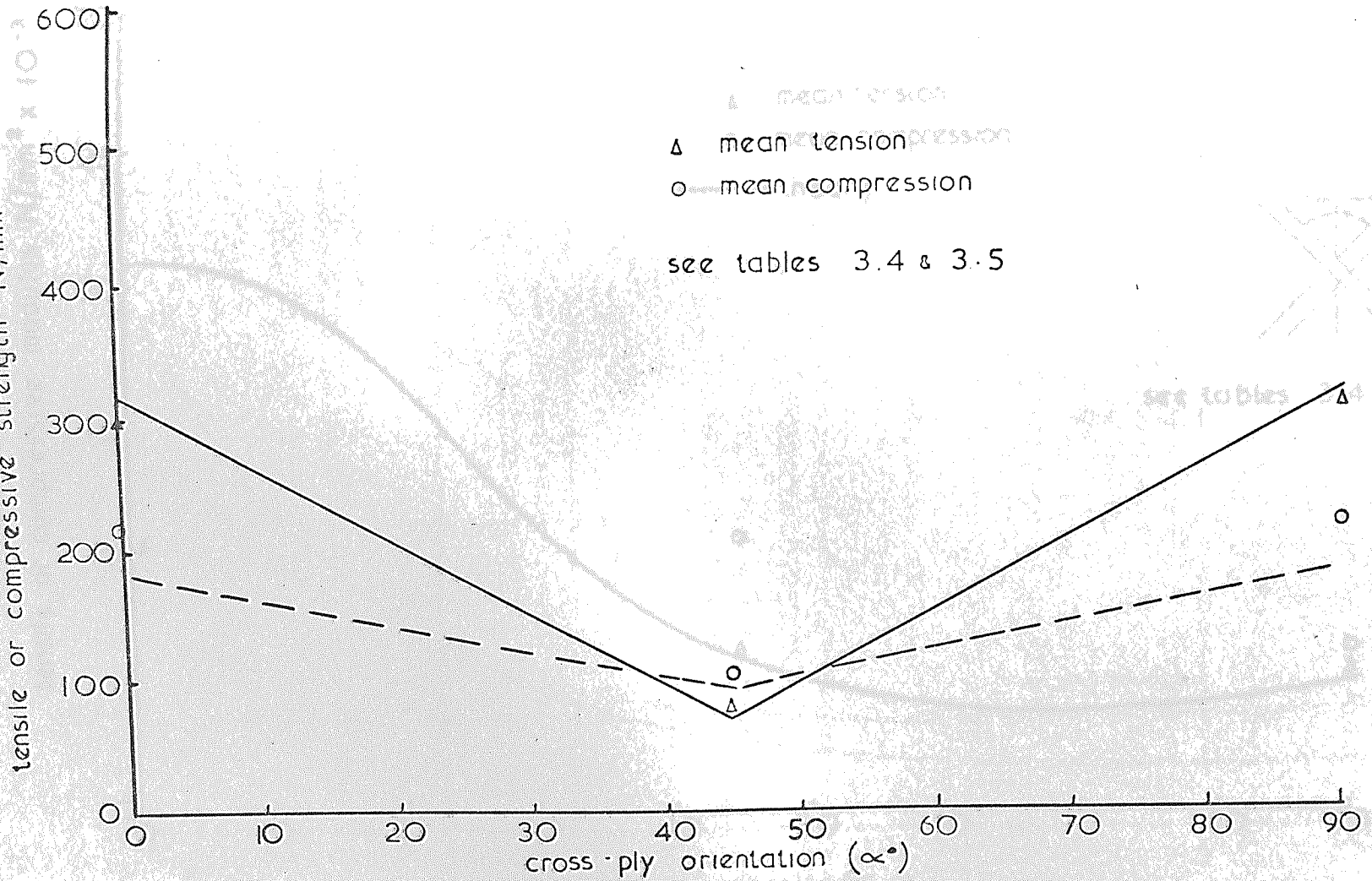
600
500
400
300
200
100
0
tensile or compressive strength N/mm²
Δ mean tension
o mean compression
see tables 3.4 & 3.5
0
10
20
30
40
50
60
70
80
90
cross-ply orientation (α°)

Fig. 3.56

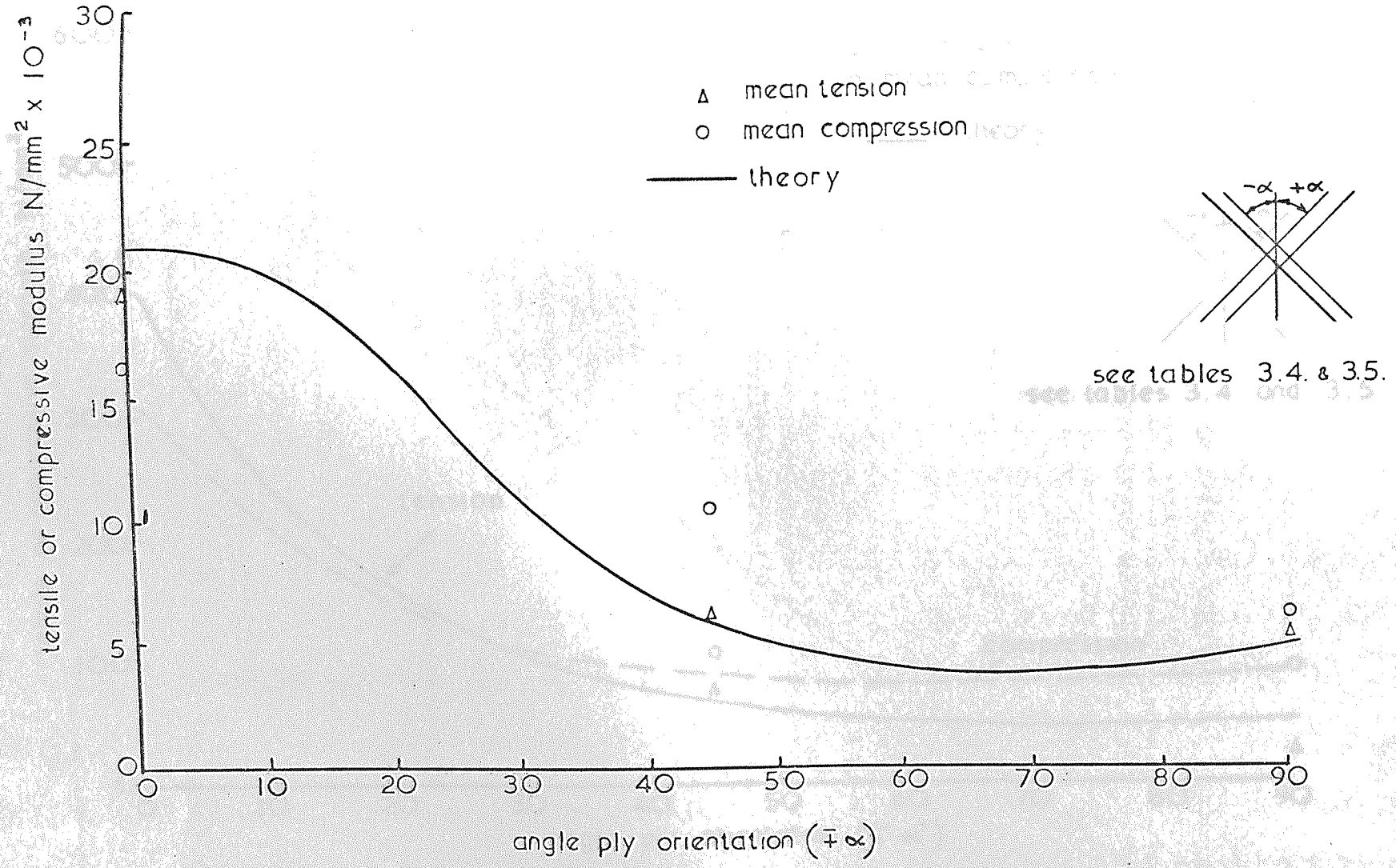
tensile or compressive modulus N/mm² x 10⁻³
30
25
20
15
10
5
0
0
10
20
30
40
50
60
70
80
90
angle ply orientation (∓∝)
mean tension
mean compression
theory
-∝
+∝
see tables 3.4. & 3.5.

Fig. 3.57

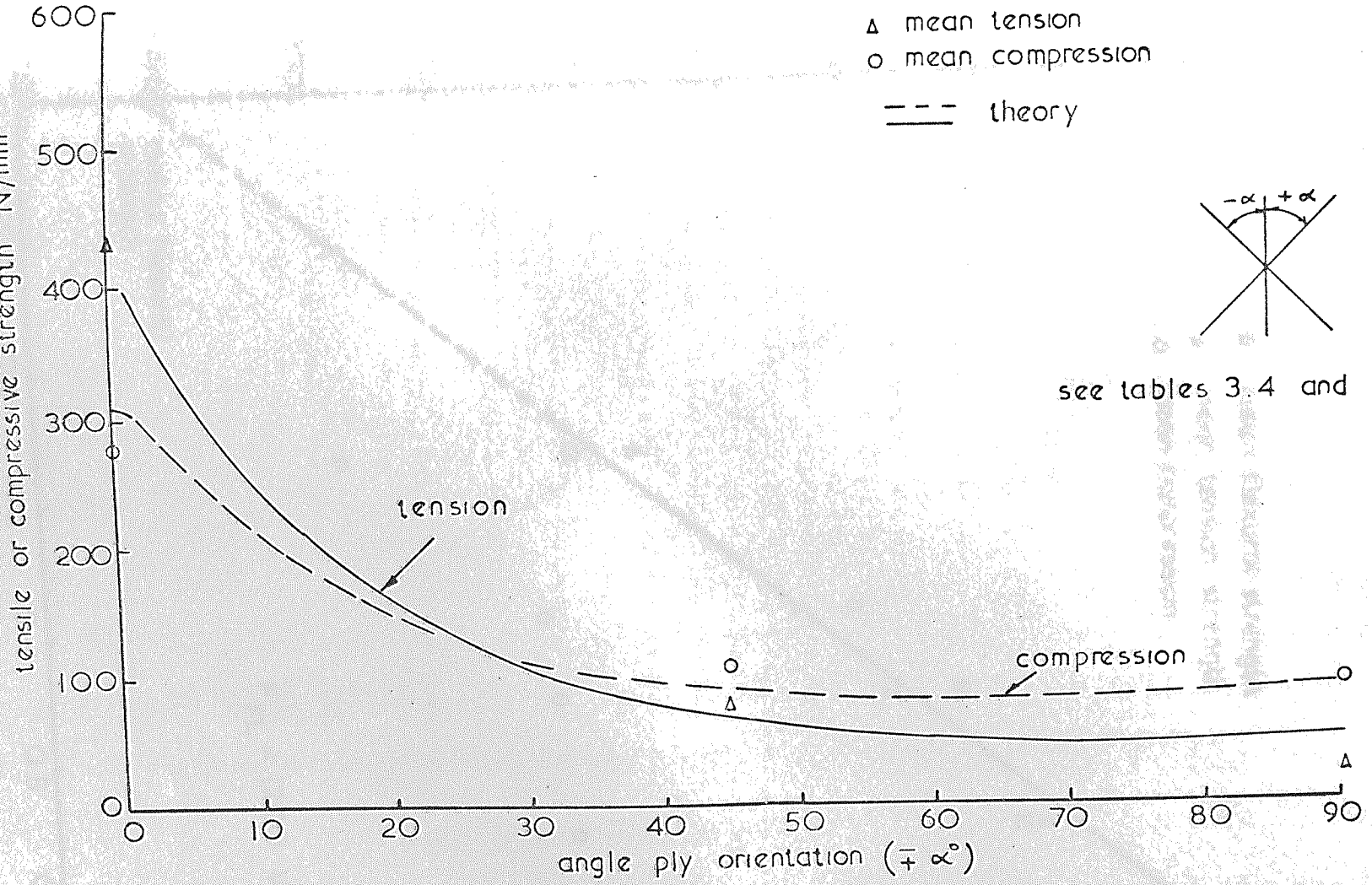
Δ mean tension
o mean compression
theory
see tables 3.4 and 3.5
tensile or compressive strength N/mm²
600
500
400
300
200
100
0
tension
compression
0
10
20
30
40
50
60
70
80
90
angle ply orientation (∓ ∝°)

Fig. 3.58

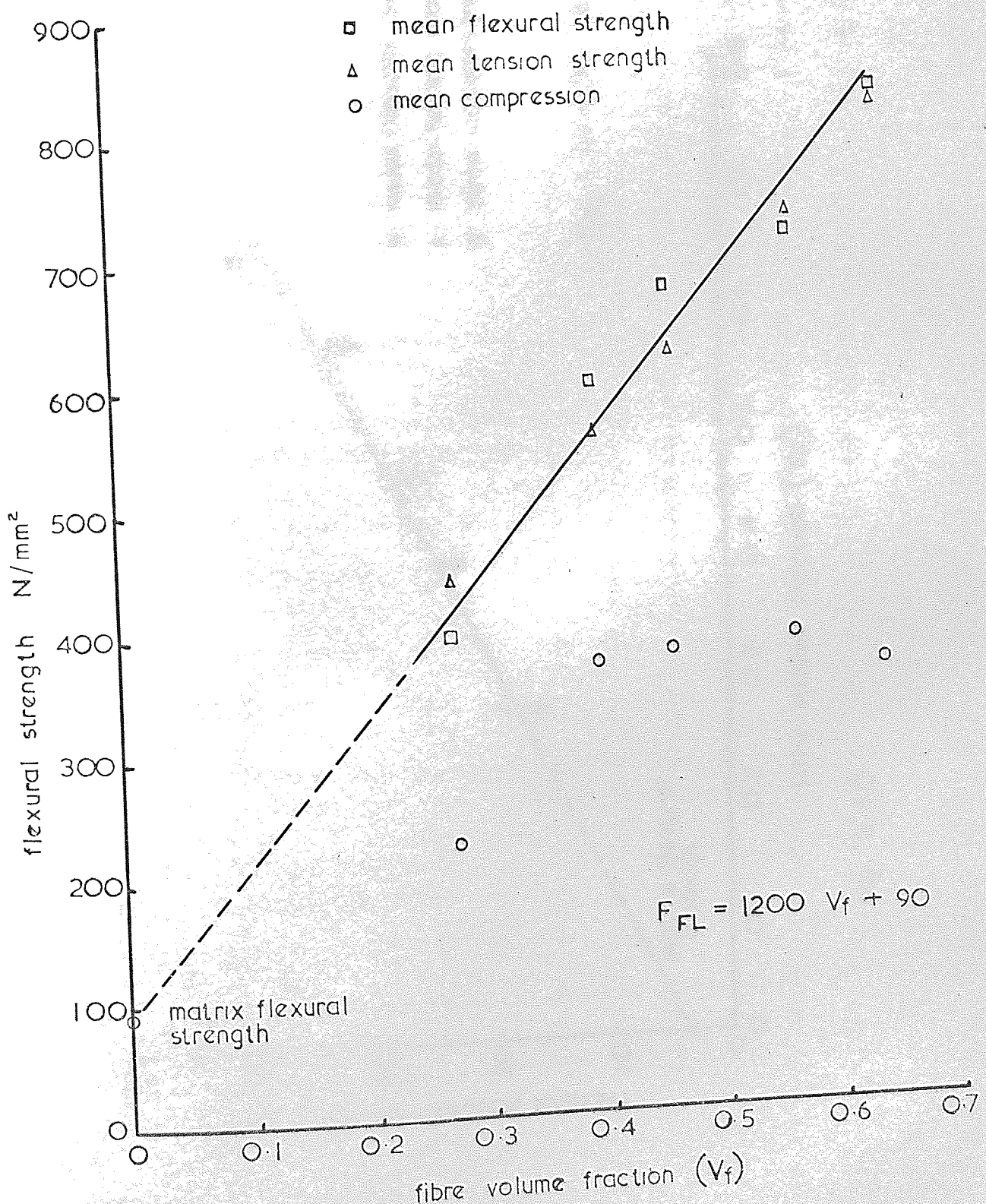
mean flexural strength
mean tension strength
mean compression
900
800
700
600
500
400
300
200
100
0
flexural strength N/mm²
matrix flexural strength
$F_{FL} = 1200\ V_f + 90$
0
0·1
0·2
0·3
0·4
0·5
0·6
0·7
fibre volume fraction (V_f)

Fig. 3.59

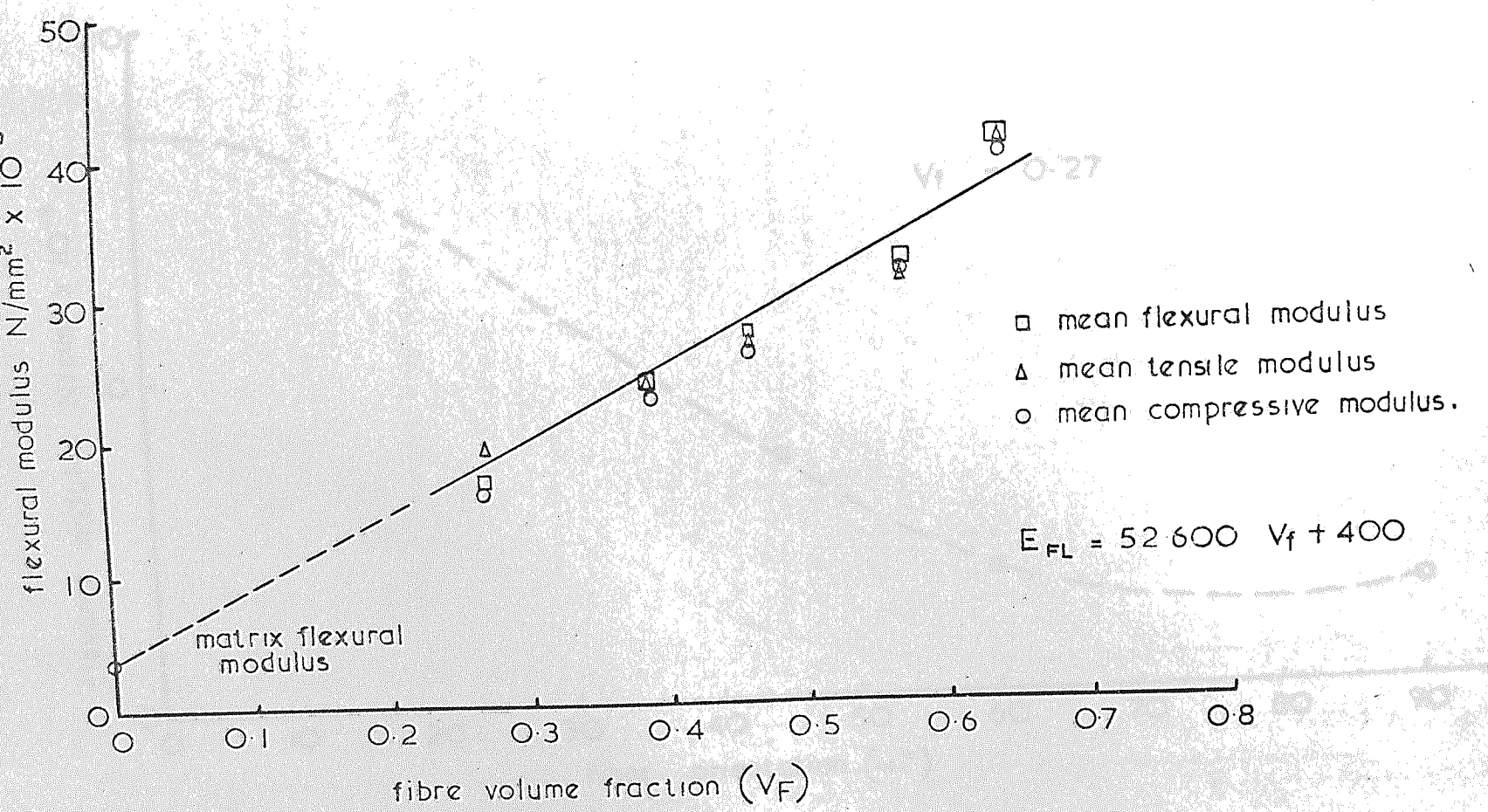
flexural modulus N/mm² x 10⁻³
50
40
30
20
10
0
0
0·1
0·2
0·3
0·4
0·5
0·6
0·7
0·8
fibre volume fraction (V_F)
matrix flexural modulus
□ mean flexural modulus
Δ mean tensile modulus
o mean compressive modulus.
E_FL = 52 600 V_f + 400

Fig. 3.60

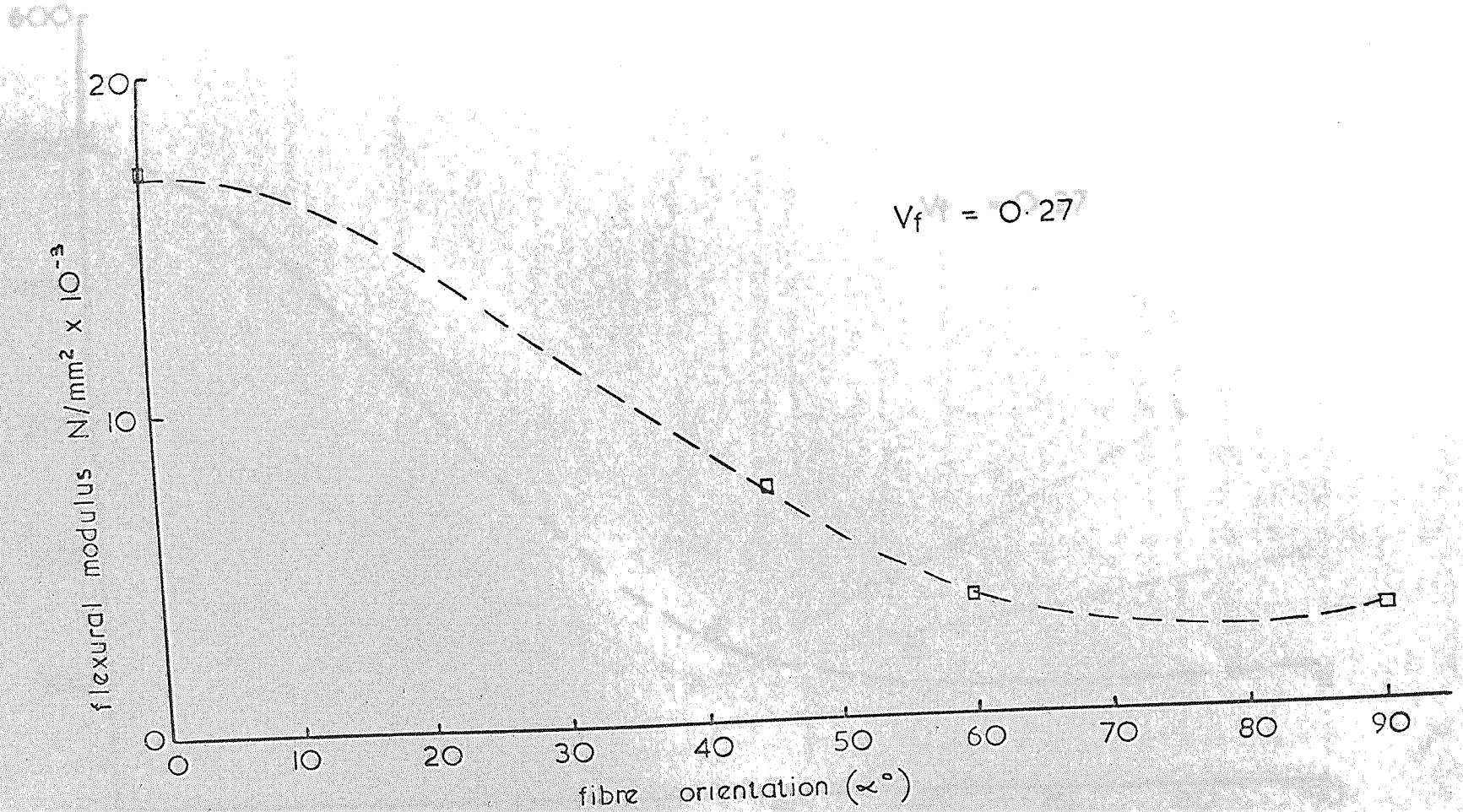
20
10
0
flexural modulus N/mm² x 10⁻³
V_f = 0·27
0
10
20
30
40
50
60
70
80
90
fibre orientation (∝°)

Fig. 3.61

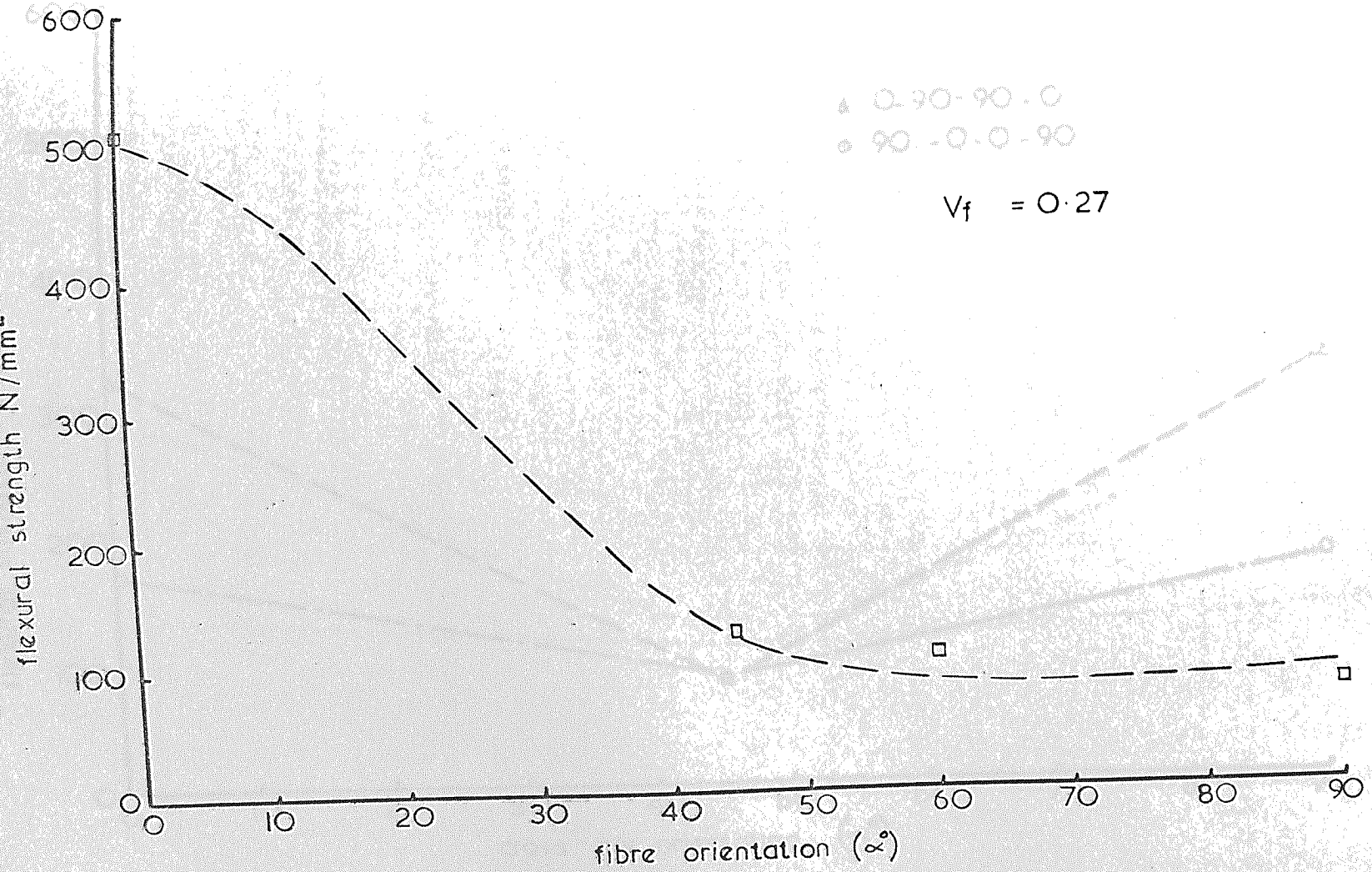
600
500
400
300
200
100
0
flexural strength N/mm²
0
10
20
30
40
50
60
70
80
90
fibre orientation (α°)
Vf = 0·27

Fig. 3.62

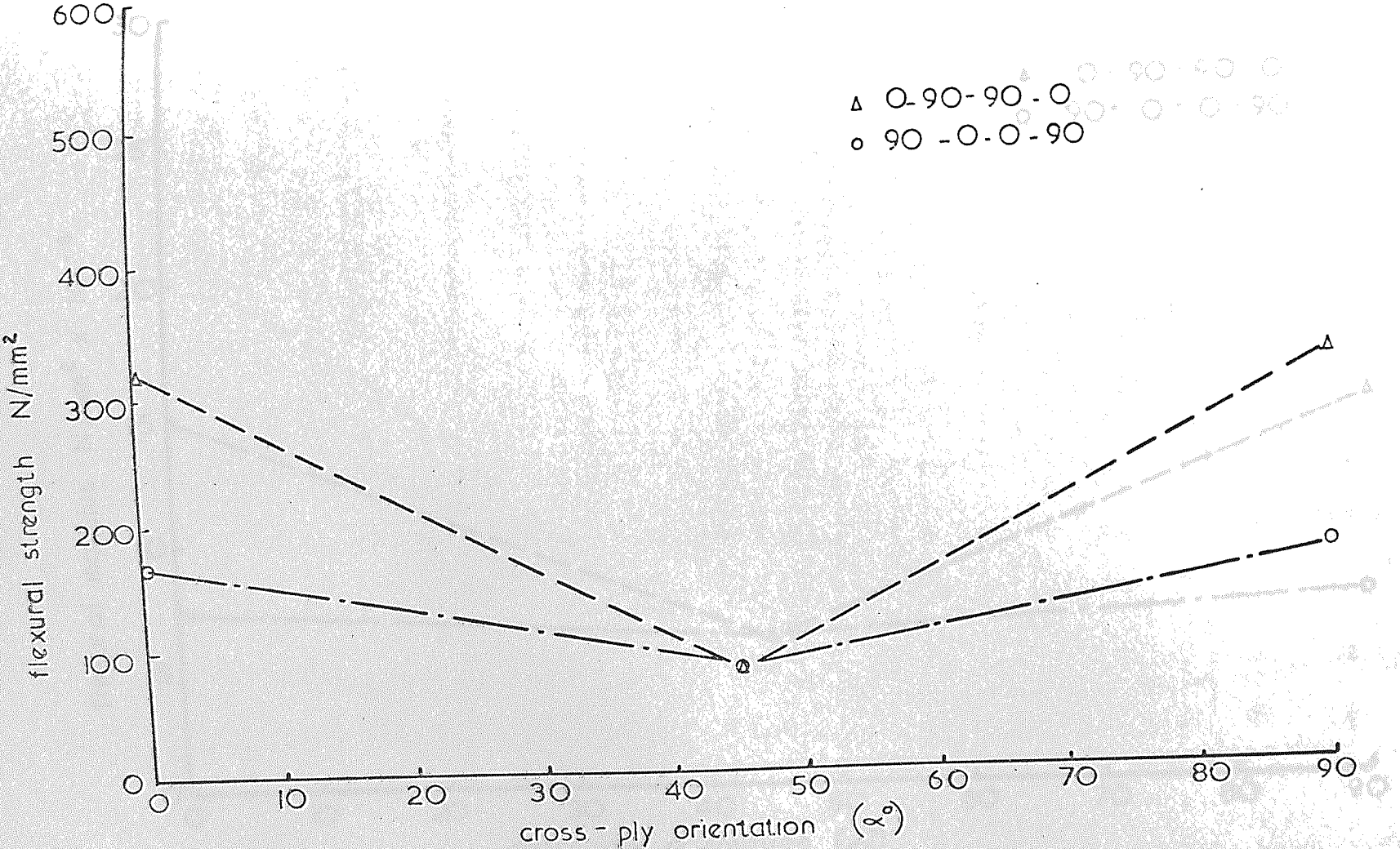
600
500
400
300
200
100
0
flexural strength N/mm²
0 10 20 30 40 50 60 70 80 90
cross - ply orientation (α°)
Δ 0-90-90-0
o 90-0-0-90

Fig. 3.63.

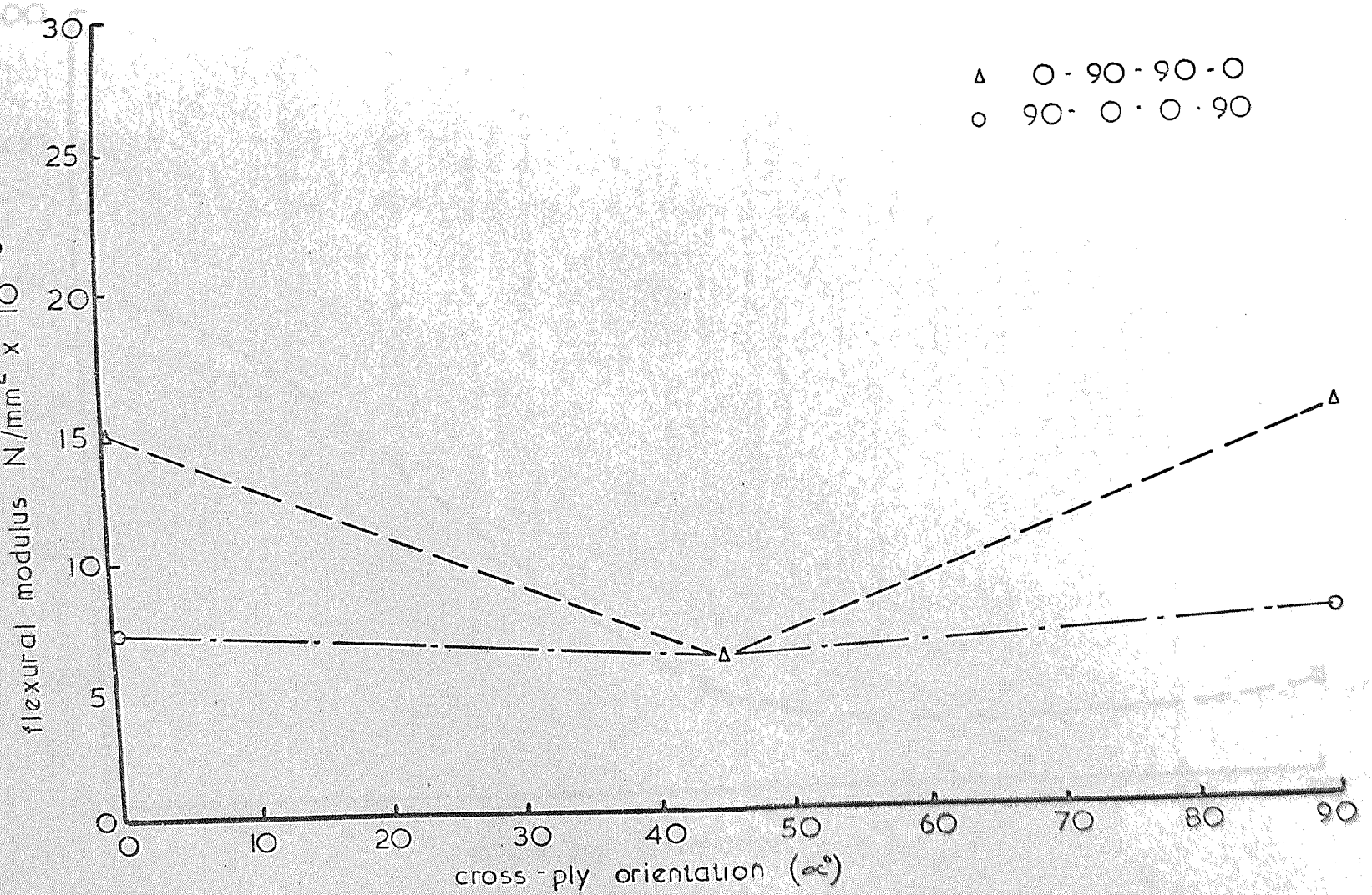
Δ 0 - 90 - 90 - 0
o 90 - 0 - 0 - 90
flexural modulus N/mm² x 10⁻³
30
25
20
15
10
5
0
0
10
20
30
40
50
60
70
80
90
cross - ply orientation (∝°)

Fig. 3.64

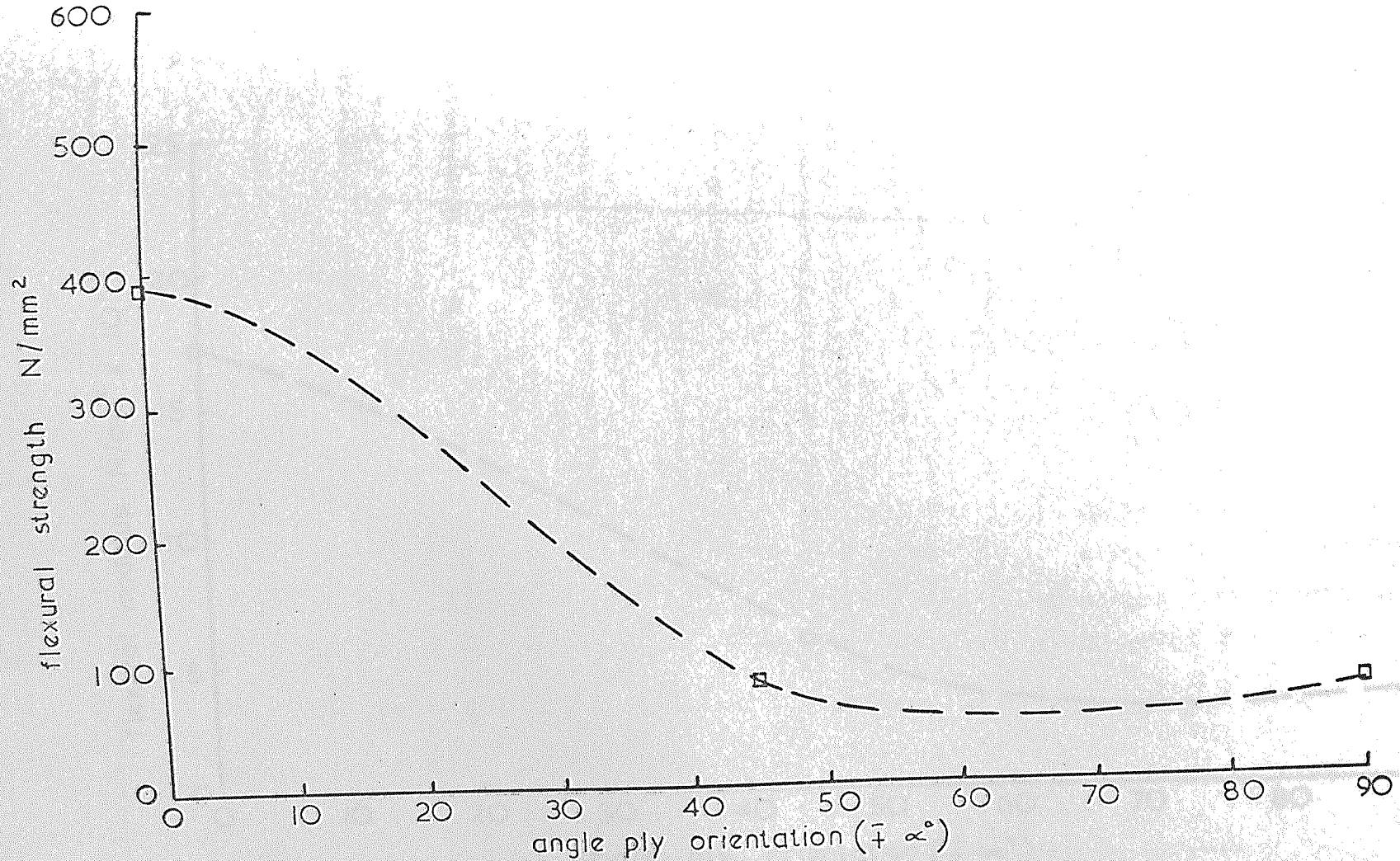
600
500
400
300
200
100
0
flexural strength N/mm²
0
10
20
30
40
50
60
70
80
90
angle ply orientation (± ∝°)

Fig. 3.65

flexural modulus N/mm² x 10⁻³
25
20
15
10
5
0
0
10
20
30
40
50
60
70
80
90
angle ply orientation (± ∝°)

Fig. 3.66

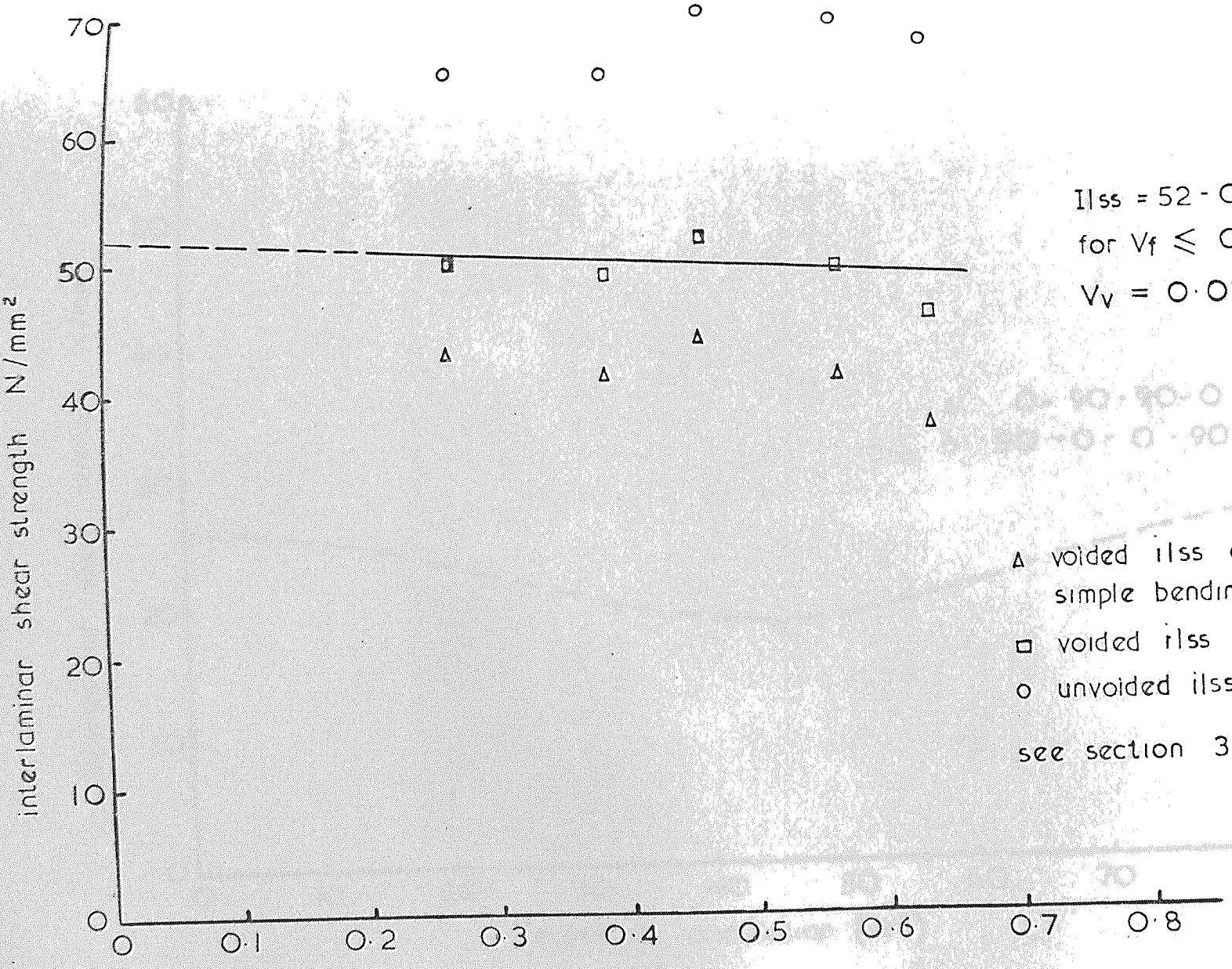

Ilss = 52 - 0·08 Vf

for $V_f \leq 0.60$

$V_v = 0.03$

Δ voided ilss calculated by simple bending theory

□ voided ilss corrected

o unvoided ilss

see section 3.7.4.

Fig. 3.67

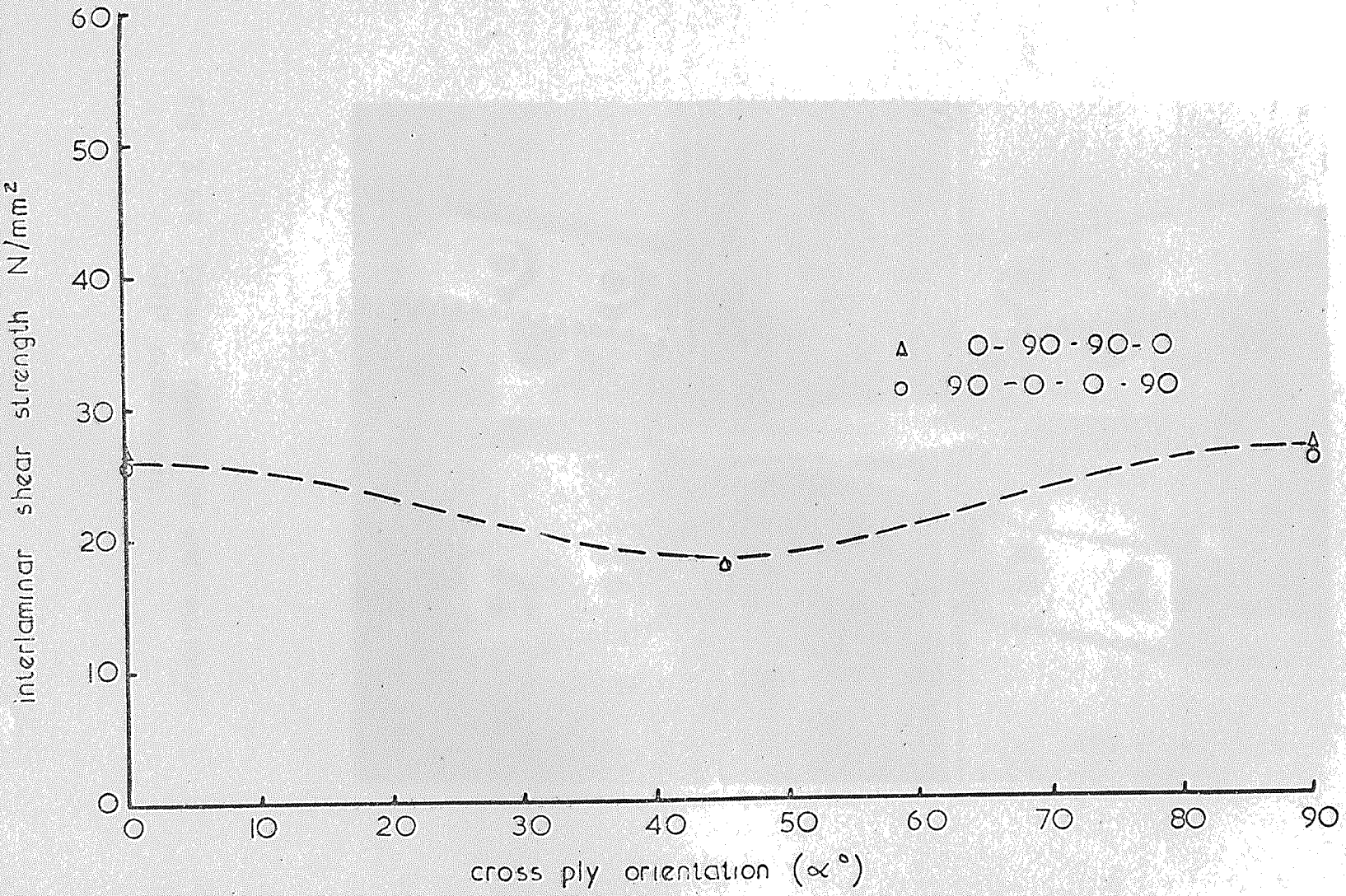
60
50
40
30
20
10
0
0
10
20
30
40
50
60
70
80
90
interlaminar shear strength N/mm²
cross ply orientation (∝°)
Δ 0-90-90-0
o 90-0-0-90

Fig. 3.68

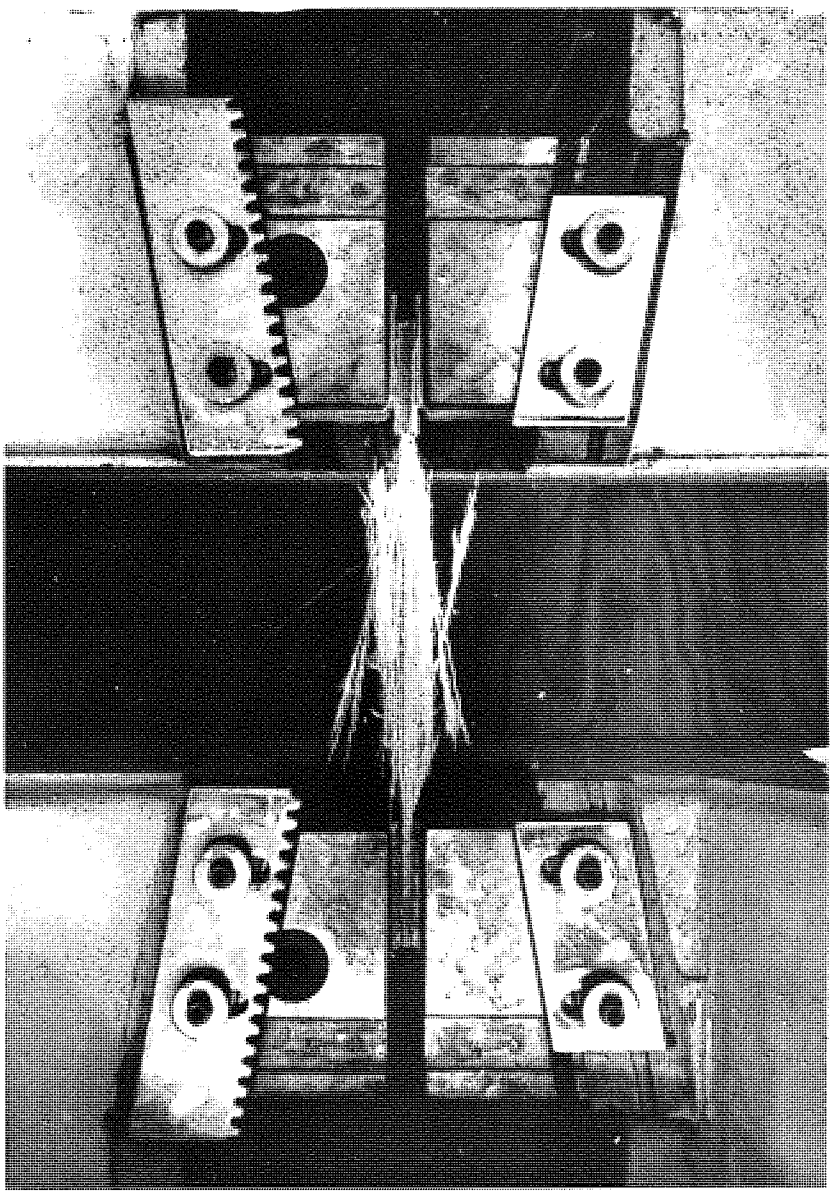

Fig. 3.69. Tensile failure of unidirectional GRP composites

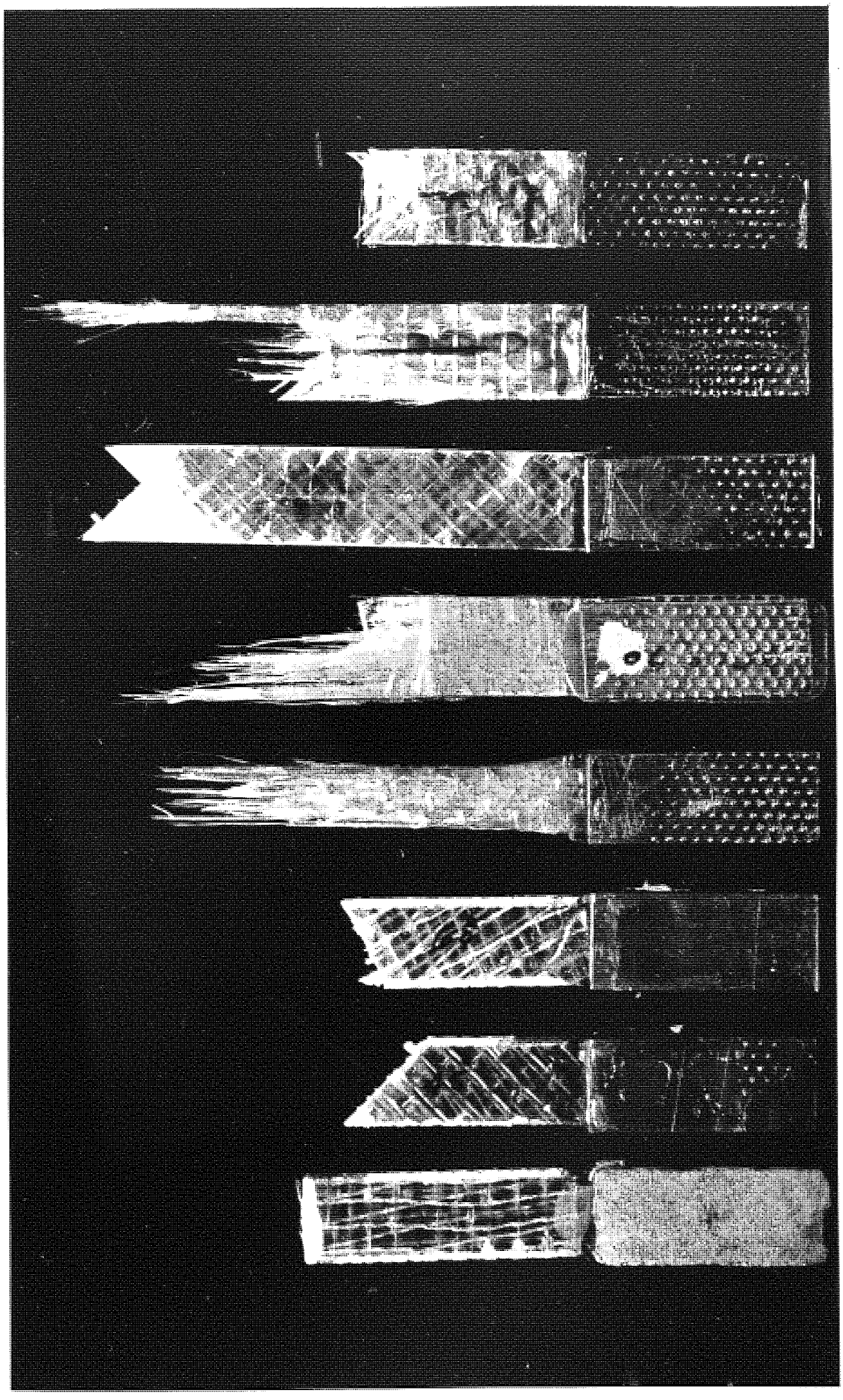

Fig. 3.70 Tensile modes of failure of GRP composites

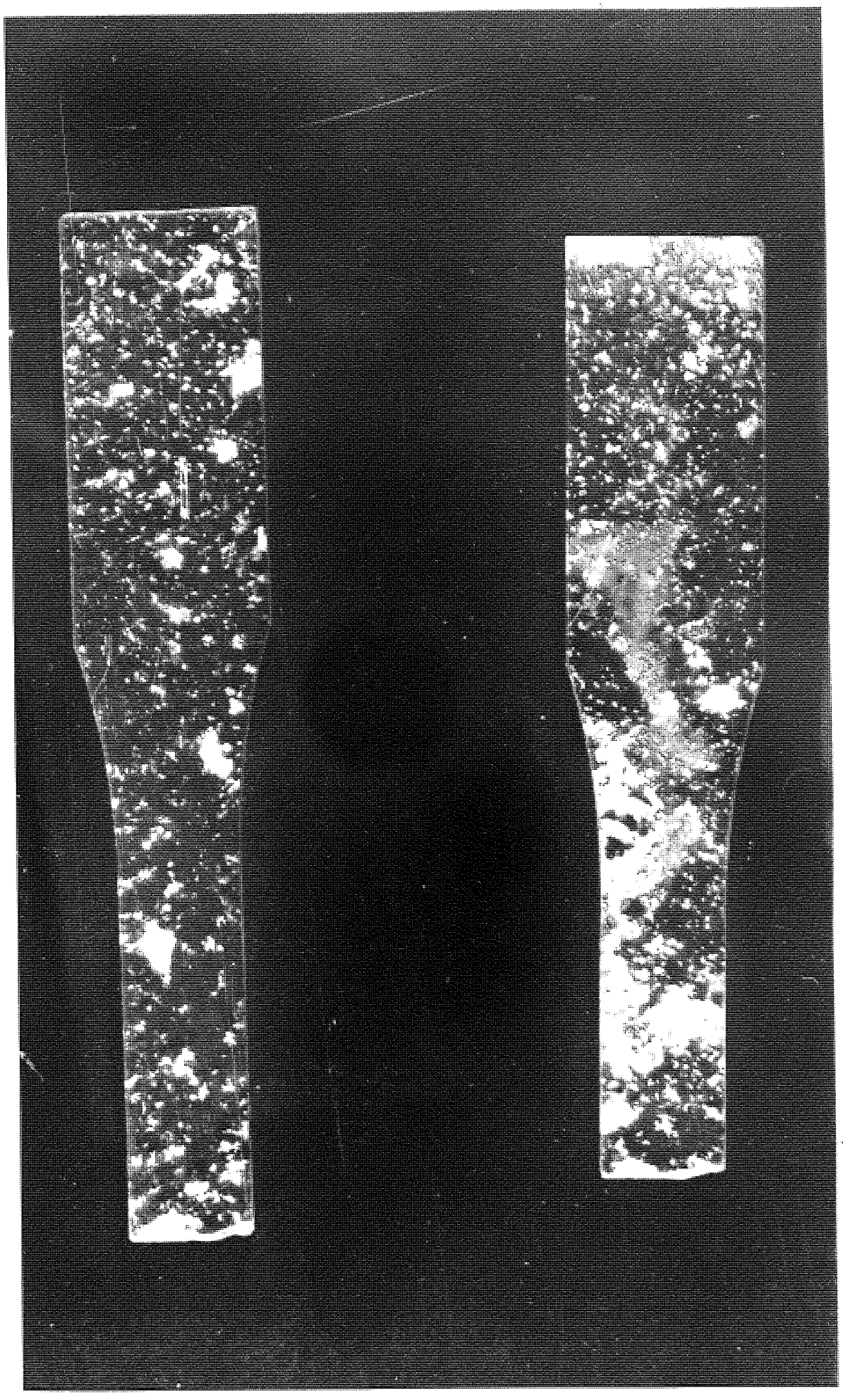

Fig 3 71 Tensile failure of polyester resin

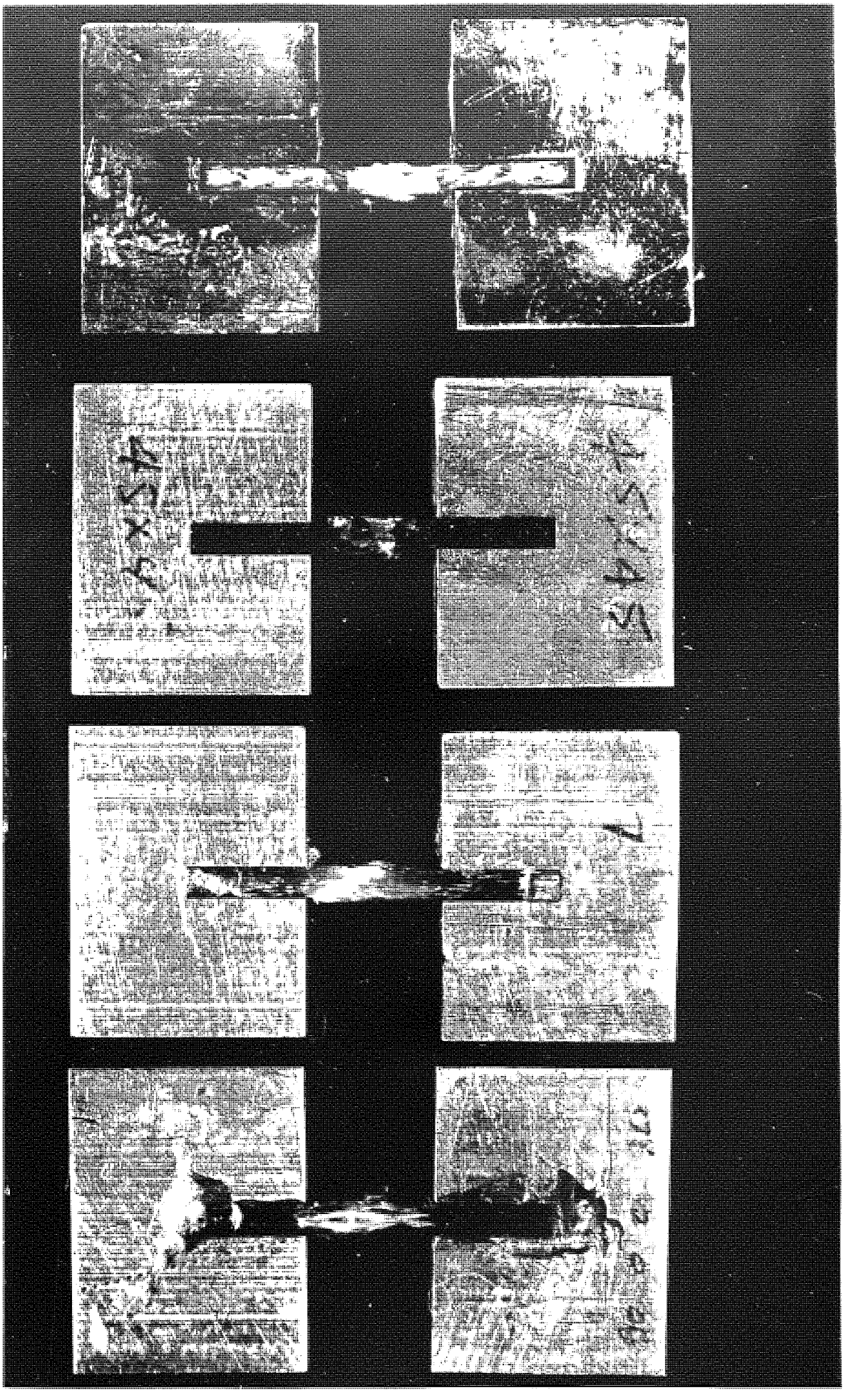

Fig. 3.72 Compressive modes of failure of GRP composites

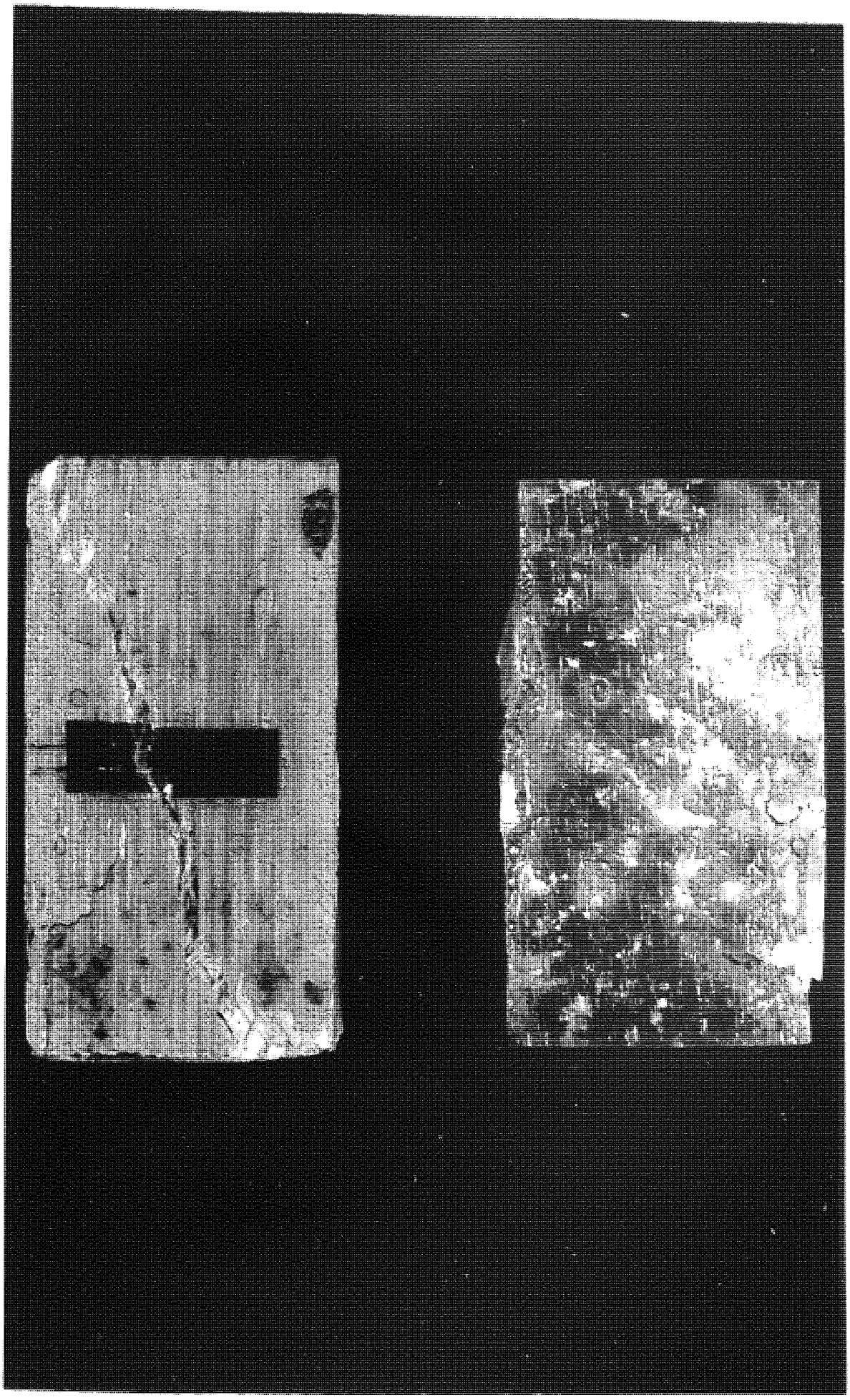

Fig. 3.73 Shear mode of failure on compressive specimens of undirectional GRP (left) and polyester resin (right)

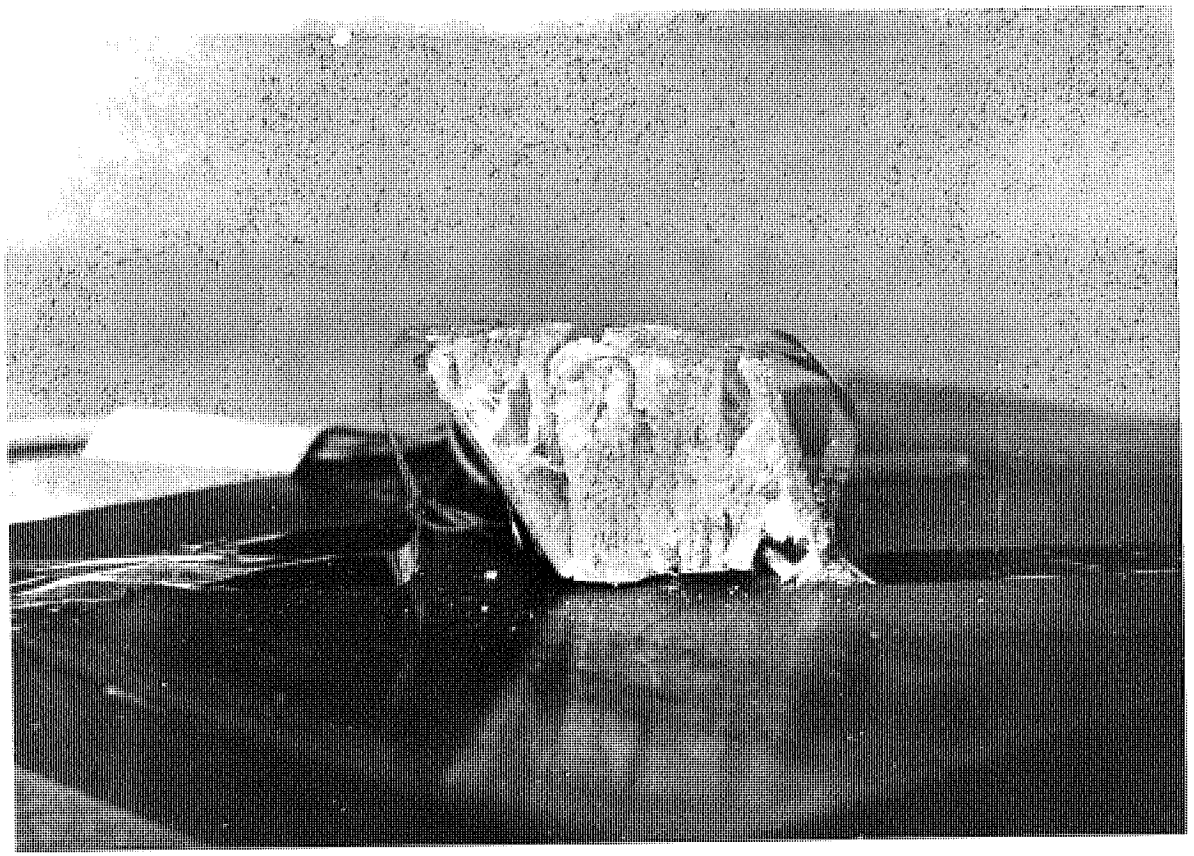

Fig 3.74 Delamination mode of failure of weak unidirectional compression specimen.

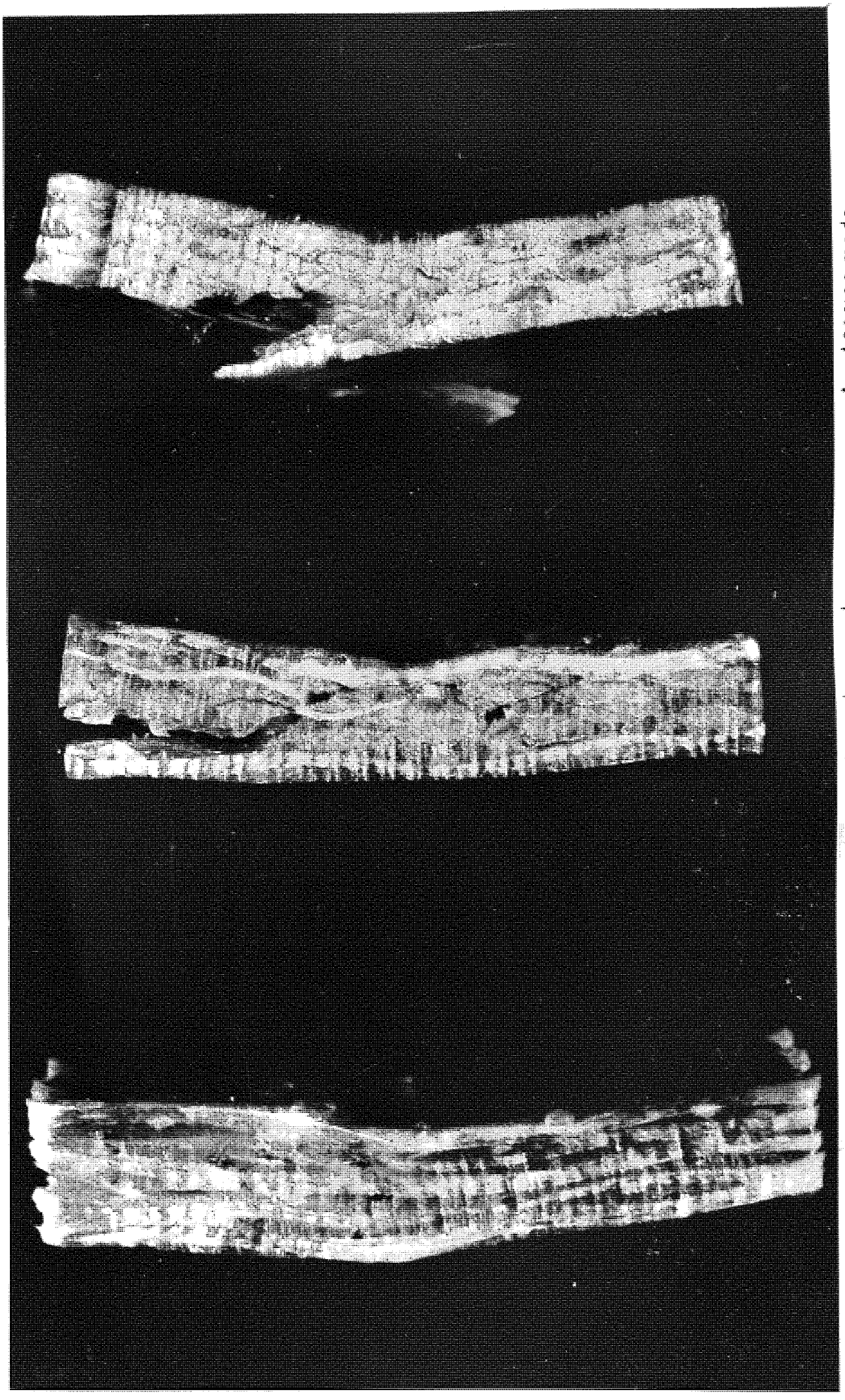

Fig 3.75 Different modes of failure of short beam speciments

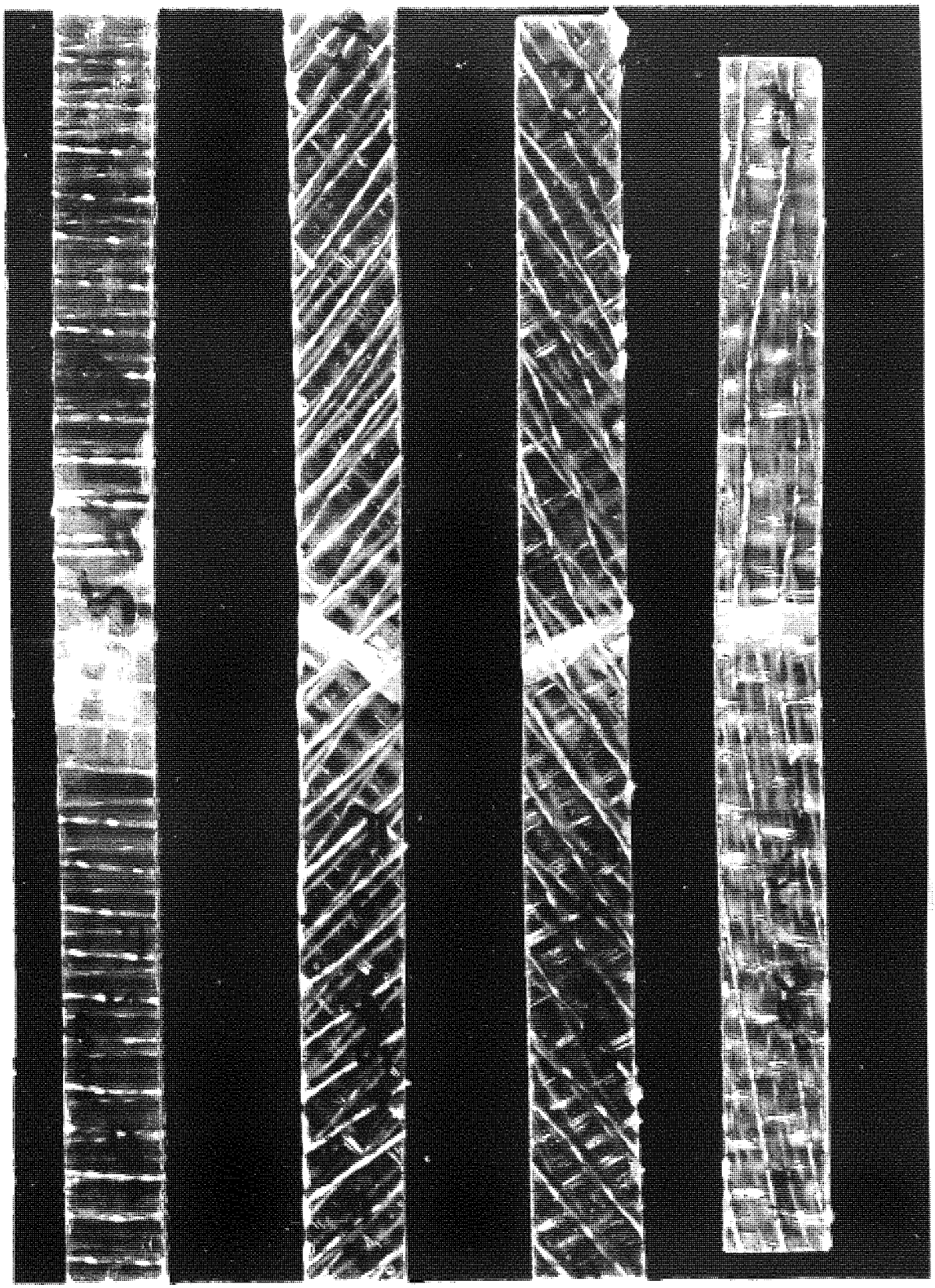

Fig. 3.76 Different modes of failure of flexural test specimens

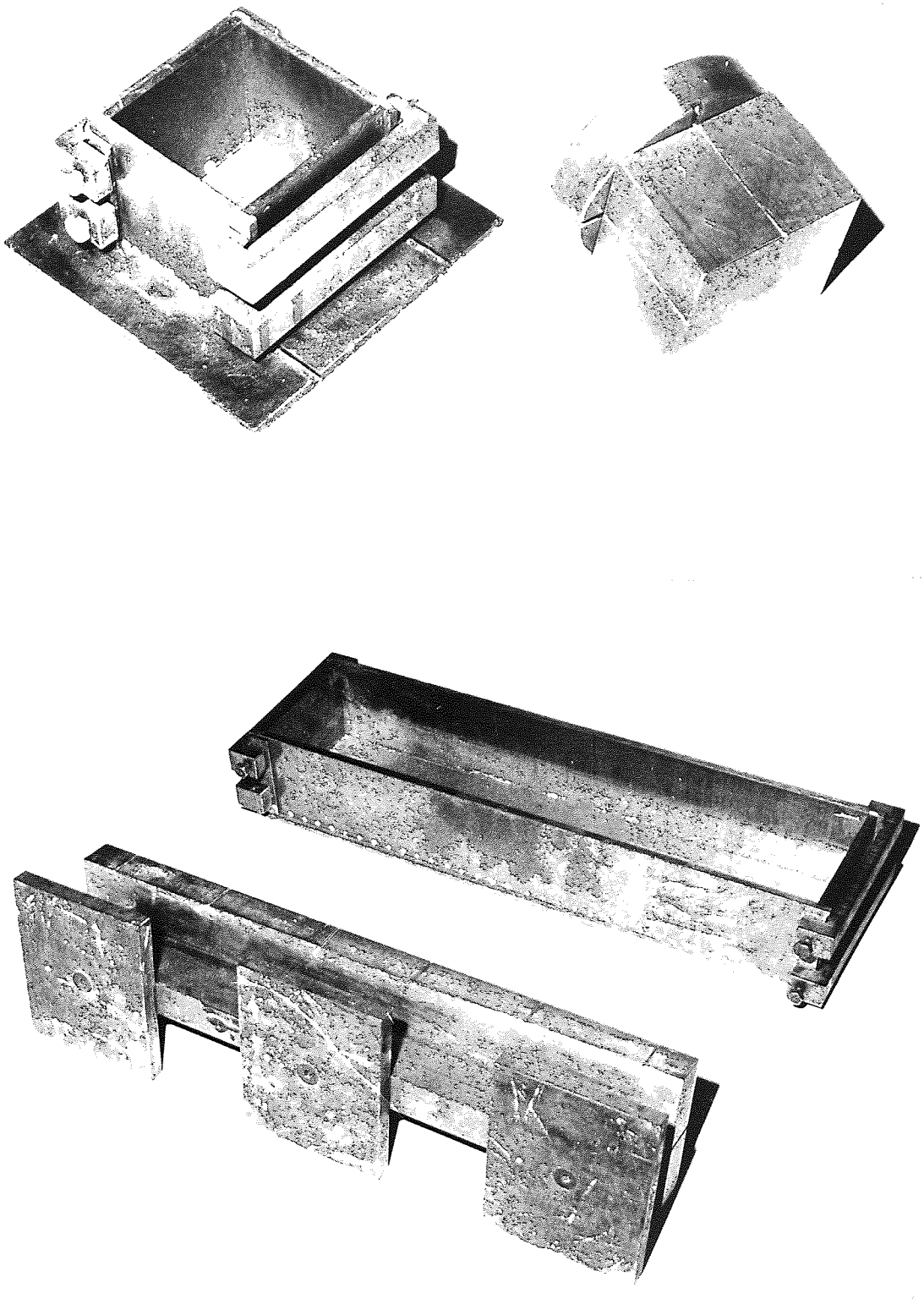

Fig. 3.77 GRP compression moulds

REFERENCES

3-1) CALCOTE,L.R., "Analysis of Laminated Composite Structures", V.N.R Publisher, July 1969.

3-2) TSAI, S.W., "Structural Behaviour of composite materials", N.S.A. CR-71, July 1964.

3-3) HASHIN,Z. and ROSEN,B.W., "The elastic moduli of fibre reinforced materials". Paper No.63, WA-175.

3-4) ADAMS,D.F. and DONER,D.R., "Journal of Composite Materials" Volume 1, No.1, 1967, P.4.

3-5) ADAMS,D.F. and DONER,D.R., "Journal of Composite Materials" Volume 1, No.2, 1967, P.152.

3-6) EKVALL,J.C., "Elastic properties of orthotropic monofilament laminates" ASME paper 61-AV-56, Presented at Aviation Conference, Los Angeles, California, March, 12-16, 1961.

3-7) EKVALL,J.C., "Structural behaviour of monofilament composite" AIAA 6th Structure and Materials Conference. Palm Springs, California, April, 1965.

3-8) ROSEN,B.W.,DOWN,N.F., and HASHIN,Z., "Mechanical properties of fibrous composites". NASA CR-31, April, 1964.

3-9) WHITNEY,J.M., RILEY, M.B., "Elastic Properties of fibre reinforced composite materials" AIAA Journals, Volume 4, No.9, September 1966.

3-10) SHAFFER,B.W., "The influence of filament orientation on the material properties of reinforced plastics", SPI Annual Conference.

3-11) BISHOP,P.H.H., "Predicting mechanical properties of fibre composite", Editor, B.PARKYN, 1970, P.1969.

3-12) ROSEN,B.W.,"Tensile failure in fibrous composite", AIAA Journal, Volume 2, No.11, 1964.

3-13) HARRIS,B., "The Strength of fibrous composite", Composite, July 1972, PP.152-167.

3-14) SCHUERCH,H., "Prediction of Composite Strength in uniaxial Boron fibre-metal matrix composite material", AIAA Journal, Volume 4, January 1966.

3-15) COLEMAN,B.D.,"On the s trength of classical fibres and fibre bundles", Journal of the Mechanics and Physics of Solids, Volume 7, 1958.

3-16) BOIT,M.,"Mechanics of incremental deformities", John Wiley and Sons, Inc. New York, 1965.

3-17) LUBIN,G., "Handbook of Fibre glass and Advanced Plastics Composite, 1969, PP.595-627.

3-18) BROUTMAN and CROCK., "Modern Composite Materials", 1967, PP.97.

3-19) DOW,N.F., and ROSEN,B.W., "Evaluation of filament-reinforced composite for aerospace structural applications", NASA CR-207, 1965.

3-20) SHU,L.S., and ROSEN,B.W., "Strength of fibre reinforced composite by limit analysis methods", Journal of Composite Materials, Volume 1, 1967.

3-21) HASHIN,Z., "Theory of fibre reinforced materials", NASA CR-1974, 1972.

3-22) DIMMOCK,J. and ABRAHAMS,M., "Prediction of composite properties from the fibre and matrix properties", Composite, Volume 1, No.2, 1969, PP.87-93.

3-23) ABRAHAMS,M., and DIMMOCK,J., "Mechanical and economic comparisons of reinforced thermoplatics", Plastic and Polymer, June 1971, PP.187-194.

3-24) HASHIN,Z., "Journal of Applied Mechanics", Volume 34, 1966, P.336.

3-25) OWEN,M.J., and FOOND,M.S., "Static and fatigue failure of glass fibre reinforced polyester resin under complex stress condition", Faraday special discussion at Nottingham, June 1972.

3-26) STOWELL,E.Z., and LU,T.S., "Journal of Mechanics and Physics" Volume 9, 1961, P.242.

3-27) NORRIS,C.B.,"Forest Products Laboratories", Report 1816, 1962.

3-28) TSAI,S.W.,"Strength characteristics of composite materials" NASA CR-224, 1965.

3-29) HOFFMAN,O., "Journal of Composite Materials" Volume 1, No.2, 1967, P.200.

3-30) ASHKENAZI,E.K., "On the problem of s trength anisotropy of construction materials" Soviet Phys. - Technical Phys., Volume 4, No.3, September 1959, PP.333-338.

3-31) MARIN,J.,"Theories of strength for combined stresses and non-isotropic materials", Journal of Aeronautical Sciences., Volume 24, No.4, April 1957, PP.265-269,274.

3-32) TSAI,S.W., and WU,E.M. "Journal of Composite Materials" Volume 5, 1971, P.58.

3-33) OGORKIEWICZ,R.M.,"Mechanical behaviour of fibre composite" Glass reinforced plastics, Editor, B.PARKYN, 1970, P.190.

3-34) HILL,R., "The mathematical theory of plasticity", Oxford University Press, London, 1950.

3-35) TSAI,W., and AZZI,V.D., "Strength of Laminated composite materials" AIAA Journal, Volume 4, No.2., 1966, PP.296-301.

3-36) AZZI,V.D., TSAI, S.W., "Anisotropic Strength of composite materials" Experimental Mechanics, Volume 5, 1965, PP.283-288.

3-37) Composite Materials, Testing and Design, ASTM, STP 460, American Society for Testing and Materials, 1969.

3-38) Second ASTM Conference on Composite Materials, Testing and Design, April 1971.

3-39) ASTM, Methods of Testing Platics, Part 26 and 27, 1973.

3-40) STURGEON,J.B., "Specimens and test methods for carbon fibres reinforced platics", RAE, Technical Report, 71026, 1971.

3-41) PURSLOW,D., and COLLINGS,T.A., "A test specimen for the compressive strength and modulus of unidirectional carbon fibres reinforced plastic latminates", RAE, Technical Reports, 72096, 1972.

3-42) EWINS,P.D., "Techniques for measuring the mechanical properties of composite materials", composite-standard testing and design, NPL Conference, April 1974.

3-43) Method of Testing Platics, British Standard Institution B.S.2782, 1970.

3-44) Grafil, Test Methods, April 1970.

3-45) Scotchply Brand, Reinforced Plastics design guide.

3-46) WADDOUPS,M.E., "Characterization and design of composite materials", TSAI,S.W., Composite materials workshops, Technomic Publ.Co.,1968, P.254.

3-47) NAIR,N.G.,MALLINDER,G.P., and PROCTOR,B.A., "Specimens and test methods for fibre reinforced materials". Pilkington Brothers Technical Report, 1972.

3-48) FOYE,R.L., and BAHER,D.J., "Design of Orthotropic laminates", Presented at the 11th Annual AIAA Structures, Structural Dynamics and Materials Science Conference, Denver , Colarado, April, 1970.

3-49) PAGANO,N.J., and PIPES,R.B., "Journal of Composite Materials" Volume 5, January 1971, PP.50-57.

3-50) CRESCZUK,L.B., In Ref.37 PP.140-149.

3-51) ISHAI,O., and LAVENGOOD,R.E., "Characterizing Strength of unidirectional composite", In ref.37, PP.271-281.

3-52) HAPLIN,J.C., et al, In ref.37, PP.37-47.

3-53) PIPES,R.B., and PAGANO,N.J., "Journal of Composite materials" Volume 4, October, 1970, P.538.

3-54) DASTIN,S., et al., In ref. 37, PP.13-26.

3-55) ELKIN,R.A. et al., In ref.37, PP.321-335

3-56) PROSEN,S.P., "Composite materials testing", Ref.37, PP.5-12.

3-57) LENDE, et al., "Preliminary evaluation of test standard for Boron-Epoxy laminates", Ref.37, PP.122-139.

3-58) SATTAR,S.A., and KELLOGG,D.H., "Effect of geometry on the mode of failure of composite in short beam shear test", Ref.37, PP.62-71.

3-59) WEST,D.C., "Experimental mechanics", Volume 4, No.7, July 1964, P.185.

3-60) HEAP,R.D., and NORMAN,R.H., "Flexural testing of plastics", Plastic Institute, 1969.

3-61) GRESCZUK,L.B., "Effect of Voids on strength properties of filamentary composites", SPI 22nd. Annual Meeting, 1967.

CHAPTER 4

THE STRENGTH AND STIFFNESS OF MULTI-PHASE LAMINATED COMPOSITES.

4.1) Introduction.

In Chapter 3 a wide structural characterization of GRP was investigated. As a result, it was shown that in contrast to most conventional materials, GRP's strength and stiffness can be controlled by the orientation angle, stacking sequence, and the fibre content of the laminates which form the GRP composite. It was also shown that although reasonably high strengths were achieved from the various types of GRP composites investigated, the modulus values associated with the strength results were very low if compared with the modulus of structural steel which is about four times that of GRP. Thus in structural uses where stiffness rather than strength are critical, it would be advantageous to improve the modulus of GRP composites.

An effective way of improving the modulous is by the introduction of steel wire sheet. A composite consisting of steel wire-glass fibre reinforced plastice, referred to as SGRP, will be described in this chapter and its properties investigated.

4.2) General Definition.

Steel-wire sheet is an arrangement of parallel wires laid on a suitable sub-base, as shown in Fig.(4-1). Normally the wire used is 0.25 mm (0.01 in.) diameter hard drawn, brass coated steel wire. Its breaking strength is equal to 2.52 to 2.75 KN/mm^2, i.e. 133-135 N/wire. Other wires can, of course, be used, for instance, rocket wire of 0.10 mm diameter with a breaking strength of 4.13 KN/mm^2, or stainless steel or nickel alloy wires where resistance to very low temperature is needed. The substratum or carrier on which

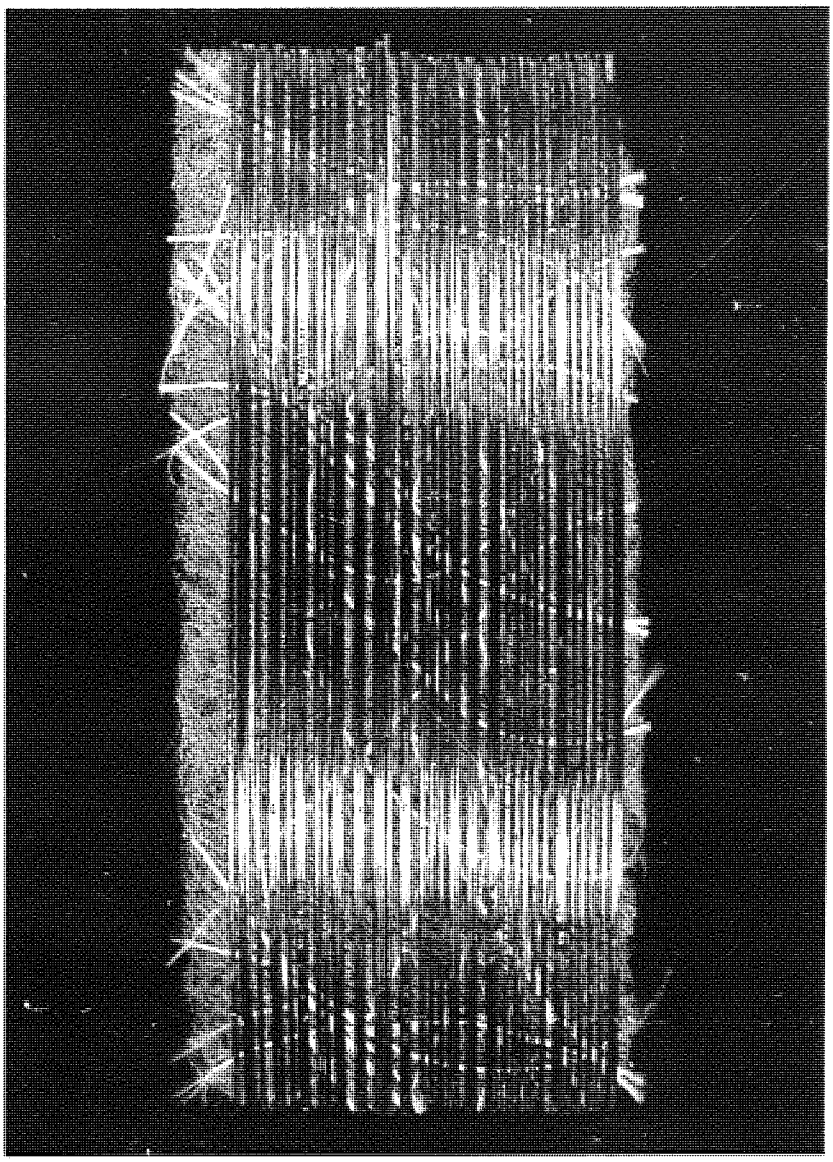

Fig. 4.1. Steel wire sheet

4.2) contd.

the wires are arranged is normally a very thin glass fibre tissue, bonded polyester cloth, woven glass cloth, thin layers of expanded polystyrene, and even paper have been used for some purposes, (ref.4-1). The resin which is used to bond the wire to the sub-base, is normally a polyester resin which adheres very well to the cleaned wire and to which the laminating resin, which is normally a polyester or epoxy resin, adheres in its turn.

The stress-strain curve of this material is linear, nearly up to failure. A slight non-linearity is usually noticed in the region of 85-90% of the ultimate stress. Fig.(4-2) shows the stress-strain relationship for the high tensile steel wires compared to E-Glassfibres, and polyester resin (ref.4-2).

The advantages of using wire sheets with GRP composites are given below:

a) Increasing the modulus of elasticity at room temperature and at elevated temperature of the composits.

b) Increasing the modulus of rigidity of the composite.

c) Reducing delamination and interlaminar shear failure. This is because of the very good wetting between resin and wires and hence the low voids content.

d) Reduced depreciation of strength with time due to static loads.

e) Fewer impregnation or wetting-out problems.

Nominal properties of commercially avaiable wire sheet produced by the National Standard Company can be found in Table (4-1). A comparison of the mechanical propertis of the wires of the sheet and other reinforcing fibres can be found in Table (4-2).

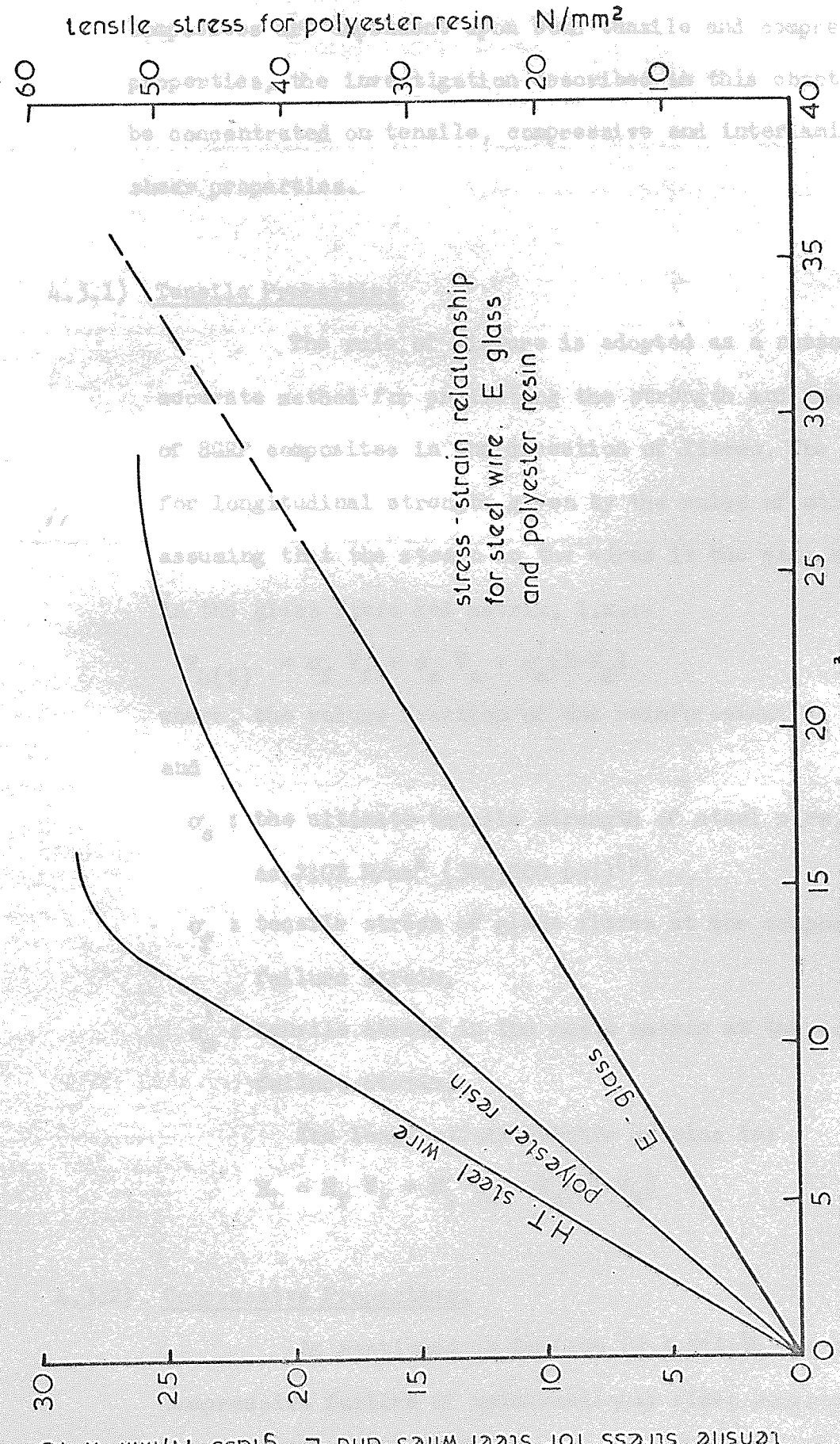
tensile stress for polyester resin N/mm²
60
50
40
30
20
10
stress - strain relationship for steel wire, E glass and polyester resin
H.T. steel wire
polyester resin
E - glass
0
5
10
15
20
25
30
35
40
strain x 10⁻³
tensile stress for steel wires and E-glass N/mm² x 10⁻²
30
25
20
15
10
5
0

Fig. 4.2

4.3) Theoretical Prediction.

Since the flexural properties of fibre reinforced composites are dependent upon both tensile and compressive properties, the investigation described in this chapter will be concentrated on tensile, compressive and interlaminar shear properties.

4.3.1) Tensile Properties

The rule of mixture is adopted as a reasonably accurate method for predicting the strength and the modulus of SGRP composites in the direction of fibres. The value for longitudinal strength given by the rules of mixture assuming that the strain in the wires is the same as that in the glass fibre and matrix, i.e.:-

$$F_{L(t)} = \sigma_f V_f + \sigma_s V_s + \sigma'_m(1-V_R) \qquad (4.1)$$

where, the volume fraction of the reinforcement $V_R = V_f + V_s$

and

σ_s : the ultimate tensile strength of steel wire, taken as 2102 N/mm² (300,000 psi)[2]

σ_f : tensile stress of glass fibres at the composite failure strain,

σ'_m : tensile stress in the resin matrix at the composite failure strain.

The longitudinal elastic modulus is:

$$E_L = E_f V_f + E_s V_s + E_m (1-V_R) \qquad (4.2)$$

4.3.2) Compressive Properties.

As mentioned in Section (3.3.2(ii)), the mode of compressive failure of unidirectional fibre composites is a micro-buckling of the reinforcement which is similar to the buckling of a column on an elastic foundation. According

Wire: Hard drawn high Carbon Steel, brass plated

Diameter	:	0.254 mm
Tensile Strength	:	2628 N/mm^2
Tensile Modulus	:	210231 N/mm^2
Breaking load per wire	:	14 kg.
Elongation to break	:	Minimum 1.5% average approximately 2%

Wire spacing per/cm	:	23.6	15.7	11.8	7.9
Weight kg/m^2	:	1.03	0.71	0.54	0.38
Weight of wire only kg/m^2	:	0.937	0.625	0.468	0.312
Width cm	:	38	57	76	76

Backing material: Glass fibre non-woven tissue

Table (4-1)

Nominal Properties of Wire Sheet

NOTE: Data taken from ref.(4-2)

	Tensile Strength N/mm	Tensile Modulus N/mm^2	Fibre Length mm	Specific Gravity
High Tensile Wire as in Wire Sheet	2803	210231	Continuous	7.8
E-Glass fibre	1752	73581	Continuous	2.55
Asbestos fibres	2978	179397	Up to 150	2.9
Carbon fibres	1752 2453	385424 245270	1000 1000	2.0 1.74

Table (4.2)

Average figures for typical figres

for comparison purposes.

4.3.2) contd.

to this, the compressive strength of SGRP is given by:-

$$F_{L(c)} = 0.25 \frac{\bar{G}_m}{1 - \bar{V}_R} \qquad (4.3)$$

where

$$\bar{V}_R = (1-V_v)V_R \qquad (4.5)$$

is the voided volume fraction of reinforcement in SGRP,

and

$$\bar{G}_m = \frac{E_m}{2(1+\nu_m)} \left(1 - \frac{V_v}{1 - \bar{V}_R}\right) \qquad (4.6)$$

is the reduced matrix shear modulus due to voids.

The compressive longitudinal modulus can be predicted in the same manner as the tensile one and by the aid of equation (4.2).

4.3.3) Interlaminar Shear Strength.

Interlaminar Shear Strength (ILSS) in SGRP composites is considered to be higher than that of GRP composites for the reason mentioned earlier (c in Section 4.2). Therefore, it is expected that the ILSS of SGRP will approach the shearing strength of the resin matrix which is assumed to be the upper bound of the interlaminar shear strength of fibre composites.

4.4) Materials for Specimens.

a) wire sheets of hard drawn high carbon steel, brass plated. Composed of about 24 wires/cm. (60 wires/in.) with an under mat of glass fibre non-woven tissue. These sheets are supplied by The National Standard Company, Kidderminster, England.

4.4) contd.

b) Glass fibres, resin and catalyst are the same as those described in Sections (3.6.3 i and ii).

4.5) Description of Moulds and Moulding Technique.

The mould used in preparing the SGRP sheets was of metal from which sheets could be produced of dimensions 1150 × 250 × 2.5 mm.

The moulding technique adopted was the same as that described in Section (3.6.4) but the number of reinforcing layers used in the composite was three, one wire sheet sandwiched between two glass fibre layers. This stacking sequence gave the following composite properties,

Volume content of steel wires:	V_s	: 7.1%
Volume content of glass fibres:	V_f	:25.9%
Volume content of resin matrix:	V_m	:64.9%
Volume content of air voids:	V_v	: 2.1%
Total volume content of reinforcement :	V_R	: 33%

The above properties were determined according to Section (3.6.9).

4.6) Details of Specimens and test procedures.

The design consideration applying to these specimens are the same as those in Section (3.6). These specimens were used to determine the material property in the direction of the reinforcement which is the major concern in this chapter.

4.6.1) Tension tests.

The uniform cross-section (un-necked) specimens described in Section (3.6.5 ii(b)) was used to characterize the SGRP composite in longitudinal tension (i.e. strength, modulus, Poisson's ratio, and stress-strain relationship). The necked specimen was not adopted because of difficulties of machining and problems of time and cost. Details of the specimen are shown in Fig.(3-11B, Chapter 3).

Preparation of specimens and test procedure are similar to that mentioned in Section (3.6.5 iv) for GRP specimens.

4.6.2) Compression tests.

The specimens used to characterize SGRP in longitudinal compression was the straight edged (unwaisted) specimens described in Section (3.6.6 ii(b)). The waisted specimen was not used for the reasons mentioned in Sections (4.6.1), and (3.6.6. ii b(2)).

The shape of the specimens was similar to the GRP specimens shown in Figs.(3-12 C and D), but the slenderness ratio used on the SGRP specimens was 17:1 which made the clear length of the specimen between the aluminium end fittings equal to 13 mm. and the overall dimensions 43 × 12.5 × 2.5 mm.

Preparation of the specimens and the test procedures were similar to those mentioned in Section (3.6.6 iii) for GRP specimens.

4.6.3) Interlaminar Shear Strength test.

The short beam specimen was adopted for the determination of ILSS of SGRP composites. In order to ensure a

4.6.3) contd.

shear failure in the specimen and in accordance with Section (3.6.7) and Fig.(3-15), the span/depth ratio chosen for the specimen was 4. This ratio being consistent with a flexural/shear strength ratio of about 14 which is about average for the SGRP composite investigated. The overall dimensions of the specimen were 15 × 10 × 2.5 mm.

The test loading system and test procedure were the same as those described in Sections (3.6.7 iii and iv) for GRP composites.

4.7) Experimental Results.

All the experimental results, compared with theory, are given in Table (4-3). A comparison between the experimental results for various GRP composites and SGRP composites are shown in Table (4.4).

4.8) Discussion of Experimental results and Comparison with theory.

4.8.1) Stress-Strain Relationship

The tensile stress-strain relationship for the SGRP specimens investigated was linear up to failure with an average ultimate strain of 1.6% which is nearly equal to the ultimate strain of the steel wire, see Fig.(4.2).

The compression stress-strain relationship was also linear up to failure and showed a lower ultimate strain than in tension which did not exceed 1%. This may be due to the effect of local instability of the reinforcement which occurred at a lower compressive strain than that occurring in tension.

Stress-strain behaviour of SGRP under repeated load in tension or compression up to 10 load cycles, proved to have an insignificant effect and no irrecoverable strain

No. of Layers = 3 (Glassfibres, Steel Wire, Glassfibres)

No. of Specimens = 5

Reinforcement Volume Content = 0.33 , V_s = 0.071, V_f = 0.259

Voids Volume Content = 0.02

	TENSION		COMPRESSION		INTER-LAMINAR SHEAR N/mm^2
	Strength N/mm^2	Modulus N/mm^2	Strength N/mm^2	Modulus N/mm^2	
Theory	488 Eq.(4.1)	36095 Eq.(4.2)	423 Eq.(4.3)	36095 Eq(4.2)	67
Experiment	447	27938	302	26667	Corrected (voided) 56
Standard Deviation	3.5	19	11.6	49	4.3

Table (4.3)

Mechanical Properties of SGRP Composites.

Type of Composite	Number of Layers	V_R	Density gm/cm^3	TENSION		COMPRESSION		Interlaminar Shear Strength N/mm^2	Shear Modulus N/mm^2
				Strength N/mm^2	Modulus N/mm^2	Strength N/mm^2	Modulus N/mm^2		
GRP	4	0.27	1.50	420	19227	241	16129	50.00	3300
GRP	5	0.39	1.69	571	24381	317	23256	48.60	2600
GRP	6	0.46	1.77	616	27655	330	26316	51.46	2800
GRP	7	0.57	1.88	725	32787	398	32787	48.38	3600
GRP	8	0.64	2.00	858	41000	385	40000	45.47	4000
SGRP	3 G-S-G	0.33	1.73	447	27938	302	26667	56.40	3846

TABLE (4-4)

Comparison of Experimental Results Between GRP and SGRP Composites

4.8.1) contd.

appeared in either case.

Stress-strain relationship in tension and compression are shown in Figs.(4-3 to 6).

4.8.2) Tensile Properties.

(i) Strength

The experimental results show excellent agreement with the theory of equation (4.1), from Table (4-3) the experimental results are seen to be within 10% of the theory. Thus the law of mixture, represented by equation (4.1), predicts the tensile strength of SGRP more accurately than GRP. This is most likely due to the lesser amount of misaligned reinforcement in the wire sheet than in the unidirectional glass mat. The lower void content of SGRP relative to GRP would also explain the improved SGRP property.

A graphical representation of equation (4.1) is shown in Fig.(4-7) illustrating the variation of longitudinal tensile strength with respect to different reinforcement volume content of GRP and SGRP composites. Fig.(4.7) is useful for design purposes as will be shown later in this chapter.

The failure mode of SGRP specimens in tension was found to be a combination of clean fracture of the steel wires across the specimen width, together with a non-uniform failure due to splintering of glass fibres. The mode of fracture of the steel wire indicates uniform stress transfer from resin to wire, whilst the splintering is a common mode of failure in unidirectional GRP composites. It's main cause, is the presence of voids trapped in the

4.8.2) contd.

(i) contd.

fibre bundles which tend to disturb the stress transfer from the resin to fibres and stress concentration takes place. A typical failure of an SGRP specimen in tension is shown in Fig.(4.8).

(ii) Longitudinal Modulus.

Like tensile strength, the experimental results of longitudinal modulus of SGRP agreed reasonably well with the theory presented by equation (4.2), which may be used to design purposes within certain limits of accuracy. For design use Fig.(4.9) shows the variation of the longitudinal modulus with different volume contents of reinforcement for both SGRP and GRP according to equation (4.2).

4.8.3) Compressive Properties.

(i) Strength.

Unlike tensile strength the experimental results for compressive strenght were not in such good agreement with the theory presented by equation (4.3). But in general they were acceptable to the same extent as those obtained for GRP specimens (see Table 3-5, Chapter 3).

A design chart showing the variation of compressive strength with different reinforcement contents of GRP and SGRP composites according to equation (4.3), is given in Fig.(4.10).

Modes of failure in compression are analogous to those observed on GRP specimens. These modes are the delamination and shear modes. The first type is common when the reinforcement is the critical phase in the composite as shown in Fig.(4.11A). From Fig.(4.11A) it can be seen that the delamination took place as a result

4.8.3) contd.

(i) contd.

of the local instability of the reinforcement, (i.e. the steel wires and glass fibres). The second mode of failure, the shear mode, is common when the resin is the critical phase in the composite (i.e. in the case of low reinforcement content and/or when the stressing is perpendicular to the unidirectional reinforcement). See Fig.(4.11B).

(ii) Longitudinal Modulus.

Compressive modulus results showed nearly the same agreement with equation (4.2) as the tensile results, so that for design purposes, Fig.(4.9) may be used for both tensile and compressive modulus.

4.8.4) Interlaminar Shear Strength.

Interlaminar Shear Strength results were in general higher than those obtained for GRP specimens. This is related to the lower amount of voids present in the composite as mentioned earlier in this chapter.

The experimental results for ILSS shown in Table (4.3) represent the corrected voided simple bending theory results due to the width/depth ratio effect. The correction factor $\overline{K} = 1.30$ was obtained from Fig.(3.16) Chapter 3. For $E_L/G_{LT} \simeq 10$ and $\frac{b}{t} = 4$. The results also showed a closer agreement with the predicted values.

4.9) Design Considerations.

The SGRP composite investigated in this program were formed from three layers stacked as Glasslayer, wire sheet, Glasslayer. This packing was considered as a basic form of SGRP composite and the intention was to substitute one layer

4.9) contd.

of wire sheet for two layers of glass fibres in the 4-layered GRP composite. A comparison could then be made between this basic SGRP and the 4-layers unidirectional GRP investigated in Chapter 3.

From Table (4.4) it can be seen that the experimental results for the tensile and compressive modulus of SGRP are much higher than the modulus of 4-layer GRP in tension and compression, in fact it more nearly matches modulus results of the 6-layers GRP. No considerable differences is evident in the strength results between SGRP and the 4-layers GRP but the SGRP showed a higher density and reinforcement content than the 4-layers GRP (see Table 4.4).

As a result of this analysis a conclusion can be drawn that the introduction of steel wire sheets into the GRP has a single benefit of increasing the stiffness.

To make the problem more unified and for the sake of rapid and safe design, design charts have been prepared showing the relation between the number of layers in the composite, the thickness of the composite and the volume content of fibres and wires in the composite. These charts are shown in Fig.(4.12) and can be used in connection with Figs.(4.7, 9 and 10) to design a composite unit according to the needand requirement.

For example, consider the design of a composite of 5 mm. thickness for a required longitudinal modulus of 100 KN/mm^2 (14.27×10^6 psi). With what reinforcement content should this composite be designed? Will this composite be manufactured from GRP or SGRP? If from SGRP what percentage of wire reinforcement and glass fibre should be used in the composite? What is the number of reinforcing layers to be

4.9) contd.

used? Finally, what tensile and compressive strengths will the composite possesses?

To answer these questions Fig.(4.9) may be used to find which volume percentage of glass fibres and steel wires will achieve the required modulus value wanted. From this figure, three types of composite are found to be suitable, viz:-

SGRP(1) with $V_f = 0.05$ and $V_s = 0.45$, gives $V_R = 0.50$

SGRP(2) with $V_f = 0.20$ and $V_s = 0.40$, gives $V_R = 0.60$

SGRP(3) with $V_f = 0.35$ and $V_s = 0.35$, gives $V_R = 0.70$.

The tensile and compressive strengths for each of the above three composites may be found from Figs.(4.7 and 10) respectively, viz:-

	V_f	V_s	Tensile Strength (N/mm^2)	Compressive Strength (N/mm^2)
SGRP (1)	0.05	0.45	1025	565
SGRP (2)	0.20	0.40	1100	710
SGRP (3)	0.35	0.35	1175	945

Table (4.5)

Table (4.5) shows that SGRP(3) is superior to the other two. To complete the design, the number of layers of glass fibre and steel wire should be known for each composite to make the total thickness of the designed unit equal to 5mm. Thus from Fig.(4.12), Table 4.6 may be prepared:-

	SGRP(1)		SGRP(2)		SGRP(3)	
	V_f	V_s	V_f	V_s	V_f	V_s
Number of layers for total 5 mm. thickness	1	9	3	7	6	8

Table (4.6)

To achieve a symmetric arrangement of layers about

4.9) contd.

the thickness centre line SGRP (3) should be chosen as the best type of composite that meets the requirements of the design.

The properties of the designed composite are repeated below:-

Total thickness of composite	:	5 mm.
Total number of layers	:	14
Number of glass fibre layers	:	6
Number of wire sheets	:	8
Total volume fraction of reinforcement	:	70%
Volume fraction of glass fibure	:	35%
Volume fraction of steel wires	:	35%
Young's Modulus	:	100 KN/mm^2
Tensile strength	:	1175 N/mm^2
Compressive strength	:	945 N/mm^2
Stacking Sequence	:	GGSSSSGGSSSSGG

where (G) refers to glass layer and (S) refers to steel wire sheet.

Note that Fig.(4.12) has been arranged only for the type of glass fibre and wire sheet used in this project. Similar charts for other types of glass fibre and wire sheet can be easily produced to meet a wider design requirement,

4.10) Conclusion.

The introduction of steel wire sheet to glass reinforced plastic effects a considerable improvement on the material modulus as shown in Tables (3.3 and 4). Design requirements may be achieved by using the design charts in Figs.(4.7, 9, 10 and 12).

Like most GRP composites, the stress-strain relation-

4.10) contd.

ship in tension and compression were linear up to failure. The ultimate tensile strain was about 1.6% which is nearly the same as the ultimate strain for steel wire, while the ultimate compressive strain did not exceed 1% (Figs.4.3 and 5). This means that SGRP composites show less deformation to failure than GRP composites which experience failure strains of about 1-3.5%.

SGRP composites shows good resistance to repeated load in tension and compression and no permanent deformation was observed after ending the cycling load, see Figs.(4.4 and 6).

Tensile properties showed an excellent agreement with equations (4.1 and 2) while compressive results, like GRP, showed less agreement with the theory presented by equation (4.3). Interlaminar shear strength showed a higher value than that obtained in GRP, probably because of the lower amount of voids present in SGRP composites under investigation.

The use of steel wire as reinforcement to improve the stiffness of GRP is a new field of design and its advantage is the combination of these two materials to form a new reinforced composite which combines the advantageous properties of both materials.

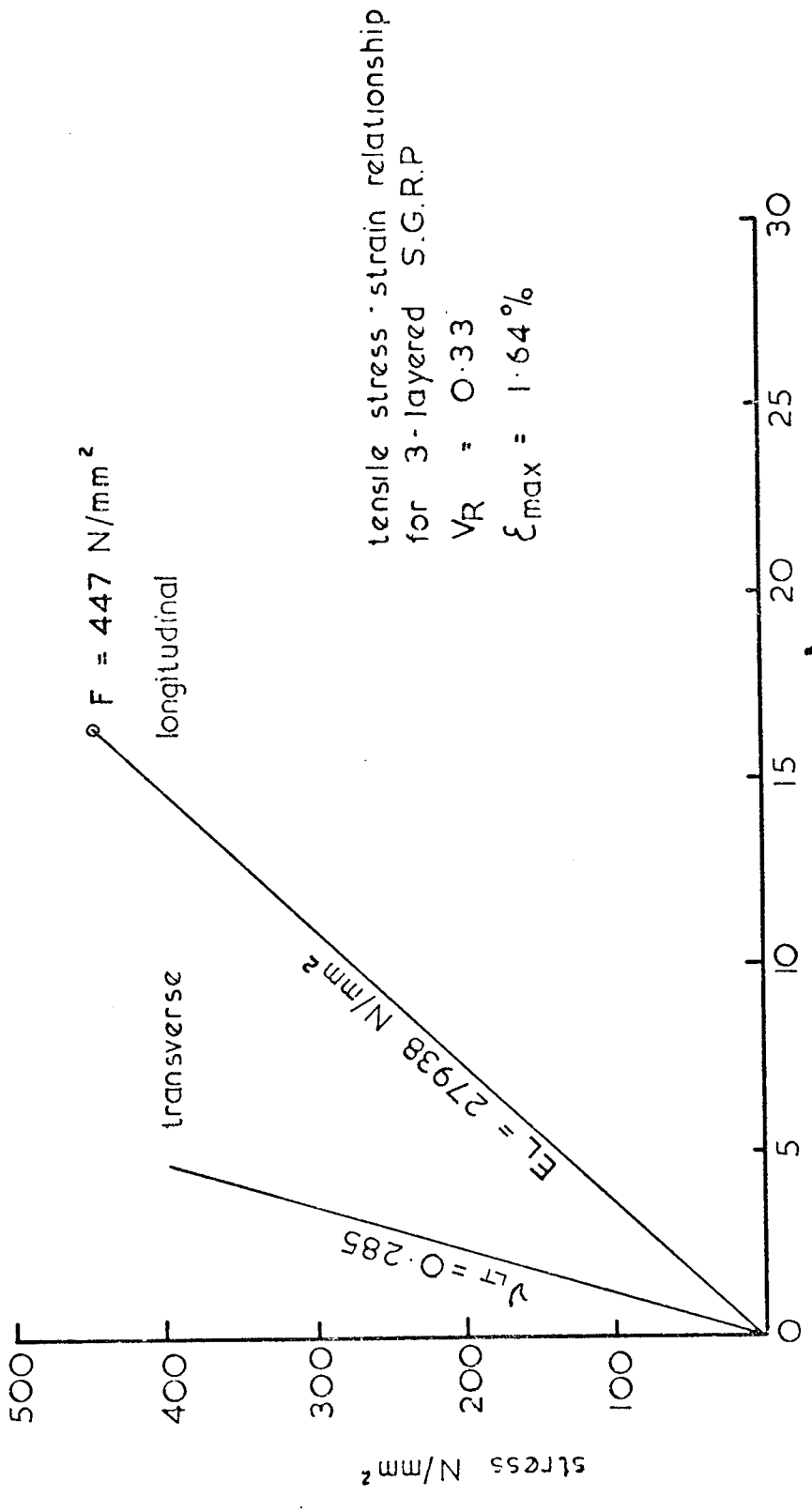
tensile stress - strain relationship
for 3-layered S.G.R.P
V_R = 0·33
ε_{max} = 1·64%
F = 447 N/mm²
longitudinal
transverse
E_L = 27938 N/mm²
ν_{LT} = 0·285
stress N/mm²
strain x 10^{-3}
0
100
200
300
400
500
5
10
15
20
25
30

Fig. 4.3

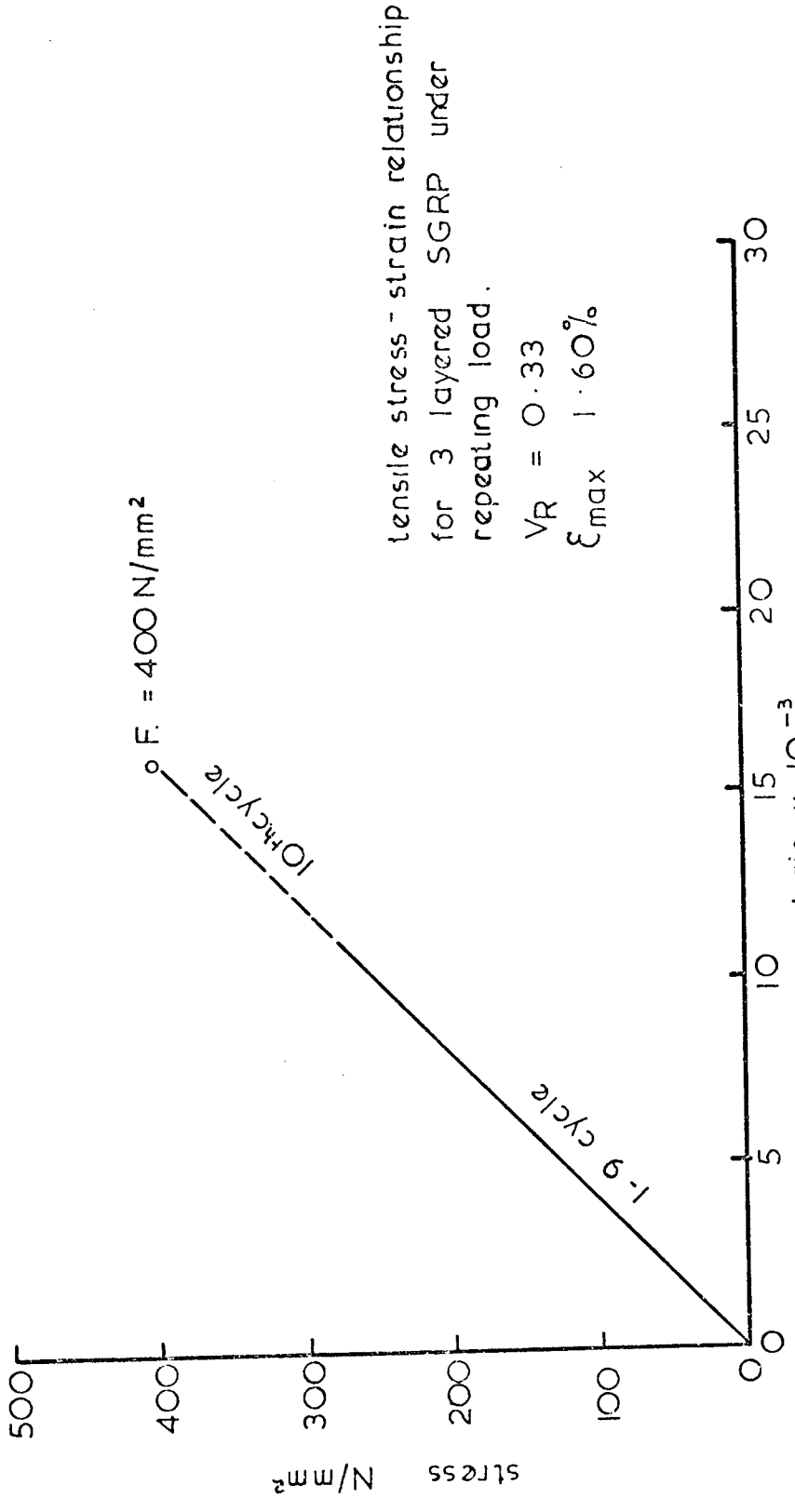
tensile stress - strain relationship
for 3 layered SGRP under
repeating load.
V_R = 0·33
ε_{max} 1·60%
F. = 400 N/mm²
10⁴ cycle
1·9 cycle
stress N/mm²
strain x 10⁻³
0
100
200
300
400
500
5
10
15
20
25
30

Fig. 4.4.

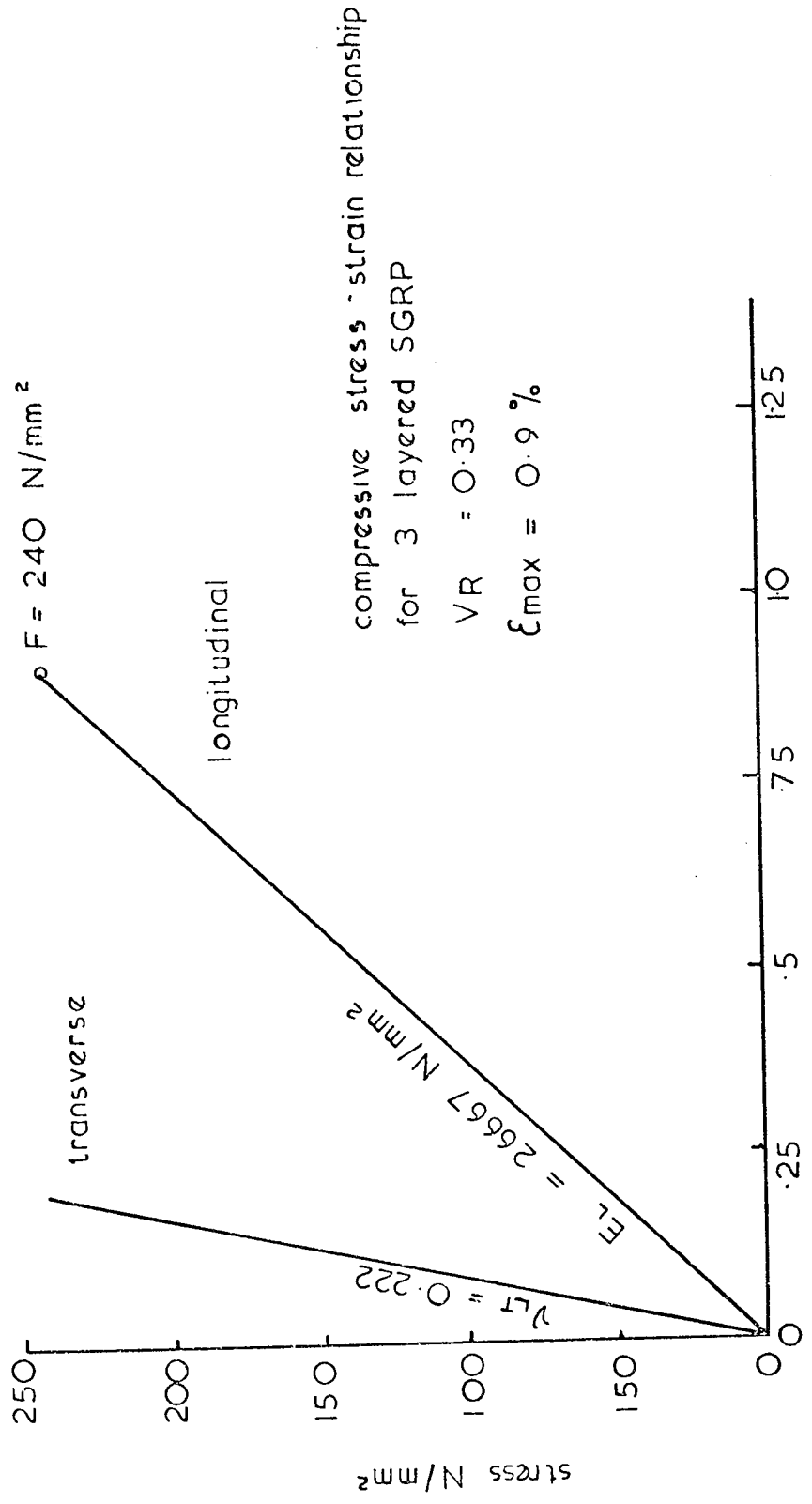
compressive stress - strain relationship
for 3 layered SGRP
VR = 0·33
ε_{max} = 0·9 %
F = 240 N/mm²
longitudinal
transverse
E_L = 26667 N/mm²
ν_{LT} = 0·22
stress N/mm²
strain x 10^{-3}
250
200
150
100
150
0
0
·25
·5
·75
1·0
1·25

Fig. 4·5

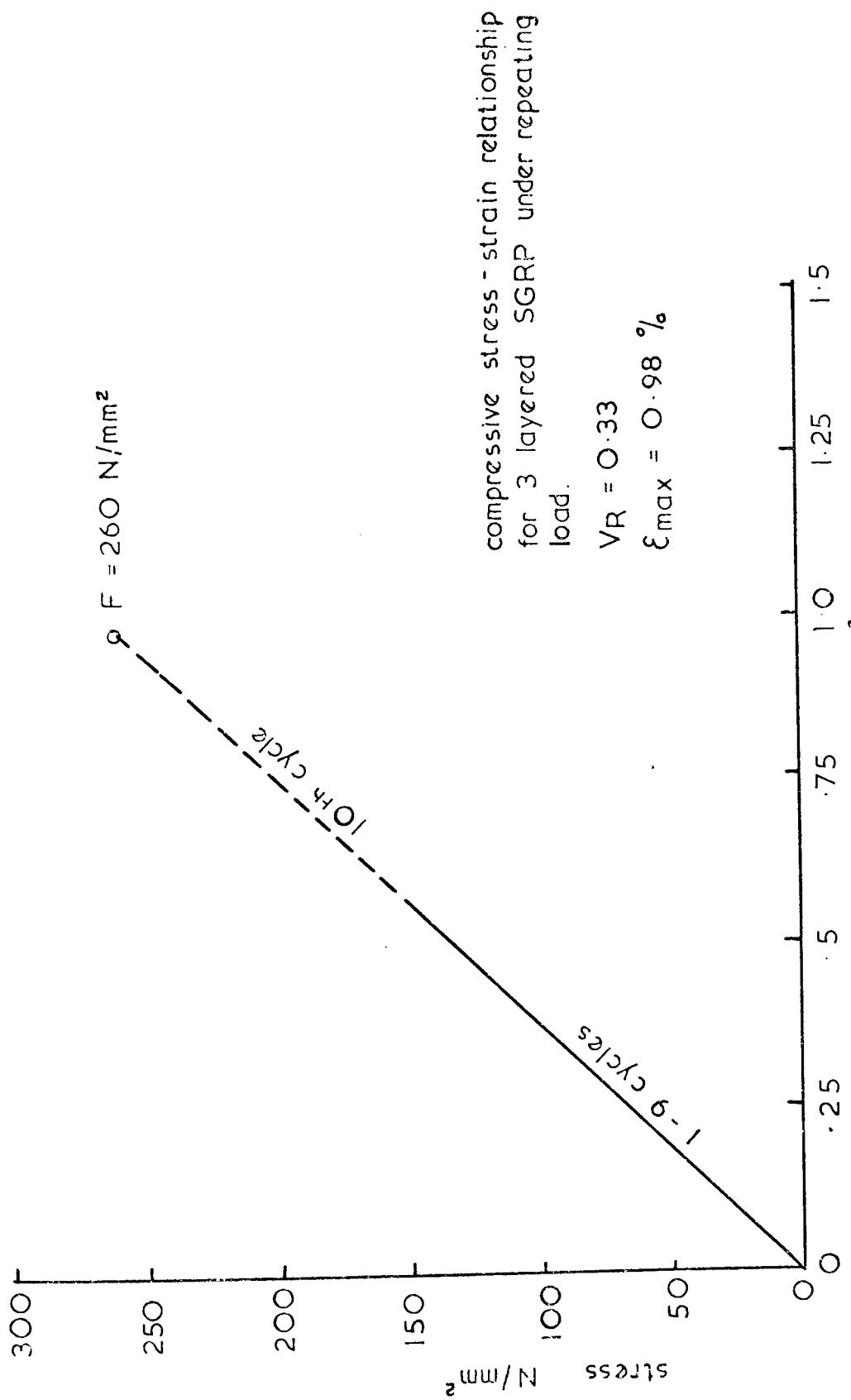
compressive stress - strain relationship
for 3 layered SGRP under repeating
load.
V_R = 0·33
ε_{max} = 0·98 %
F = 260 N/mm²
10^{4} cycle
1·9 cycles
stress N/mm²
strain x 10^{-3}
0
50
100
150
200
250
300
·25
·5
·75
1·0
1·25
1·5

Fig. 4.6.

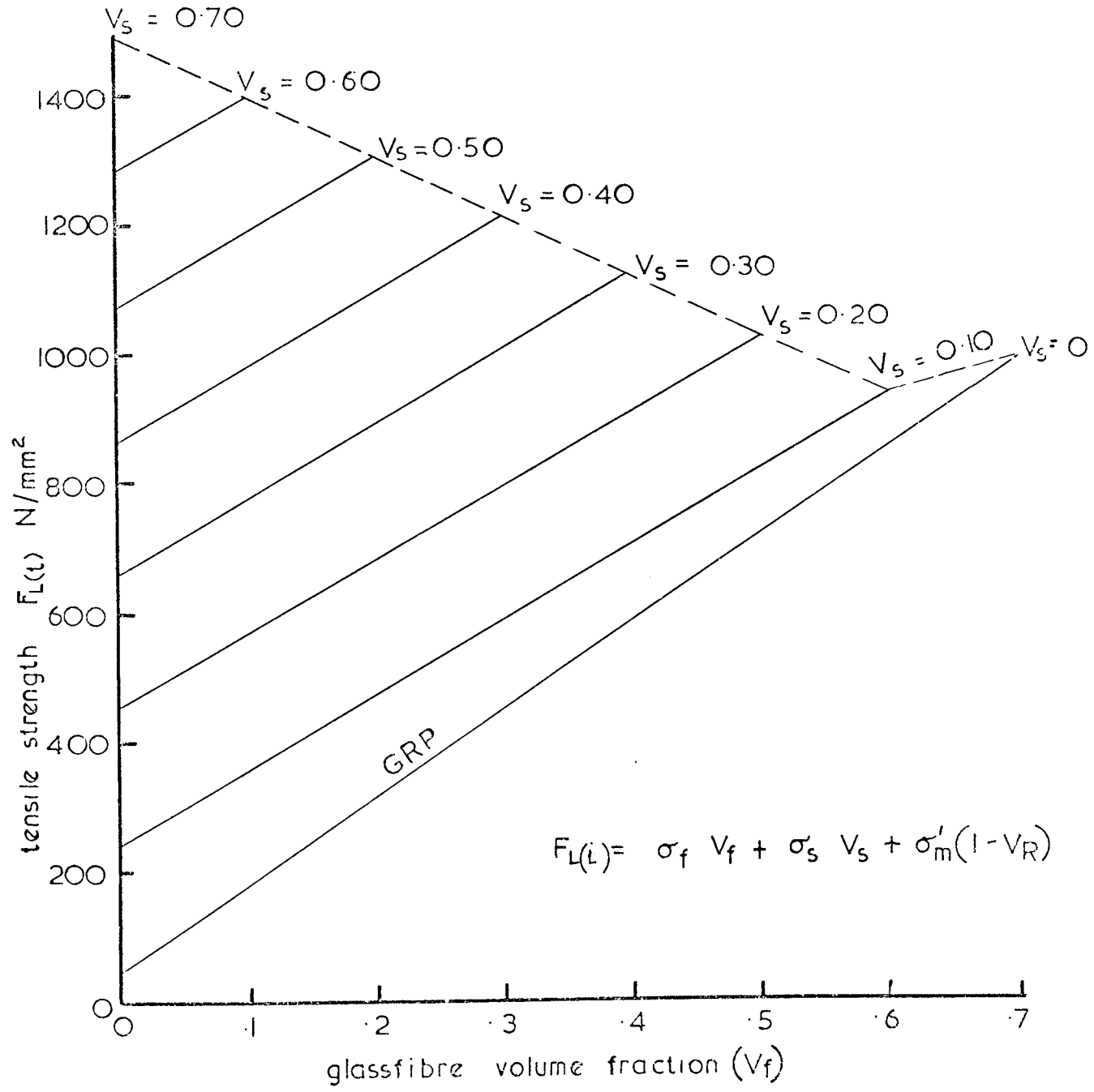
V_s = 0·70
V_s = 0·60
V_s = 0·50
V_s = 0·40
V_s = 0·30
V_s = 0·20
V_s = 0·10
V_s = 0
GRP
1400
1200
1000
800
600
400
200
0
tensile strength $F_{L(t)}$ N/mm²
0
·1
·2
·3
·4
·5
·6
·7
glassfibre volume fraction (V_f)
$F_{L(t)} = \sigma_f V_f + \sigma_s V_s + \sigma'_m(1 - V_R)$

Fig. 4.7.

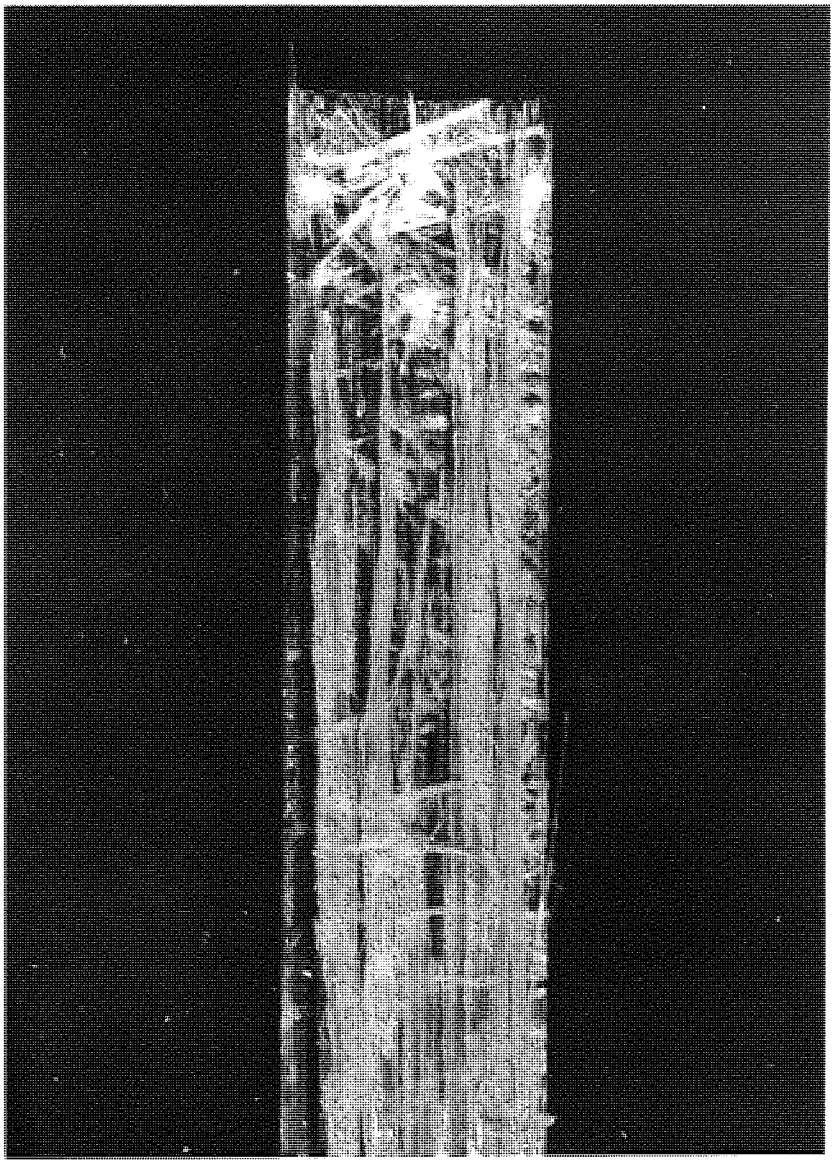

Fig. 4.8 Typical tensile failure of SGRP specimen

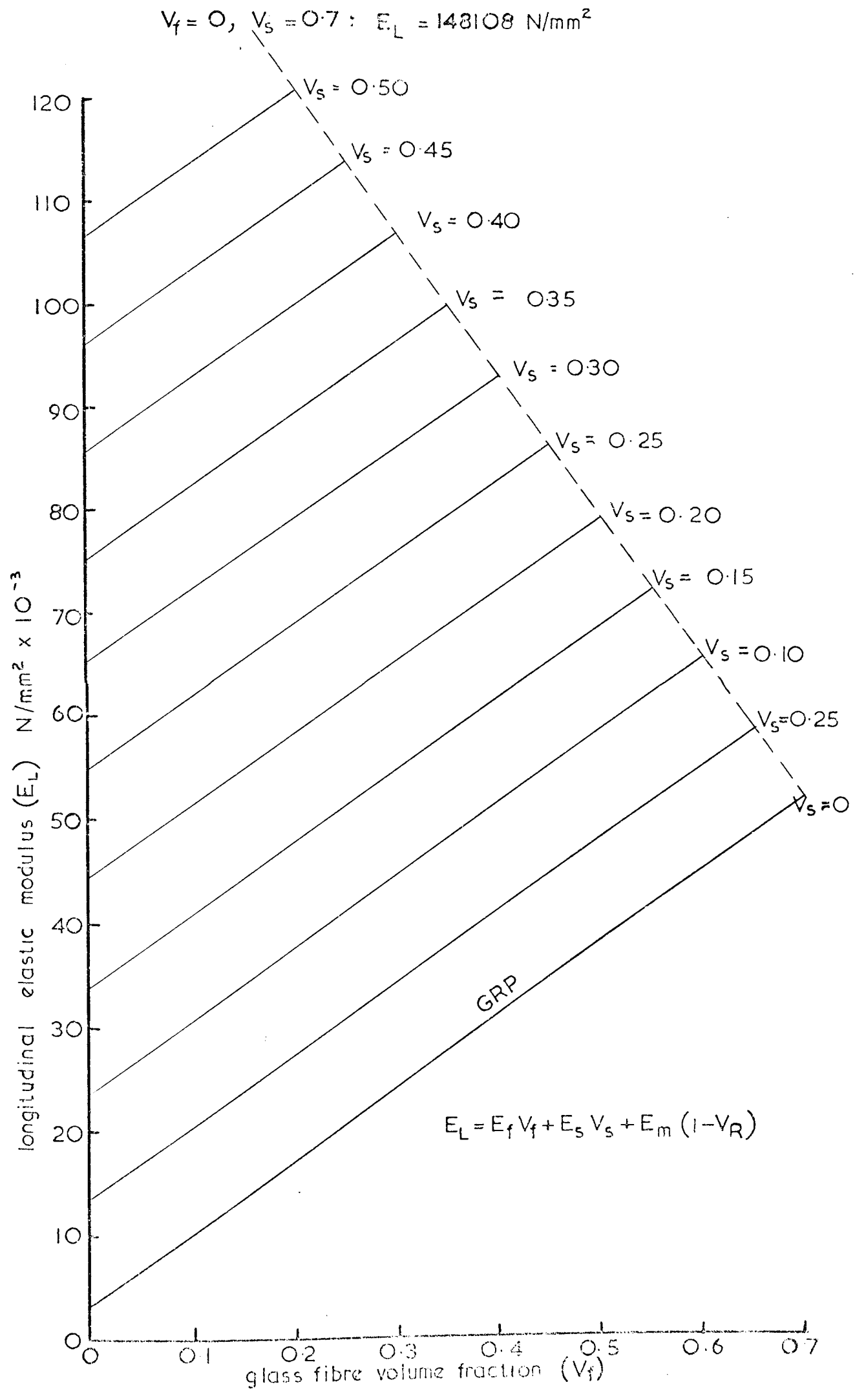
$V_f = 0$, $V_s = 0.7$: $E_L = 148108$ N/mm²
$V_s = 0.50$
$V_s = 0.45$
$V_s = 0.40$
$V_s = 0.35$
$V_s = 0.30$
$V_s = 0.25$
$V_s = 0.20$
$V_s = 0.15$
$V_s = 0.10$
$V_s = 0.25$
$V_s = 0$
GRP
$E_L = E_f V_f + E_s V_s + E_m (1 - V_R)$
longitudinal elastic modulus (E_L) N/mm² x 10^{-3}
glass fibre volume fraction (V_f)
0
10
20
30
40
50
60
70
80
90
100
110
120
0.1
0.2
0.3
0.4
0.5
0.6
0.7

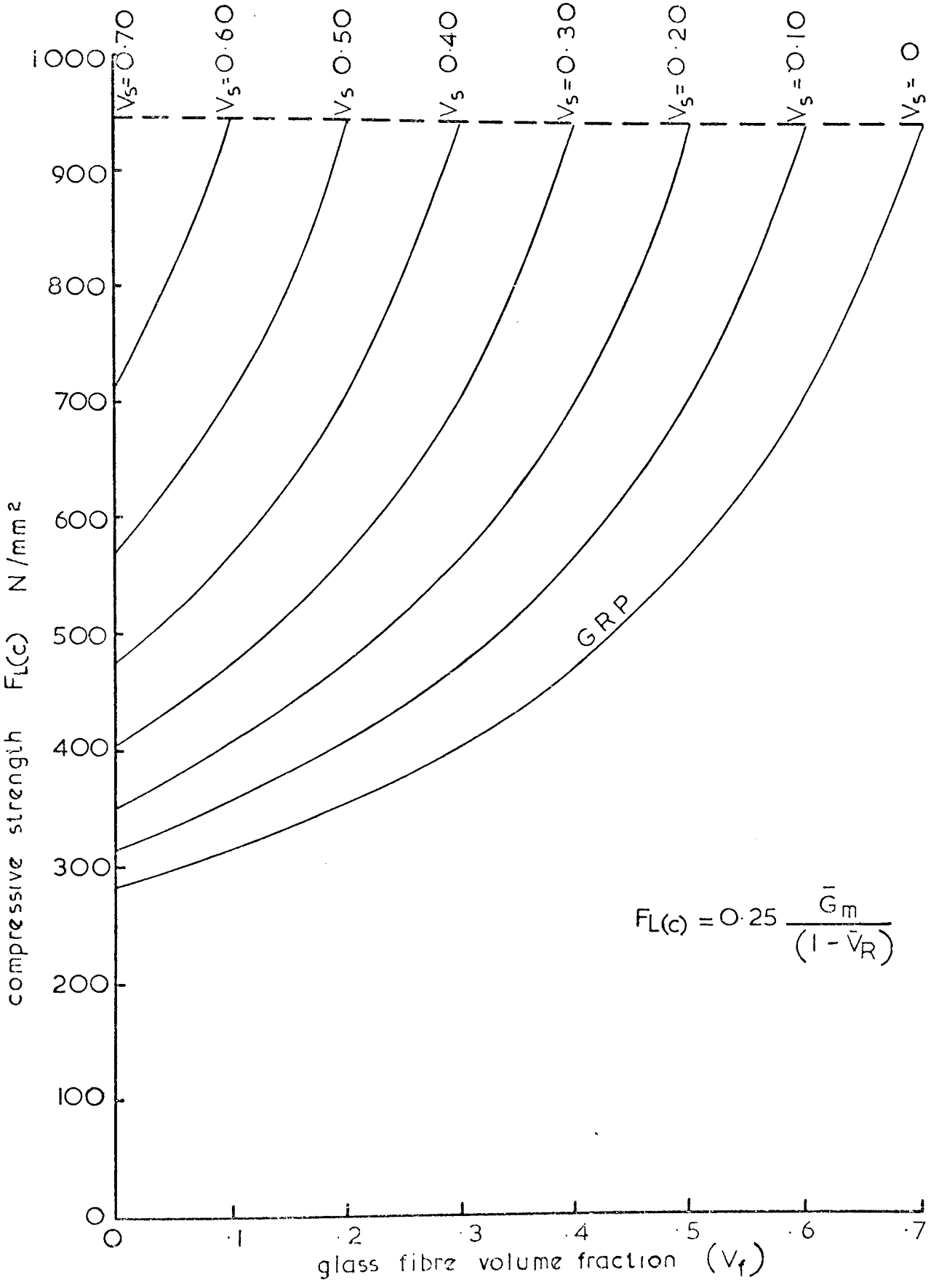
Vs=0·70
Vs=0·60
Vs 0·50
Vs 0·40
Vs=0·30
Vs=0·20
Vs=0·10
Vs= 0
GRP
1000
900
800
700
600
500
400
300
200
100
0
compressive strength FL(c) N/mm²
0
·1
·2
·3
·4
·5
·6
·7
glass fibre volume fraction (Vf)
FL(c) = 0·25 Ḡm / (1 - V̄R)

Fig. 4·10

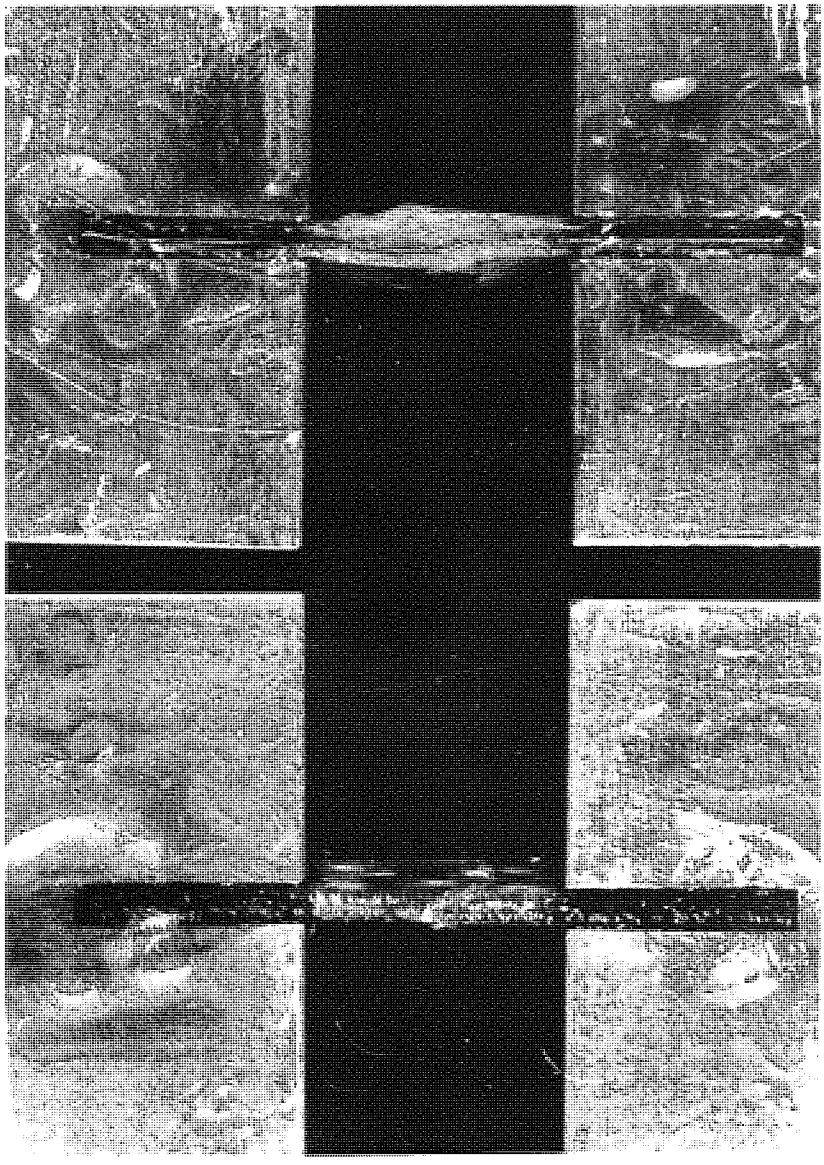

A

B

Fig. 4.11. Modes of compressive failure of SGRP specimens

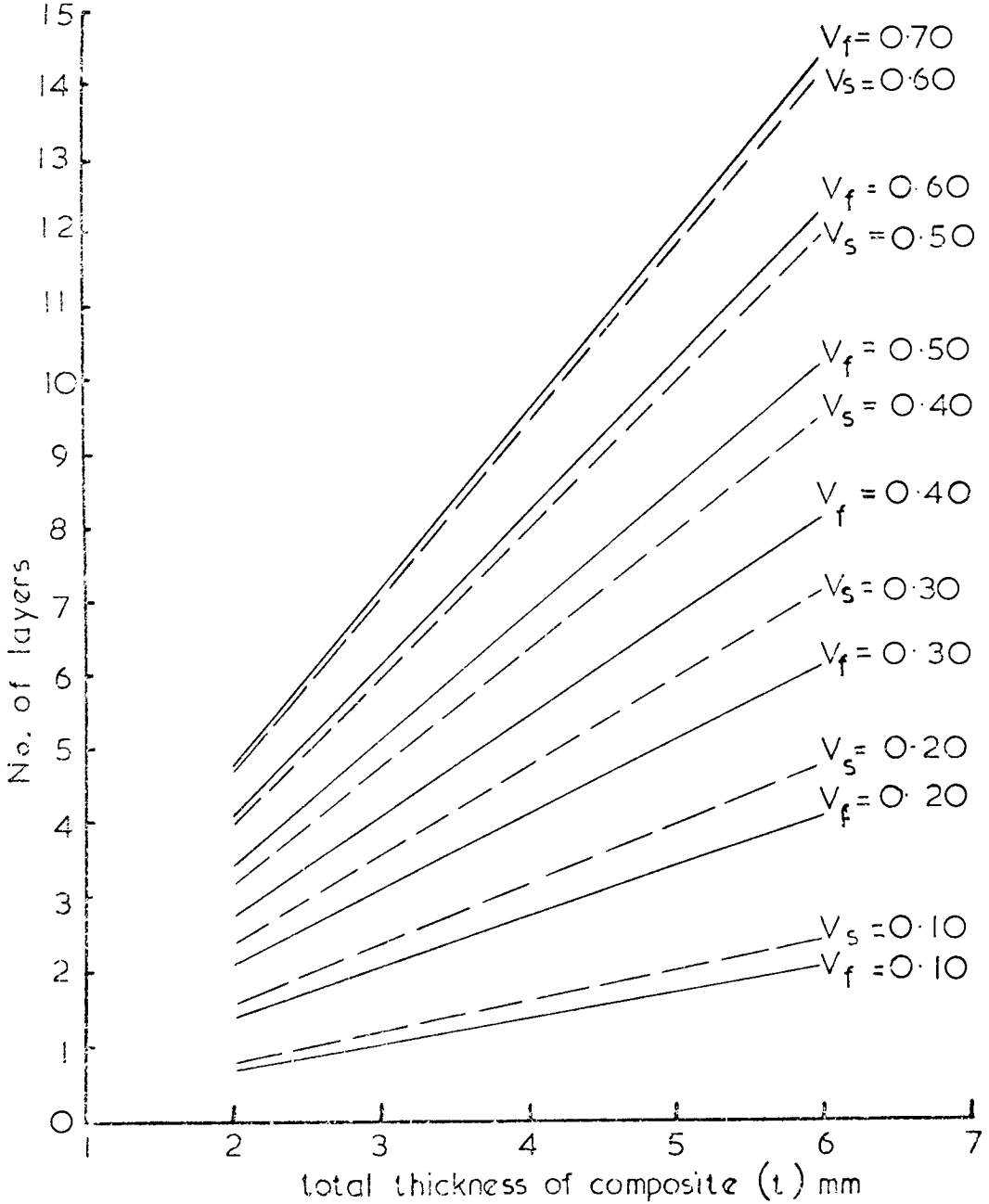

Fig. 4.12

$$\text{No. of layers} = \frac{V_R}{t_{layer}} \times t_{compt.}$$

glass laminations

thickness = 0·295 mm
weight = 750 gm/m²

steel wire layer

thickness = 0·254 mm
weight = 10 30 gm/m

REFERENCES.

4-1) JARAY,F.F., "Hard-drawn steel wires as reinforcement for thermosetting laminate", The Chemical Engineer, October, 1970.

4-2) National Standard Company Technical Data.

4-3) JARAY,F.F., "Behaviour of wire reinforced plastic using the wire sheet as reinforcing material", 22nd Annual Meeting, SPI Reinforced Plastics Division, 1967.

CHAPTER 5

THE STABILITY OF GRP PLATES.

5.1) Introduction.

As previously mentioned in Chapter 2, GRP sections should preferably be thin in order to maintain a reasonable overall cost of the element to be manufactured and to reduce the effect of the exothermic action during the curing stage, this is of considerable importance if the thickness of the GRP element is greater than 12 mm and the moulding technique is by a mechanised method (i.e. single stage moulding).

Thin walled sections create no problems if used in tension but the situation is completely different if these sections are used under compression or shearing when instability becomes a major problem.

Flat rectangular plates may be considered as the basic elements of thin walled open or closed sections, so this chapter will cover an investigation on the stability of flat GRP plates under uniaxial compression or pure shear. The investigation will be concentrated on the effect of fibre arrangement and plate dimensions (i.e. aspect ratio) on the buckling load under certain boundary conditions which will be defined later in this chapter. The design consideration of GRP plates that fail by instability and yielding simultaneously will also be considered.

5.2) Basic assumptions:

In most practical applications of thin plates the magnitude of the stresses acting on the surface parallel to the middle plane are small compared to the bending and membrane stresses. Since the plate is thin, this implies that the tractions on any surface parallel to the midplane are relatively small. In particular, an approximate state of plane stress exists.

5.2) contd.

A standard x,y,z coordinate system, as shown in Fig.(5.1), is used in deriving the equations. The displacements in the x,y,z direction are denoted by u,v,w, respectively. The following basic assumptions are made (ref.5-1):

1. The plate is constructed by an arbitrary number of layers of orthotropic sheets moulded together. However, the orthotropic axes of material symmetry of an individual layer need not coincide with the x-y axes of the plate.
2. The plate is thin, that is, the thickness h is much smaller than the other physical dimensions.
3. The displacements u,v,w are small compared to the plate thickness.
4. In-plane strains ϵ_x, ϵ_y and ϵ_{xy} are small compared to unity.
5. All plates are symmetrically laminated so that B_{ij} matrix all vanished, see Section (3.3.5).
6. Transverse shear strains ϵ_{xz} and ϵ_{yz} are negligible.
7. Tangential displacement u and v are linear functions of the z-coordinate.
8. The transverse normal strain ϵ_z is negligible.
9. Each ply obeys Hooke's law.
10. The plate has constant thickness.
11. Rotary inertia terms are negligible.
12. There are no body forces.
13. Transverse shear stresses σ_{xz} and σ_{yz} vanish on the surfaces $z = \pm h/2$.

It should be noted that assumption 6 is a direct consequence of plane stress. Together 6 and 7 constitute the classical assumptions of Kirchhoff. Assumption 8 allows the problem to be reduced to a two dimensional study of the middle

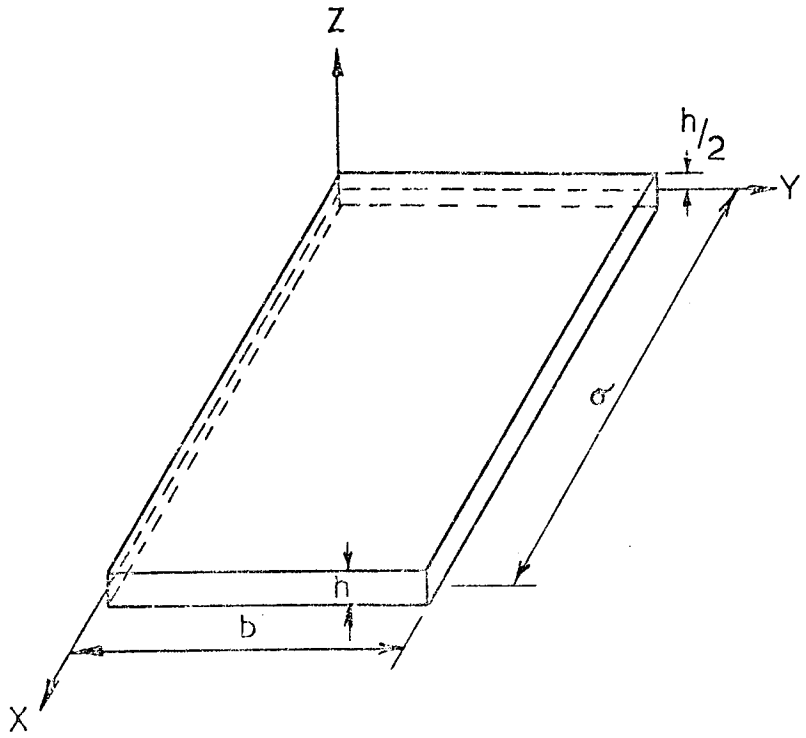

Fig. 5.1 Coordinate system of plate

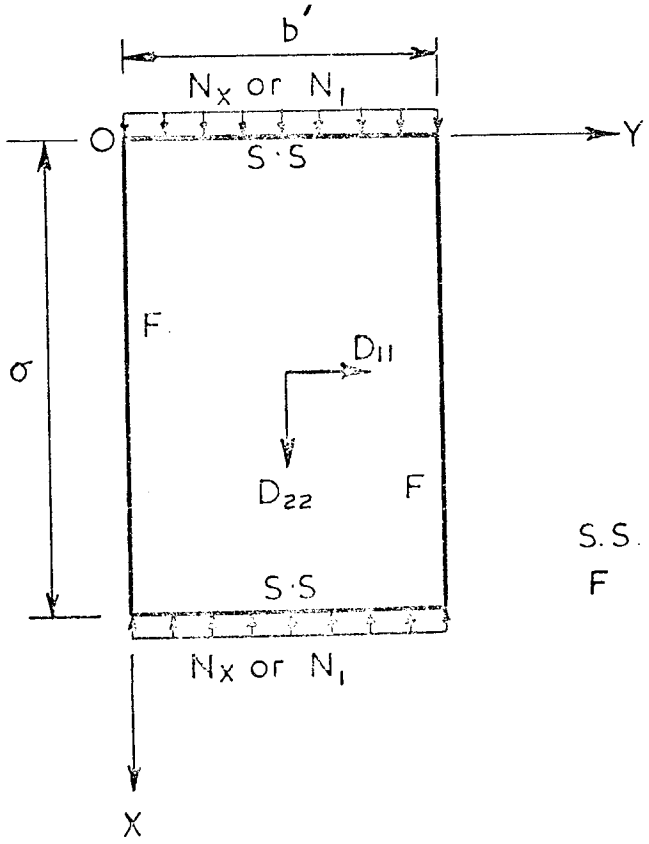

S.S. Simple support
F Fixed

Fig. 5.2 Schematic diagram of a typical test specimen with assumed load and boundary conditions

5.2) contd.

plane.

5.3) Theoretical Prediction of buckling load.

The classical anisotropic plate formulation is represented by the differential equation which describes the bending of an anisotropic plate subjected to an in-plane edge loading and neglecting any bending-membrane coupling terms: (refs.5-2 and 5-3),

$$D_{11}\frac{\partial^4 w}{\partial x^4} + 4D_{16}\frac{\partial^4 w}{\partial x^3 \partial y} + 2D_3\frac{\partial^4 w}{\partial x^2 \partial y^2} + 4D_{26}\frac{\partial^4 w}{\partial x \partial y^3} + D_{22}\frac{\partial^4 w}{\partial y^4} + N_x\frac{\partial^2 w}{\partial x^2} + 2N_{xy}\frac{\partial^2 w}{\partial x \partial y} + N_y\frac{\partial^2 w}{\partial y^2} = 0 \qquad (5.1)$$

where $D_3 = D_{12} + 2D_{66}$

and $w = f(y)\ \mathrm{Sin}\ \frac{m\pi x}{a}$.

Many other equations have been derived which represent special conditions of the fibre and layer arrangement in the plate. The theories behind these equations are presented in the following.

5.3.1) Specially orthotropic plate theory.

Specially orthotropic laminated plates have been shown to be governed by equations which are less formidable than those governing more general laminated plates, in fact these plates can usually be analysed with the same techniques used frequently for isotropic plates.

Since the analysis of specially orthotropic plates is more easily handled, laminated plates have in the past often been assumed to behave as such specially orthotropic plates. It is important to note, however, that the only laminated plates which strictly qualify as specially orthotropic plates are those laminated symmetrically where the laminate principle axes

5.3.1) contd.

coincide to those of the plate. Because of this, the normal stress-twist curvature terms D_{16} and D_{26} will vanish from equation (5.1) which becomes, (see ref.5-1,3 to 5-8),

$$D_{11}\frac{\partial^4 w}{\partial x^4} + 2D_3\frac{\partial^4 w}{\partial x^2 \partial y^2} + D_{22}\frac{\partial^4 w}{\partial y^4} + N_x\frac{\partial^2 w}{\partial x^2} + 2N_{xy}\frac{\partial^2 w}{\partial x \partial y} + N_y\frac{\partial^2 w}{\partial y^2} = 0 \qquad (5.2)$$

Equation (5.2) is the specially orthotropic plate formulation under general in-plane edge loading. A thorough discussion on this theory and its derivation may be found in ref.(5-1).

5.3.2) Mid-Plane Symmetric Laminated Plates:

In this section, a more general laminated plate than the orthotropic plate will be considered. In particular, the D_{16} and D_{26} are considered in the analysis, ref.(5-1), and also appear in the general equation as will be shown later. The stiffness coupling matrix terms - the B_{ij} - are also assumed to be zero.

Laminated plates for which the B_{ij} terms do not exist but which exhibit non-zero D_{16} and/or D_{26} terms are an important class of plates. They are equivalent mathematically to homogeneous anisotropic plates. Such plates occur when the laminate possesses mid-plane symmetry, (i.e. when there is a lamina above the geometrical mid-plane at the same distance from the mid-plane and having identical orientation and properties for each lamina below the mid-plane). The laminate principle axes are not necessarily coincident with the principle axes of the plate.

The general formulation for this type of plate is similar to equation (5.1).

A detailed analysis of these plates may be found in ref.(5-1).

5.3.3) General Laminated Plates theory:

In the previous two sections, the types of plates presented were for laminates exhibiting mid-plane symmetry with regard to the stacking sequence of the individual layers.

General laminated plate theory covers the analysis of those plates which are unsymmetrically laminated. Because of this, the effect of the B_{ij} coupling terms has been considered in deriving the general equation which may be found in detail in ref.(5-1).

5.3.4) Numerical Methods.

Buckling loads for plates for which the D_{16} and D_{26} terms are of the same order of magnitude as the other flexural stiffness terms cannot be found by classical orthotropic theory. A number of numerical methods are available which can be applied to plates of this type and represented by the Ritz method and Galerkin method. A thorough discussion on these methods and others may be found in ref.(5-4).

5.4) Buckling of GRP rectangular Plates under uniaxial compression:

The general aim of studying the stability of GRP plates under uniaxial compression, is to determine their characteristics under this type of loading, in order that they may be used for design purposes if these plates happen to be used as a compression flange of a GRP flexural member or as a part of a thin walled compression member.

In order to achieve this purpose it was necessary to meet the following requirements:

1. Suitable test specimens had to be fabricated with a good surface and thickness uniformity in order to minimize the amount of irregularities that may have a major effect on the buckling load. Also, the size of specimens made had to

5.4) contd.

1. contd.

be adequate to extract strength and modulus coupons for mechanical properties determination after buckling tests took place.

2. A method had to be found to determine when the critical load was reached in a plate.

3. A test arrangement capable of imposing the desired boundary and load conditions had to be designed.

5.4.1) Test Specimens:

The plate specimens listed in Table (5.1), were simply supported at the loaded ends and fixed at the unloaded edges.

No.of specimens	Type	Material	Plate Configuration	Dimensions (mm)
2	1	GRP	Unidirectional -0°- 6 layers	420x176x4.51
2	2	GRP	Angle - PLY +45,-45,-45,+45	420x176x5.03
2	3	GRP	Cross- PLY 0,90,90,0	420x176x4.85
2	4	SGRP	Unidirectional -0°- G.S.G.	420x176x2.95
2	5	GRP	Unidirectional -0°- 4-Layers	651x176x4.87
2	6	GRP	Multidirectional 0,+45,-45,-45,+45,0	420x176x4.46
2	7	GRP	Cross - PLY 0,90,90,0	651x176x4.06
2	8	GRP	Angle-Ply +45,-45,-45,+45	651x176x4.22

Table (5.1)

The boundary condition mentioned above will be called simple-fixed support throughout this chapter.

5.4.2) Theoretical Predictions

It is clear from Table (5.1) that all the GRP

5.4.2) contd.

plates investigated were symmetrically reinforced about the middle verticle and horizontal planes. So that, the theory that fits these requirements is the specially orthotropic plate theory which has been adopted to predict the buckling load theoretically. This theory is represented by equation (5.2) which has been contracted to take the following form for uniaxial compression,

$$D_{11}\frac{\partial^4 w}{\partial x^4} + 2D_3\frac{\partial^4 w}{\partial x^2 \partial y^2} + D_{22}\frac{\partial^4 w}{\partial y^4} + N_x\frac{\partial^2 w}{\partial x^2} = 0 \qquad (5.3)$$

where

$$D_1 = D_{11} = \frac{E_x t^3}{12(1-\nu_x\nu_y)} \quad \text{in the longitudinal direction,}$$

$$D_2 = D_{22} = \frac{E_y t^3}{12(1-\nu_x\nu_y)} \quad \text{in the transverse direction} \qquad (5.3a)$$

and

$$D_3 = \tfrac{1}{2}(\nu_x D_y + \nu_y D_x) + 2(GI)_{xy}$$

where $2(GI)_{xy} = 2\frac{Gt^3}{12}$ is the average torsional rigidity, see Fig.(5.2).

An approximate solution for orthotropic plates with both unloaded edges fixed was given in refs.(5-3 and 9), from which the buckling load may be predicted by the following,

$$N_{x(cr)} = \frac{\pi^2\sqrt{D_1 D_2}}{b^2}\left[\sqrt{\frac{D_1}{D_2}}\left(\frac{m'}{\phi}\right)^2 + \frac{8}{3}n^2\frac{D_3}{\sqrt{D_1 D_2}} + \frac{16}{3}n^4\sqrt{\frac{D_2}{D_1}}\left(\frac{\phi}{m'}\right)^2\right] \qquad (5.4)$$

where $\phi = \frac{a}{b}$, is the aspect ratio of the plate. The smallest value of $N_{x(cr)}$ occurs for $n' = 1$. Consequently the critical load will be determined from,

$$N_{x(cr)} = \frac{\pi^2\sqrt{D_1 D_2}}{b^2}\left[\sqrt{\frac{D_1}{D_2}}\left(\frac{m'}{\phi}\right)^2 + 2.67\frac{D_3}{\sqrt{D_1 D_2}} + 5.33\sqrt{\frac{D_2}{D_1}}\left(\frac{\phi}{m'}\right)^2\right] \qquad (5.5)$$

Let the buckling coefficient take the following form,

5.4.2) contd.

$$K_b = \sqrt{\frac{D_1}{D_2}}\left(\frac{m'}{\phi}\right)^2 + 2.67\,\frac{D_3}{\sqrt{D_1 D_2}} + 5.33\,\sqrt{\frac{D_2}{D_1}}\left(\frac{\phi}{m'}\right)^2 \qquad (5.6)$$

to minimize equation (5.6). Consider $\dfrac{d\,K_b}{d\left[\left(\frac{m'}{\phi}\right)^2\right]} = 0$

from which the minimum K_b occurs when

$$\frac{m'}{\phi} = 1.52\,\sqrt[4]{\frac{D_2}{D_1}} \qquad (5.7)$$

substituting equation (5.7) inot equation (5.6) yields,

$$K_{b(min)} = 2.67\left(1.73 + \frac{D_3}{\sqrt{D_1 D_2}}\right) \qquad (5.8)$$

and the critical buckling load is given by

$$N_{x(cr)} = \frac{\pi^2\sqrt{D_1 D_2}}{b^2}\cdot K_{b(min)} \qquad (5.9)$$

From equation (5.7),

$$\phi = 0.658\,m'\,\sqrt[4]{\frac{D_1}{D_2}} \qquad (5.10)$$

where m' is always an integer.

Ref.(5-3) gives the boundary conditions of the plate aspect ratio ϕ, when the same value of $N_{x(cr)}$ occurs from m' and $m'+1$ half-waves in the x-direction. These boundary conditions are as follows:-

$$\text{If} \quad 0 < \phi < 0.931\,\sqrt[4]{\frac{D_1}{D_2}}, \text{ then } m' = 1$$

$$\text{If} \quad 0.931\,\sqrt[4]{\frac{D_1}{D_2}} < \phi < 1.61\,\sqrt[4]{\frac{D_1}{D_2}}, \text{ then } m' = 2 \qquad (5.11)$$

$$\text{If} \quad 1.61\,\sqrt[4]{\frac{D_1}{D_2}} < \phi < 2.28\,\sqrt[4]{\frac{D_1}{D_2}}, \text{ then } m' = 3$$

Finally, in order to determine the critical buckling load for a given aspect ratio, the value of m' should be determined from equation (5.11), (i.e., establish the location of a given ratio in this formula), and by finding m', the critical

5.4.2) contd.

buckling load can easily be found from equation (5.5). For plates with a higher aspect ratio than those given by equation (5.11), their critical buckling load can be predicted by equations (5.8 and 9).

5.4.3) Test Arrangements:

The plates were subjected to compressive loads as shown in Fig.(5.3). The edges of the plates were supported by an aluminium frame in order to simulate the boundary conditions assumed in the theory. The frame was adjustable to accommodate plates of different thickness, (see Figs.5.3 and 4). The load was either read out through a load cell or else read directly off the testing machine. Deflections were measured by dial gauges for an accuracy of 0.01 mm., (see Fig.5.5). Strain was measured by electrical strain gauges similar to those mentioned in Chapters 3 and 4 and shown in Fig.(5.3).

5.4.4) Test Procedure:

The plate was positioned under the loading machine in an accurate verticle position. Then the load was applied to the plate and released repeatedly for two or three times until uniform and constant readings were obtained from the dial gauges. This takes out much of the misalignment in the fixtures. The test was then run and,deflections were normally taken after every load increment up to at least one-half the plate thickness and often higher than this limit.

Strain gauge readings were obtained after every load increment by the aid of a computerized data logger.

The loading was usually stopped after a clear

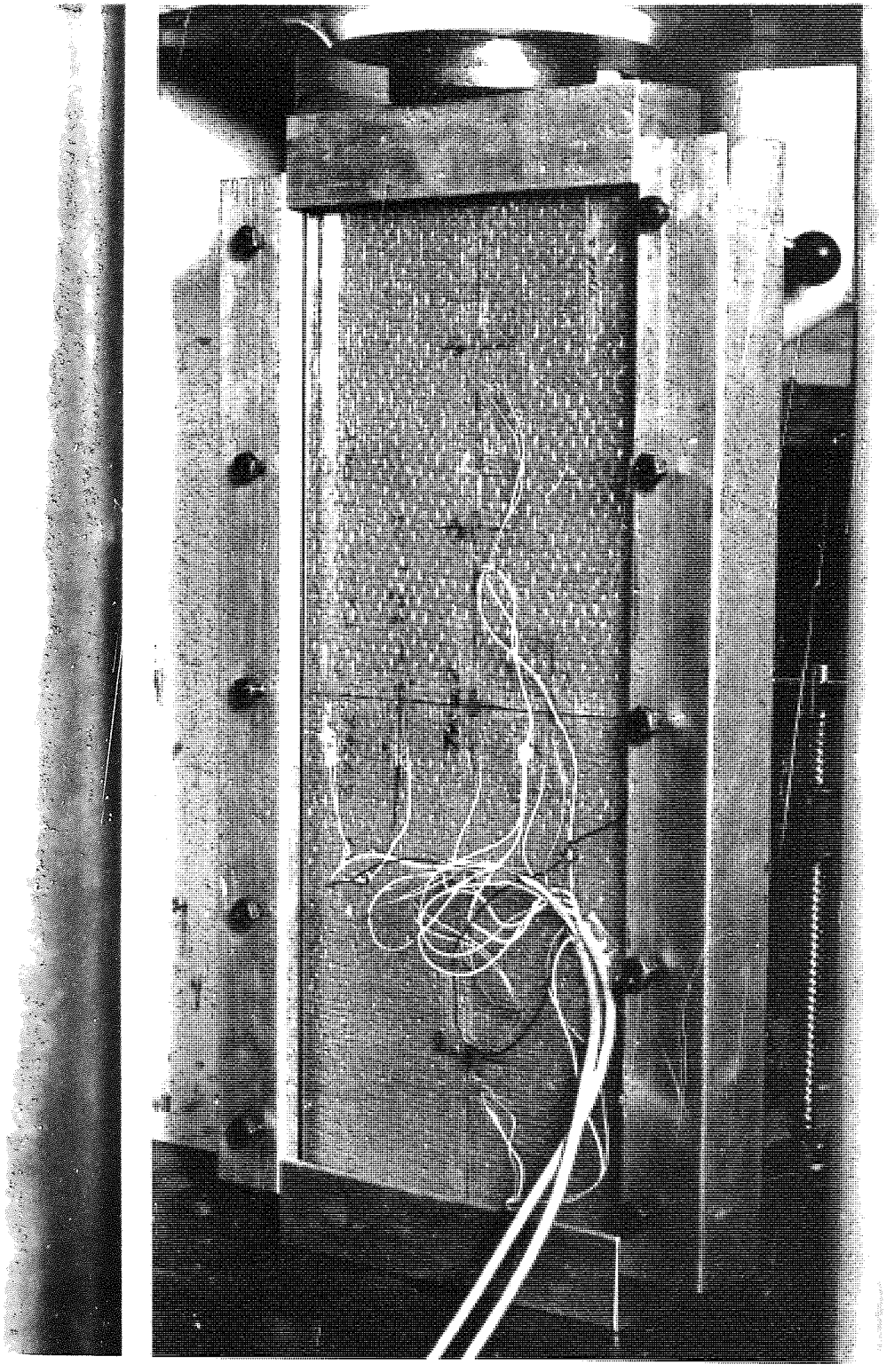

Fig 5.3. Plate under test, view showing the supporting frame and the strain guage position

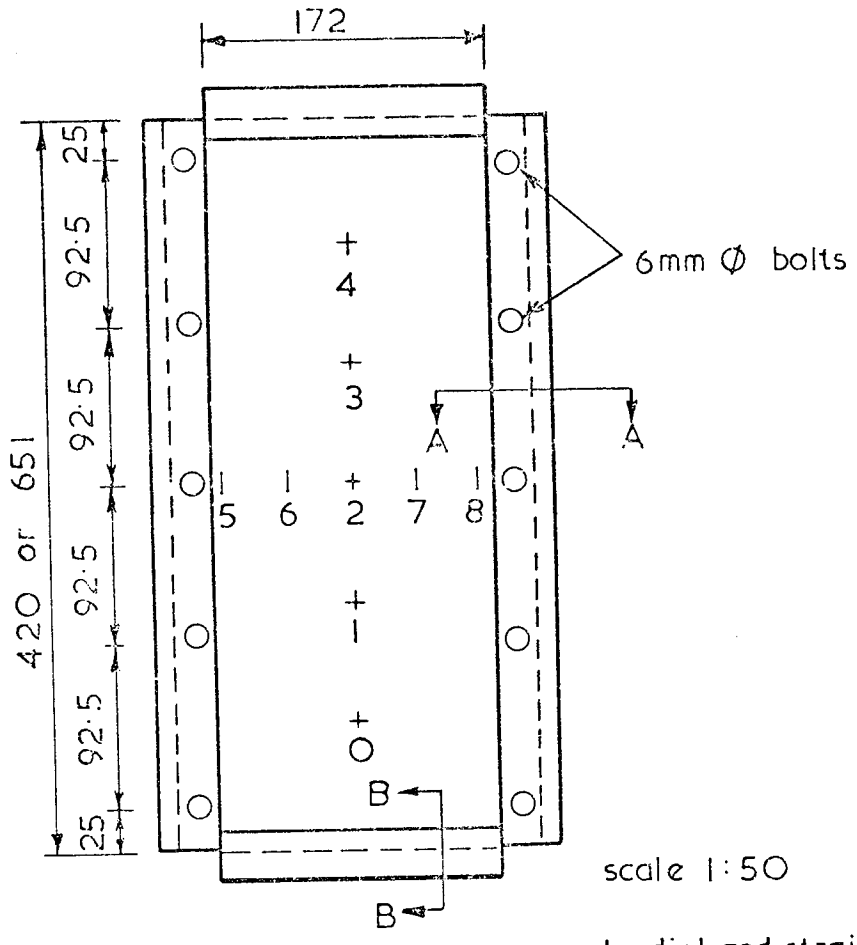

A : General set up

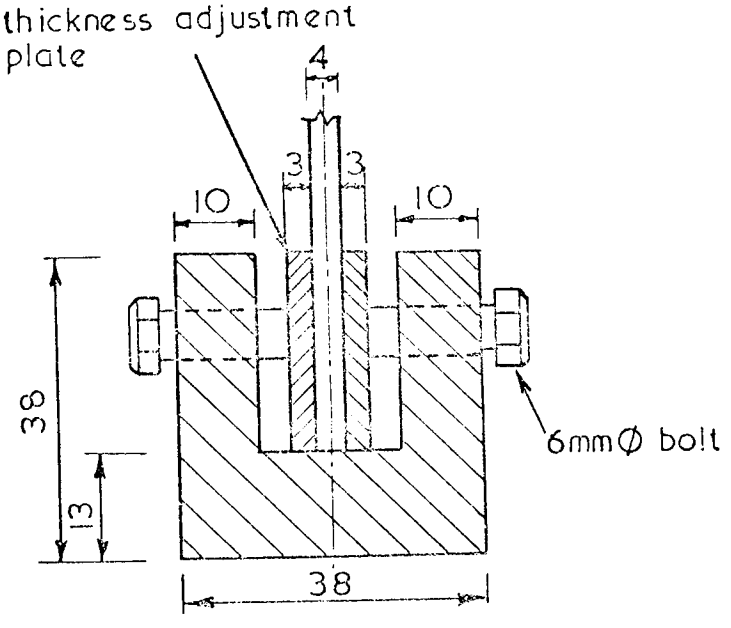

B Section A-A

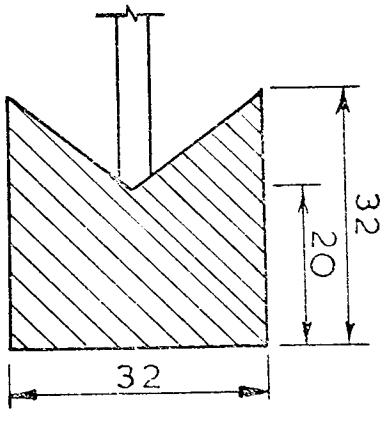

C Section B-B

scale 1:1

NOTE : All dimensions are in millimeters

Fig 5.4 Test fixture

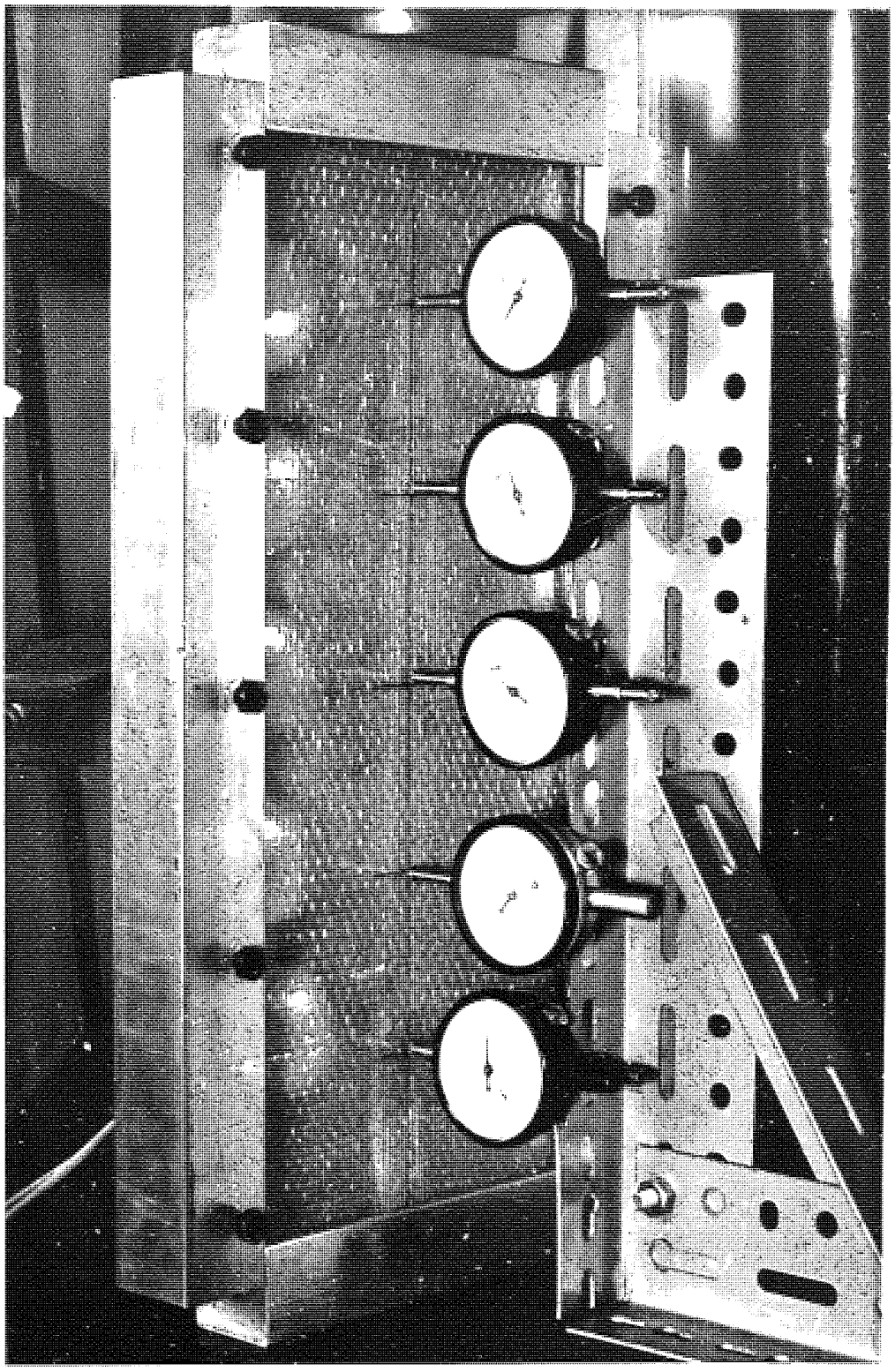

Fig. 5.5 . Plate under test view showing the supporting frame and the dial guage positions

5.4.4) contd.

buckling pattern could be observed on the plate under test, after which test coupons were extracted from the plate for modulus and strength determination according to the methods mentioned in Chapter 3.

5.4.5) Southwell Plot:

Classical plate buckling theory assumes that a plate remains flat as it is loaded until the critical load is reached, at which time the plate assumes some deflected shape. All real plates, however, have some initial curvature or are loaded eccentrically and will deflect as they are loaded. The experimental verification of most buckling theories, then, will require some criteria for determining when the actual plate would have reached its critical load, had it remained flat during loading.

Southwell (ref.5-10) has shown that near the critical buckling load the relationship between the deflections, externally applied load, and the critical buckling load can be expressed as:

$$\delta = \frac{a_1}{\frac{N_{x(cr)}}{P} - 1} \qquad (5.12)$$

where

δ = deflection,

a_1 = constant,

P = applied load, and

$N_{x(cr)}$ = critical buckling load.

Rewriting equation (5.12) in a more usable form

$$\frac{\delta}{P} N_{x(cr)} - \delta = a_1 \qquad (5.13)$$

it is apparent that a plot of δ/P versus δ should yield a

5.4.5) contd.

straight line (near the critical buckling load). Furthermore, the slope of this line is equal to $^{1}/N_{x(cr)}$.

Care must be taken in selecting the region in which the Southwell hypothesis applies. Points on the δ/p versus δ plots corresponding to a maximum deflection greater than $\frac{1}{2}$ the plate thickness cannot be used (membrane stiffening action begins to become important), and points well below the buckling region will also not follow a straight line relationship (ref.5-11).

In the present work, the results obtained from this method are compared with those obtained from the strain gauge readings for the same points at which the Southwell method has been applied.

5.4.6) Results:

All buckling results are shown on Table (5.2) which contains the experimental observations and theoretical predictions of buckling loads. The elastic properties of the various types of composite plates used are shown on Table (5.3). These properties were obtained by the methods discussed in Chapter 3.

The mode of buckling of simple-fixed GRP plates under uniaxial compression is shown in Fig.(5.6).

The graphical determination of the experimental buckling loads by Southwell plot and the strain gauge methods are shown in Figs.(5.7 to 5.14) for all types of plates investigated.

Plate Type	Type of Composite	Fibre Arrangement	Buckling Load $[N_{x(cr)}]$ N/mm		
			Theory Eq.(5.5) or Eq.(5.9)	Experiment	
				Southwell Plot	Strain Gauge Reading
1	GRP	Unidirectional (0°) -6-layers	220.60	199	199
2	GRP	Angle-Ply (45,-45,-45,45)	287.85	277	284
3	GRP	Cross-Ply (0,90,90,0)	234.00	227	227
4	SGRP	Unidirectional (0°)	70.88	63	65
5	GRP	Unidirectional (0°) -4-layers	186.41	170	182
6	GRP	Multi-directional (0,45,-45,-45,45,0)	247.86	213	222
7	GRP	Cross-Ply (0,90,90,0)	137.00	106	122
8	GRP	Angle-Ply (45,-45,-45,45)	170.00	135	154

TABLE (5.2) COMPRESSIVE BUCKLING RESULTS.

(See Table (5.1))

Plate Type	Type of Composite	Fibre Arrange-ment	Fibre Volume Cement	Longitudinal Modulus E_L (N/mm^2)	Transverse Modulus E_T (N/mm^2)	Shear Modulus G_{LT} (N/mm^2)	Longitudinal Poisson's Ratio ν_{LT}	Transverse Poisson's Ratio ν_{TL}
1	GRP	Uni-Directional (0°)	0.46	34795	6200	2700	0.283	0.050
2 & 8	GRP	Angle -Ply 45.-45,-45,45	0.27	5777	5777	6887	0.530	0.530
3 & 7	GRP	Cross-Ply 0,90,90,0	0.27	12931	12931	1774	0.167	0.167
4	SGRP	Uni-Directional (0°)	0.33	36073	7657	2800	0.285	0.060
5	GRP	Uni-Directional (0°0)	0.27	21408	4740	1800	0.309	0.068
6	GRP	Multi-Directional 0,45,-45, -45,45,0	0.46	19525	6500	7200	0.485	0.161

TABLE (5.3) ELASTIC PROPERTIES

(See Table (5.1))

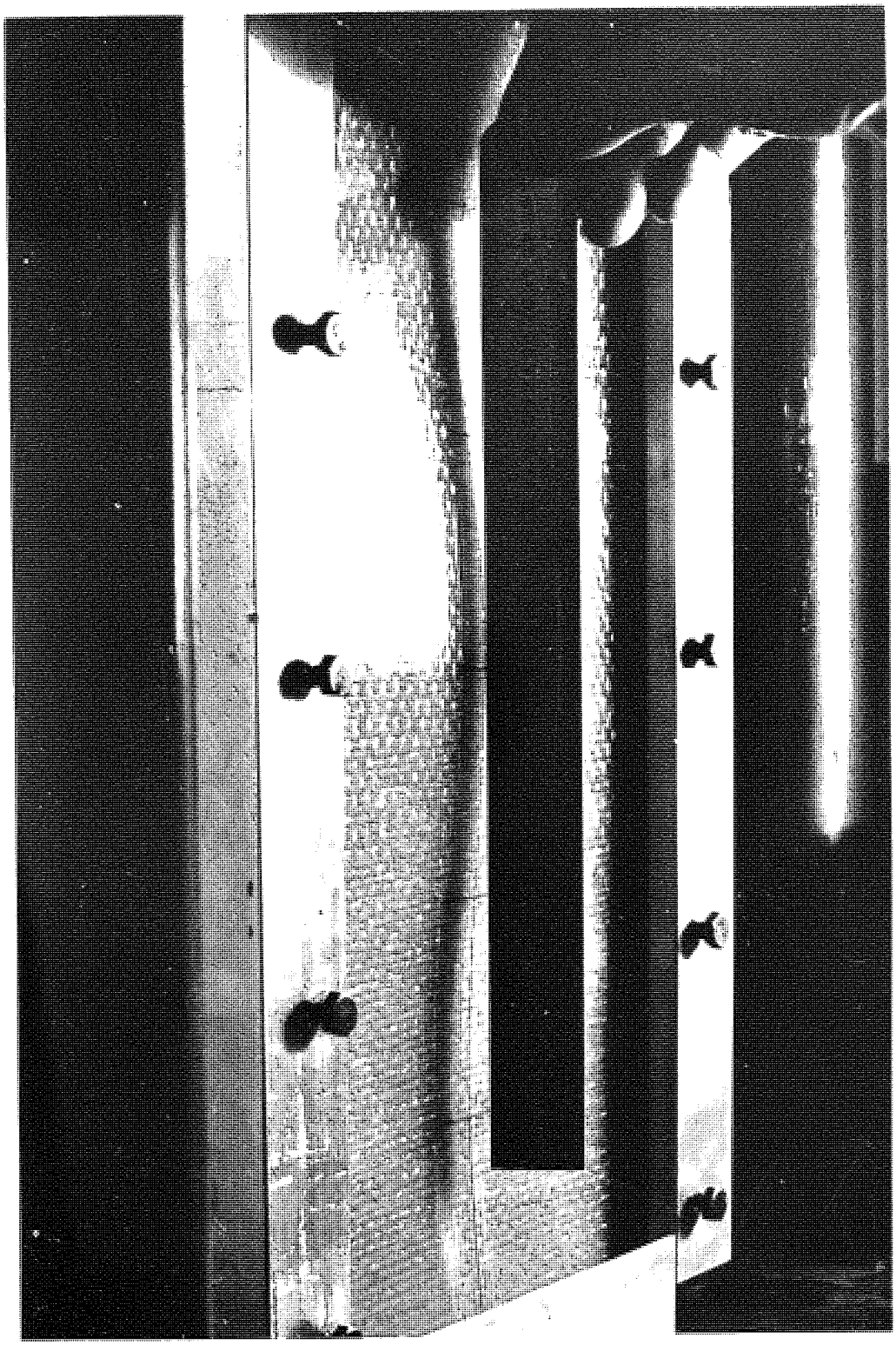

Fig 5.6. Buckling mode of simple - fixed supported GRP plate under uni - axial compression

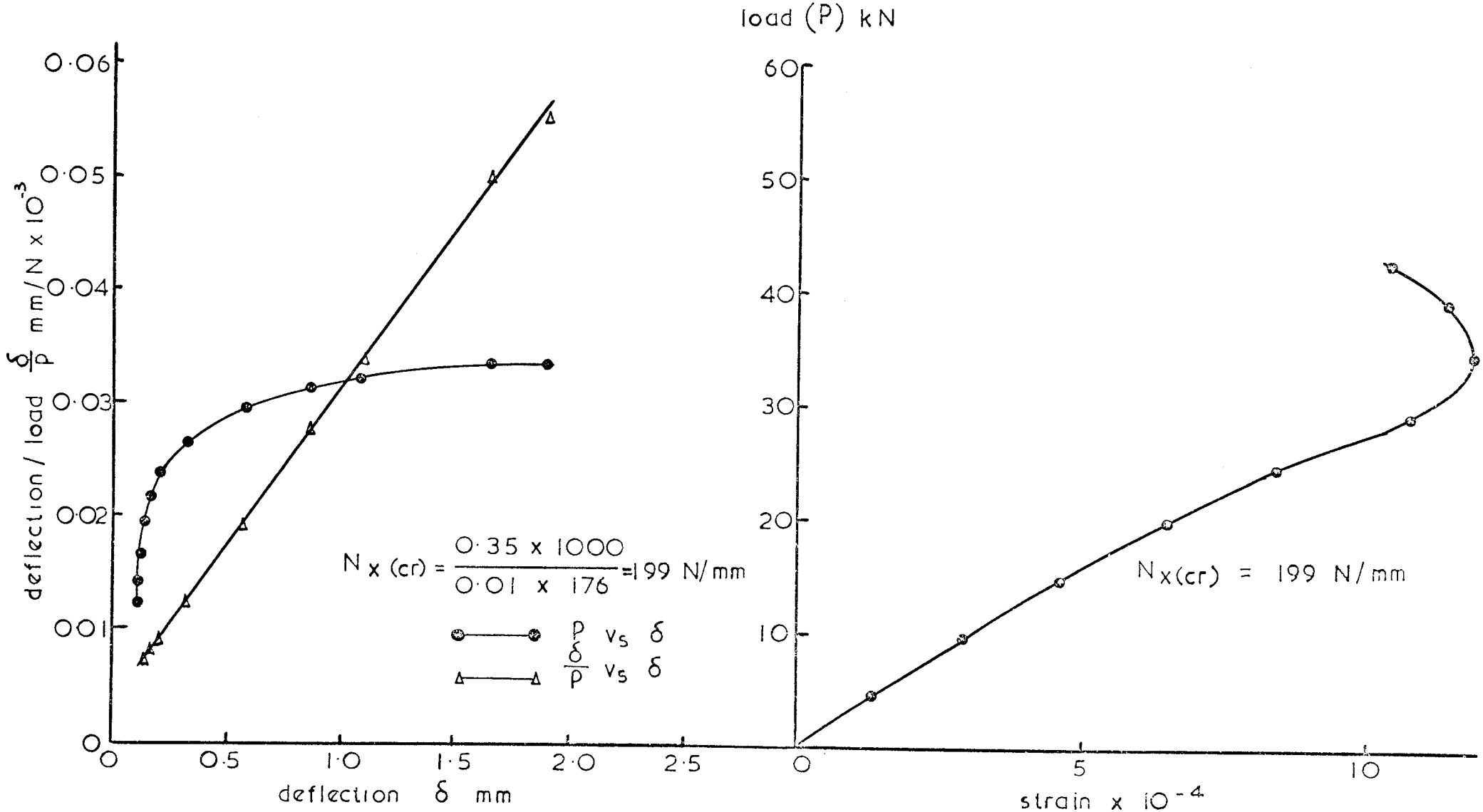

Fig 5.7 Plate type 1

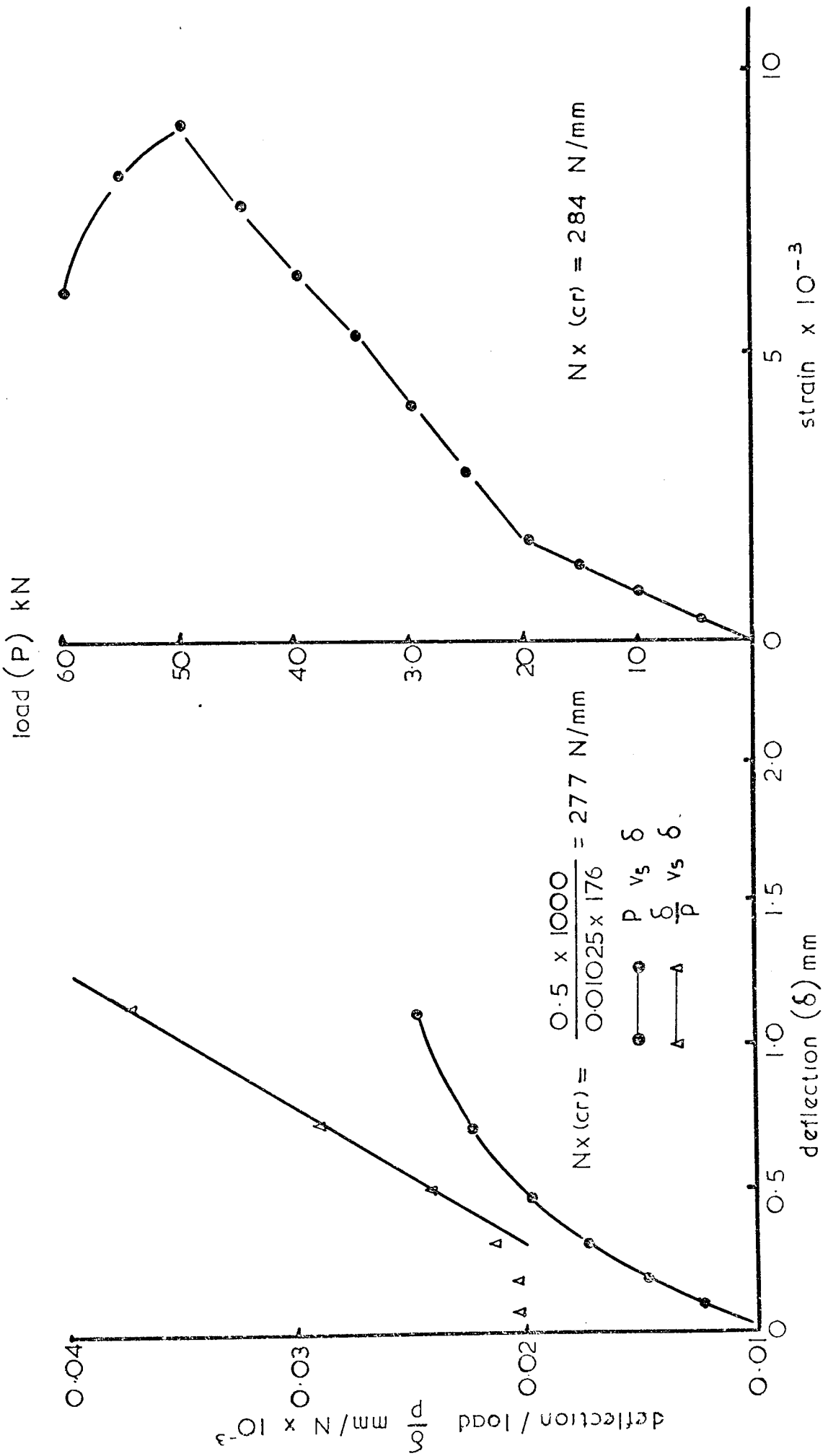

Fig 5.8 Plate type 2

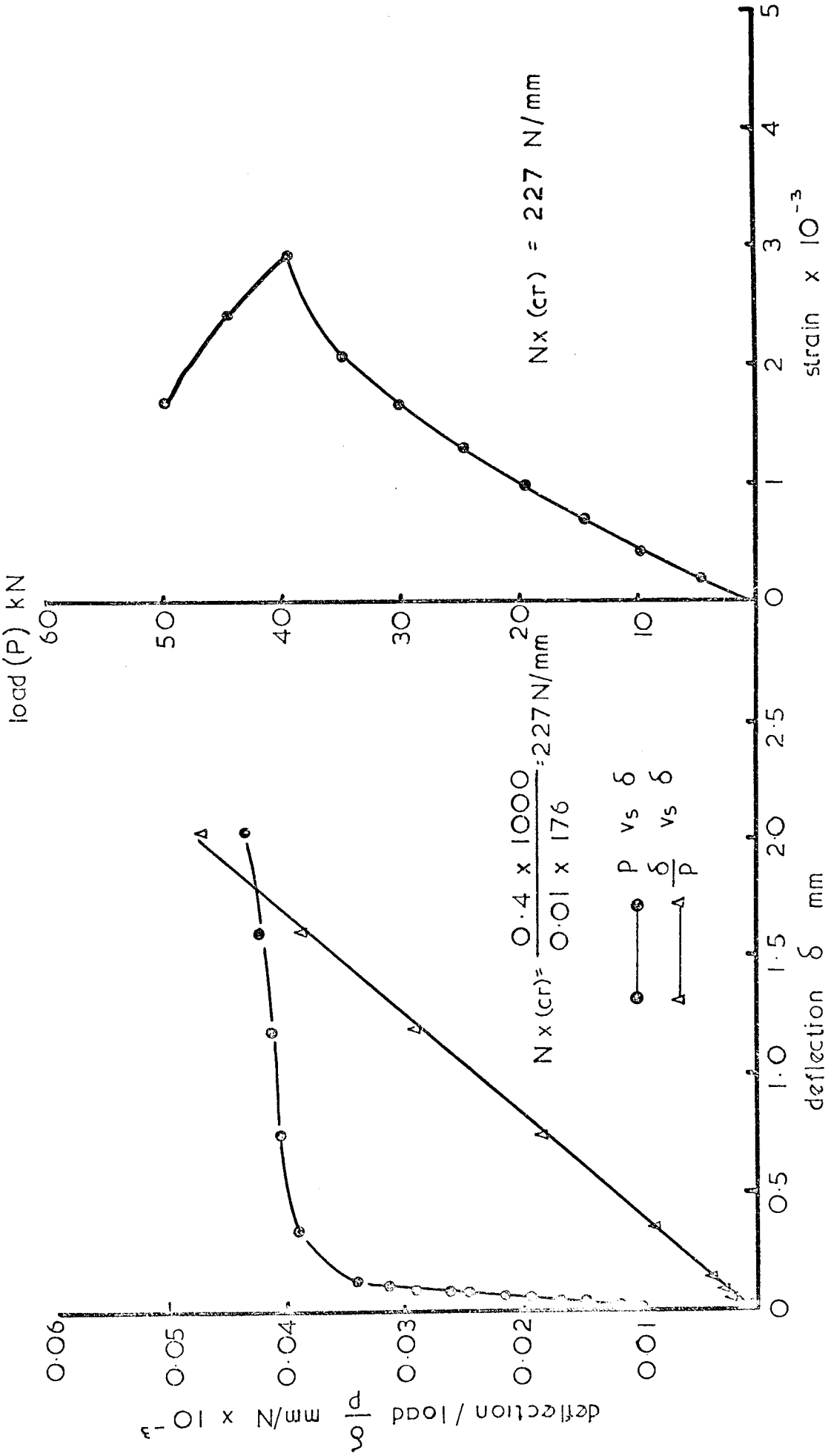

Fig. 5.9. Plate type 3

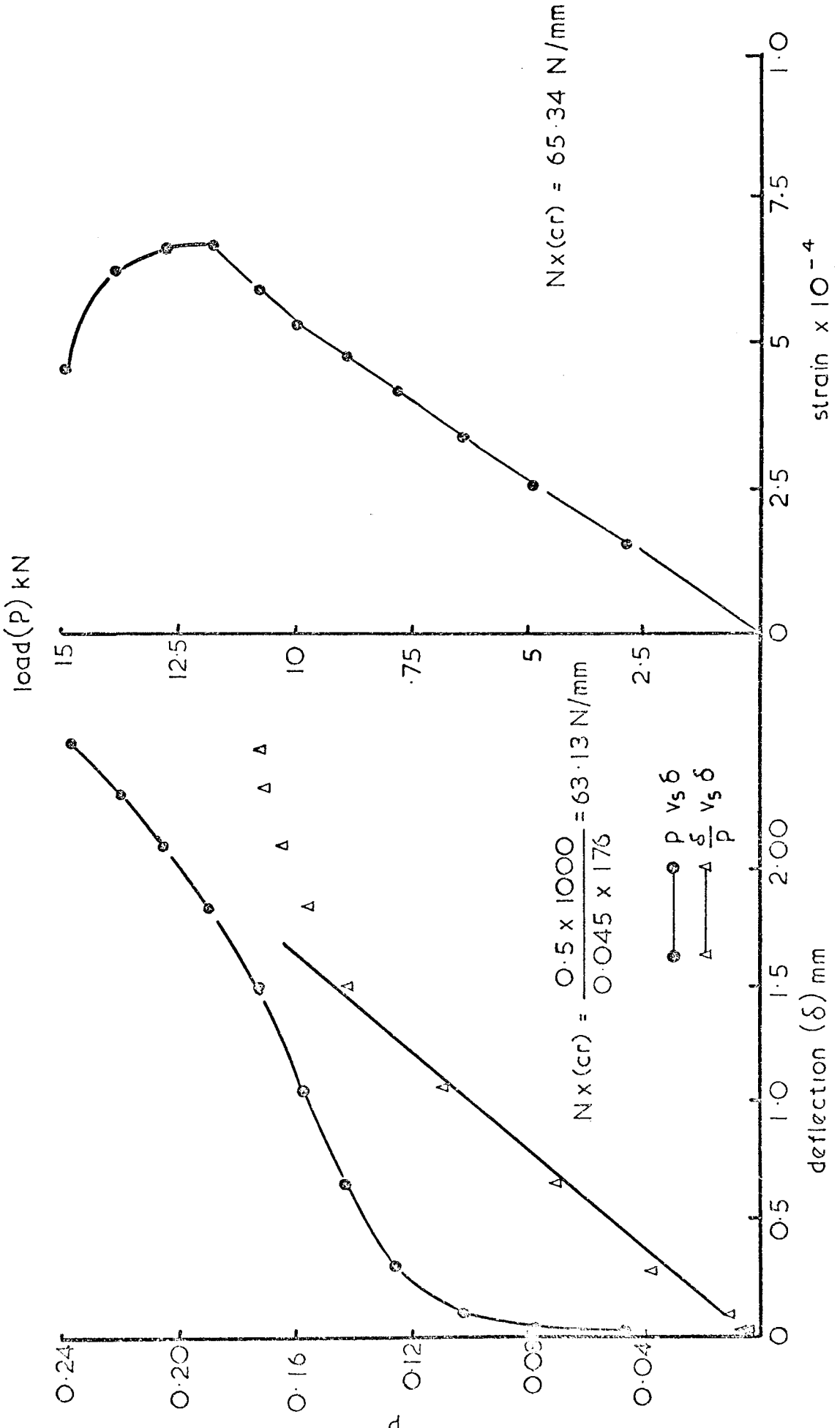

Fig 5.10 Plate type 4

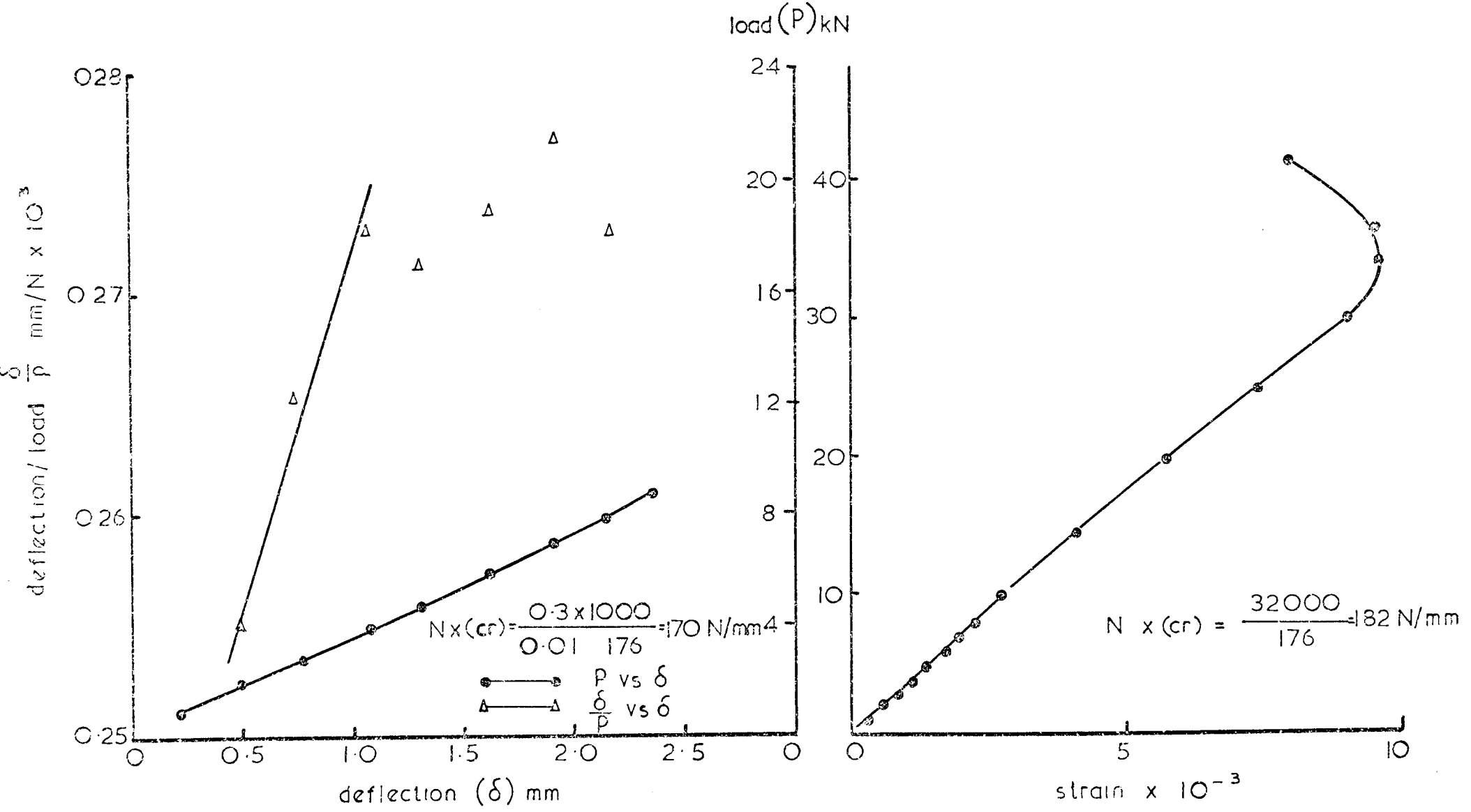

Fig. 5.11. Plate type 5

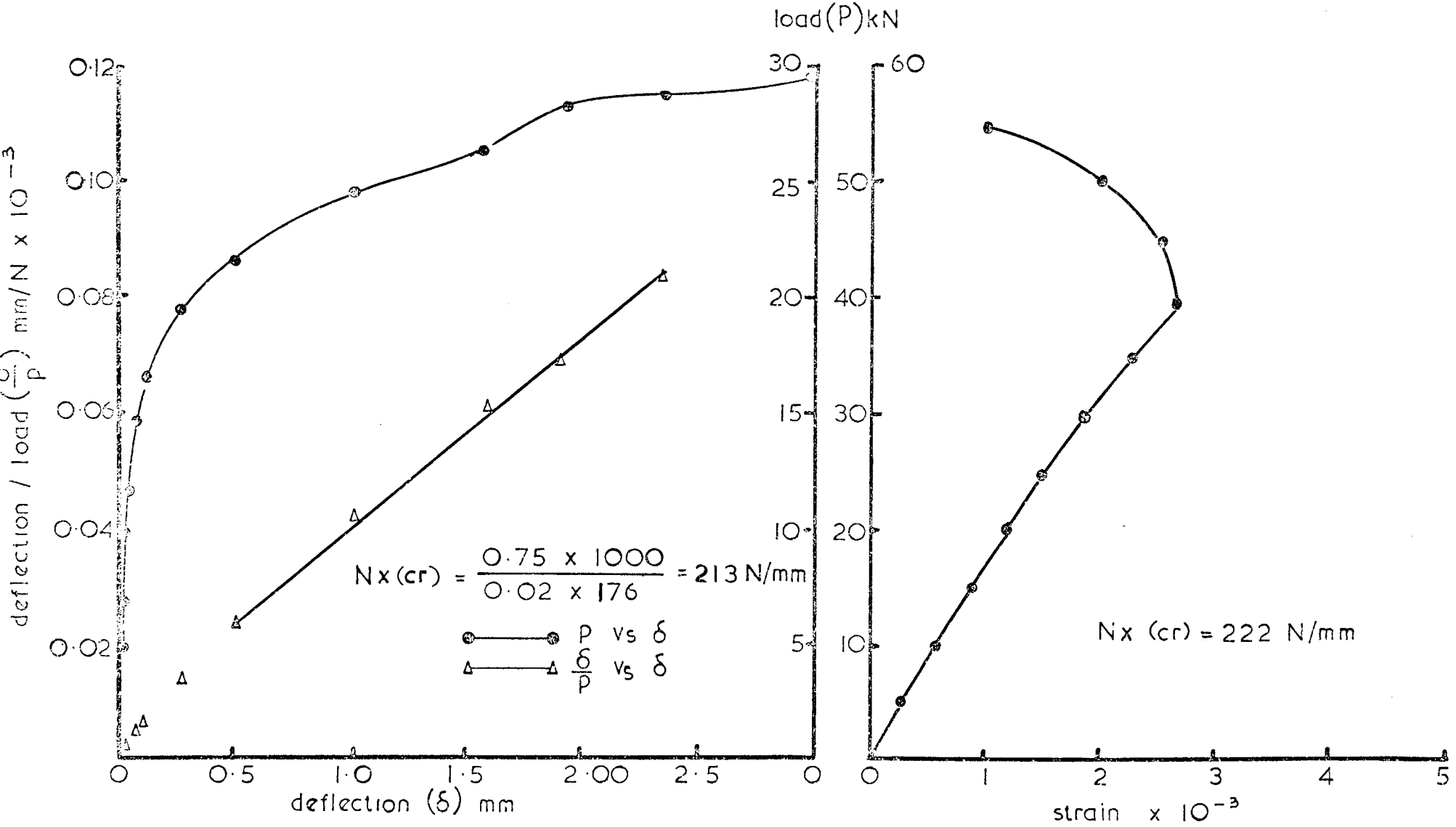

Fig. 5.12 Plate type 6

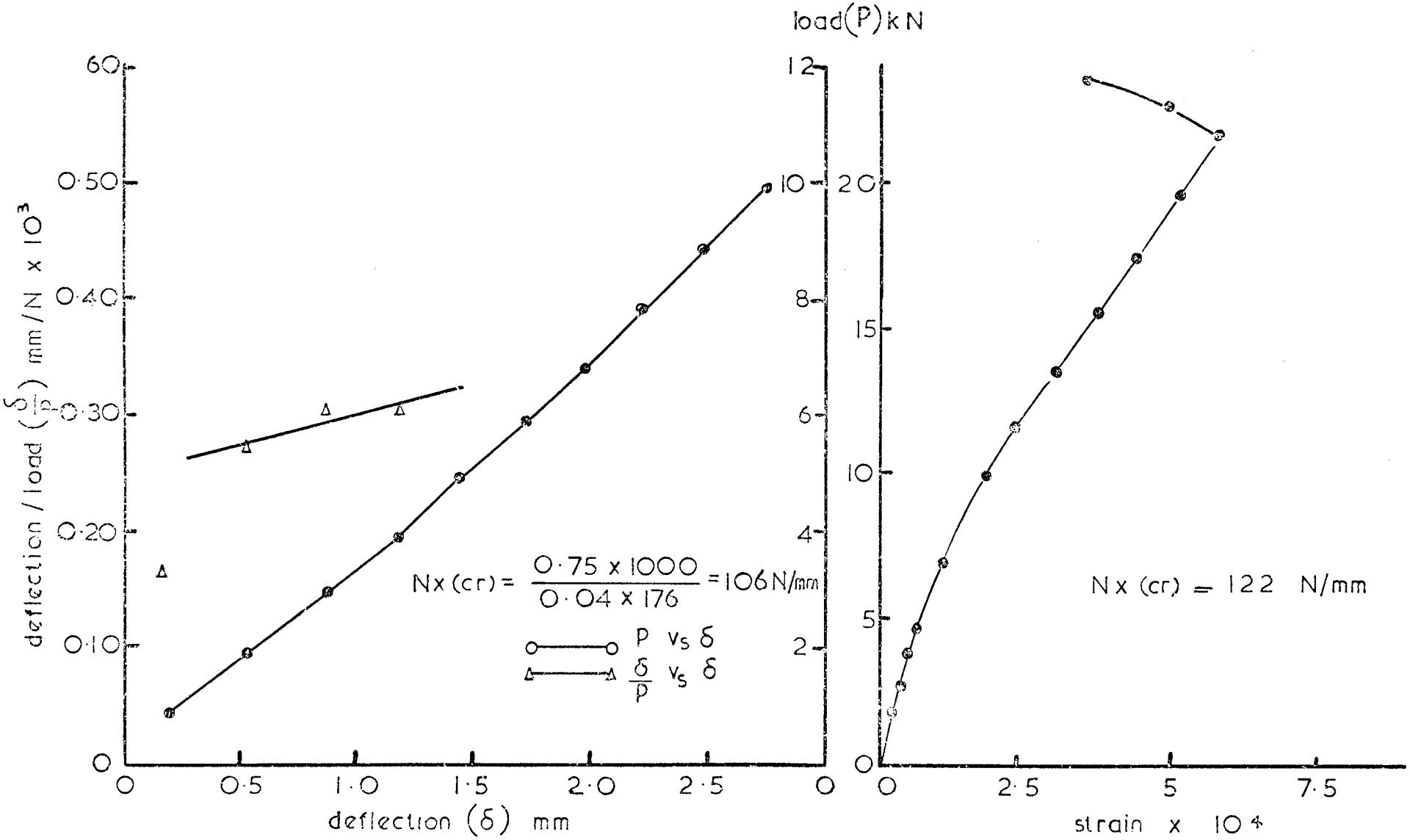

Fig. 5.13 Plate type 7

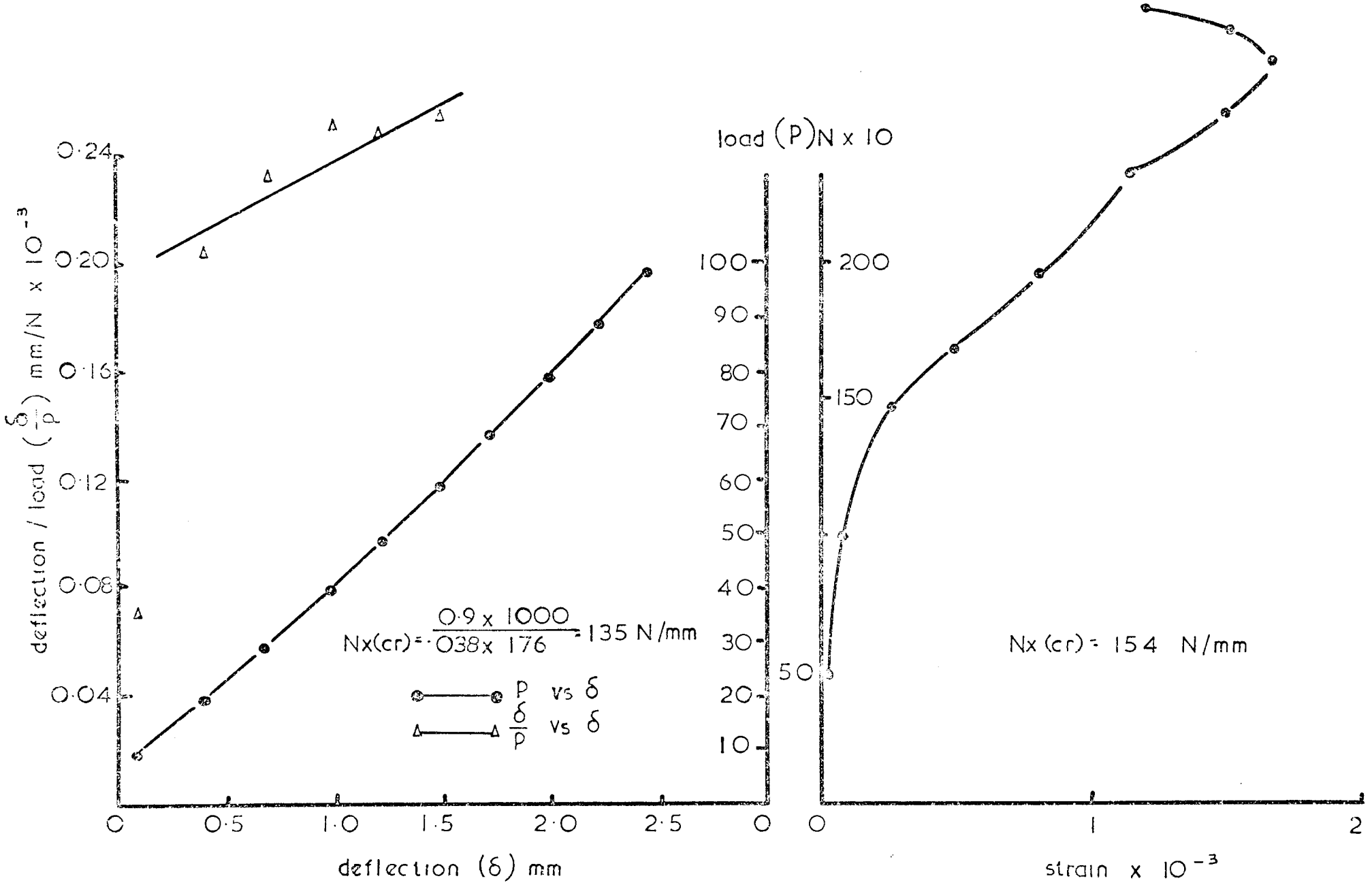

Fig. 5.14 Plate type 8

5.4.7) Discussion:

Table (5.2) shows that the theory and experiments are in reasonable agreement especially with the strain gauge results. This close agreement is due to the minimisation of irregularities by the moulding technique adopted and the good alignment of the plates under the loading machine and within the test arrangements.

The results obtained from the strain gauges were closer to the theory than those obtained by Southwell plots for the following reasons:

1) The electric strain gauges are very sensitive to the detection of any changes in the pattern of the plate surface and a sudden deviation in the strain gauge reading can be observed as soon as the initial buckling takes place and hence the initial buckling load can be found, as shown in Figs.(5.7 to 14).

2) In the Southwell plot, the points $\frac{\delta}{P}$ versus δ plots corresponding to a maximum deflection greater than $\frac{1}{2}$ the plate thickness and points well below the buckling region should be neglected from the calculation. Any error in defining the slope of the straight line that passes through the points in the buckling region in the above mentioned plot could give a completely false determination of buckling load.

3) During the actual testing of plates, the deflections must be large enough so that any initial misalignment in the test fixture, as well as any initial imperfection, is overshadowed by the deflection due to the load. This may require that the deflections be larger than those acceptable for the small deflection theory and the material behaviour may deviate from Hooke's law on both of which

5.4.7) contd.

3) contd.

the Southwell plot is based. The problem of non-linear elastic stability, as it relates to the Southwell plot, has been investigated in ref.(5-11) and suggests that the critical load is overestimated by the Southwell plot in the case of non-linearities associated with large deflection (stable-symmetric buckling). The critical load associated with the small deflection theory was assumed by Southwell is reasonably predicted by this method, (neutral case).

Because of the variation of thickness in the test specimens and for the sake of obtaining a reasonable comparison concerning the effect of the type of reinforcement employed and the fibre arrangement on the buckling load, Table (5.4) was prepared to show the buckling resistance of four types of GRP plates in addition to one type of SGRP plate of the same thickness. From this table, a conclusion can be drawn that the buckling resistance of SGRP plate is higher than the GRP plates for the values of fibre volume fraction mentioned in the table, and the angle-ply (45 x 45) GRP plate has greater buckling resistance than the unidirectional at 0° and the cross-ply (0.90) GRP plates for the same fibre content. So that, for design application when compressive buckling is the major design criteria, it is feasible to employ either a unidirectional SGRP or angle-ply GRP composites.

Another case was considered in the design of GRP plates, the case where failure of simple-fixed plates under uniaxial compression is caused by simultaneous yielding and buckling. This case is applicable where reasonably thick

Type of Composite	Fibre Arrangement	Fibre Volume Content	Thickness (mm)	Plate Aspect Ratio a/b	Theoretical Buckling Load (N/mm)	Normalized Value
SGRP	Unidirectional at (0°)	0.30	2.95	2.39	70.88	1
GRP	Unidirectional at (0°)	0.27	2.95	2.39	44.00	0.63
GRP	Angle-Ply at 45,-45,-45,45	0.27	2.95	2.39	58.06	0.82
GRP	Cross-Ply at 0,90,90,0	0.27	2.95	2.39	52.57	0.74
GRP	Multi-directional at 0,45,-45,-45,45,0	0.46	2.95	2.39	71.42	1.01

TABLE (5.4) COMPARISON OF COMPRESSIVE BUCKLING LOAD OF VARIOUS COMPOSITES.

5.4.7) contd.

plates are employed in a structure provided their use does not affect the economical aspects of the design. Fig.(5.15) shows the relationship between the thickness/width ratio $\left(\frac{h}{b}\right)$, ultimate compressive resultant (N_1 or N_x), and the composite fibre volume fraction (V_f) for four types of GRP composite plates, (i.e. unidirectional, multidirectional, cross-ply and angle-ply). This figure can supply the designer with the optimum cross-section of infinitely long simple-fixed GRP plates that fail by buckling and yielding simultaneously.

In Fig.(5.15), the cruves that show the relationship between N_1 and V_f were obtained according to Section [3.3.2(ii)] for unidirectional GRP and Section [3.5] for the other types of GRP investigated in the figure. The curves showing the relationship between $\frac{h}{b}$ and V_f were obtained with the aid of the following equation,

$$\frac{h}{b} = \frac{3}{\pi}\left[\frac{N_1}{2(\sqrt{C_{11}C_{22}}+C_{33})}\right]^{\frac{1}{2}} \qquad (5.13)$$

which is derived as follows,

The critical buckling load for an infinitely long simple-fixed plate is given by equation (5.9) which can be presented in the following form

$$N_{x(cr)} = \frac{8}{3}\frac{\pi^2}{b^2}(\sqrt{3D_1D_2}+D_3) \qquad (5.13a)$$

by putting $D_3 = D_{12}+2D_{66}$ and letting D_1, D_2 be D_{11}, D_{22} respectively in equation (5.13a) yields

$$N_{x(cr)} = \frac{8}{3}\frac{\pi^2}{b^2}\left[\sqrt{3D_{11}D_{22}}+(D_{12}+2D_{66})\right] \qquad (5.13b)$$

substituting now the D_{ij} part of equation (3.83) into equation (5.13b), the following equation can be obtained,

——— $\frac{h}{b}$ vs vf

——·—— N_x or N_1 vs. vf

1. unidirectional GRP at O.
2. multidirection " " O. 45. 45. 45 · 45 . O.
3. cross-ply " " O. 90 .90 . O.
4. angle-ply " " 45. 45. 45 · 45.

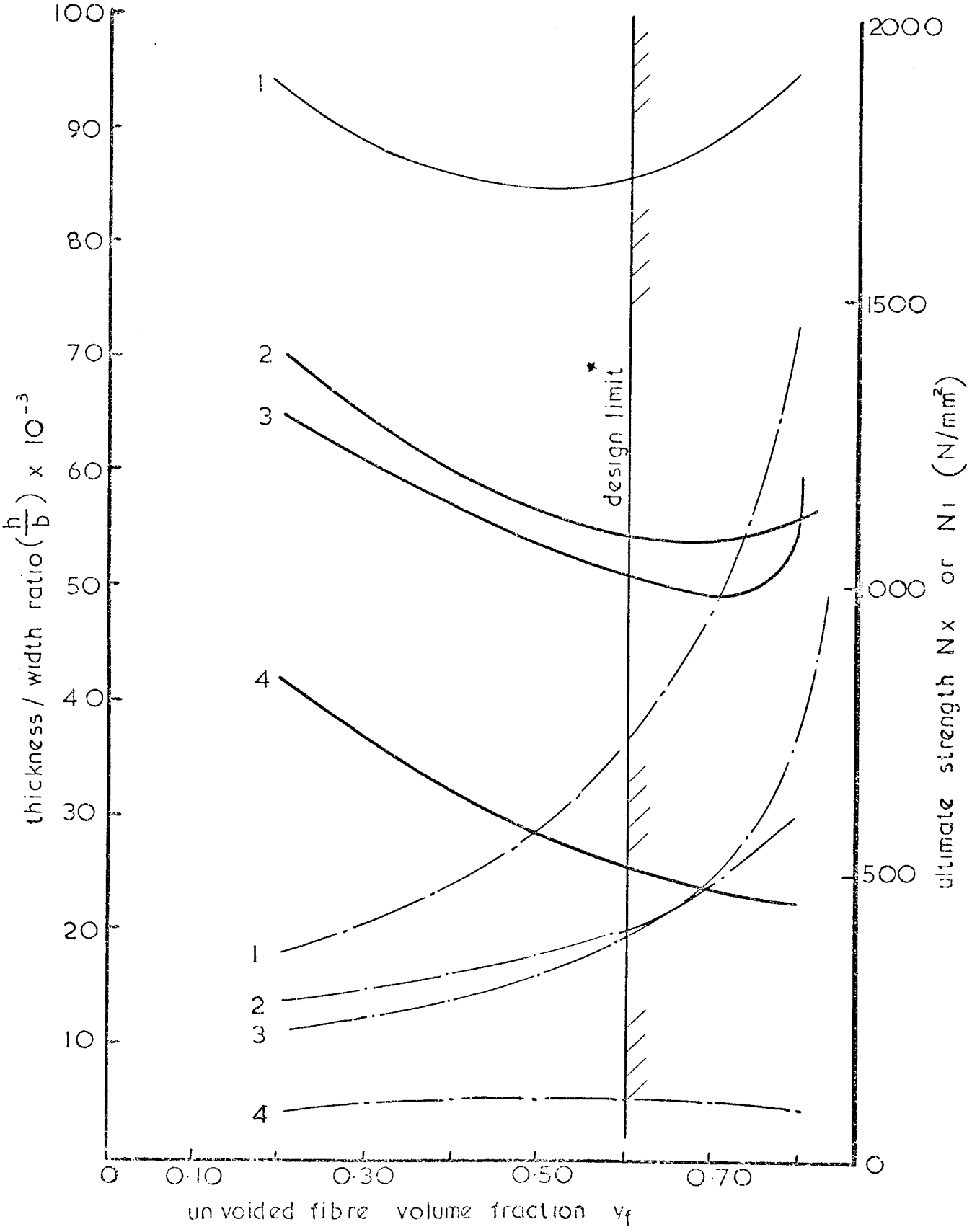

Fig 5.15 *(Design limit is defined by the optimum resin content to provide and effective matrix see (Sec 3.73))

5.4.7) contd.

$$N_{x(cr)} = \frac{8}{3}\frac{\pi^2}{b^2}\frac{h^3}{12}\left[\sqrt{3C_{11}C_{22}}+(C_{12}+2C_{66})\right] \qquad (5.13c)$$

because of the symmetric fibre arrangement in the composite investigated the C_{ij} values in equation (5.13c) may be obtained from equation (3.16). In the case of simultaneous failure in yielding and buckling, the buckling stress should be equal to the material ultimate compressive resultant $\left(\text{i.e. } \frac{N_{cr}}{h} = N_1\right)$, thus equation (5.13c) can be written,

$$\frac{N_{cr}}{h} = N_1 = \frac{2\pi^2}{9}\left(\frac{h}{b}\right)^2\left[\sqrt{3C_{11}C_{22}}+(C_{12}+2C_{66})\right] \qquad (5.13d)$$

rearranging equation (5.13d), equation (5.13) can be obtained, i.e.

$$\frac{h}{b} = \frac{3}{\pi}\left[\frac{N_1}{2(\sqrt{3C_{11}C_{22}}+C_{33})}\right]^{\frac{1}{2}} \qquad (5.13)$$

where

$$C_{33} = C_{12} + 2C_{66}.$$

5.5) Buckling of GRP rectangular Plates in Pure Shear:

The objective of studying the buckling behaviour of GRP plates under pure shear is to understand their response under this type of loading system and hence enable safe design of these plates as shear webs. Again, to achieve this purpose it is necessary to prepare suitable test specimens, a reliable method of determining the buckling load, and finally a test arrangement that is adequate to simulate the boundary and load conditions assumed in the design.

5.5.1) Test Specimens:

The plate specimens shown on Table (5.5), were

5.5.1) contd.

tested with fixed edges under pure shear loading.

No. of specimens	Type	Plate Configuration	Dimensions (mm).
2	1	Unidirectional (0°).	876 × 176 × 4.35
2	2	Angle-Ply (+45,-45, -45,+45	876 × 176 × 4.20
1	3	Cross-Ply (0, 90, 90, 0)	876 × 176 × 3.69
2	4	Unidirectional (+45°)	876 × 176 × 4.25
2	5	Unidirectional (-45°)	876 × 176 × 3.14
1	6	Unidirectional (-45°)	1105 × 176 × 4.16

Table (5.5)

5.5.2) Theoretical Predictions.

It is clear from Table (5.5) that the three first types of plates investigated are of symmetrical arrangement about the vertical and horizontal middle plane and therefore the specially orthotropic plate theory will be applied to these plates, (Section 5.3.1). The other three types are symmetric about the middle horizontal plane but not about the middle vertical plane (i.e. the laminate principle axes are not parallel to the plate axes) and hence the mid-plane symmetric plate theory will be applied for the theroetical prediction, (Section 5.3.2). Because the plates under consideration are assumed to be unstiffened flat plates that may be used as shear webs in built up box sections, the theoretical prediction will be concentrated on the shear buckling of long CRP plates.

5.5.2(i) Specially orthotropic plates under pure shear:

If the aspect ratio of the plate is large (i.e. $\phi > 4$), then the plate may be considered as an infinitely long strip. Ref.(5-12) introduced the quantity $v = \frac{\sqrt{D_1 D_2}}{D^3}$ and expresses the numerical results of the critical load as a function of the plate characteristics factor v. The buckling load is given by the same reference as

when $D_3 < \sqrt{D_1 D_2}$ (i.e. $1 \leq v \leq \infty$)

$$N_{xy(cr)} \text{ or } N_{12(cr)} = \frac{K_s \pi^2}{b^2} (D_1)^{\frac{1}{4}} (D_2)^{\frac{3}{4}} \qquad (5.14)$$

when $D_3 > \sqrt{D_1 D_2}$ (i.e. $0 \leq v \leq 1$)

$$N_{xy(cr)} \text{ or } N_{12(cr)} = \frac{K_s \pi^2}{b^2} \sqrt{D_2 D_3} \qquad (5.15)$$

where the relationship between K and v is shown in Fig.(5.16).

To find the buckling load in shear theoretically, first find the plate characteristics factor v, then from Fig.(5.16) find the value of K_s that corresponds to the value of v, and finally substitute the value of K_s into either equation (5.14) or (5.15) depending on the v value.

5.5.2(ii) Mid-Plane Symmetric plate theory in pure shear:

This theory will be applied to plates type 4,5 and 6 shown in Table (5.5). For these types of plates subjected to pure shear, the general differential equation (5.1) will be reduced to the following

$$D_{11} \frac{\partial^4 w}{\partial x^4} + 4D_{16} \frac{\partial^4 w}{\partial x^3 \partial y} + 2D_3 \frac{\partial^4 w}{\partial x^2 \partial y^2} + 4D_{26} \frac{\partial^4 w}{\partial x \partial y^3} + D_{22} \frac{\partial^4 w}{\partial y^4} = 2N_{xy} \frac{\partial^2 w}{\partial y \partial x} \qquad (5.15)$$

Thielemann (5-9) presented an approximate solution for

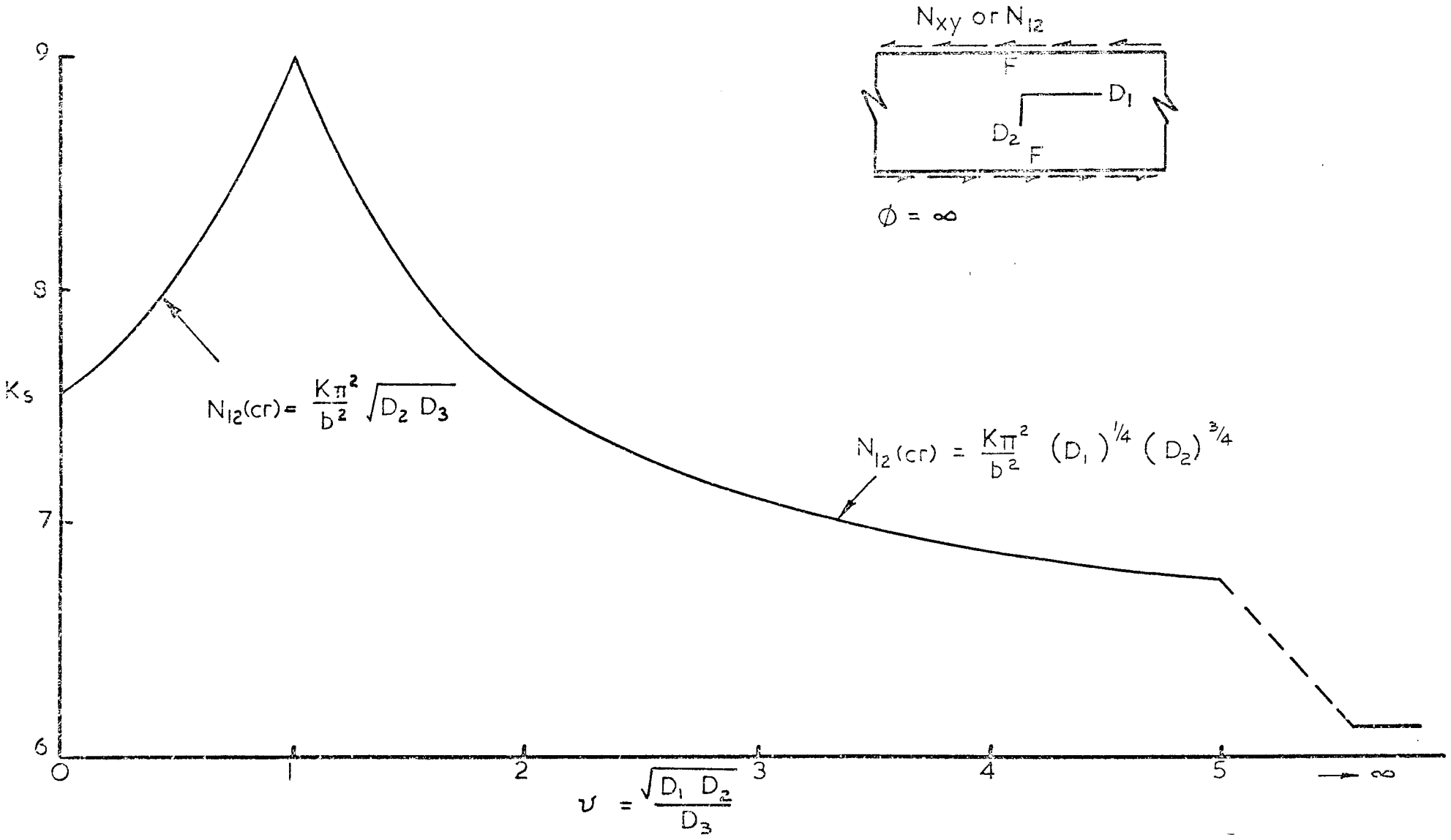

Fig 5.16. Infinite long orthotropic plates in shear (SEYDEL) ref. 5.12

5.5.2(ii) contd.

infinitely long anisotropic plates clamped along their longitudinal edges and gave the critical shear load as:-

$$N_{xy(cr)} = \frac{4}{3}\frac{\pi^2}{\psi b^2} D_{22}\left(4\frac{L^2}{b^2} + 3\psi^2 + \frac{D_3}{D_{22}} - 6\frac{D_{26}}{D_{22}}\psi\right) \qquad (5.16)$$

also the relationship between $\left(\frac{L}{b}\right)$ and ψ is given by the following equation

$$\frac{b^2}{L^2}\left(3\psi^4 - 8\frac{D_{26}}{D_{22}}\psi^3 + 2\frac{D_3}{D_{22}}\psi^2 - \frac{D_{11}}{D_{22}}\right) + 8\psi^2 - \frac{8}{3}\frac{D_3}{D_{22}} - \frac{16}{3}\frac{L^2}{b^2} = 0 \qquad (5.17)$$

Solution of equation (5.17) was obtained for the types of plates under consideration by feeding various values of ψ and $\left(\frac{L}{b}\right)$ into a computer for the ranges assumed by ref.(5-9) of $\frac{D_{26}}{D_{22}}$ and $\frac{D_3}{D_{22}}$ for simply supported plates and with $\frac{D_{11}}{D_{22}}$ assumed to be 1 for +45 and -45 orientation (these plates have equal stiffness in the longitudinal and transverse directions). The values of ψ and $\frac{L}{b}$ that satisfied the equation (i.e. when the right hand side of equation (5.17) was equal to or approach zero) are shown on Table (5.6) together with the corresponding value of K_s which was obtained as follows:-

By rearranging equation (5.16):-

$$\frac{N_{xy(cr)}\, b^2}{\pi^2 D_{22}} = \frac{4}{3\psi}\left(4\frac{L^2}{b^2} + 3\psi^2 + \frac{D_3}{D_{22}} - 6\frac{D_{26}}{D_{22}}\psi\right) \qquad (5.18)$$

let $K_s = \dfrac{N_{xy(cr)}\, b^2}{\pi^2 D_{22}}$

$$\therefore K_s = \frac{4}{3\psi}\left(4\frac{L^2}{b^2} + 3\psi^2 + \frac{D_3}{D_{22}} - 6\frac{D_{26}}{D_{22}}\psi\right) \qquad (5.19)$$

Examinations of the values mentioned in Table (5.6) indicates that the actual value of the critical shear load depends upon the sign of the ratio

From ref.(5-9),

$$\frac{D_3}{D_{22}} = \frac{-4\frac{G_{LT}}{E_L}(1-\nu_{LT}\nu_{TL}) + \frac{E_T}{E_L}(3-2\nu_L) + 3}{4\frac{G_{LT}}{E_L}(1-\nu_{LT}\nu_{TL}) + \frac{E_T}{E_L}(1+2\nu_L)+1} \quad \text{for } \alpha = +45 \text{ or } -45^\circ$$

$$\frac{D_{26}}{D_{22}} = + \frac{1 + \frac{D_3}{D_{22}}}{4} \text{ for } \alpha = 45$$

$$\frac{D_{26}}{D_{22}} = - \frac{1 - \frac{D_3}{D_{22}}}{4} \text{for } \alpha = -45$$

$N_{xy(cr)} = \pi^2 K_s \frac{D_{22}}{b^2}$

$\frac{D_3}{D_{22}}$	$\frac{D_{26}}{D_{22}} = +0.5$			$\frac{D_{26}}{D_{22}} = 0.0$			$\frac{D_{26}}{D_{22}} = -0.5$			$\frac{D_{26}}{D_{22}} = -1.0$		
	$\frac{L}{b}$	ψ	K_s	$\frac{L}{b}$	ψ	K_s	$\frac{L}{b}$	ψ	K_s	$\frac{L}{b}$	ψ	K_s
0				0.70	0.65	6.62						
1	0.50	0.80	2.53	0.80	0.775	9.22	1.00	0.76	17.07			
2	0.70	0.38	5.57	1.00	0.88	12.61	1.10	0.86	18.05			
3	0.95	1.00	8.81	1.15	1.00	15.05	1.25	1.00	20.33	1.35	1.00	25.72

Table (5.6) Shear Buckling Constants for clampled plates.

5.5.2(ii) contd.

$\frac{D_{26}}{D_{22}}$. When this ratio is positive the buckling loads are smaller than that predicted from the specially orthotropic case, while when the ratio is negative the actual buckling loads are greater than those predicted by the specially orthotropic analysis. Physically, the case of positive D_{26}/D_{22} indicates that the minimum plate stiffness ocurs parallel to the direction of the resolved compressive load (pure shear resolved at 45°) while a negative value of this ratio occurs when the maximum plate stiffness occurs parallel to the direction of the resolved compressive load. Reversing the sign of the ratio $\frac{D_{26}}{D_{22}}$ is equivalent to reversing the applied shear. Consequently these results show the buckling resistance to be highly dependent upon the direction of the applied shear load, see Fig.(5.17).

At this stage all the constants related to the shear buckling of infinitely long clamped plate are known and shown on Table (5.6) which is similar to that prepared by Thielemann (5-9) for simply supported edges.

5.5.3) Test Arrangements:

The plates were subjected to a compressive load applied diagonally to generate a shearing stress along the edges of the specimen as shown in Figs.(5.18 to 20). The aluminium frame that supported the edges of the plate and the details of the connections through which the load was transmitted from the testing machine to the plates are shown in Fig.(5.20). Other details of the test arrangements are similar to those mentioned in Section (5.4.3) for plates under uniaxial compression.

The test procedure is exactly the same as that mentioned in Section (5.4.4).

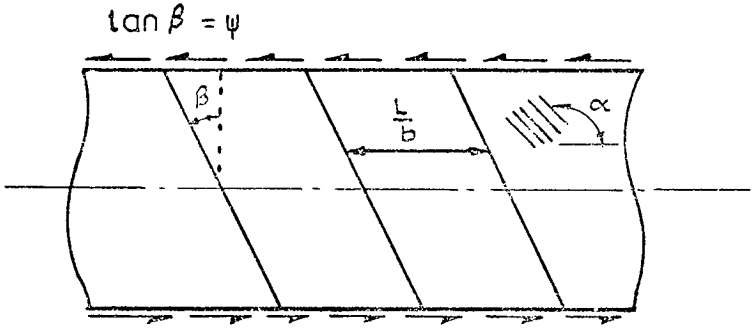

a.

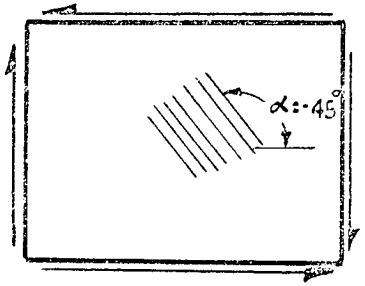

b. $\frac{D_{26}}{D_{22}} < 0$

$\alpha = -45°$ or $135°$

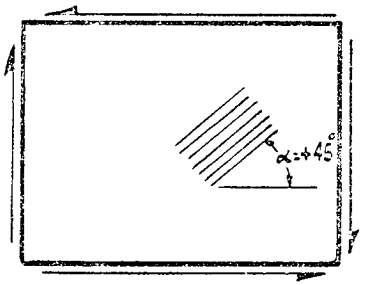

c. $\frac{D_{26}}{D_{22}} > 0$

$\alpha = +45°$

Fig. 5.17. Details of direction of the applied load with respect to the fibre orientation

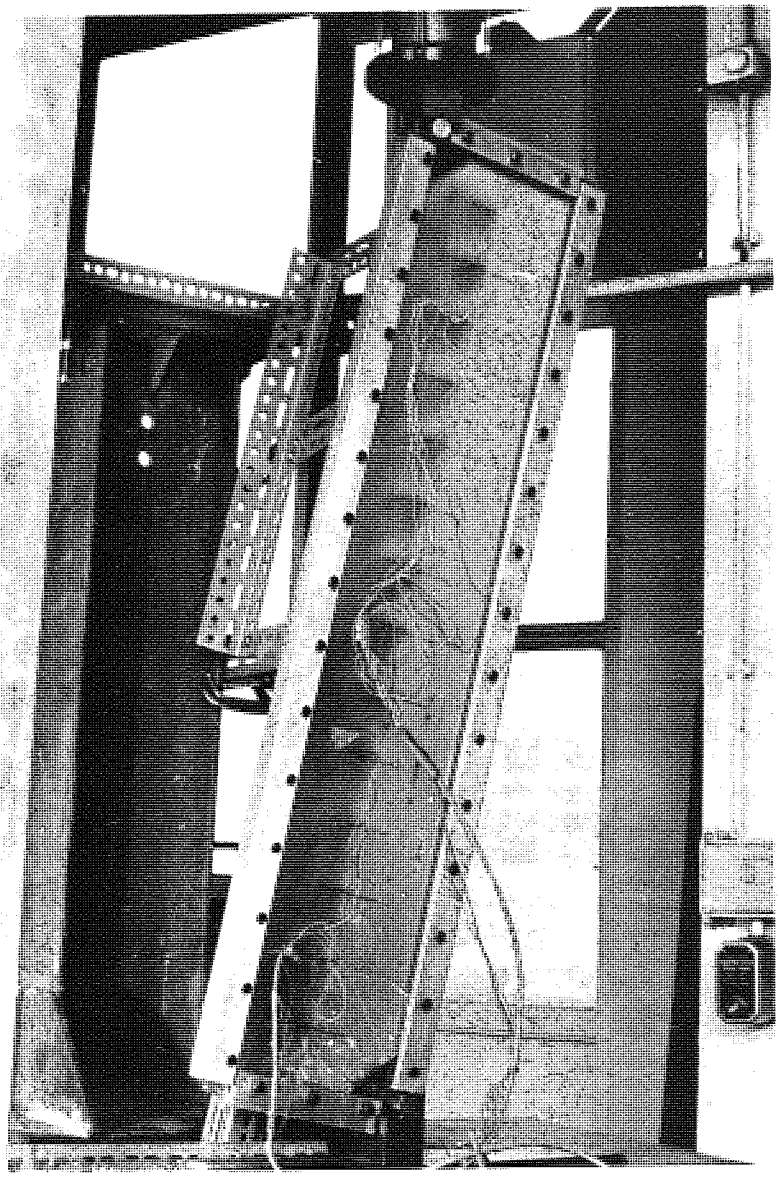

Fig. 5.18 Long G.R.P. plate under shear loading

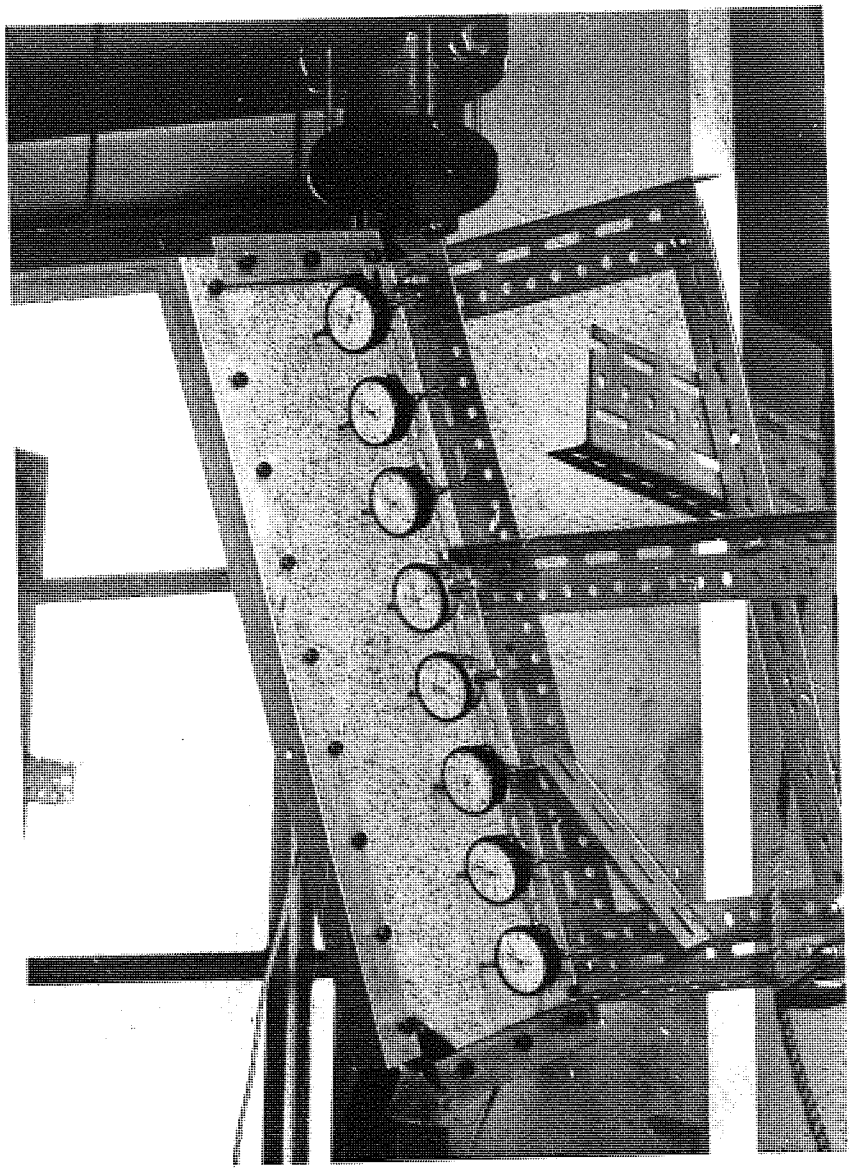

Fig. 5.19. G.R.P. plate under testing in shear

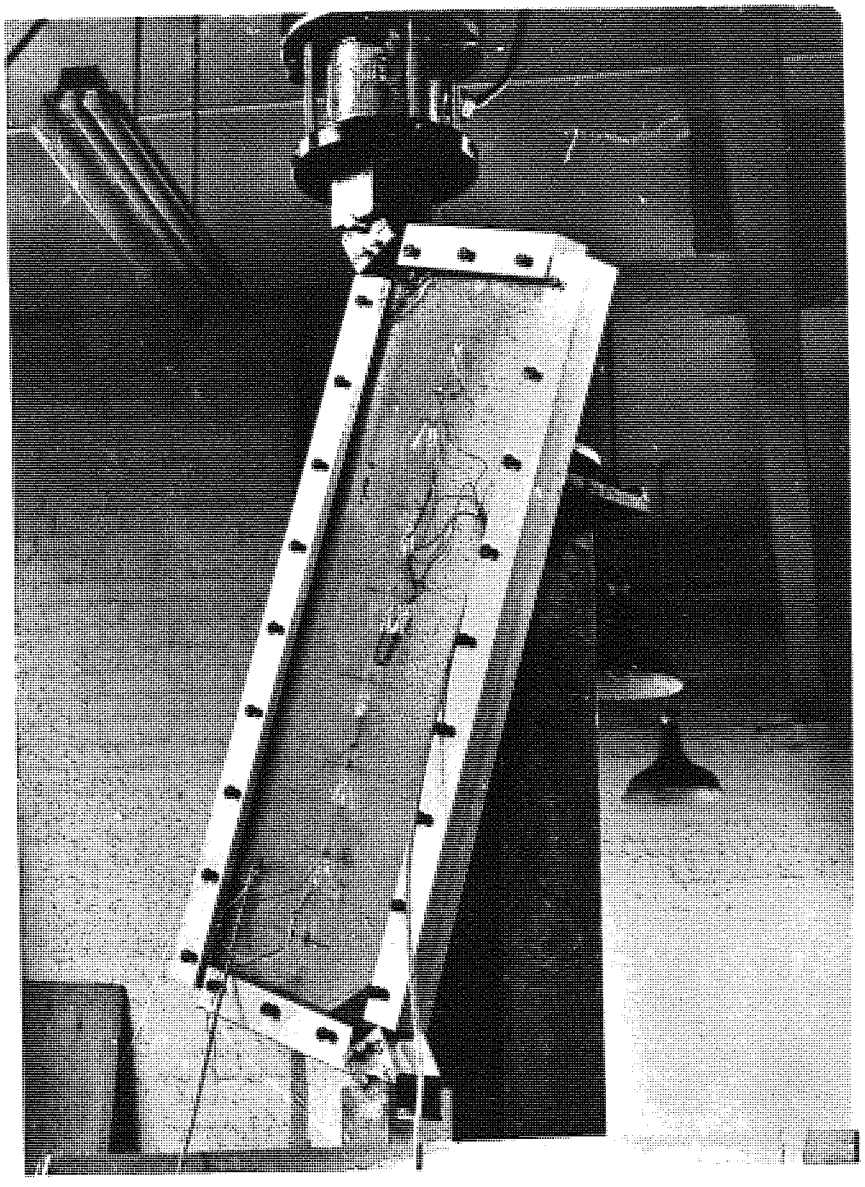

Fig. 5.20 Test fixture of GRP plate under shear loading

5.5.4) Results:

The theoretical and experimental results for the shear buckling loads of all types of plate mentioned on Table (5.5) are presented on Table (5.7). The elastic properties of the material of the plates under investigation shown in Table (5.8) were obtained by the methods discussed in Chapter 3.

The graphical determination of buckling loads by the Southwell plot method are shown in Figs.(5.21 to 5.26).

5.5.5) Discussion:

The experimental and theoretical results shown in Table (5.7) exhibit a reasonable agreement which is nearly of the same order as that obtained from compressive buckling, except for the cross-ply plates which suffer from a considerable amount of irregularities.

The Southwell plot was the only method used to determine the buckling load experimentally, as shown on Figs.(5.21 to 26). Unlike the compressive buckling case, the strain gauge method of determining the buckling load was not reliable under shear because of the disturbed results which were obtained from the strain gauge readings. This disturbance may be due to the non-uniform and complex stress field which is generated in the plate under this type of stressing system.

The edge supports and the aspect ratio chosen for the plates were ideal to simulate the conditions assumed in the theory. In addition triangular stiffening plates of dimensions 95 × 95 × 2 mm were bonded to each side of the plate corners on which the load was applied to prevent any material yield in those areas as shown in Fig.(5.20).

Again as in the compression case, the variation

Plate Type	Type of Composite	Fibre Arrangement	Buckling Load $N_{xy(cr)}$ N/mm	
			Theory	Experiment (Southwell Plot)
1	GRP	Unidirectional (0°)	113.60 (Eq.5.14)	75.75
2	GRP	Angle-Ply (+45,-45,-45,+45)	189.00 (Eq.5.15)	142.00
3	GRP	Cross-Ply (0, 90, 90, 0)	116.00 (Eq.5.14)	56.80
4	GRP	Unidirectional (+45°)	66.10 (Tbl.5.6)	66.84
5	GRP	Unidirectional (-45°)	105.30 (Tbl.5.6)	90.90
6	GRP	Unidirectional (-45°)	245.00 (Tbl.5.6)	189.39

TABLE (5.7) SHEAR BUCKLING RESULTS

(See table (5.5))

Plate Type	Fibre Arrangement	Fibre Volume Fraction	Longitudinal Modulus E_L (N/mm^2)	Transverse Modulus E_T (N/mm^2)	Shear Modulus G_{LT} (N/mm^2)	Longitudinal Poisson's Ratio ν_{LT}	Transverse Poisson's Ratio ν_{TL}
1	Unidirectional (0°)	0.27	21408	4740	1800	0.309	0.068
2	Angle-Ply (45,-45,-45,45)	0.27	5777	5777	6887	0.580	0.530
3	Cross-Ply (0, 90, 90, 0)	0.27	11300	11300	1774	0.167	0.167
4,5 & 6	Unidirectional (45°), (-45°)	0.27	5410*	5410**	13004***	0.500+	0.500++

* E_1

** E_2

*** G_{12}, for E_L = 15280 N/mm^2

\+ ν_{12}

++ ν_{21}

TABLE (5.8) ELASTIC PROPERTIES

(See table (5.5))

Type of Composite	Fibre Arrangement	Fibre Volume Fraction	Thickness (mm)	Plate Aspect Ratio a/b	Theoretical Buckling Load (N/mm)	Normalised Value
GRP	Unidirectional at (-45°)	0.27	4.35	4.98	279	1
GRP	Unidirectional at (+45°)	0.27	4.35	4.98	71	0.25
GRP	Unidirectional at (0°)	0.27	4.35	4.98	114	0.41
GRP	Angle-Ply (45,-45,-45,45)	0.27	4.35	4.98	210	0.75
GRP	Cross-Ply (0, 90, 90, 0)	0.27	4.35	4.98	190	0.68

TABLE (5.9) COMPARISON OF SHEAR BUCKLING LOAD OF VARIOUS GRP COMPOSITES.

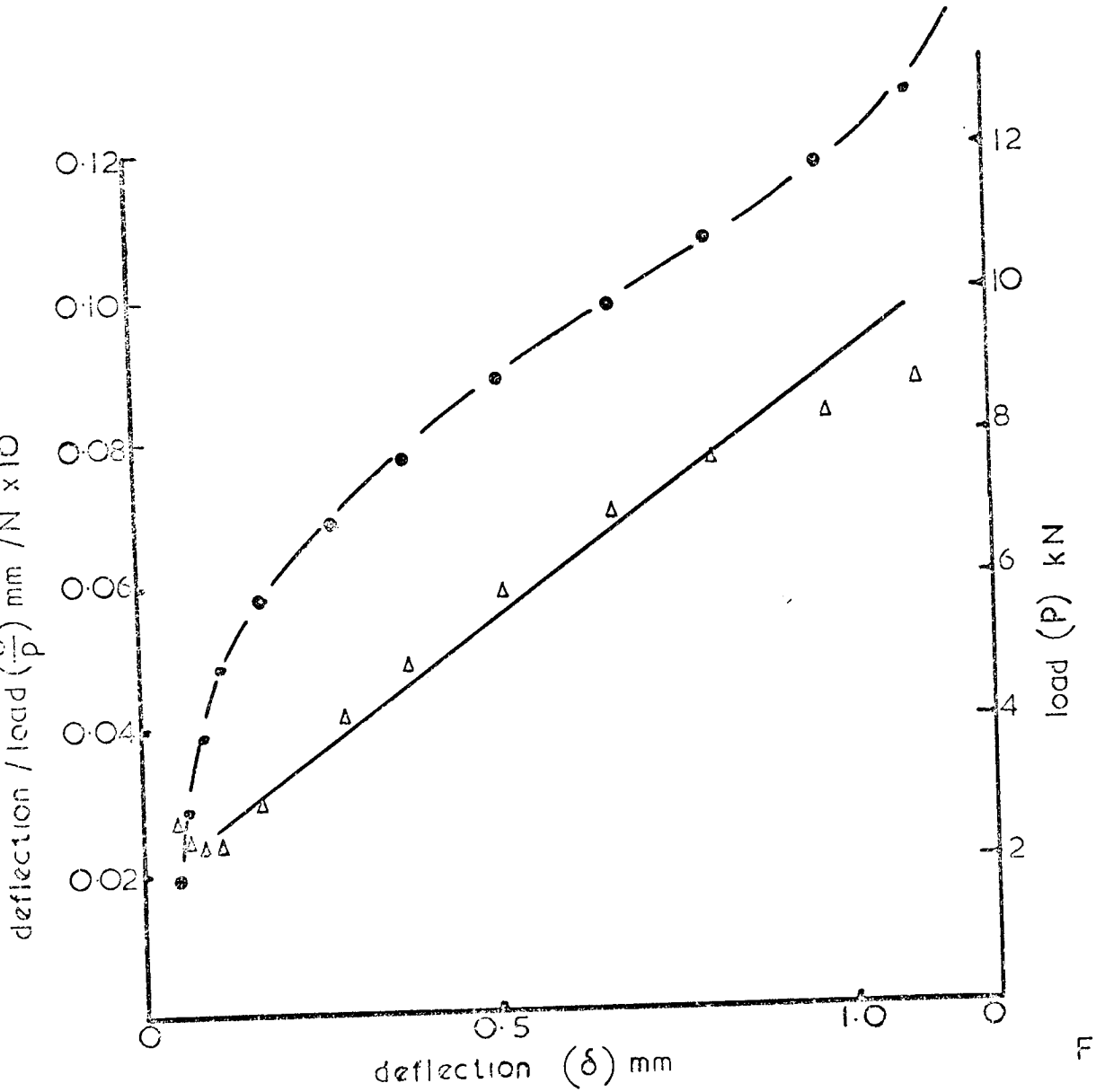

$$N_{xy(cr)} = \frac{0.4 \times 1000}{0.03 \times 176} = 75.75$$

P vs δ

δ/p vs δ

Fig. 5.21 Plate type 1

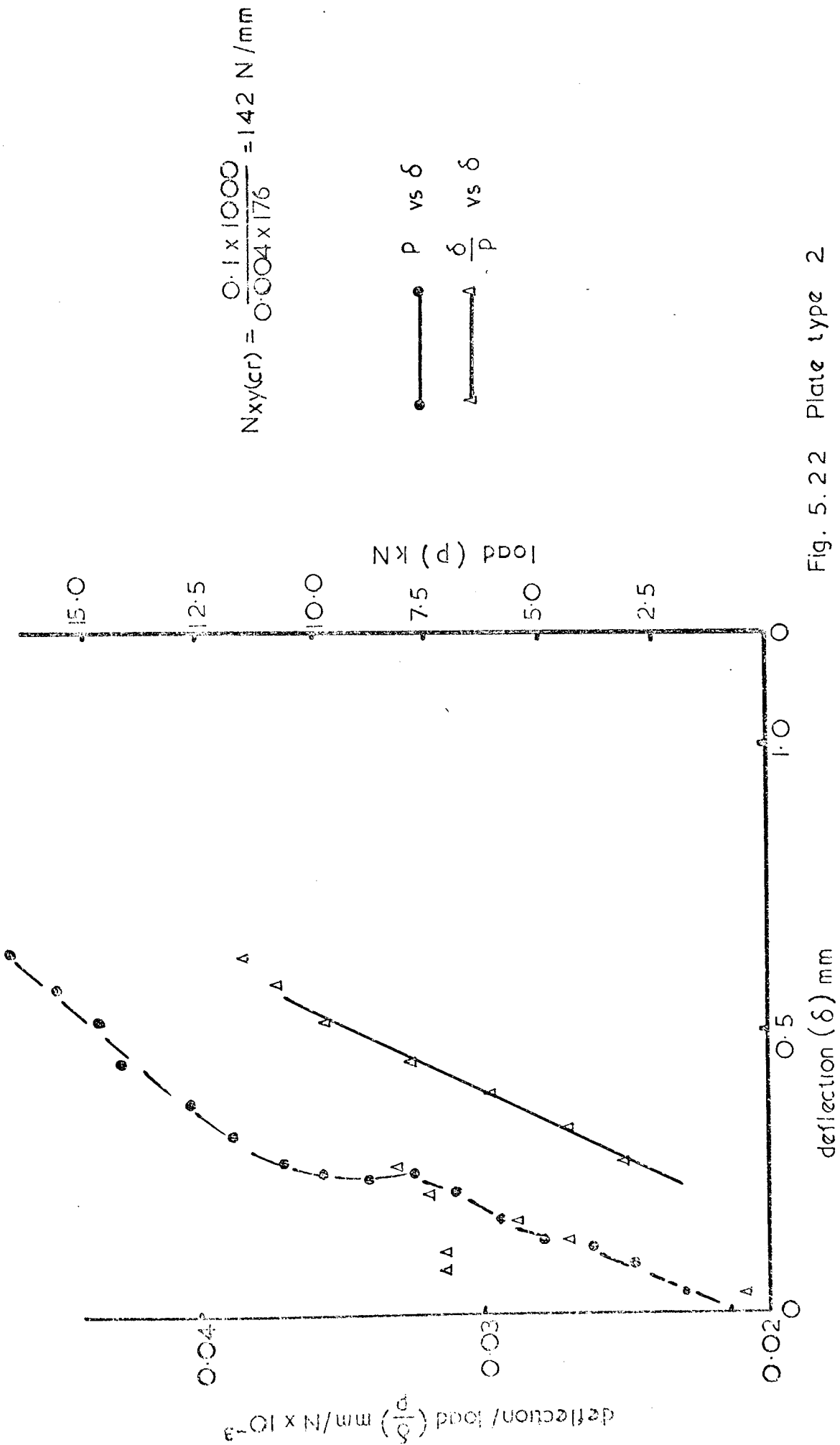

Fig. 5.22 Plate type 2

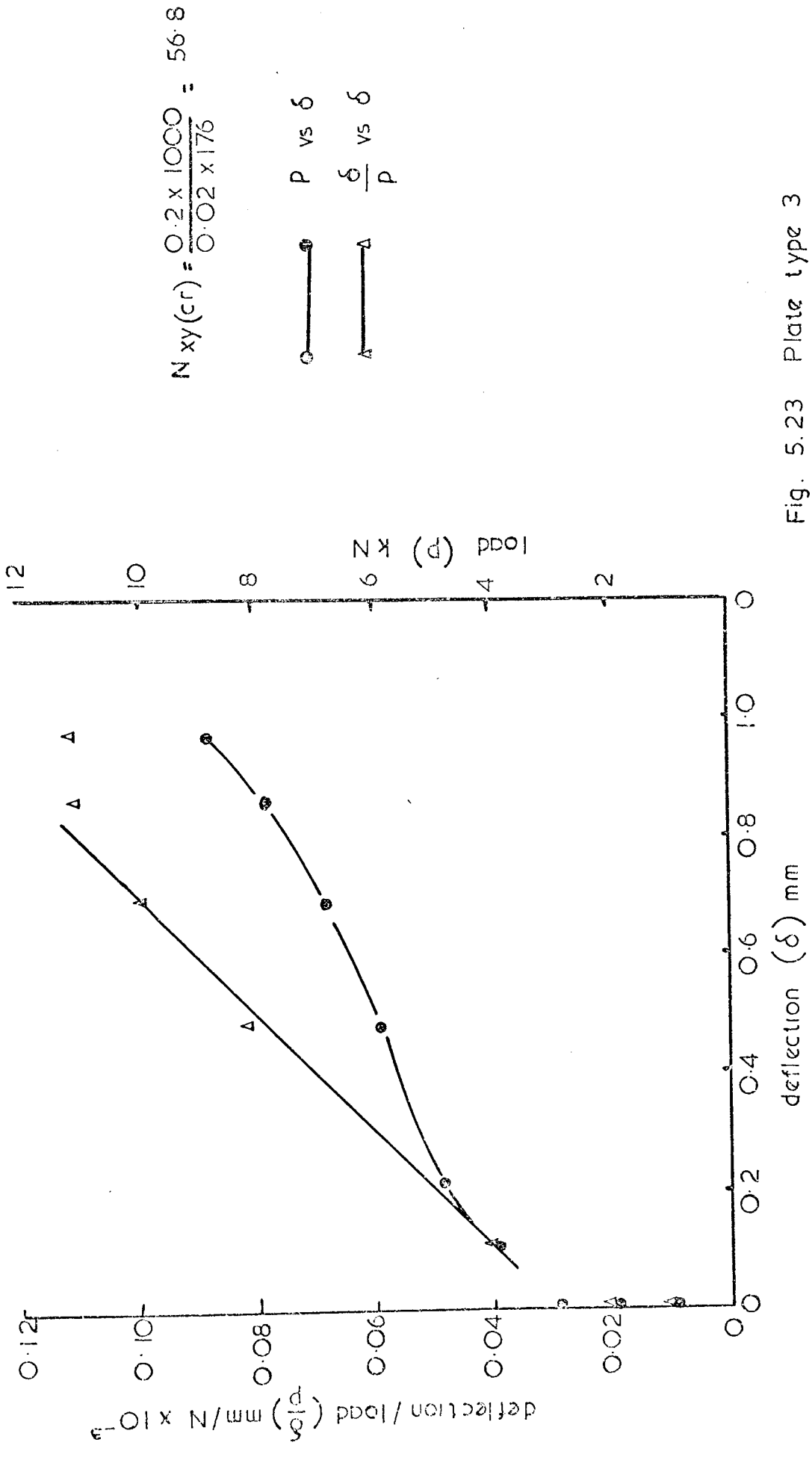

Fig. 5.23 Plate type 3

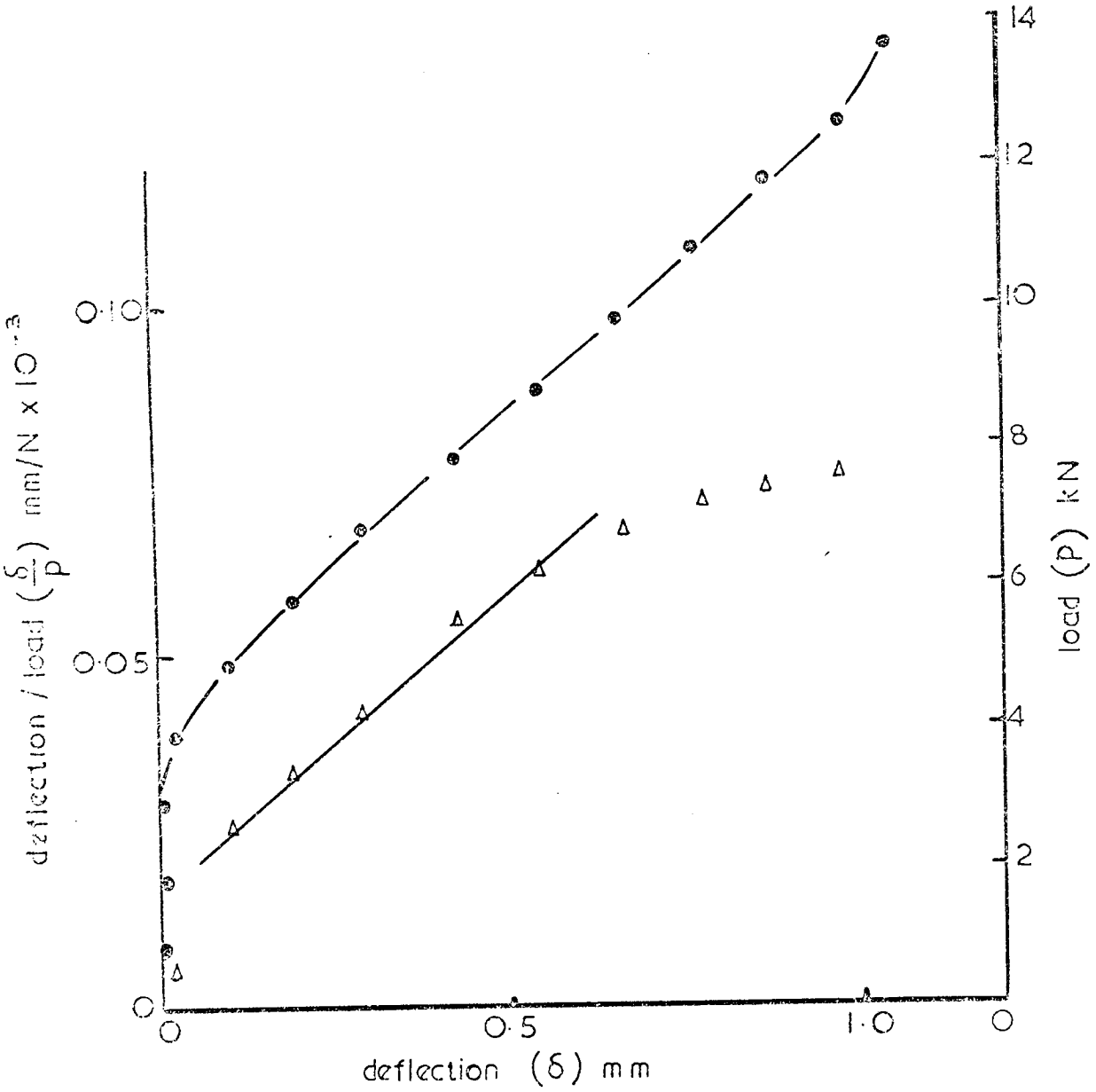

$$N_{xy(cr)} = \frac{0.20 \times 1000}{0.017 \times 176} = 66.84 \text{ N/mm}$$

p vs δ

$\frac{\delta}{p}$ vs δ

Fig. 5.24 Plate type 4

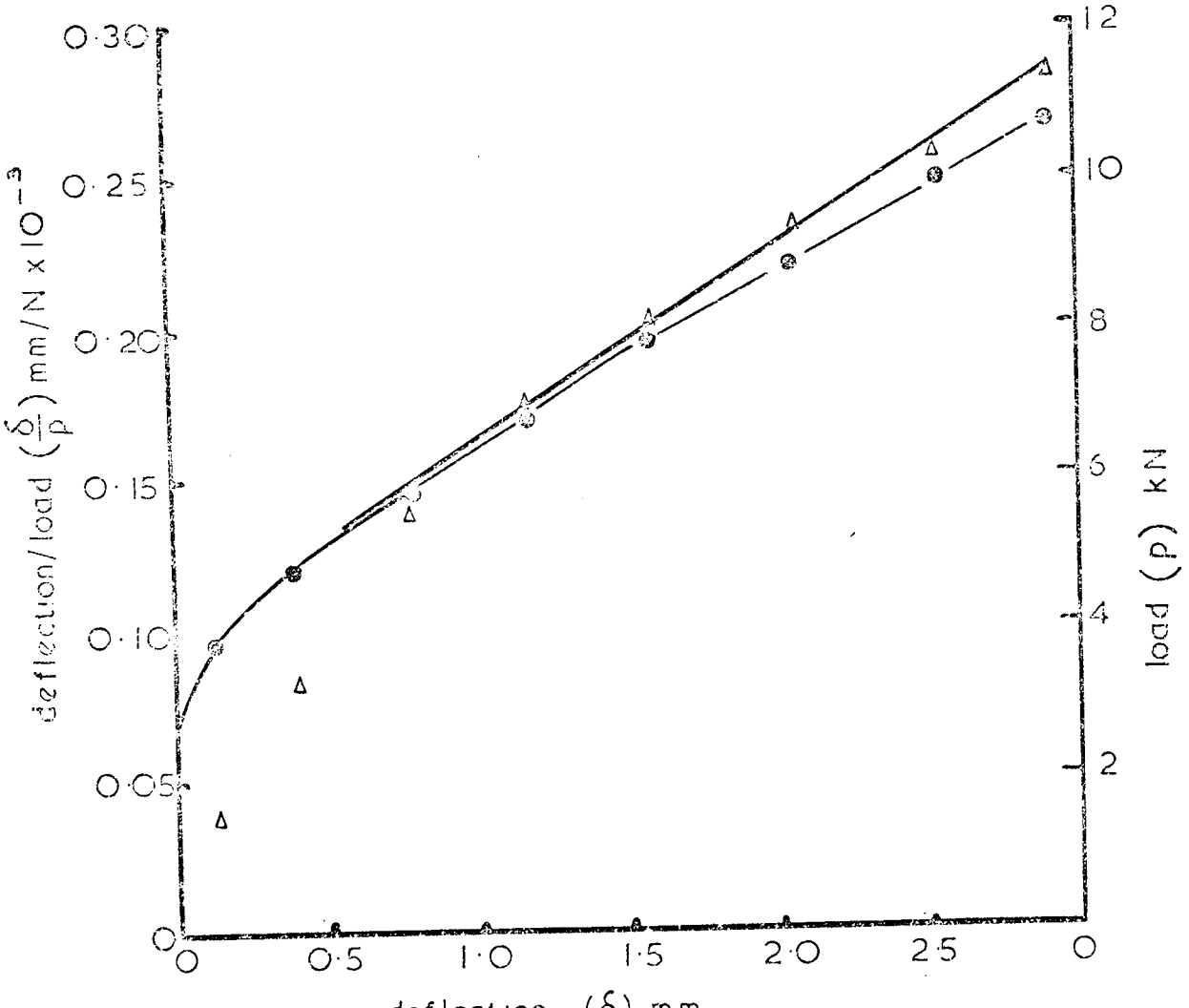

$$Nxy\,(cr) = \frac{1{\cdot}00 \times 1000}{0{\cdot}0625 \times 176} = 90{\cdot}90\ N/mm$$

P vs δ

$\frac{\delta}{P}$ vs δ

Fig. 5.25 Plate type 5

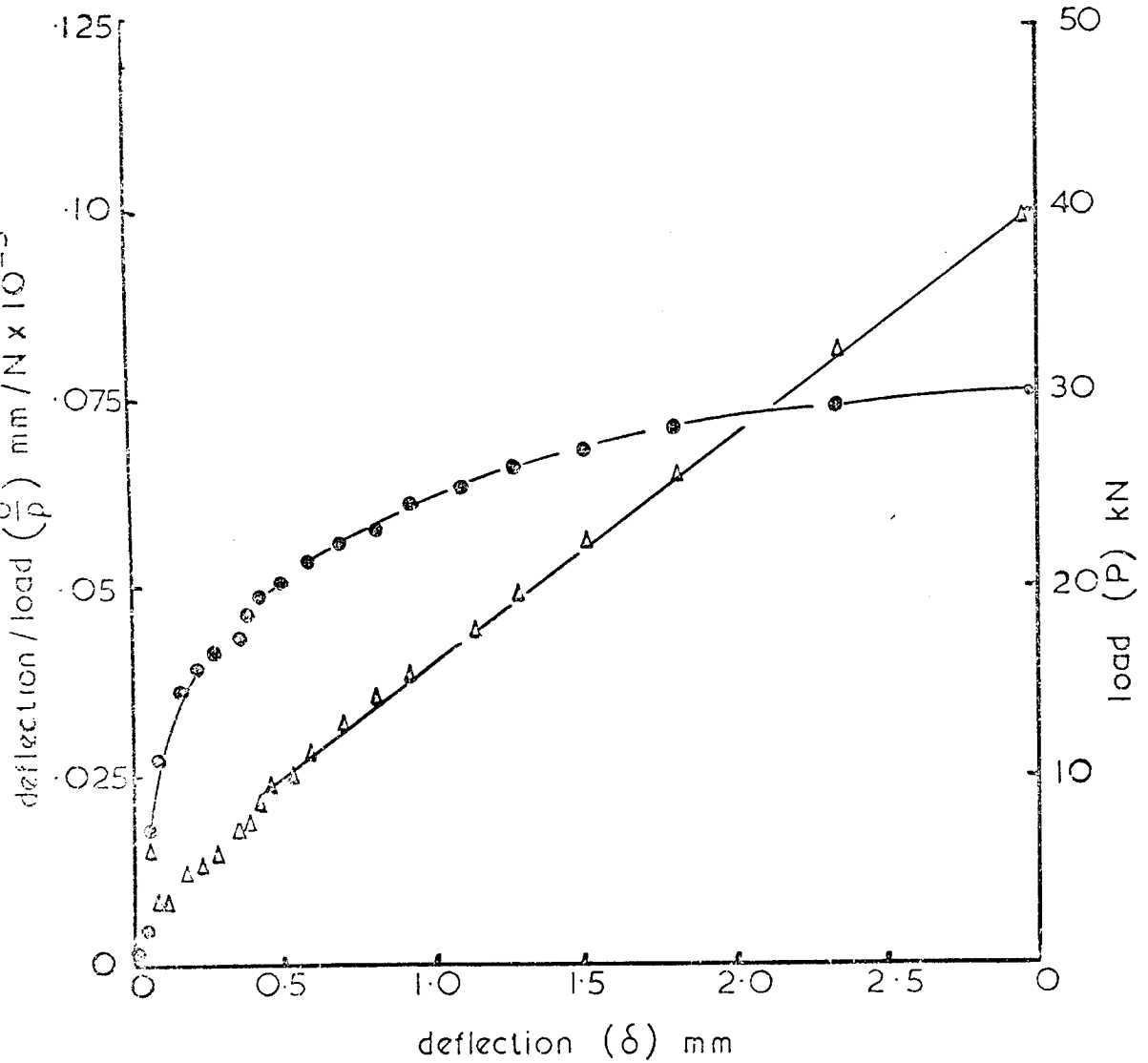

$$N_{xy(cr)} = \frac{0{\cdot}5 \times 1000}{0{\cdot}015 \times 176} = 189{\cdot}39 \text{ N/mm}$$

P vs δ

$\frac{\delta}{p}$ vs δ

Fig. 5.26 Plate type 6

5.5.5) contd.

in thickness between the test specimens did not allow direct comparison of buckling loads between the GRP composites investigated. Table (5.9) was prepared showing a theoretical comparison based on the experimental observations obtained from the tests. This shows that the GRP composite of unidirectional fibre arrangement at -45° has a higher buckling resistance againstshear than any other GRP composite investigated for the same fibre content and plate thickness. So when shear buckling is the major design criteria it is better to use unidirectional GRP at -45° as the optimum fibre arrangement.

5.6) Conclusion.

Theory and experiment were generally in acceptable agreement for both buckling loads in compression and shear which proved that the adopted specially orthotropic plate and mid-plane symmetric theories were ideal for the theoretical prediction.

The test arrangements and edge supports were reasonably designed to bring the theoretical assumptions with the experimental conditions.

The strain gauge method of determining the buckling load experimentally was more reliable in the compression case than Southwell plot method, while the later is superior to the former in the shear case.

SGRP plates proved to have more buckling resistance than GRP ones in compression, which is expected because of the higher modulus of steel wire than that of glass fibres. Within the GRP composites themselves, the angle-ply composite plates showed a higher resistance to compressive buckling than the

5.6) contd.

cross-ply and unidirectional arrangement of the same thickness and fibre content, see Table (5.4).

-45° GRP plates proved to have highest resistance to shear buckling for equal thickness and fibre content, see Table (5.9).

For the design of a built up GRP box section beam, the compression flange should be made of either cross-ply (0-90) or multidirectional (0, $\overline{+}$ 45) in order to achieve a reasonably strong, stiff compression flange, (see Fig.5.15). The web should be made of -45° unidirectional arrangement to suit the sign of the applied shear force. The tension flange should be made of 0° unidirectional arrangement to achieve the maximum strength.

Finally, GRP composites have been shown to have a low buckling resistance if compared to steel. This is because of their low modulus which is a major weakness in this material. It has been shown in this chapter that some improvement may be achieved of the buckling load by changing the fibre arrangement within the composite, but this improvement is not sufficient to make GRP really suitable for use under compression or pure shear. Hence a mechanical stiffening (i.e. ribs or corrugation) is preferable to achieve a higher buckling resistance than can be obtained from flat plates.

REFERENCES.

5-1) ASHTON,J.E., and WHITNEY,J.M., "Theory of laminated plates", Technomic Publishing Co.,Inc.,1970.

5-2) HEARMON,R.F.S., "An introduction to applied elasticity", Oxford University Press, London ,1961.

5-3) LEKHNITSKI,S.G.,"Anisotropic plates", Translated from the second Russian edition by S.W.Tsai and T.Cheron, Gordon and Breach, 1968.

5-4) BULSON,P.S.,"The Stability of flat plates", Chatto & Windus, London, 1970.

5-5) CALCOTE,L.R.,"The analysis of Laminated Composite Structures", Van Nostrand Reinhold Co., 1969.

5-6) DAS,V.C.,"Buckling of rectangular orthotropic plates", Applied Scientific Research, Section A, Volume 11, 1963, PP.97-103.

5-7) WITTRICK,W.H., "Correlation between some stability problems for orthotropic and isotrpic plates ... etc." Aeronautical Quarterly, Volume 4, August 1952, P.83.

5-8) SHULESHKO,P., "Reduction method for buckling problems of orthotropic plates" Aeronautical Quarterly, Volume 8, 1957, pp.145-156.

5-9) THIELEMANN,W., "Contribution to the problems of buckling of orthotropic plates, with special reference to plywood", NACA Tech.Memo, 1263, August 1950.

5-10) SOUTHWELL,R.V., "Proceeding of the Royal Society,London", Series A, Volume 135, 1932, P.601.

5-11) ROORDA,J., "Some thoughs on the Southwell plot" Journal of the Engineering Mechanics Division, American Society of Civil Engineers, Volume 93, No. EM6, December 1967.

5-12) SEYDEL,E.Z., "Fur flugtechnik U. Motorluftsch", Volume 24, No.3, 1933, P.78.

CHAPTER 6

DESIGN AND TESTING OF GRP BEAMS

6.1) Introduction:

At this stage, the structural properties of GRP and SGRP composites have been reasonably understood. In this chapter, the consideration of manufacturing GRP beams will be discussed and a beam cross-section that suits the properties of the composites under consideration will be designed.

So far most designs in GRP take advantage of the high axial strength and overcome the weakness in shear by designing sandwich beams and plates composed of thin GRP skin sheets at the top and bottom of the cross-section to resist the tensile and compressive stresses respectively. A light weight, high shear resisting core material is then embedded between these two faces. The design of this type of structure is discussed in ref.(6-1,4) with sandwich construction of GRP for large spans, and single skin construction for small spans.

In the present chapter, the design and manufacture of a single skin GRP beam unit that can be used for long or short span application will be discussed.

6.2) GRP Beam Cross-Section:

It is obvious that the maximum tensile or compressive stress in a beam is proportional to the distance of the most remote fibre from the neutral axis. Hence, if the material has the same strength in tension and compression, it will be logical to choose shapes of cross-section in which the centroid is at the mid-depth of the beam. In this manner the same factor of safety for fibres in tension and for those in compression will be obtained. This is the underlying idea in the choice of section symmetrical with respect to the neutral axis for materials such as structural steel which has about the same yield point in tension

6.2) contd.

and compression.

For materials of different strength in tension and compression (i.e. cast iron, concrete, or GRP) the best section for a beam is not symmetrical with respect to the neutral axis, in other words the neutral axis is not at the mid-depth of the beam section but is at a position from the extreme fibres in the same proportion as the strengths of the material in tension and compression. In this manner a balance effect of stresses along the cross-section can be obtained.

In designing a beam, not only the conditions of strength should be satisfied but also the condition of economy in the weight of the beam. If two cross-sections having the same section modulus, (i.e. satisfying the condition of strength with the same factor of safety), the one with the smaller area is more economical.

The developed GRP cross-section was taken as a double web open section with a flat tension flange and two semi-circular compression flanges which tend to increase the local buckling resistance in the compression region, see Figs.(6.1) and (6.2).

The constants that define the newly developed cross-section is given by the following relationships,

(i) Area (A)

$$A = t(2\pi r + 2D + b) \tag{6.1}$$

(ii) Neutral axis position taken from the top of the cross-section,

$$y_N = \bar{r} - \frac{2r^2 - \frac{1}{2}(D^2 + bD - \frac{t^3}{12})}{\pi r + D + \frac{b}{2}} \tag{6.2}$$

(iii) Moment of Inertia about the neutral axis

6.2) contd.

(iii) contd.

Case 1 : When neutral axis below the line x-x (Fig.6.1)

$$I_{TL}=2\left[\frac{\pi}{8}rt(4r^2+t^2)+\frac{4}{3}\bar{y}(3r^2+\tfrac{1}{4}t^2)+\pi rt\,\bar{y}^2\right]$$

$$\frac{bt^3}{12}-\frac{t^4}{12}+tbD^2-2t\bar{y}bD+tb\,\bar{y}^2-t^2D^2+2t^2\,\bar{y}D-t^2\bar{y}^2$$

$$+2\left(\frac{tD^3}{3}-tD'^2\,\bar{y}+6D'\,\bar{y}^2\right) \qquad (6.3)$$

Case 2 : When neutral axis is above the Line x-x (Fig.6.2)

$$I_{TU}=2\left[\frac{\pi}{8}rt(4r^2+t^2)-\frac{4}{3}\bar{y}t(3r^2+\tfrac{1}{4}t^2)+\pi rt\,\bar{y}^2\right]+$$

$$\frac{bt^3}{12}-\frac{t^4}{12}+btD^2+2btD\bar{y}+bt\,\bar{y}^2-t^2D^2-2D\bar{y}t^2-\bar{y}^2t^2$$

$$+2\left(\frac{tD'^3}{3}+tD'^2\,\bar{y}+tD'\,\bar{y}^2\right) \qquad (6.4)$$

The derivation of equations (6.2 to 6.4) may be found in the Appendix.

The advantages of this cross-section may be summarized below,

(a) The beam unit can be manufactured in one stage only and hence there is no problem of connections in this cross-section which generate stress concentration.

(b) Although the problem of torsional instability is a major one in an open cross-section, this may be eliminated by structural arrangement between adjacent members.

(c) Because of the longtudinal support mentioned in (b) above, there is no problem of lateral instability and hence these sections may be used for long and/or deep heavily loaded spans.

(d) Shearing stresses may be easily controlled by either changing the fibre arrangement or employing transverse stiffeners in the webs.

6.2) contd.

(e) The semi-circular shape of the compression flanges make the cross-section very rigid against compressive local buckling.

A comparison has been made between the newly developed cross-section (corrugated) and some of the competitors to this section, the box and rectangular section, which shows the superiority of the former on the latter cross-sections as shown on Table (6.1)

Section Property	Corrugated Section	Rectangular Section	Box Section*
Area (A) mm	2022.40	2022.48	2022.40
Width (b_T) mm	202	31.8	202
Thickness (t) mm	2	-	2
Depth (D_T) mm	402	63.6	307.6
Moment of Inertia (I) $mm^4 \times 10^6$	34.89	0.68	28.19
Neutral axis position (y_N)mm	177.08	31.80	153.80
Section modulus (Z) $mm^3 \times 10^4$	19.70	2.14	18.32
Critical Local buckling stress in compression (σ_{cr}) N/mm^2	151.43	-	3.61

Table (6.1)

*Sectional properties of I-Section can be considered the same as those of the box section.

Note that the critical local buckling stress in compression shown on Table (6.1) was determined by:-

for corrugated section, from ref.(6-2)

$$\sigma_{cr} = K\left(\frac{t}{r}\right)\left[\frac{E}{\sqrt{3(1-\nu^2)}}\right] \qquad (6.5)$$

where $K = 0.5$ (This coefficient was chosen for design purposes.)

and, for box section

6.2) contd.

$$\sigma_{cr} = K \frac{\pi^2 E}{12(1-\nu^2)} \left(\frac{t}{b}\right)^2 \qquad (6.6)$$

where K = 4.

The comparison in Table (6.1) was made on the basis that the material of all cross-sections was isotropic, and homogeneous (i.e. chopped strand mat.) with the following elastic properties

Young's modulus (E) = 10000 N/mm^2

Poisson's ratio (ν) = 0.30

The critical buckling stress due to shear is equal in both corrugated and box cross sections as the webs are considered to be infinitely long strips which have equal shear buckling coefficients, (see Chapter 5).

6.3) Description of test specimens:

Nine type of beam specimen were tested. These specimens differed from each other mainly by the number, type and arrangement of glass layers in the specimens. A description of each of the specimens may be found in Table (6.2), the beam cross-section is shown in Fig.(6.1).

6.4) Moulding technique:

All the materials (glassfibres, resins and catalysts) were supplied by The Application Department, Fibreglass Limited, St.Helens, Lancashire, the same as those mentioned in Section (3.6.3) of Chapter 3.

The moulding technique used in manufacturing the beam specimens was the conventional hand lay up technique which is widely used in the reinforced plastics industry. The moulding

6.4) contd.

took placed at the establishment mentioned above.

6.5) Test arrangement and procedure:

The beam specimens were tested under a simply supported four point loading system that divided the beam into three equal parts of 530 mm each. The adoption of this loading system gave a pure bonding zone at the middle of the beam in order to get a good assessment of the neutral axis position and stress and strain distribution along the cross-section. Electric strain gauges were fixed to the cross-section of the beam in order to measure the bending and shearing strains respectively. Four wooden saddles were fixed at the supports and load points to maintain the cross-sectional shape during load application. The load was applied automatically by a load cell at a load increment varying between 1.0 to 0.25 metric tone. The strain readings were taken by a computerized data logger, while deflection readings were taken after each load increment. The loading was discontinued as soon as a mode of failure was observed on the test specimen. A general view of the test arrangement and the strain gauge positions may be found in Figs.(6.3) and (6.4) respectively.

6.6) Results:

Table (6.3) shows the load carrying capacities with their corresponding deflections and the mode of failure of each beam under test. The modes of failure are shown in Figs.(6.5) to (6.13).

6.6) contd.

The experimentally determined stress and strain distributions along the beam cross-sections are shown in Figs.(6.14) to (6.22). While the theoretical and experimental values of tensile, compressive and shear stress are shown on Table (6.4).

The elastic and sectional properties of the beams are shown in Tables (6.5) and (6.6) respectively.

The strength and elastic properties were obtained from coupons extracted from the beams under test and according to the test methods mentioned in Chapters 3 and 4.

6.7) Discussion:

It is clear from Table (6.3) that all the beams failed at a reasonably high load. The strain gauge readings showed that at this stage the load-deformation relationship was non-linear, the load at which non-linearity commenced is also shown in Table 6.3. The reason for this non-linearity in the load-deformation relationship is partly due to crack formation in certain parts of the beam, but the main reason is that at the end of the linear limit the beam cross-section starts to deform or warp and hence the neutral axis position changes. This behaviour is to be expected from an open section and the employment of the wooden saddles was designed to minimize this effect. The part played by the change in cross-sectional shape was also indicated in most of the specimens by the fact that the load/deflection curve retunred to the origin. If major cracking had been the cause of the non-linearity this would not have been the case.

Up to the onset of non-linearity the theory and

6.7) contd.

experimental observations agreed reasonably well, as will be discussed below.

The experimental maximum tensile and compressive stresses showed an acceptable agreement with the theory predicted by the simple bending theory given by the following equation,

$$f = \frac{M}{Z} \qquad (6.7)$$

The experimental observations of the maximum shearing stresses at the neutral axis position agreed well with the simple bending theory given by the following equation,

$$\tau_{xy} = \frac{F[(D'-\bar{y})^2 + (b-t)(D-\bar{y})]}{2\, I_{TL}} \qquad (6.8)$$

where I_{TL} is given by equation (6.3).
The derivation of equation (6.8) may be found in the Appendix.

The maximum experimental shearing stresses were obtained from the analysis of 45° strain gauges rosettes fixed on the beam face as shown in Fig.(6.4). The details of the equations used in the calculations of the shearing stresses and strains are mentioned in the Appendix.

The experimental and theoretical maximum tensile, compressive and shear stresses are shown in Table (6.4).

Table (6.3) shows the experimentally observed and the theoretically predicted deflections at the end of the linear stage which are in good agreement. The theoretical determination of the deflection was by the aid of the simple bending theory which is given by the following equation,

$$\delta_{max} = \frac{Wa(3L^2 - 4a^2)}{48\, E_L\, I_{TL}} \qquad (6.9)$$

The derivation of equation (6.9) may be found in the Appendix.

6.7) contd.

Table (6.6) and Figs.(6.14 to 22) show that the neutral axis position is reasonably well predicted by equation (6.2) up to the onset of non-linearity.

No sign of local instability in the compression flanges and webs was observed in the linear region but in the non-linear stage web instability was observed as soon as the shape of cross-section began to deform. This developed into the prime mode of failure especially with beams which were not reinforced transversely (i.e. at 90°) as shown in Figs.(6.5 and 9).

After a thorough examination of the results, beam type 7 proved to be the best of all types investigated. It failed in a very clean compressive mode of failure as shown in Fig.(6.11). Also, no tearing in the corners below the points of load application was observed in contrast to beam type 5 and 6 which suffered from this mode of failure, see Figs.(6.9 and 10). The strength and modulus of the GRP composite from which this type of beam was manufactured were relatively high compared to the other types under investigation which resulted in this beam having the best performance under load. The transverse reinforcement employed in this type of beam gave it a greater stiffness against vertical deflections and produced a web which was stiffer in bending and buckling. Because of this, its load carrying capacity at the end of the linear region (3 tonne) was better than other beams for a given deflection.

For long term design under static load, if a factor of safety of 4 is employed (ref.6-3,4), the working stresses will be equal to the ultimate strength at failure (see Table 6.4) divided by 4. Table (6.7) shows the long term design

6.7) contd.

stresses with their corresponding design and alloable deflections. From this table a conclusion may be drawn that with this factor of safety the design deflections are within the limit of $^{1}/_{120}$th of the beam span.

6.8) Economical Design Consideration:

From Section (6.7), it was seen that the experimental results agreed reasonably well with the simple bending theory up to the point at which cross-sectional deformation began. The beams under test were not designed to give the most economical cross-sections but in this section a step further will be taken in the design of GRP beams by investigating the possibility of designing the most economical cross-section (i.e. the cross-section that shows the maximum $\frac{Z}{A}$ ratio if compared with other cross-sections of the same area). A computer program was run using equations (6.1) to (6.4) for a wide range of the ratios $\left(\frac{D}{r}\right)$, $\left(\frac{t}{r}\right)$ and $\left(\frac{b}{r}\right)$ in order to find the values of A,I, and Z for a unit value of r. Figs.(6.23 to 25) represent a sample of the results produced by this program. The unit values of A,I and Z may be converted to the real design value by multiplying them by r^2, r^3 and r^4 respectively where the value of r is the only value needed in the design in addition to the other design information (ie. span, applied load and allowable stresses), as will be shown in the following numerical example.

To find the most economical cross-section of a 2 meter simply supported GRP beam to carry a live load of 1500 kg. and the material of the beam is similar to that of beam type 7 on Table (6.2). The design data are as follows:-

6.8) contd.

Ultimate compressive strength = 120 N/mm^2

Radius of the compression flange (r) = 40 mm.

Factor of safey to be used = 4 (for long term design)

Material longitudinal modulus = 12083 N/mm^2

The design steps are as follows:-

The design allowable stress $f_c = \frac{120}{4} = 30\ N/mm^2$

Maximum bending moment due to the live load = $\frac{WL}{8}$

$$\therefore \text{B.M.} = \frac{1500 \times 9.81 \times 2000}{8} = 36 \times 10^{+5}\ \text{N.mm}$$

the required section modulus (Z) = $\frac{36\times10^{+5}}{30} = 1.2\times10^5\ mm^3$

$\therefore$ the required section modulus per unit radius

$$Z_{(unit)} = \frac{1.2 \times 10^5}{(40)^3} = \underline{1.875}$$

From Fig.(6.23) the ratios of $\left(\frac{D}{r}\right)$, $\left(\frac{t}{r}\right)$ and $\left(\frac{b}{r}\right)$ that satisfy the required value of $Z_{(unit)}$ are shown below,

for $Z_{(unit)} = 1.875$ and $\left(\frac{b}{r}\right) = 3.00$, the values of $\left(\frac{D}{r}\right)$ and $\left(\frac{t}{r}\right)$ are in the following:-

$\left(\frac{D}{r}\right)$	$\left(\frac{t}{r}\right)$
3.2	0.10
3.8	0.08
4.9	0.06
6.9	0.04

From the previous section the allowable deflection was limited to $^1/_{120}$th of the span and hence $\delta_{(allowable)}$ is 16.67 mm. Then the required moment of inertia will be obtained by the following formula:-

6.8) contd.

$$I = \frac{5\ WL^3}{384\ E_L\ \delta_{(allowable)}}$$

$$\therefore \quad I = \frac{5\times1500\times9.81\times8\times10^9}{384\times12083\times 15.67} = 7610 \times 10^3 \text{ mm}^4$$

$\therefore$ The required moment of inertia per unit radius

$$I_{(unit)} = \frac{7610\times10^7}{(40)^4} = \underline{\underline{2.97}}$$

from Fig.(6.24) the ratios of $\left(\frac{D}{r}\right)$, $\left(\frac{t}{r}\right)$ and $\left(\frac{b}{r}\right)$ that satisfy the required value of $I_{(unit)}$ are shown below,

for $I_{(unit)} = 2.47$ and $\left(\frac{b}{r}\right) = 3.00$, the value of $\left(\frac{D}{r}\right)$ and $\left(\frac{t}{r}\right)$ are in the following:-

$\left(\frac{D}{r}\right)$	$\left(\frac{t}{r}\right)$
2.7	0.10
3.0	0.08
3.6	0.06
4.5	0.04
6.4	0.02

It can be seen that the value obtained for the $Z_{(unit)}$ associated with higher values of $I_{(unit)}$ than the required value (i.e. the deflection requirement has been satisfied by the cross-sections represented by the value of $Z_{(unit)}$) are shown by the position of the crosses on Fig.(6.24). Now putting the values of $\left(\frac{D}{r}\right)$ and $\left(\frac{t}{r}\right)$ which correspond to the value of $Z_{(unit)}$ in Fig.(6.25) in order to find the minimum area required for this section modulus, the minimum area of the cross-section that satisfies the requirement is 1.9 mm^2 for a unit value of the radius r and for the values of $\left(\frac{D}{r}\right) = 6.9$, $\left(\frac{t}{r}\right) = 0.04$ and

6.8) contd.

$\left(\frac{b}{r}\right)$ = 3.00 as shown in Fig.(6.25). Now the design values of the optimum case may be obtained from the unit values as follows:-

for $r_{(Design)}$ = 40 mm

The area of the cross-section $A_{(Design)} = 1.9\times(40)^2 = 3040$ mm^2.

The section modulus $Z_{(Design)} = 1.875\times(40)^3 = 120\times10^3$ mm^3.

The moment of inertia $I_{(Design)} = 7.3\times(40)^4 = 18.69\times10^6$ mm^4 (see Fig.6.24)

The lower depth of the section (D) = 40×6.9 = 2.76 mm.

The thickness of the section (t) = 40×0.04 = 1.60 mm.

The lower width of the beam (b) = 40×3 = 120 mm.

For the sake of design, a wide range of curves can be produced as an output of the computer program previously mentioned and similar to those presented in Fig.(6.23) to (6.25) for values of $\left(\frac{b}{r}\right)$ ratio varying from 1 to 5 in increments of $\frac{1}{2}$ and for the same values of $\left(\frac{D}{r}\right)$ and $\left(\frac{t}{r}\right)$ shown in the same figures.

6.9) Conclusions.

The simple bending theory proved to be satisfactory in predicting the stresses and deflections of GRP beams provided the cross-section is not deformed due to excessive load or the lack of lateral support.

A factor of safety of 4 is considered to be reasonable for the long term design of GRP beams subjected to static lead.

Compared to structural steel, GRP gives lower stiffness so that the allowable deflection of GRP beams has been limited to $^1/_{120}$th of the span. It is considered that this limit is acceptable for many design purposes, but the designer may need

6.9) contd.

to vary this according to design requirement.

The designed cross-section proved to be stable up to nearly 60% of its ultimate load carrying capacity after which it suffered cross-sectional deformation due to lack of support offered by the test arrangement. Practically full lateral support can be achieved by compatibility with other structural units and hence its deformation would be expected to be less noticeable than under laboratory conditions.

GRP beams should be generally reinforced in the same manner as the reinforcement of beam type 7. This beam was reinforced with a combination of unidirectional layers and balanced bidirectional fabric. This type of reinforcement has the advantage of increasing the resistance to cross-sectional deformation, and of improving the transverse and shear modulus. The unidirectional layers resist the main axial stresses and provide stiffness in the longitudinal direction.

Finally the introduction of GRP beams to structural engineering seems to be promising but further investigation is badly needed in order to obtain useful data that can be used for long term design, in particular to put firm limits to the factor of safety and the allowable deflections.

Beam Type	No.of Layers	Type of * Layers	Arrangement of Layers (Degrees)	Fibre Content By Weight (%)	Total Length (mm)	Length Between Supports (mm)	Radius+ r (mm)	Total+ Depth D_T (mm)	Thickness+ t (mm)	Lower+ Width b (mm)	Total+ Width b_T (mm)
1	4	U,F,F,U	0, $\overline{+}$ 45, $\overline{+}$ 45, 0	~ 40	1890	1590	52.08	140.42	4.17	150	358.34
2	4	S,S,S,S	-	~ 40	1890	1590	52.38	141.01	4.76	150	359.52
3	6	U,U,U,U,U, U	0	~ 50	1890	1590	52.60	140.45	5.19	150	360.40
4	4	U,U,U,U	0,90,90,0	~ 40	1890	1590	52.25	140.76	4.51	150	359.02
5	4	U,ST,ST, U (SGRP)	0,0,0,0	~ 40	1890	1590	52.52	141.28	5.03	150	360.06
6	4	U,U,U,U	0,0,0,0	~ 40	1890	1590	51.95	140.15	3.89	150	357.80
7	4	U,F,F,U	0-90	~ 40	1890	1590	52.16	140.57	4.32	150	358.64
8	4	W,W,W,W	0-90	~ 40	1890	1590	51.77	139.79	3.54	150	356.08
9	3	W,S,W	0-90	~ 40	1890	1590	52.16	140.57	4.32	150	358.64

Table (6.2) Description of GRP Beam Specimens

* U : Unimat (unidirectional)
F : Fabmat (bidirectional fabric with mat underlay)
S : Suprimat (choppet strand mat)
W : Balanced Woven Rovings
ST : Steel wire layer

These commercial names are used by Fibreglass Ltd.,

+ See Fig.(6.1)

Beam Type	Ultimate Load Carrying Capacity (Metric Tonne)	Ultimate Deflection (mm)	Load Carrying Capacity Up to End of Linear Regions (Metric Tonne)	Max Linear Deflection (mm)		Mode of Failure
				Theory	Experiment	
1	4.97	81.30	3.0	27,83	30.59	Shear (Fig.6.5)
2	1.68	30.32	1.1	13.70	14.75	Tension (Fig.6.6)
3	8.08	68.88	5.5	23.59	28.35	Shear (Fig.6.7)
4	3.54	71.41	2.6	27.09	32.01	Compression (Fig.6.8)
5	1.64	19.33	1.4	5.95	9.25	Shear and end crushing at supports (Fig.6.9)
6	3.54	48.29	2.2	17.06	21.59	Shear and tearing under the points of load application (Fig.6.10)
7	3.50	43.26	3.0	23.77	20.27	Compression (Fig.6.11)
8	3.11	39.78	2.2	22.42	25.05	Compression (Fig.6.12)
9	3.76	49.53	3.0	24.03	26.95	Compression (Fig.6.13)

Table (6.3) Load Carrying Capacity and deflections of GRP Beams.

Beam Type	TENSION				COMPRESSION				SHEAR			
	Ultimate Tensile Strength (N/mm^2)	Max.Tensile Stress (N/mm^2)		Factor* of Safety	Ultimate Compressive Strength (N/mm^2)	Max.Compressive Stress (N/mm^2)		Factor* of Safety	Inter-Laminar Shear Strength (N/mm^2)	Max.Shear Stress (N/mm^2)		Factor* of Safety
		Theory	Experiment			Theory	Experiment			Theory	Experiment	
1	171.0	81.57	73.00	2.34	105.0	72.00	63.00	1.67	23.7	15.71	15.34	1.54
2	95.6	25.10	47.76	2.00	117.9	23.18	36.32	3.25	31.4	4.96	6.60	4.75
3	334.0	109.65	107.40	3.11	203.0	103.55	95.27	2.13	27.5	21.81	17.85	1.54
4	141.0	59.74	63.26	2.23	101.0	55.15	47.85	2.11	24.1	11.86	12.88	1.87
5	266.0	31.78	35.26	7.54	118.0	29.35	33.30	3.54	21.7	6.23	6.59	3.29
6	305.0	70.08	51.65	5.40	198.0	61.70	43.04	4.60	28.6	13.34	10.62	2.69
7	261.5	78.29	65.26	4.00	120.3	71.67	53.16	2.26	29.9	15.55	20.36	1.47
8	217.0	66.59	62.69	3.46	108.7	62.36	48.27	2.25	25.6	13.61	10.74	2.38
9	170.0	78.47	48.40	3.51	111.2	71.67	44.81	2.48	30.5	15.51	14.21	2.15

Table (6.4) Strengths and Stresses in GRP Beams

* This is the test factor of safety which is equal to the ultimate strength divided by the experimental maximum stress.

Beam Type	Longitudinal Modulus (E_L) N/mm^2	Transverse Modulus (E_T) N/mm^2	Shear Modulus (G_{LT}) N/mm^2	Longitudinal Poisson's Ratio ν_{LT}	Transverse Poisson's Ratio ν_{TL}
1	10406	4750	5200	0.432	0.197
2	6727	6727	2050	0.412	0.412
3	17322	4340	2280	0.293	0.073
4	8111	8111	1570	0.185	0.185
5	19591	4120	1480	0.275	0.058
6	14348	4150	1850	0.315	0.091
7	12083	8755	1950	0.192	0.139
8	11076	11076	2320	0.175	0.175
9	8963	8963	2250	0.225	0.225

Table (6.5) Elastic Properties of GRP Beams.

Beam Type	Radius (r) mm	Area (A) mm^2	Distance of N.A* From Line x-x ($\bar{y}$) mm	Neutral Axis+ Position From Line Z-Z (y_N) mm	Moment of Inertia (I) $mm^4 \times 10^{-6}$	Section Modulus (Z) $mm^3 \times 10^{-3}$
1	52.1	2665.5	-12.87	67.05	7.25	108
2	52.4	3034.1	-12.94	67.70	8.35	123
3	52.6	3397.6	-12.99	68.22	9.42	138
4	52.3	3022.5	-12.92	67.57	8.28	123
5	52.5	3046.6	-12.97	67.83	8.41	124
6	52.0	2325.4	-12.84	67.86	6.29	93
7	52.2	2675.8	-12.89	67.18	7.31	109
8	51.8	2307.6	-12.79	67.60	6.20	92
9	52.2	2675.8	-12.89	67.18	7.31	109

Table (6.6) Sectional Properties of GRP Beams.

* The negative sign represents that the neutral axis is below the line x-x, see Fig.(6.1)

+ Theoretical Neutral axis position. The experimental can be found in Figs.(6.14 to 22)

Beam Type	Ultimate Strength at Failure (N/mm^2)	Type of Strength	Design Factor of Safety	Design Working Stress (N/mm^2)	Design Deflection (δ) mm	Allowable Deflection = $\frac{\text{Span}}{120}$ mm
1	23.7	Shear	4	5.92	10.49	13.25
2	95.6	Tension	4	23.90	13.04	13.25
3	27.5	Shear	4	6.87	7.43	13.25
4	101.0	Compression	4	25.25	12.40	13.25
5	21.7	Shear	4	5.42	5.18	13.25
6	28.6	Shear	4	7.15	9.14	13.25
7	120.3	Compression	4	30.07	9.97	13.25
8	108.7	Compression	4	27.17	9.77	13.25
9	111.2	Compression	4	27.80	9.32	13.25

Table (6.7) Working Stresses and Deflections.

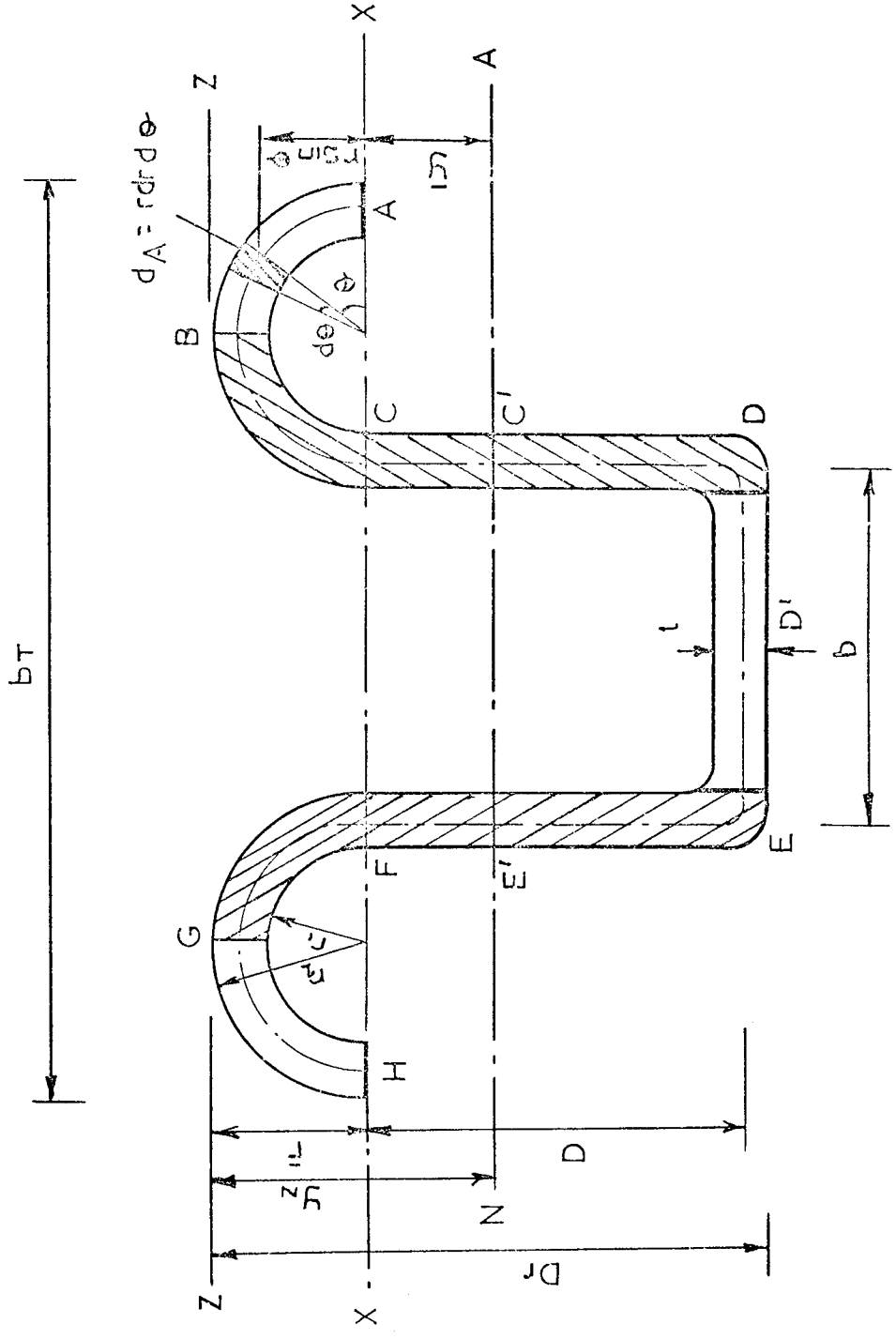

Fig 6.1 The nutral axis below the line X - X

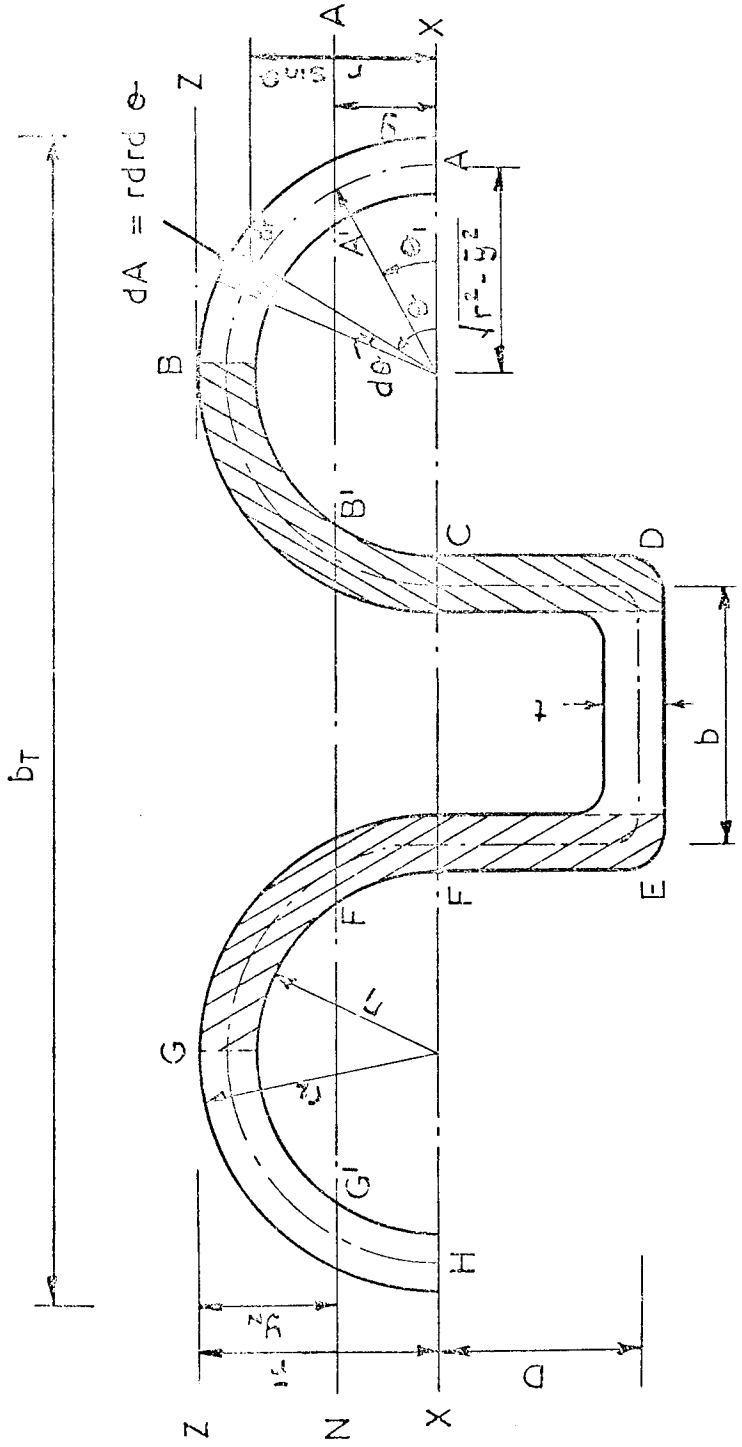

Fig. 6.2. The nutral axis above the line x-x

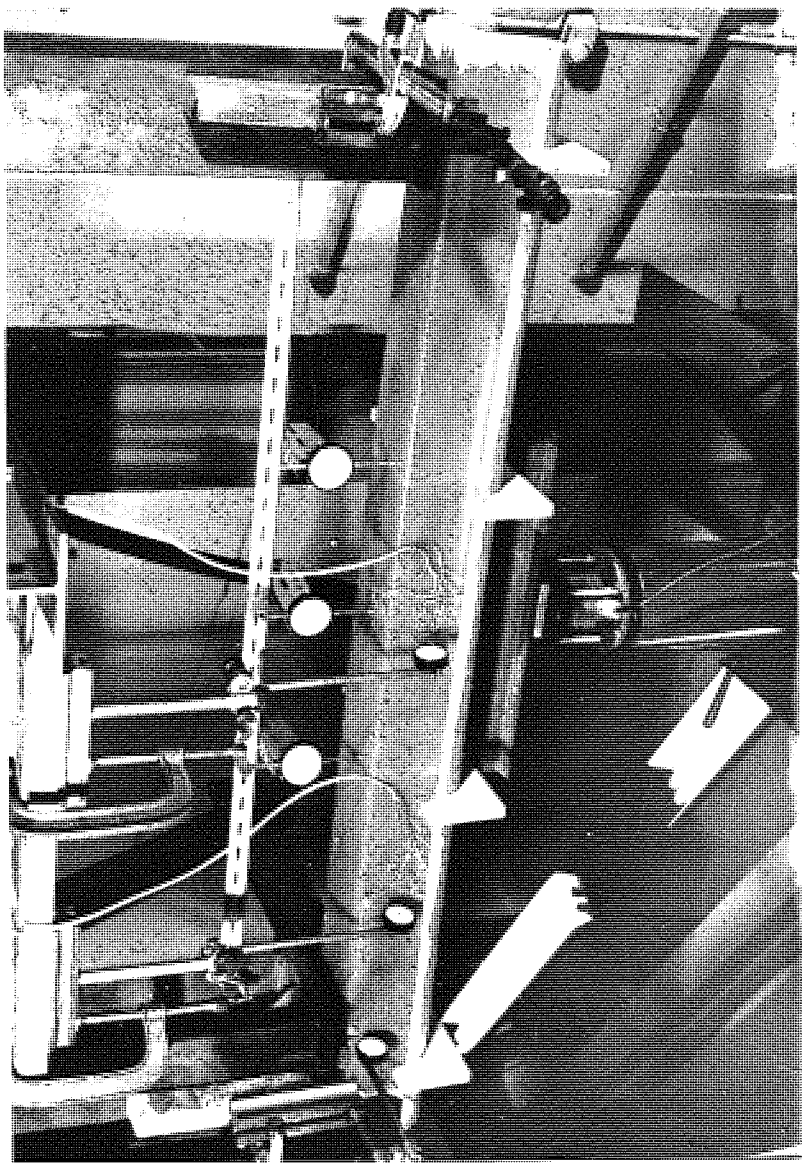

Fig. 6.3 Test fixture

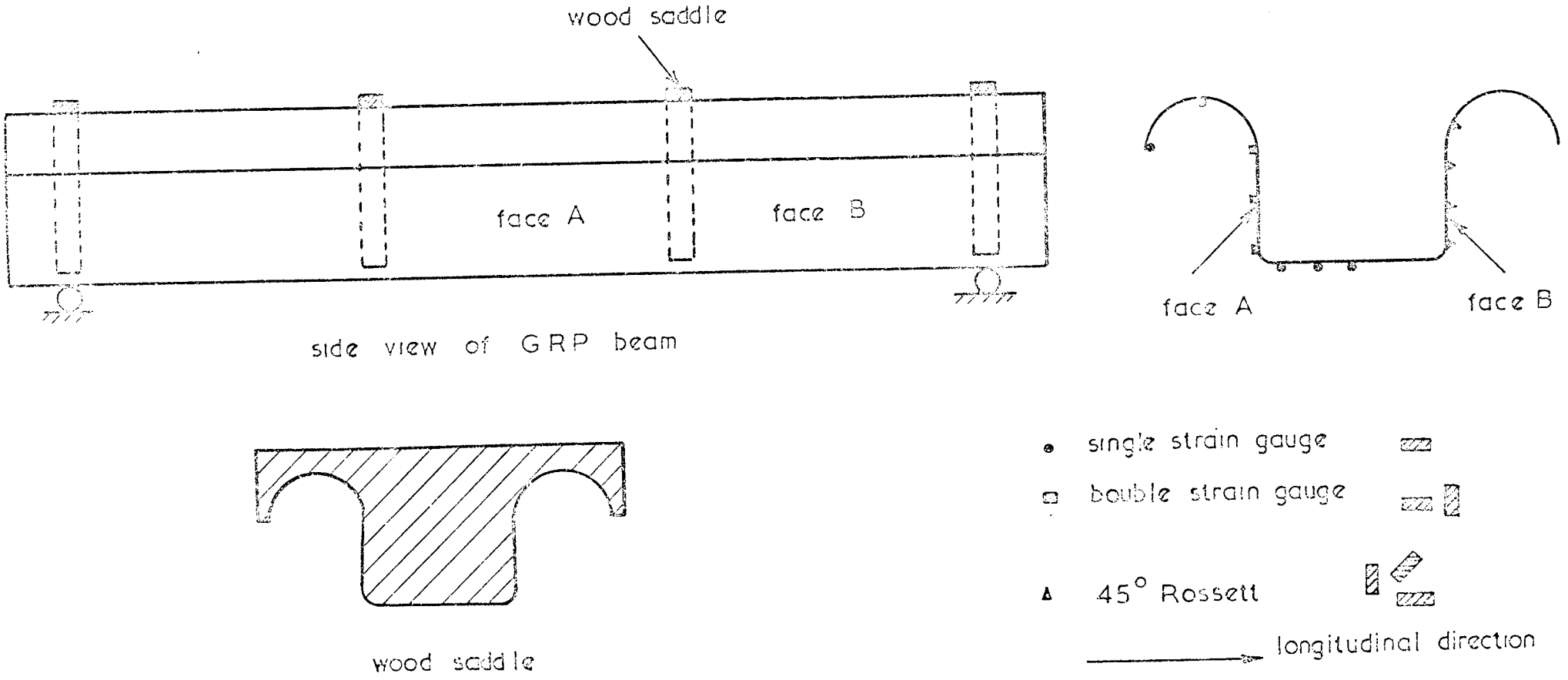

Fig. 6.4. Details of strain gauges positions and wood suddles

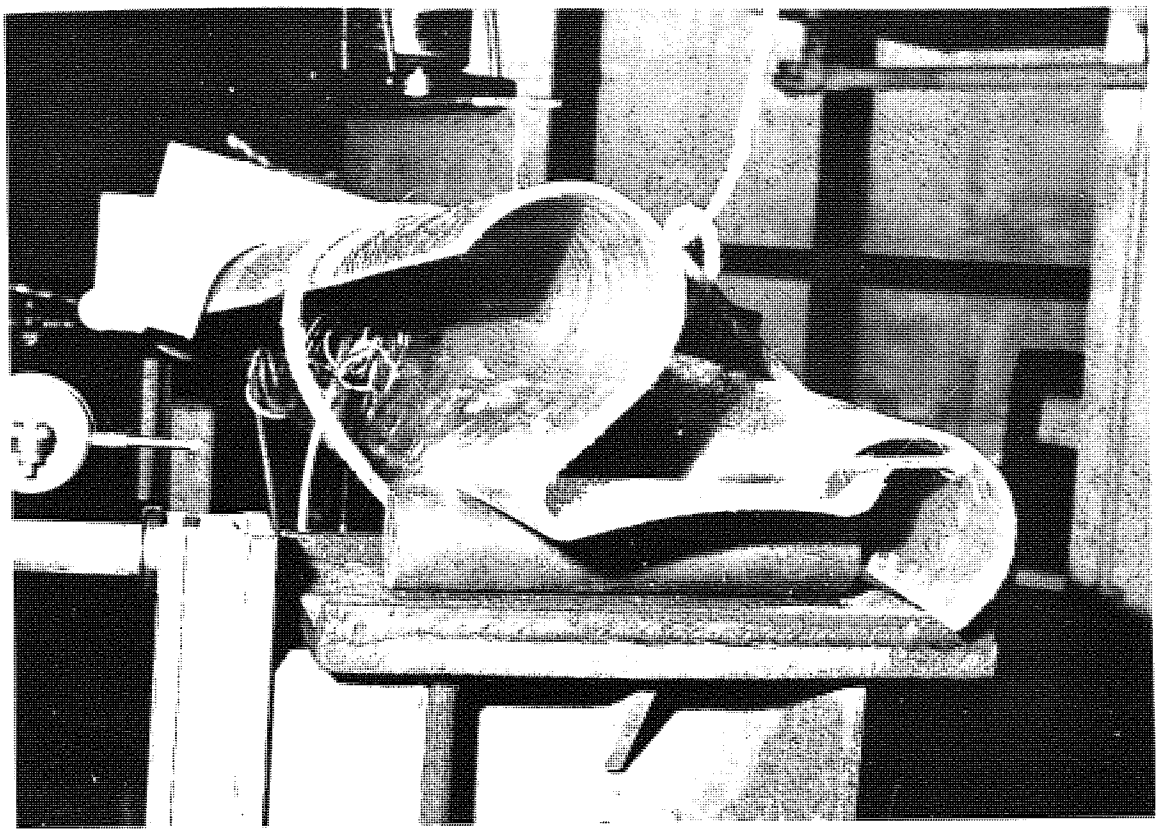

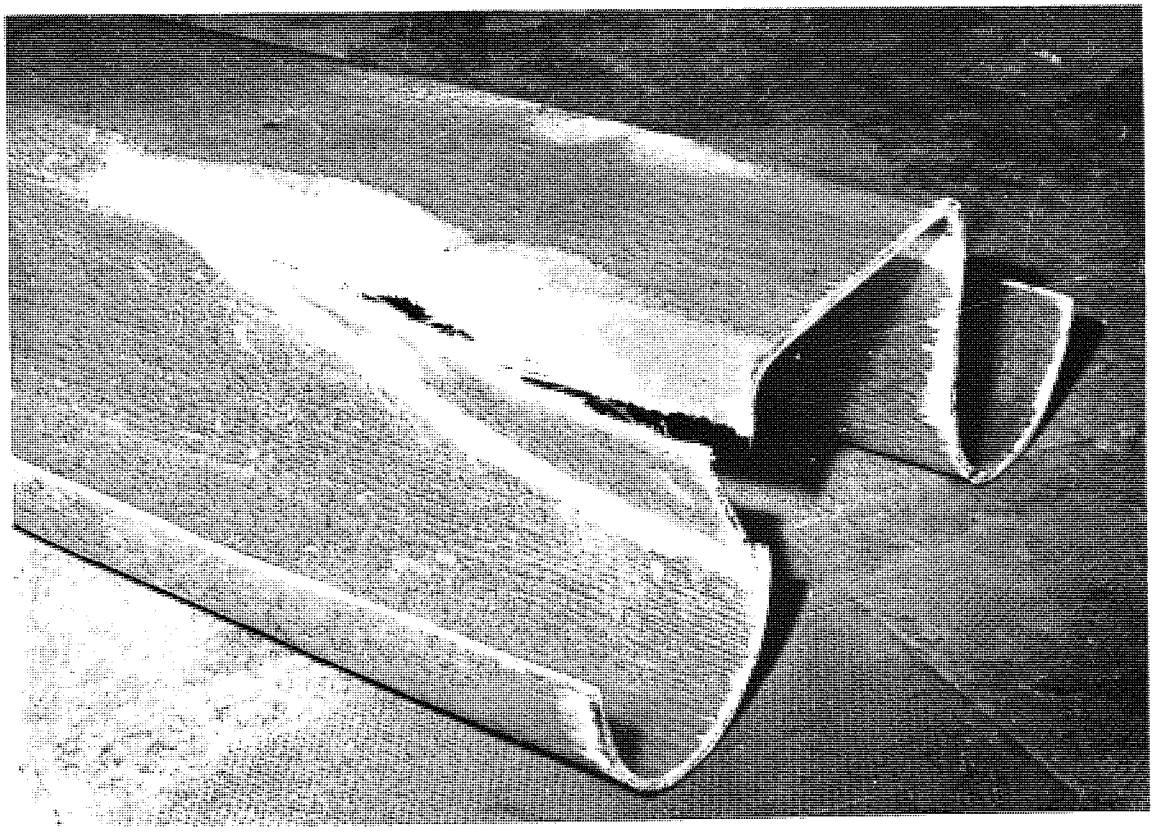

Fig. 6.5. Mode of failure of beam type I

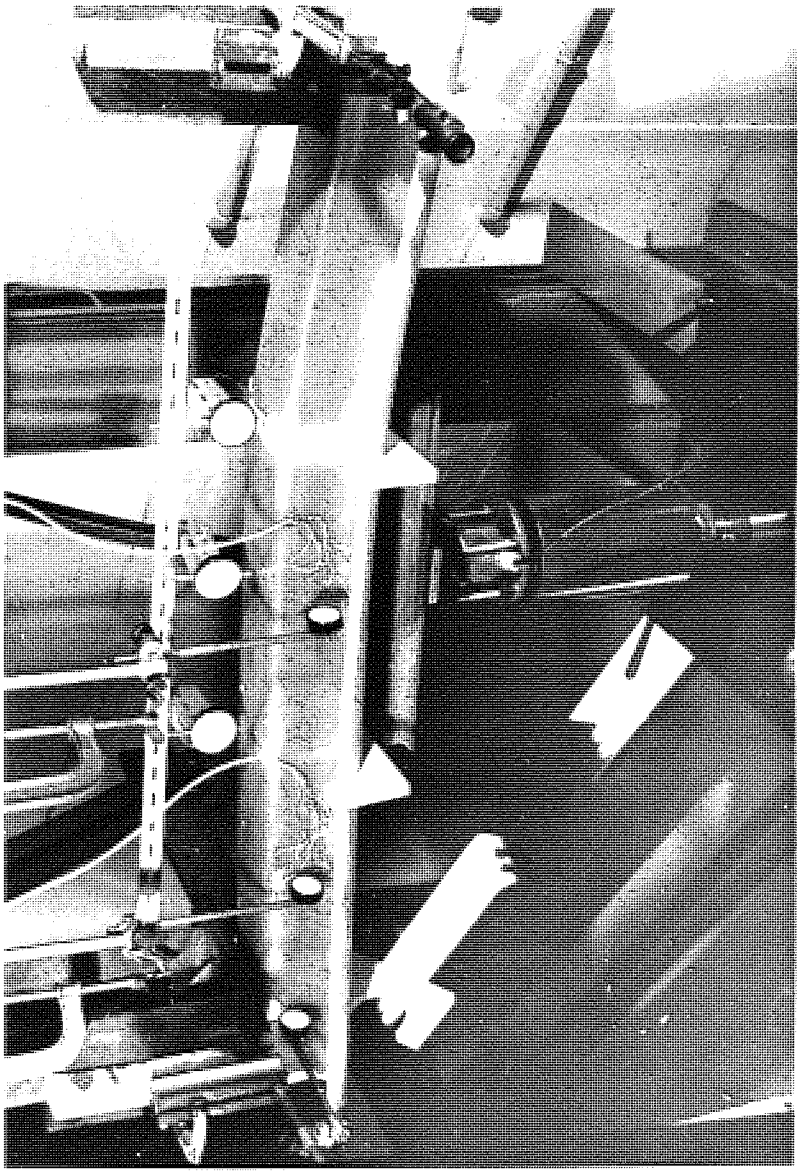

Fig. 6.6 Mode of failure of beam type 2

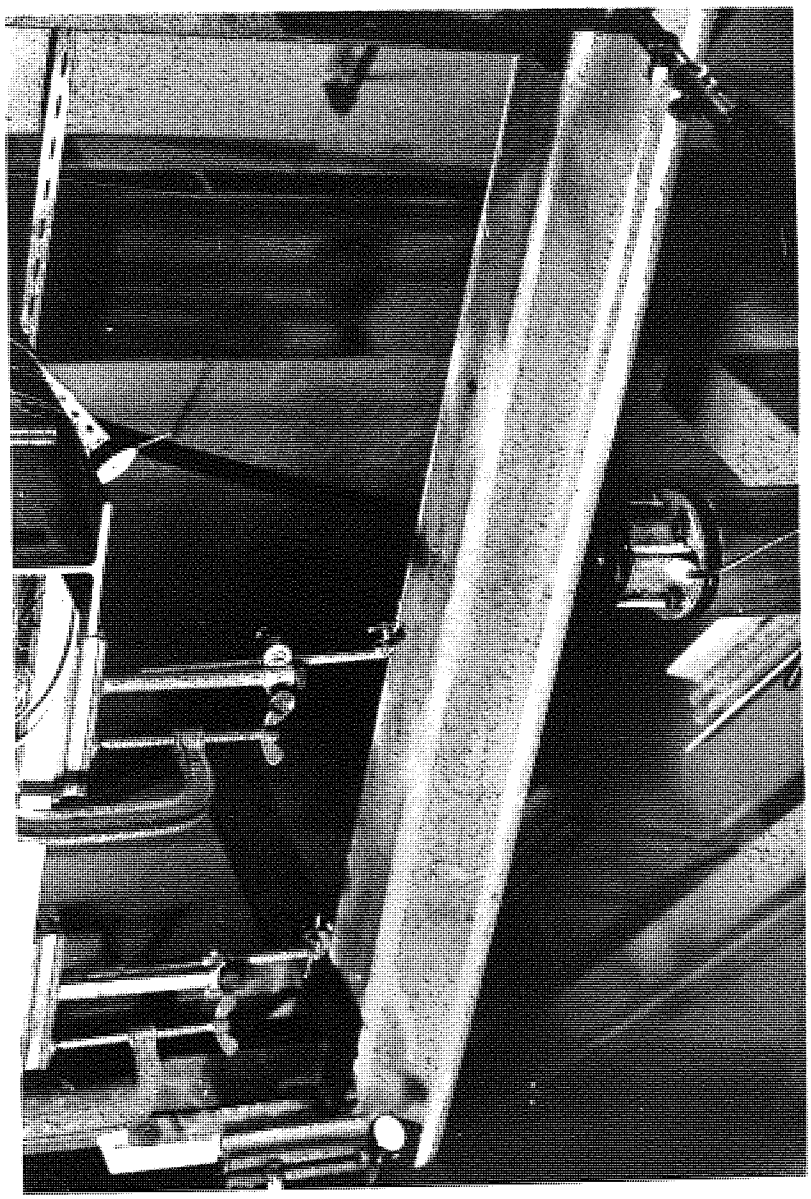

Fig. 6.7. Mode of failure of beam type 3

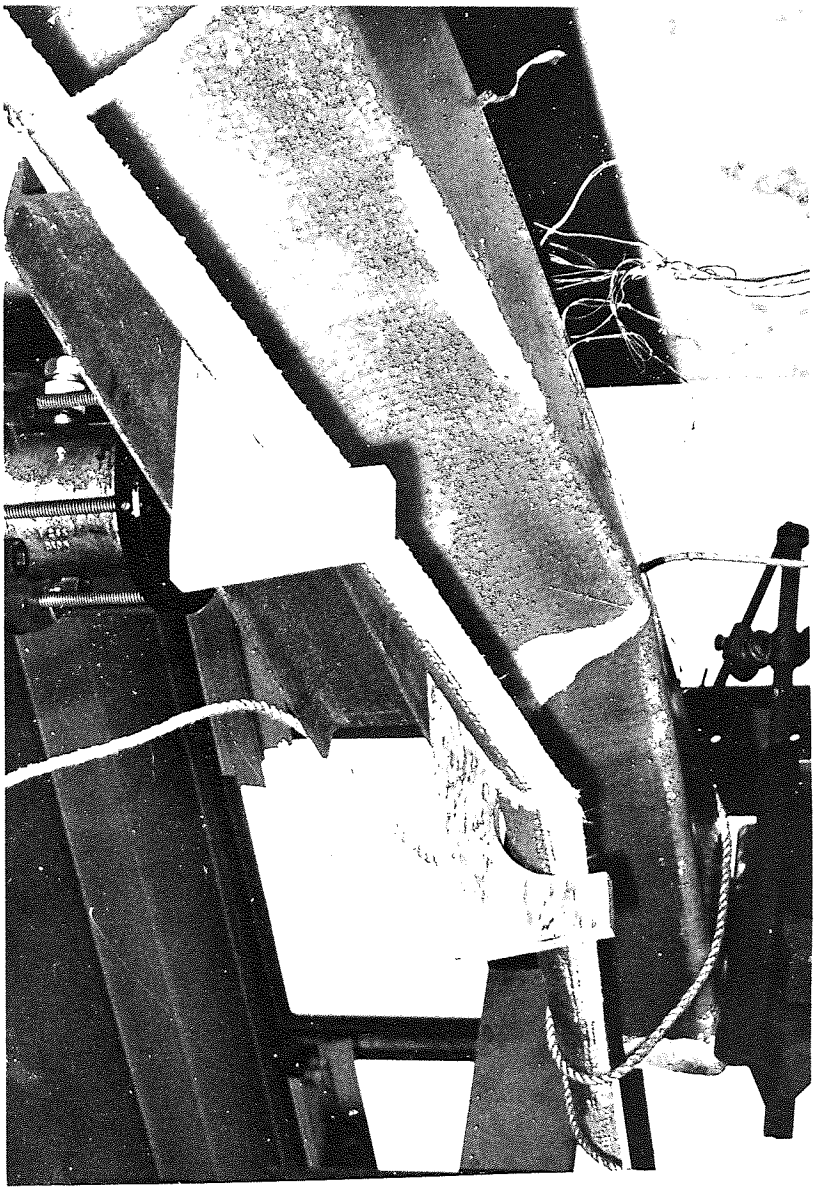

Fig. 6.8. Mode of failure of beam type 4

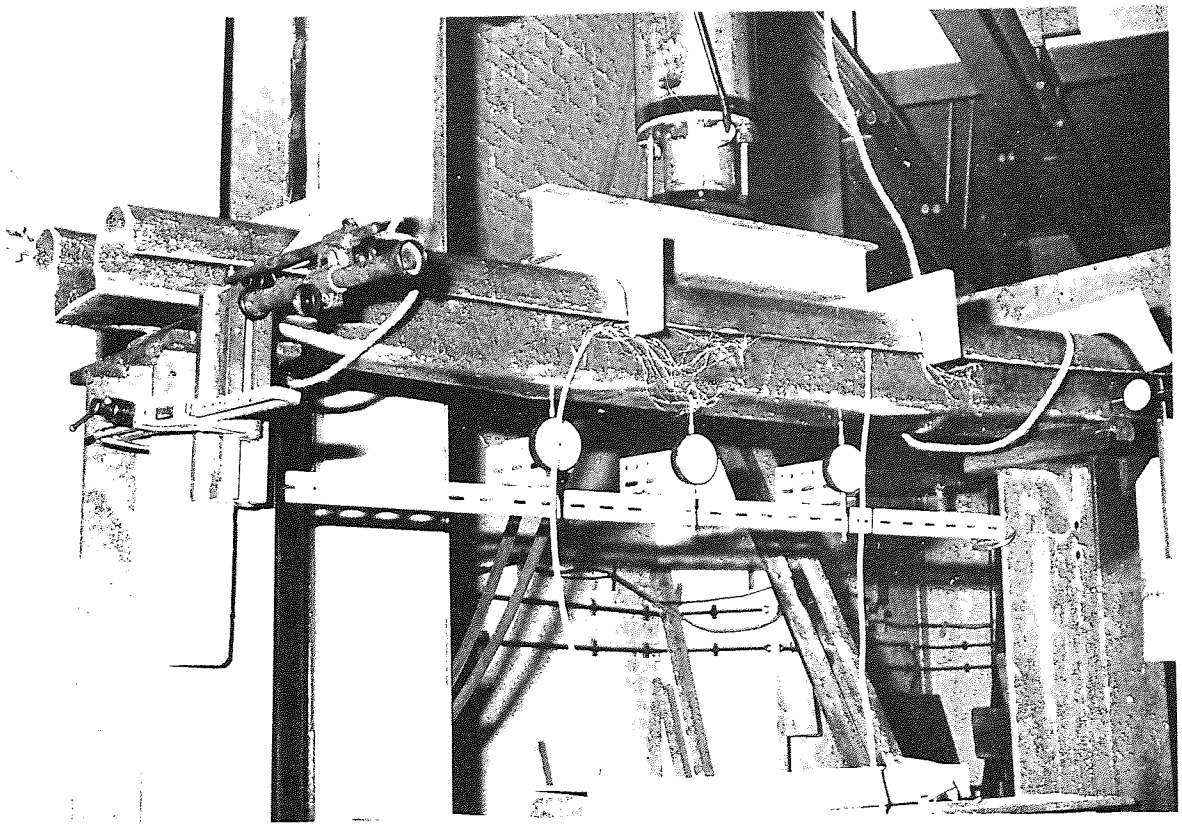

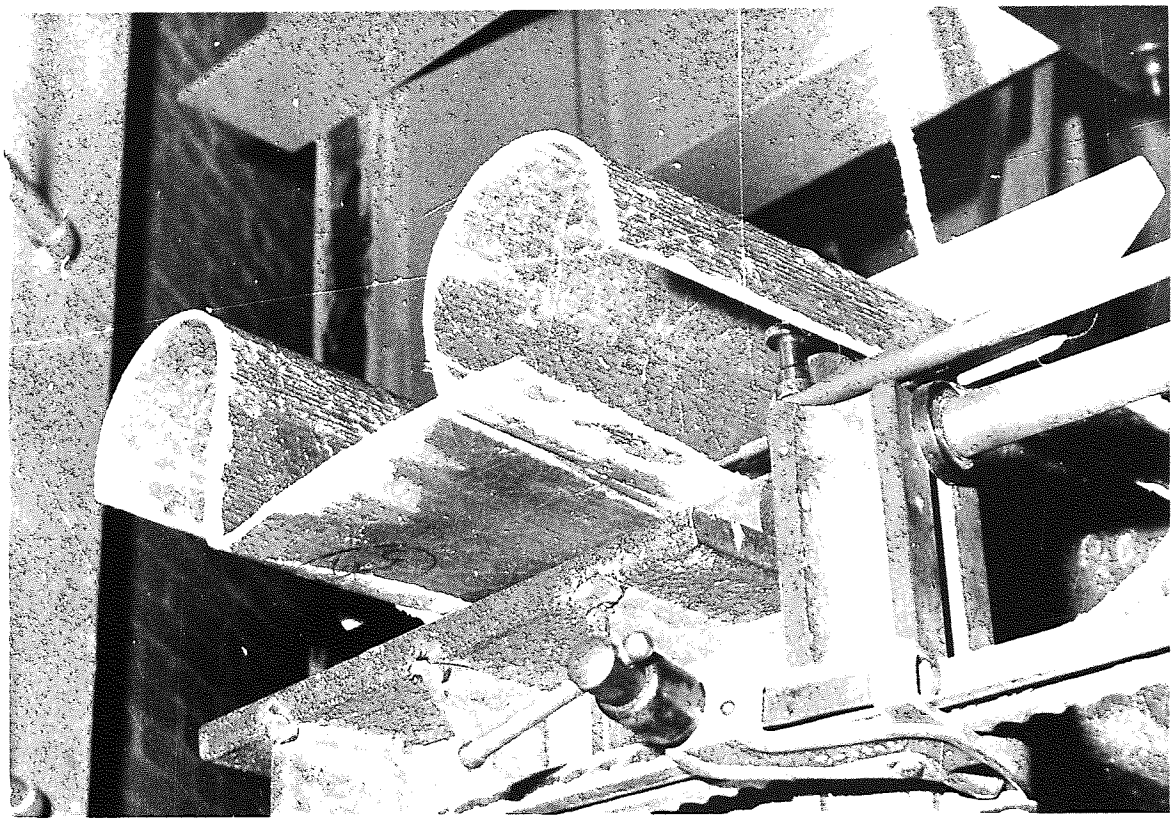

Fig. 6.9. Mode of failure of beam type 5

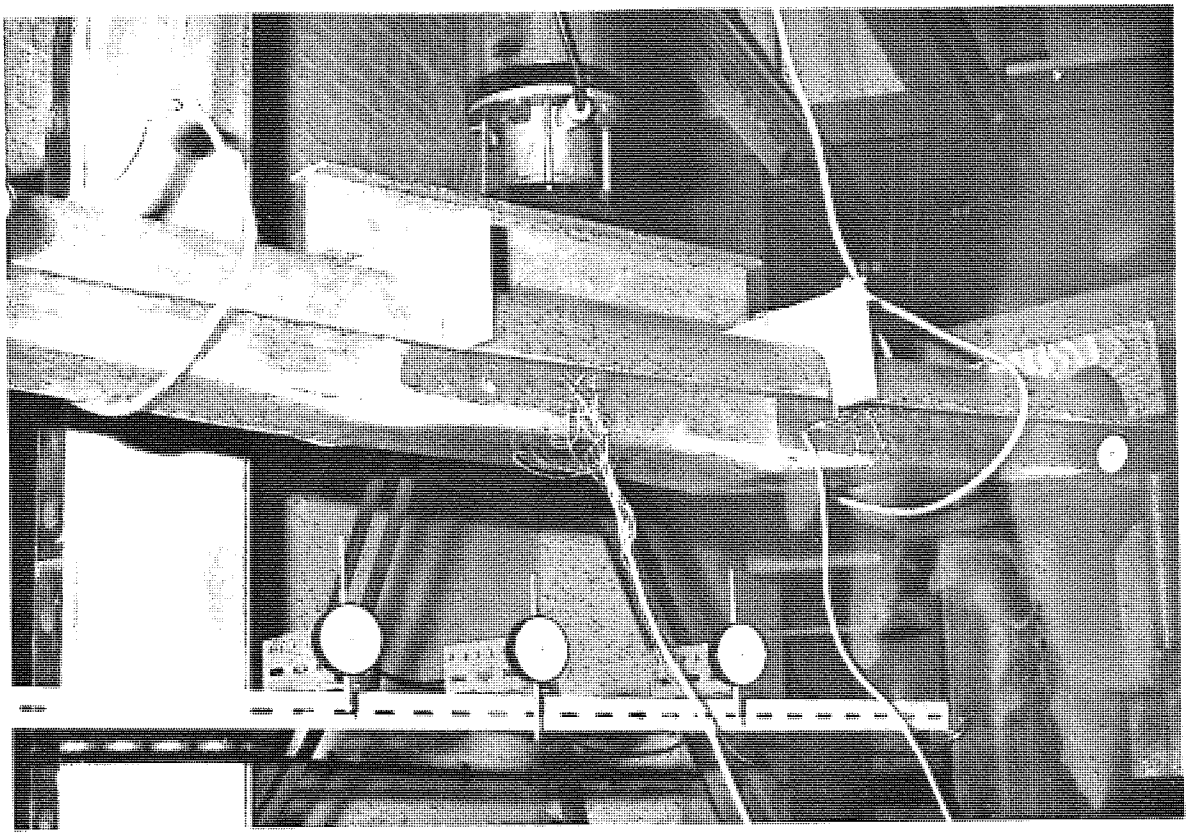

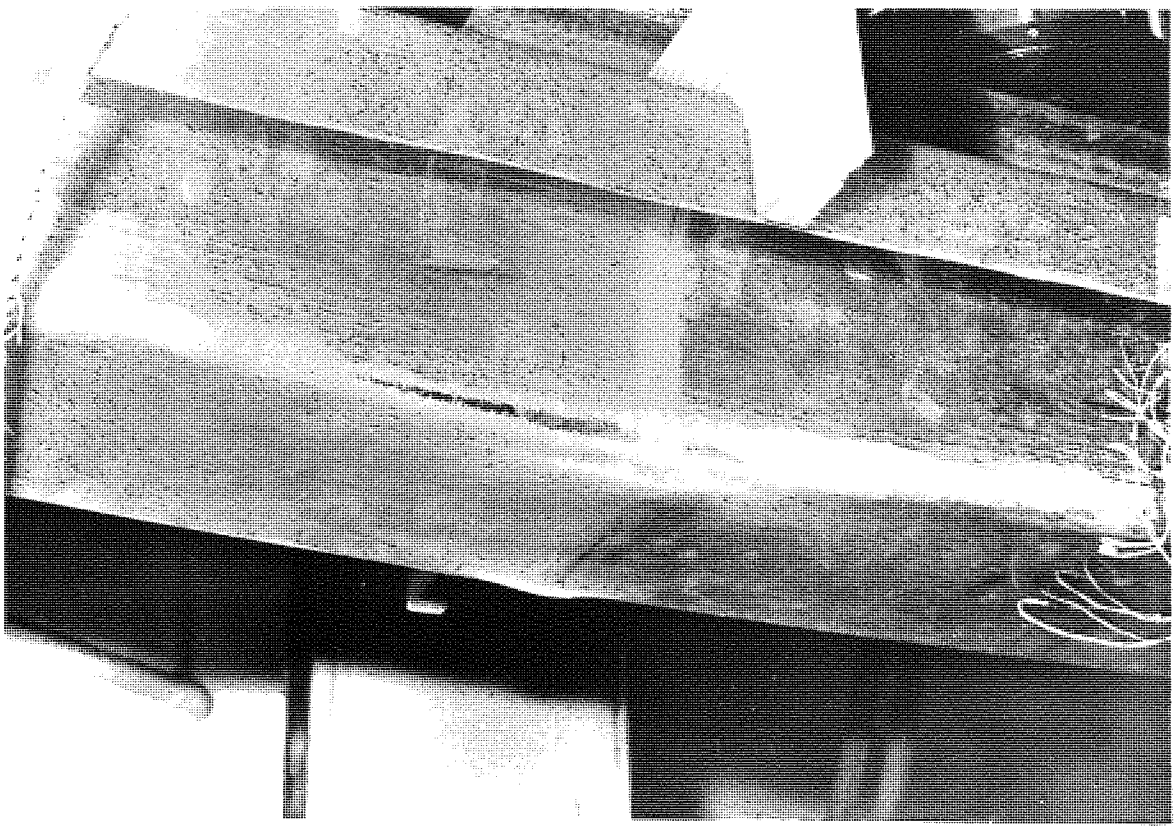

Fig. 6.10 Mode of failure of beam type 6

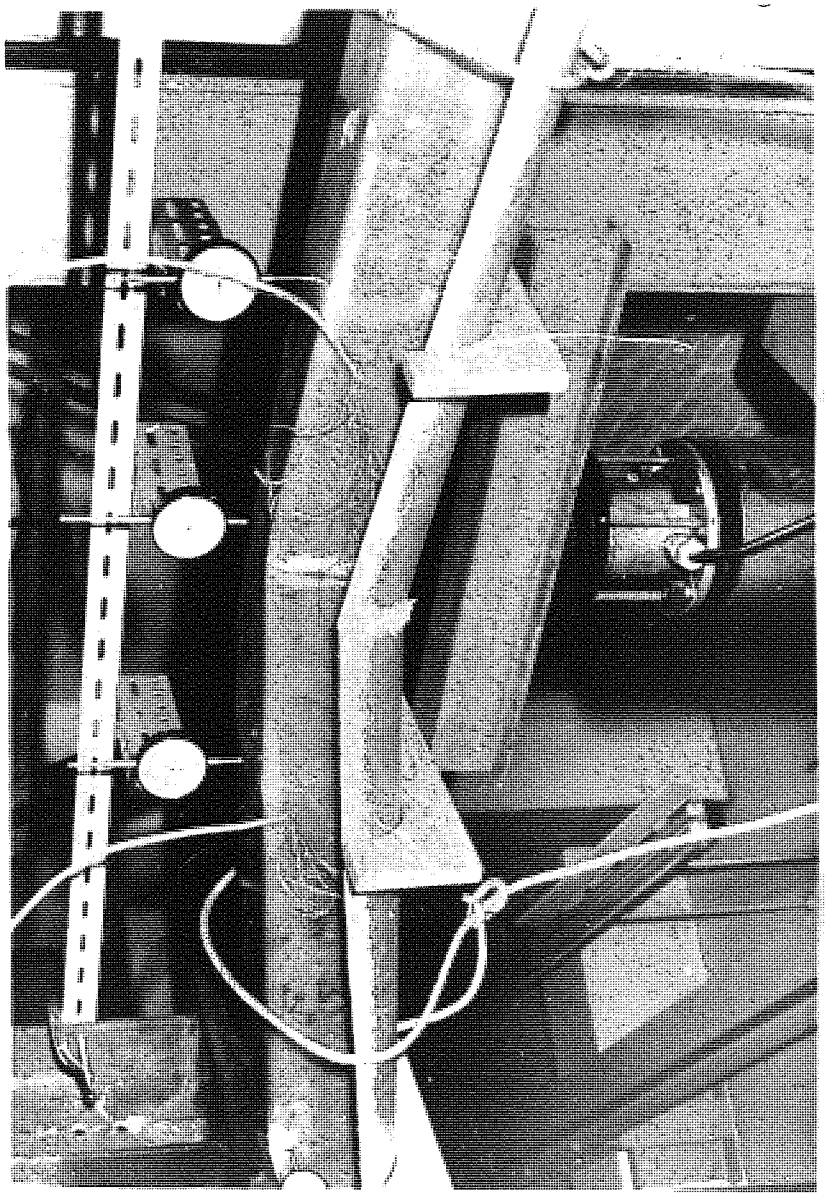

Fig. 6.11. Mode of failure of beam type 7

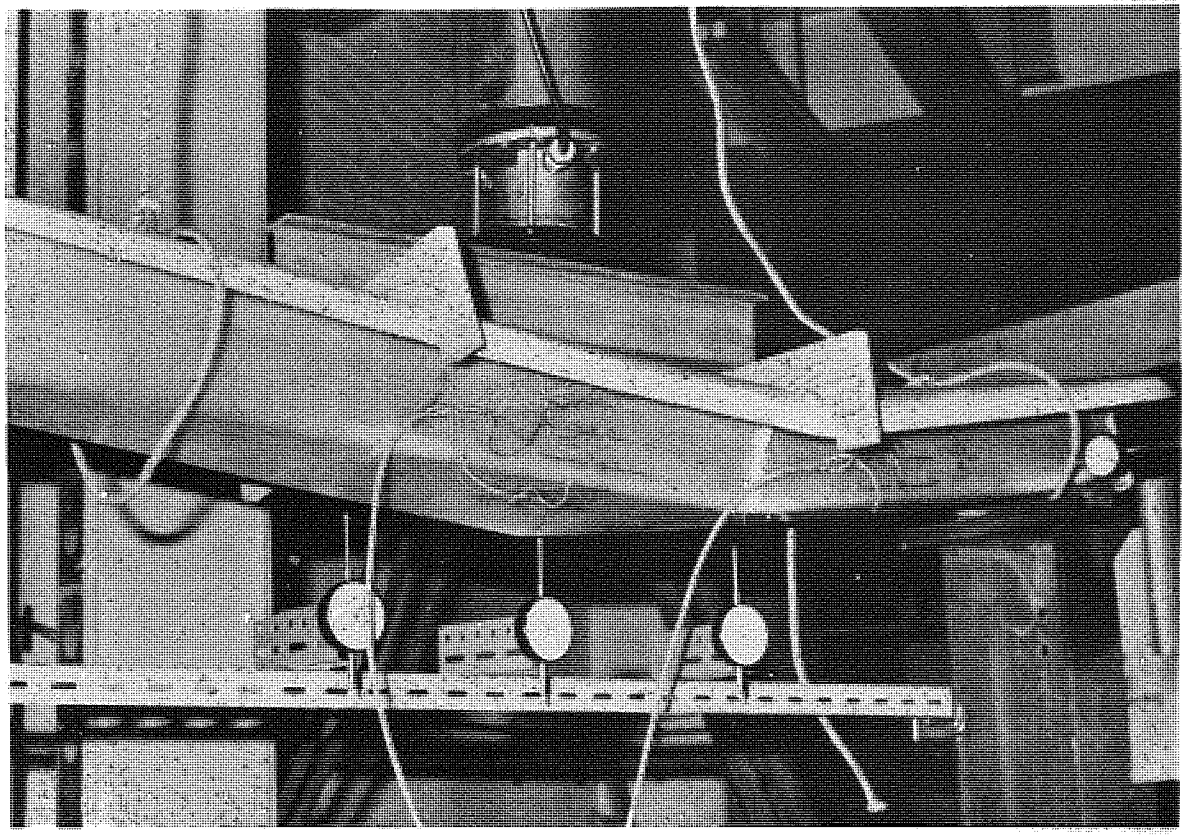

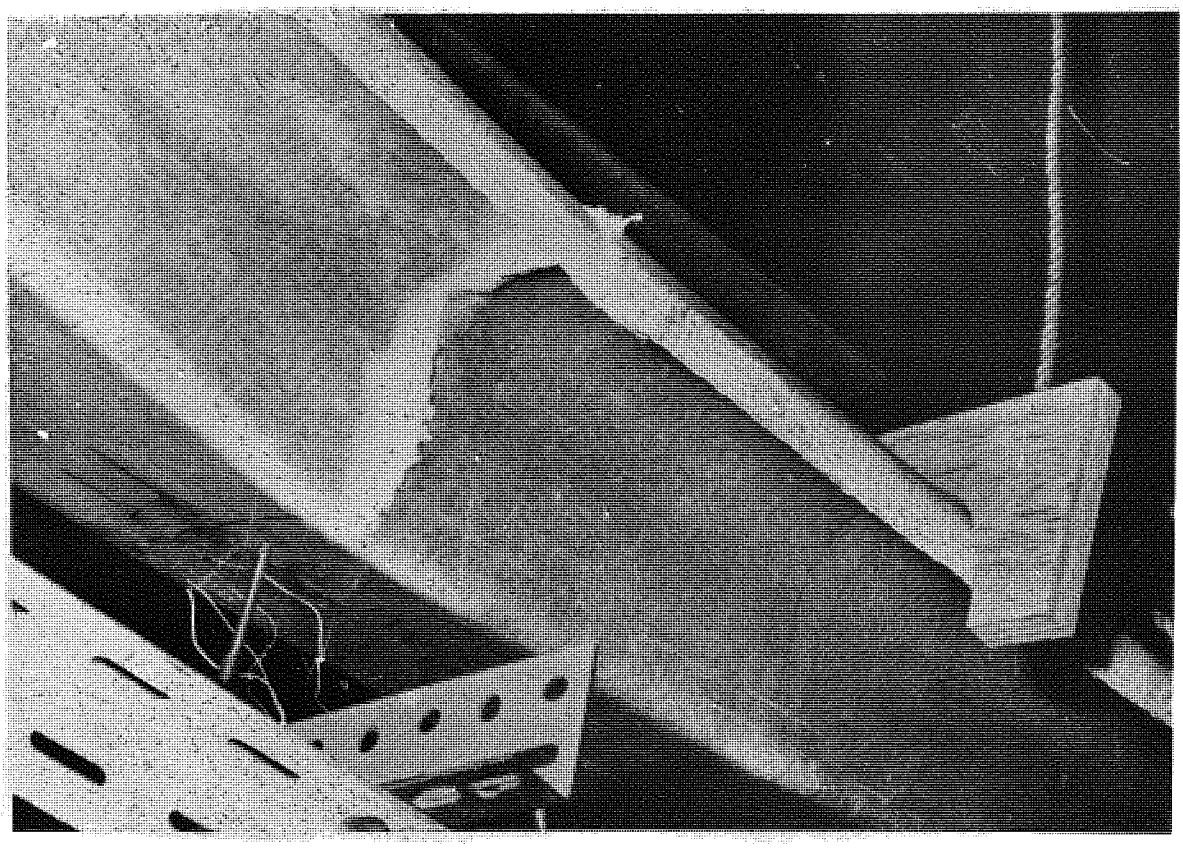

Fig 6.12 Mode of failure of beam type 8

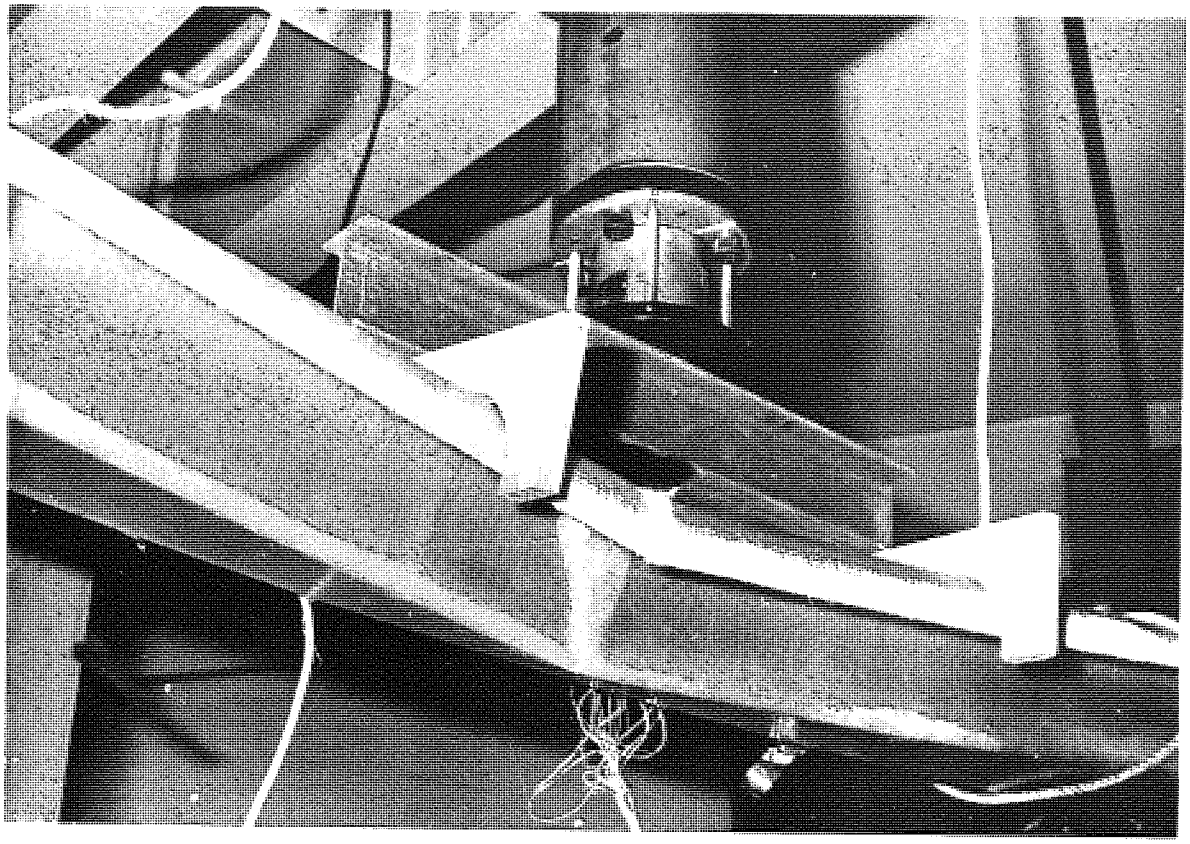

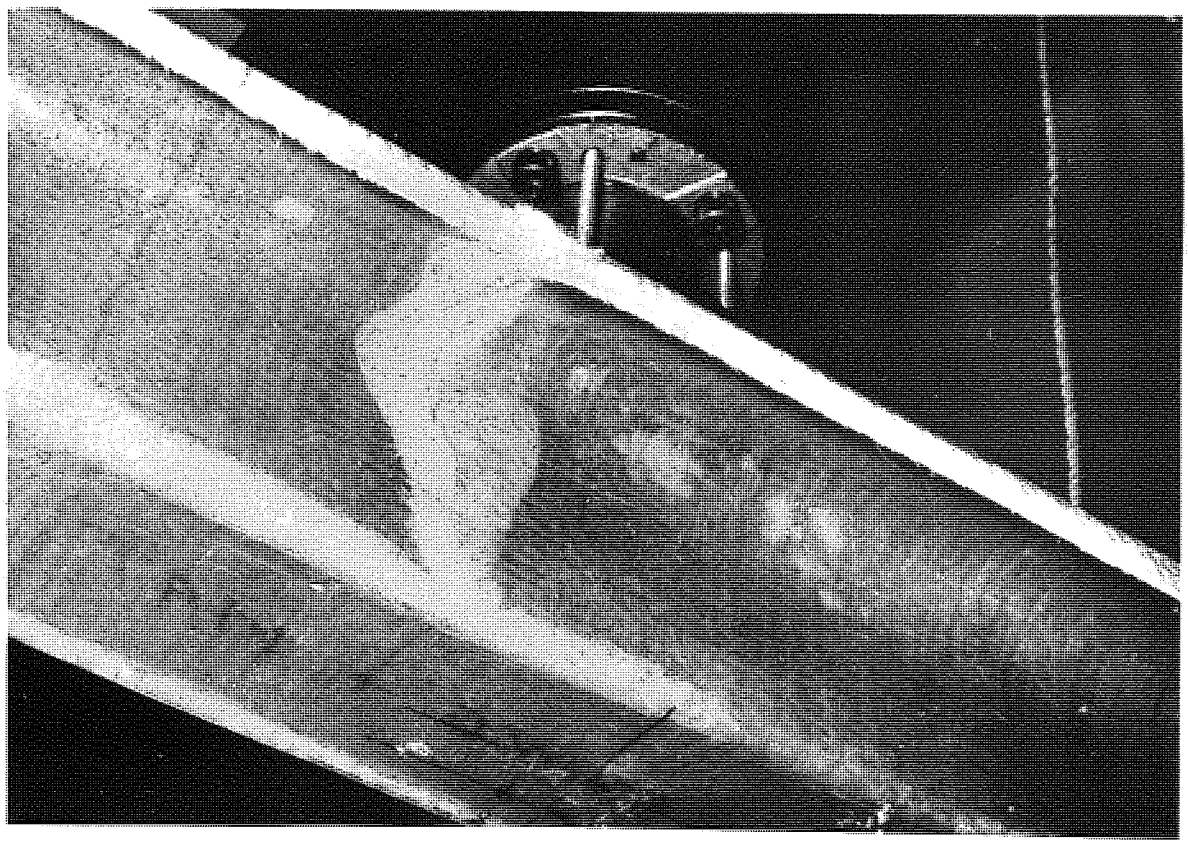

Fig. 6.13 Mode of failure of beam type 9

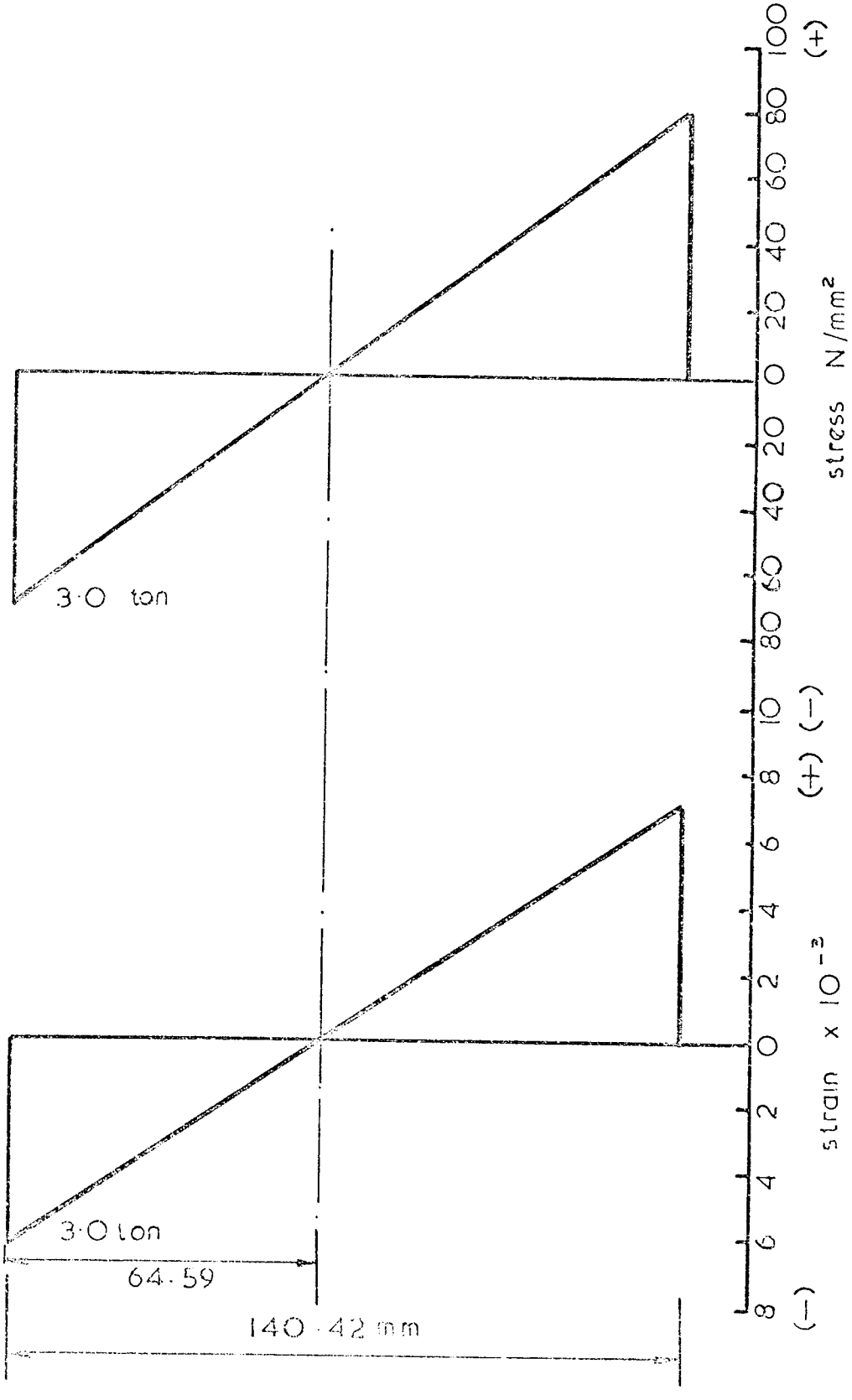

Fig. 6.14 Beam type 1

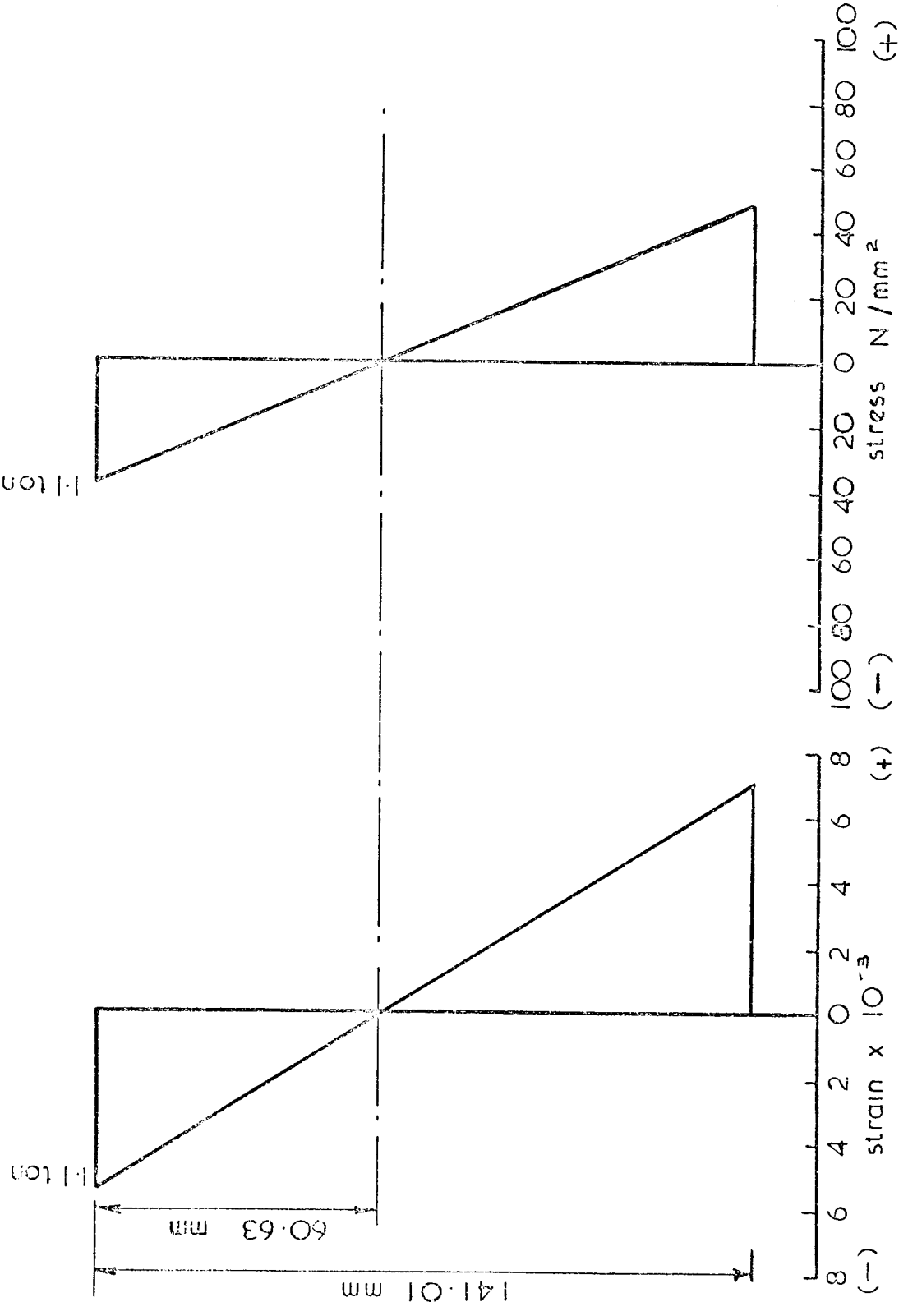

Fig. 6.15 Beam type 2

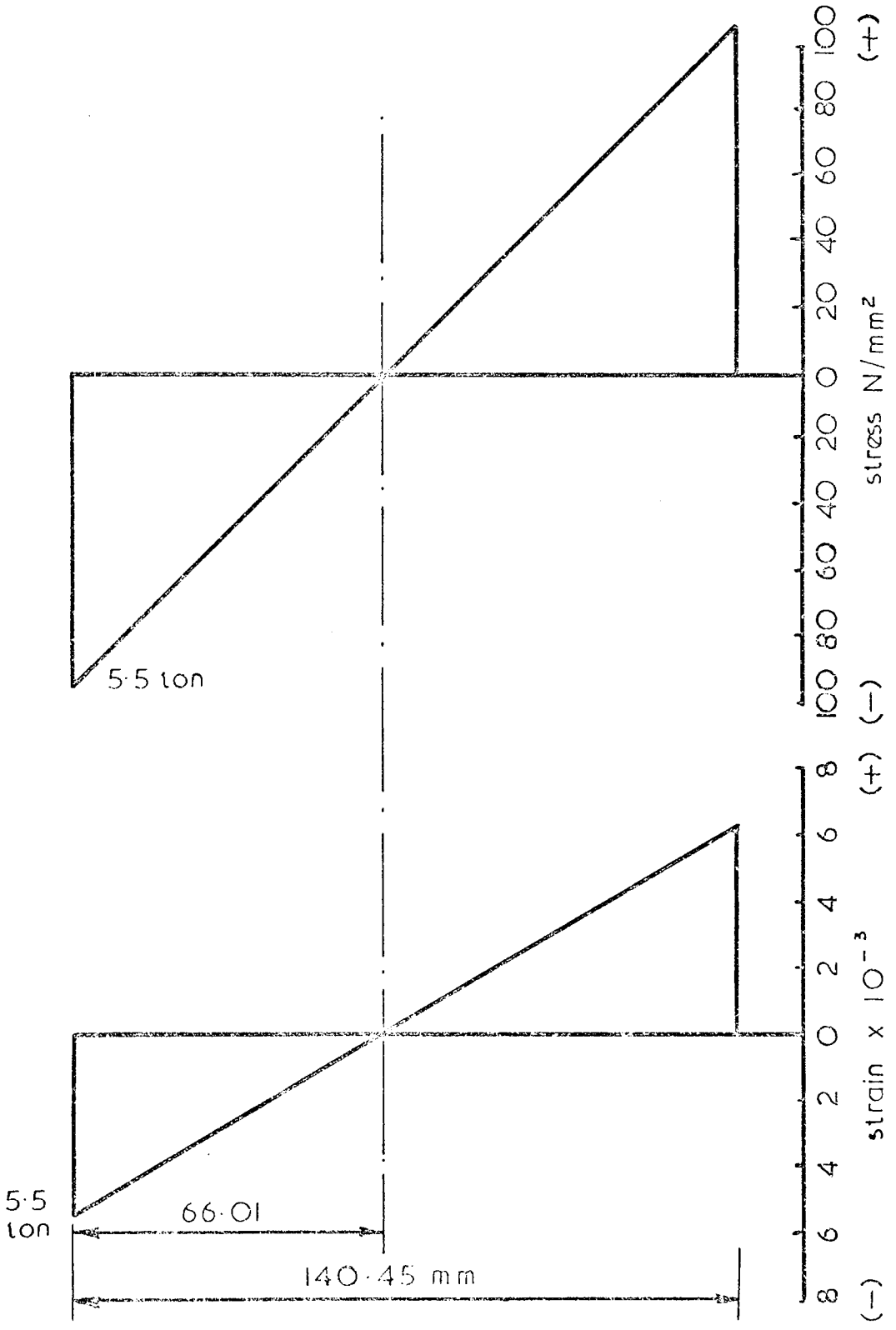

Fig .616 Beam type 3

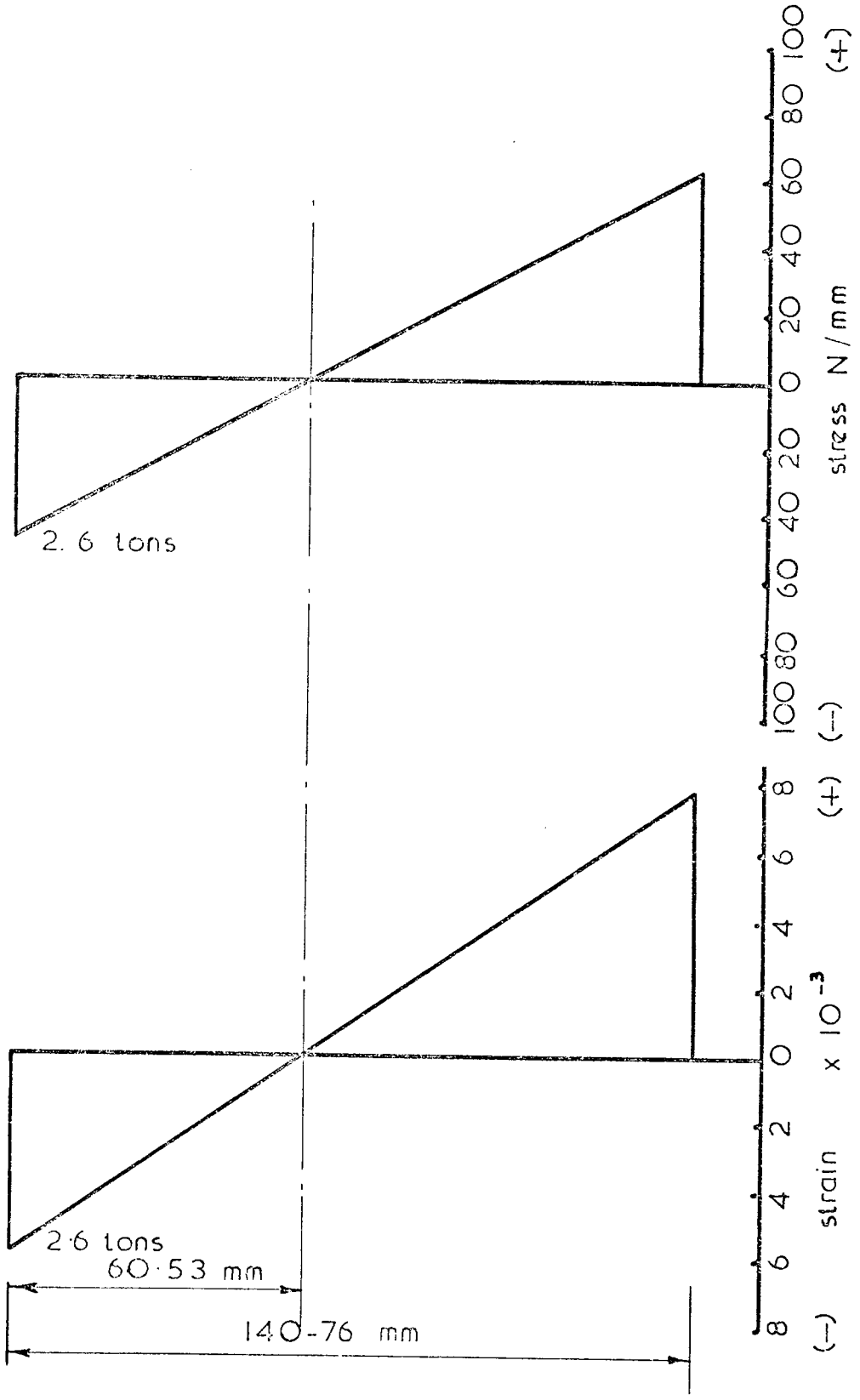

Fig. 6.17 Beam type 4

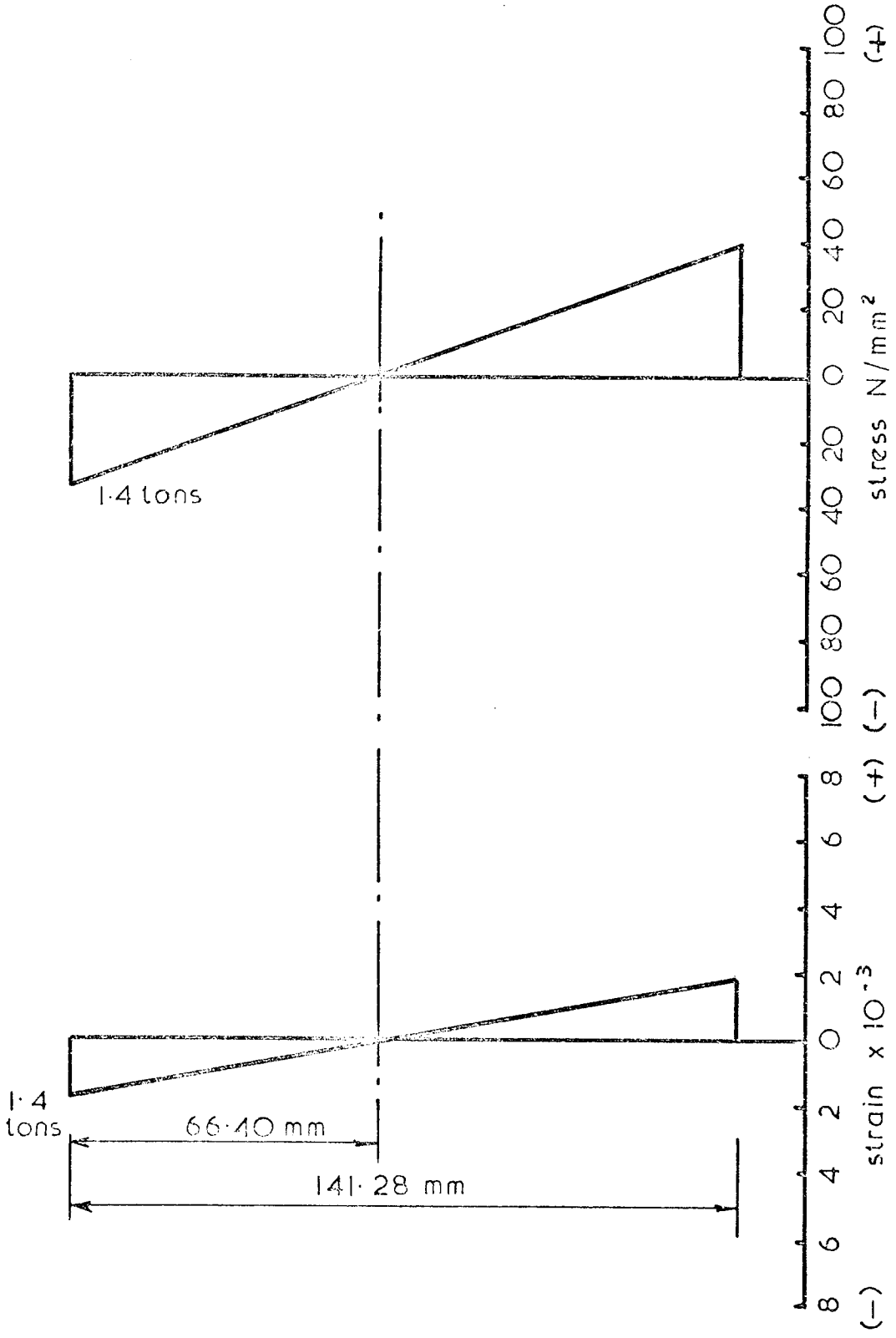

Fig. 6.18 Beam type 5

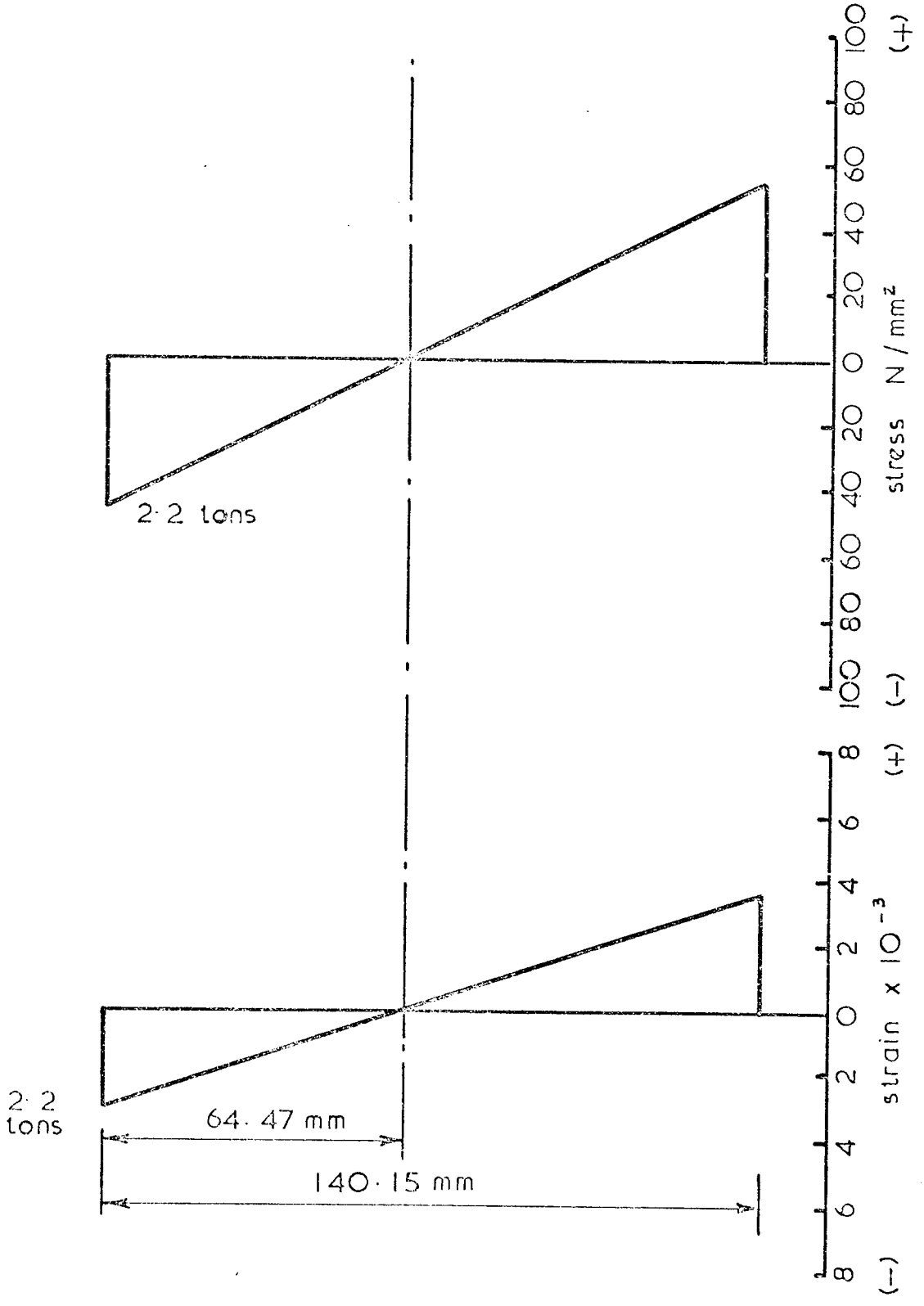

Fig 6.19 Beam type 6

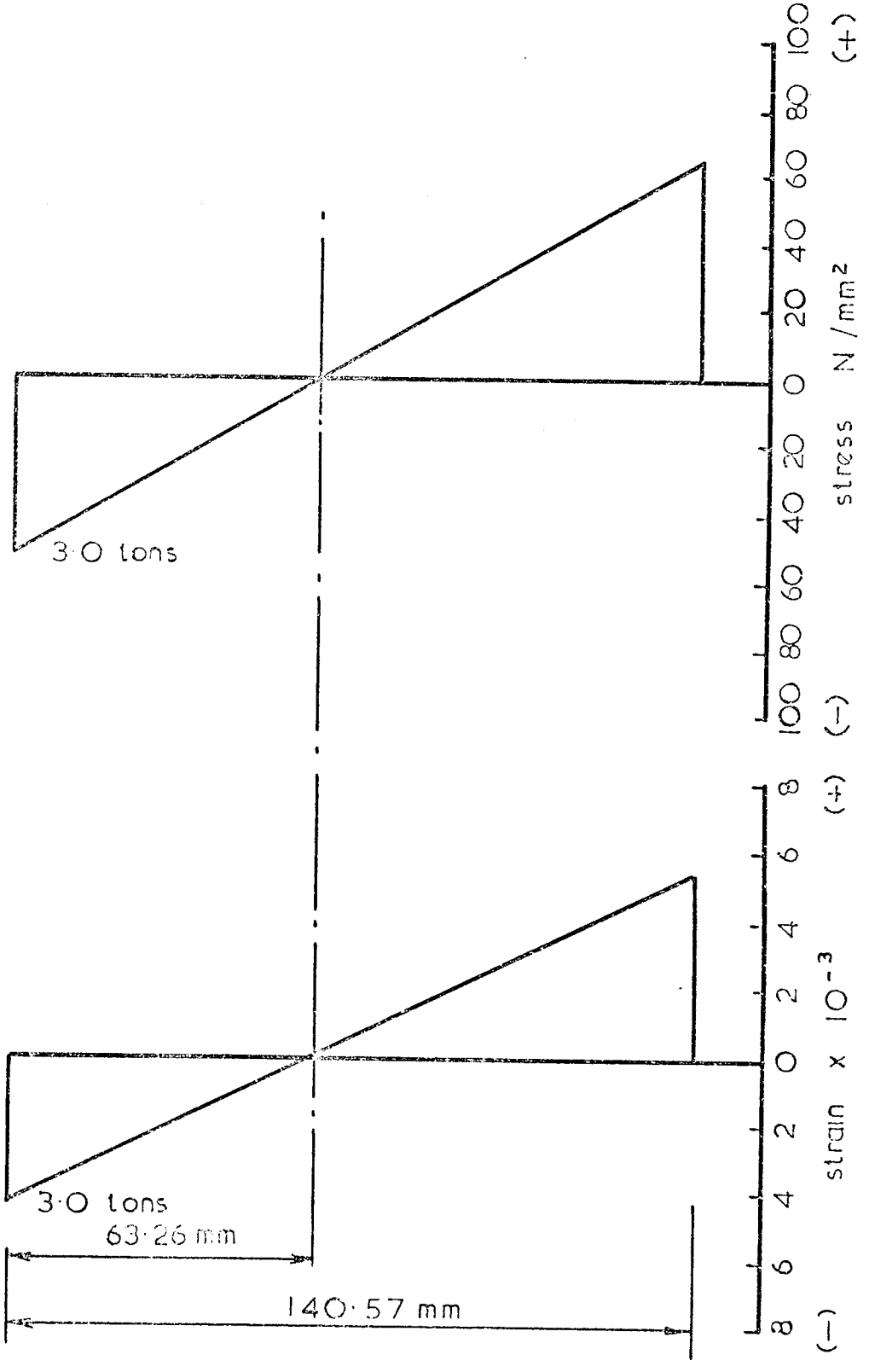

Fig 6.20 Beam type 7

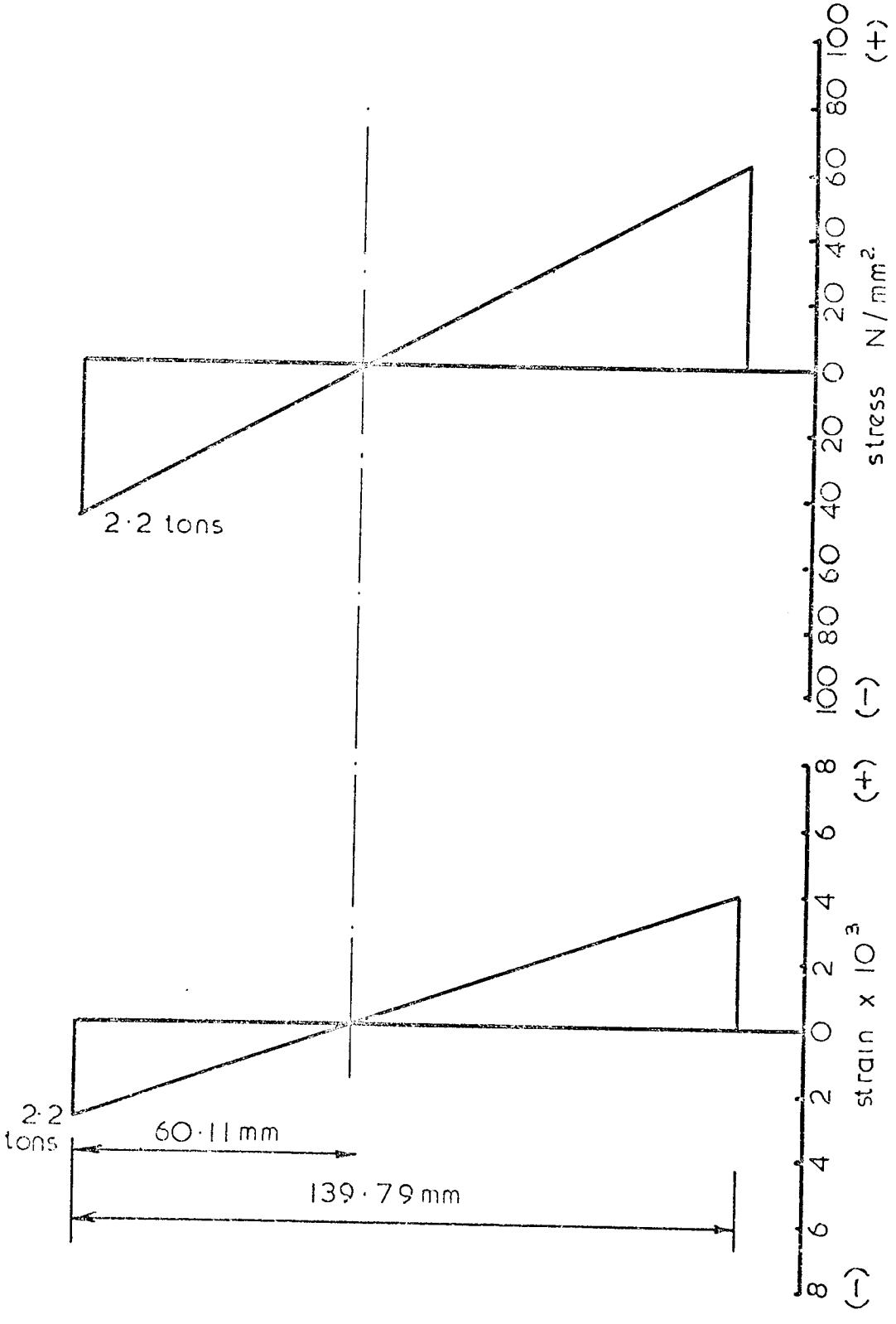

Fig. 6.21 Beam type 8

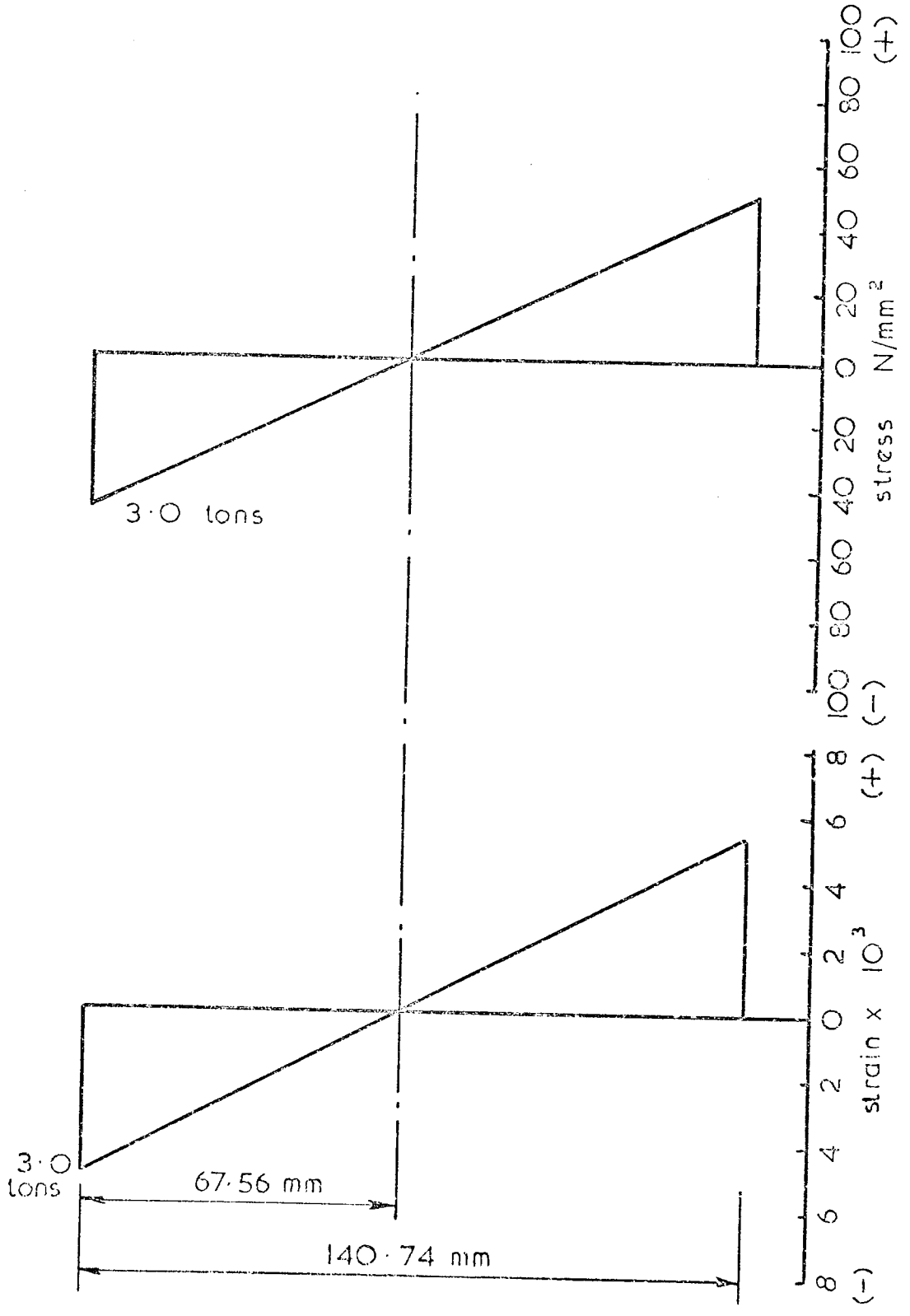

Fig. 6.22 Beam type 9

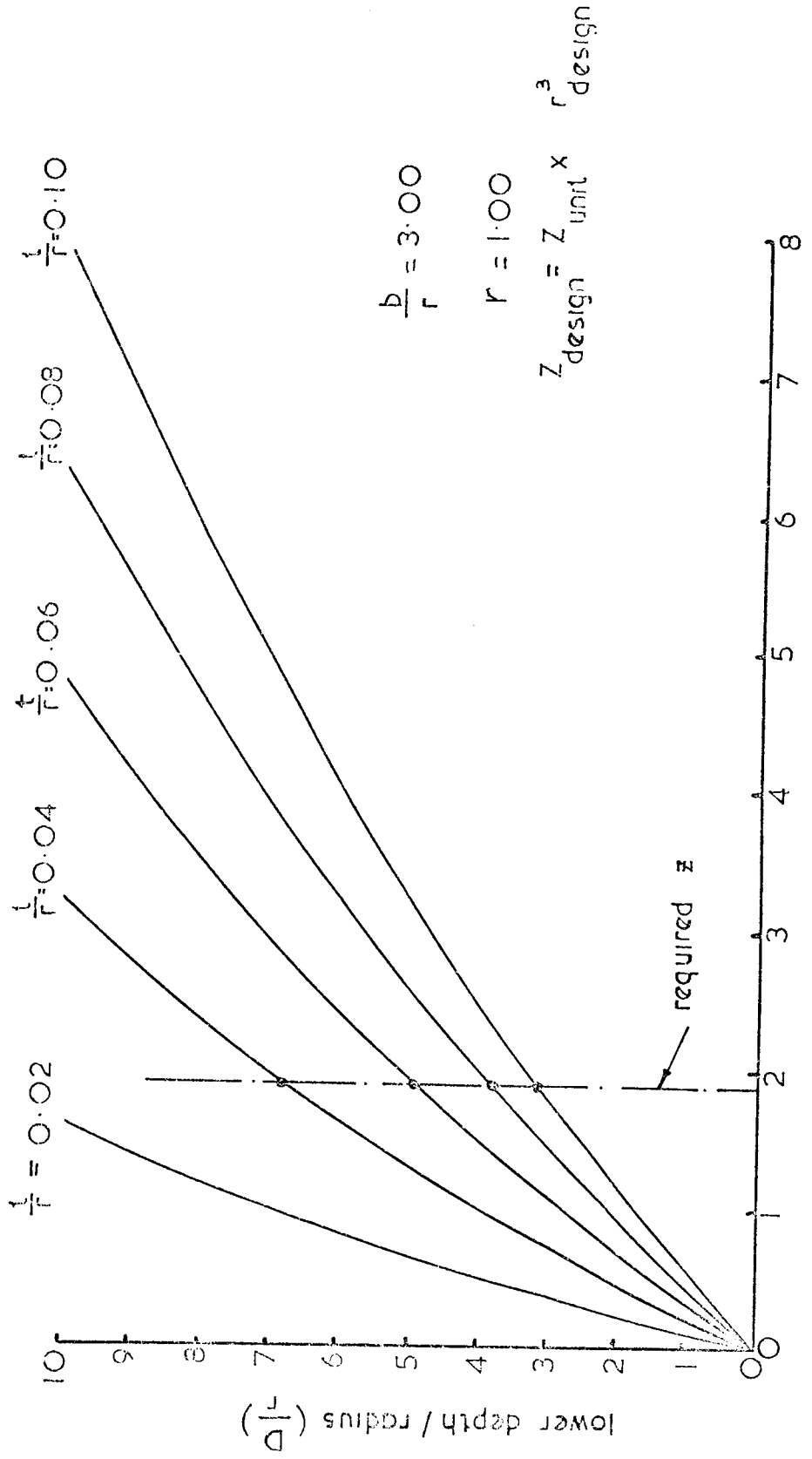

Fig 6.23 (see figs 6·1 & 2)

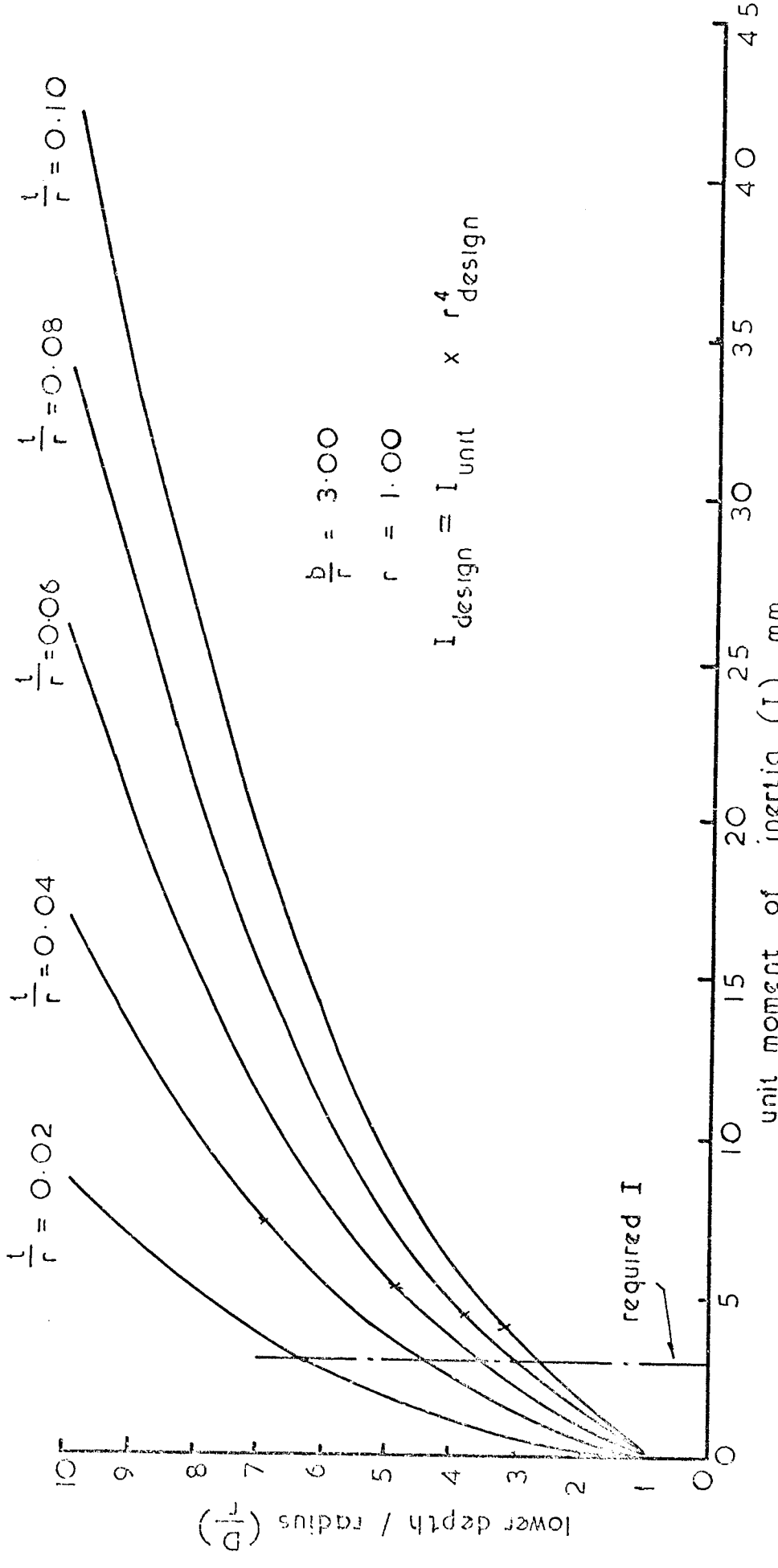

Fig 6.24. see figs 6.1 & 2

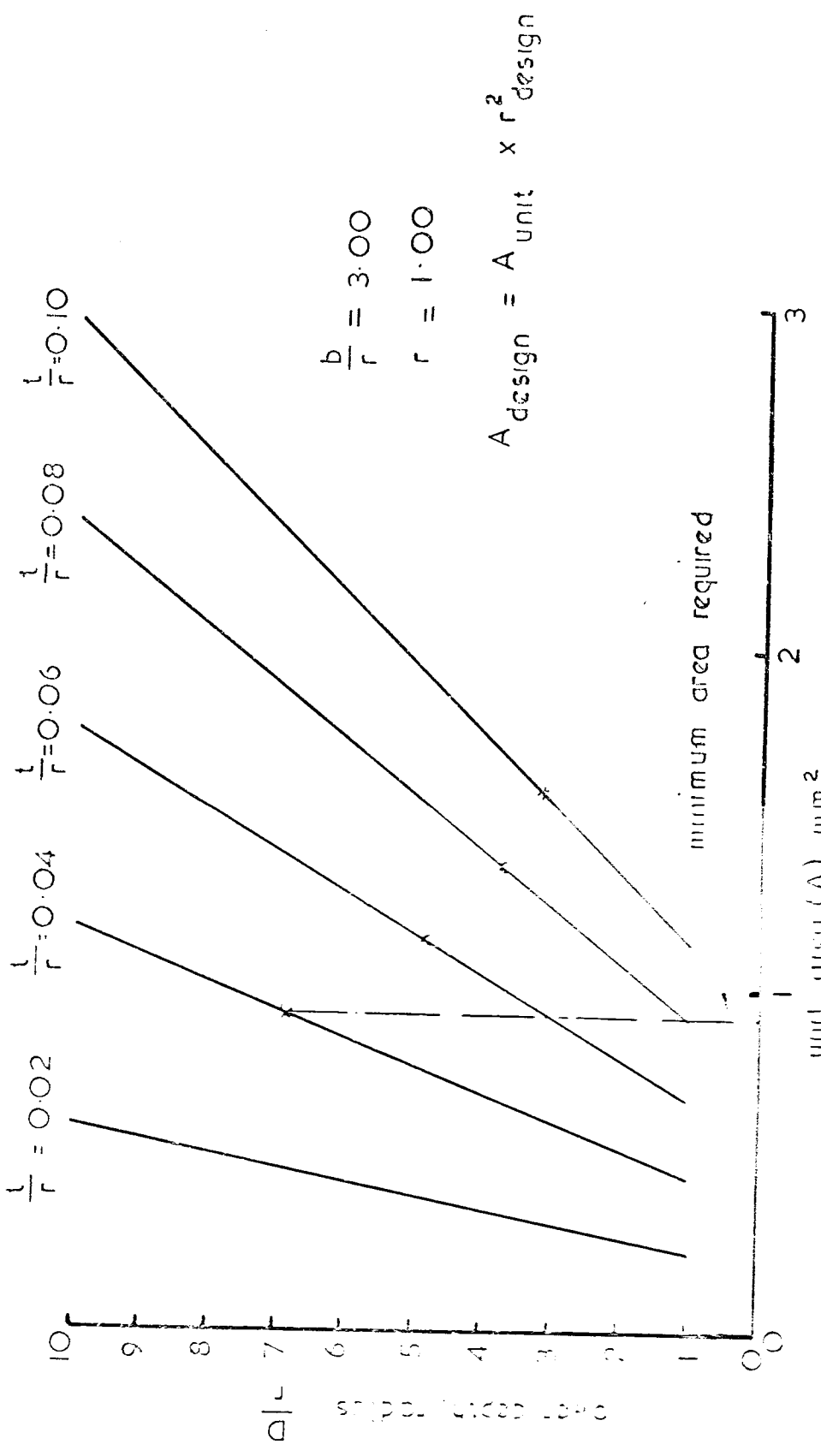
$\frac{t}{r} = 0.02$
$\frac{t}{r} = 0.04$
$\frac{t}{r} = 0.06$
$\frac{t}{r} = 0.08$
$\frac{t}{r} = 0.10$
$\frac{b}{r} = 3.00$
$r = 1.00$
$A_{design} = A_{unit} \times r^2_{design}$
minimum area required
unit area (A) mm²
$\frac{r}{b}$

Fig 6.1. & 2.

REFERENCES.

6-1) BENJAMIN,B.S ., "Structural design with plastics", Van Nostrand Reinhold, 1969.

6-2) TIMOSHENKO,S.P., and GERE,J.M., "Theory of elastic stability" McGraw-Hill, New York, 1961.

6-3) COOK,D.J., "Factor influencing the design of GRP Structures", Uniciv Report No.R.101, University of New South Wales, Australia, December 1972.

6-4) SMITH,C.S., "Application of fibre reinforced composite in marine technology" Composite,Standard,Testing and Design, NPL Conference, April 1974.

C H A P T E R 7

CONCLUSIONS AND SUGGESTIONS FOR A FURTHER RESEARCH.

7.1) Conclusion:

Although each of the previous chapters contains its own conclusions this section will show the general conclusion of the project.

The method of cold setting pressure moulding adopted in manufacturing most of the elements tested throughout the program proved to be efficient in reducing the void content and minimizing the thermal effect due to curing. This method could not be applied in manufacturing the beam specimens because of their doubly curved shape which would have required mould beyond the financial means of the project.

For design purposes it has been shown that the stress/strain relationship is linear and that the Tsai approach for predicting the elastic modulii was in good agreement with experimental observations.

Tensile and compressive strengths showed an acceptable agreement with the theory, although the compressive strength showed poorer agreement at high fibre content.

Interlaminar shear strength showed little variation with increasing fibre content and, as for the compressive strength, it was highly effected by the void content in the composite.

Flexural properties were found to approach the tensile properties and varied directly with the fibre content in the composite. The effect of fibre content and arrangement on stranght and stiffness may be found in Chapter 3.

The introduction of steel wire sheet to glass reinforced plastics made a considerable improvement in the material modulus, this improvement was also shown in the interlaminar shearing strength of SGRP because of the lower amount of voids present in this type of composite relative to GRP.

7.1) contd.

GRP composites showed a lower buckling resistance under uniaxial compression or pure shear than steel, because of the lower modulus. It was shown in Chapter 5 that some improvement may be achieved in the buckling load by changing the arrangement of the fibres within the composite, but this improvement was not sufficient to make GRP really suitable for use under the above mentioned loading systems. To achieve a higher buckling resistance, either steel wire sheets may be used in the composite (according to the design method mentioned in Chapter 4) for uniaxial compression, or, mechanical stiffening (i.e. ribs or corrugation) may be used for uniaxial compression or pure shear.

The simple bending theory proved to be satisfactory in predicting the stresses and deflections of GRP beams provided the cross-section shape does not become deformed.

A factor of safety of 4 and an allowable deflection limited to $^{1}/_{120}$th of the span are considered to be acceptable for many design pruposes for GRP beams, but the designer may need to vary this according to the design requirement.

At this stage, GRP beams should be generally reinforced in the same manner as the reinforcement of beam type 7, which showed the best performance of all the beam tested with the exception of beam type 5 which was manufactured from SGRP. Beam type 5 showed much smaller deflections than the others, but the nature of the steel wire sheets was such that it possessed a curvature after manufacture which made it unsuitable for hand lay up technique. This curvature resulted in a large amount of air voids being trapped beneath its curved pattern and hence the strength performance dropped sharply. These air voids would be eliminated if compression moulding were used. Thus the behaviour

7.1) contd.

of steel wire sheet in the hand lay-up technique prevented a full assessment of its potential in the type of beam investigated.

Finally, GRP beams were shown to be promising for structural engineering uses and they could be strong competitors to steel beams. For example for the same load carrying capacity at the end of the linear stage, a5"×5"×$\frac{1}{2}$" steel angle beam would be equivalent to beam type 7. The steel beam is about 1.15 times the GRP beam area and about five times heavier than the GRP beam. The deflection of the steel beam however is about $\frac{1}{10}$ th of the GRP beam for the fibre content used in the experiment for the same load. The deflection ratio could be improved by increasing the fibre content in the longitudinal direction in order to improve the stiffness.

7.2) Recommendation for further research:

The suggestions for further work are as follows:-

Firstly, further research should be undertaken to improve the buckling resistance of rectangular plates by the introduction of corrugations, stiffeners, or steel wire. In the case of stiffeners these should be longitudinal and/or transverse and should be moulded integrally with the plate rather than moulded separatly and subsequently attached to the plate.

Secondly, as the work described here showed that open sections were deficient in cross-sectional rigidity further work is required to overcome this problem. The beams tested showed that due to cross-sectional deformation only about 60% of the potential bending strength was achieved. This cross-sectional deformation may be reduced or even eliminated by introducing diaphragms fixed along the beam at suitable spacing, depending on design requirement. Such diaphragms are used in

7.2) contd.

many structural applications e.g. on steel thin walled sections when the stability of the cross-section may be the critical factor.

APPENDIX

(i) Determination of the Neutral axis position of GRP Beams Cross-Sections:

From the simple bending theory, the neutral axis of the section may be found by the following relationship,

$$y_N = \frac{\Sigma Ay}{\Sigma A} \tag{A.1}$$

where ΣAy is the sum of the moment area of the cross-section about the line Z-Z and ΣA is the area of the cross-section. Because of the symmetry of the cross-section about the vertical axis, only one side of the section will be considered in the analysis as shown in Fig.(A.1).

From Fig.(A.1), let $\Sigma Ay = Ay_{(AD')}$, then

$$Ay_{(AD')} = Ay_{(AC)} + Ay_{(CD)} + Ay_{(DD')} \tag{A.2}$$

by finding each moment area of equation (A.2) separately and then add them together and as the following.

In determining $Ay_{(AC)}$, consider the element dA in Figure (A.1) the area of which is equal $rdrd\theta$. Taking the moment of this area about the line Z-Z and integrating within the portion AC yields the following,

$$Ay_{(AC)} = \int_0^{\pi} \int_{r_1}^{r_2} r(\bar{r} - \sin\theta)\, dr\, d\theta \tag{A.3}$$

there $Ay_{(AC)}$ then becomes equal to the following

$$Ay_{(AC)} = \int_0^{\pi} \int_{r_1}^{r_2} \bar{r}\, r\, dr\, d\theta - \int_0^{\pi} \int_{r_1}^{r_2} r^2 \sin\theta\, dr\, d\theta \tag{A.4}$$

integrating equation (A.4) and solve for $Ay_{(AC)}$ yields the following,

(i) contd.

$$Ay_{(AC)} = \pi \bar{r}\, rt - \frac{2t}{3}\left(3r^2 + \frac{t^2}{4}\right) \qquad (A.5)$$

Equation (A.5) is the moment area of part AC about the line Z-Z.

$$Ay_{(CD)} = \left(D + \frac{t}{2}\right) t \left[\frac{1}{2}\left(D + \frac{t}{2}\right) + \bar{r}\right] \qquad (A.6)$$

Equation (A.6) is the moment area of part CD about the line Z-Z.

$$Ay_{(DD')} = \left(\frac{b}{2} - \frac{t}{2}\right) t(D + \bar{r})$$

$$Ay_{(DD')} = \frac{1}{2}\, t(b-t)(D + \bar{r}) \qquad (A.7)$$

Equation (A.7) is the moment area of part DD' about the line Z-Z.

By adding equations (A.5,6 and 7) and dividing them by the area AD' yields equation (6.2) which is written again below

$$y_N = \bar{r} - \frac{2r^2 - \frac{1}{2}(D^2 + bD - \frac{t^2}{12})}{\pi r + D + \frac{b}{2}}$$

when the value of the second term on the right hand side of equation (6.2), which is labelled $\bar{y}$ in Fig.(A.1), is negative. The neutral axis position is below the line x-x while if the value is positive, the neutral axis position is above the line x-x, as shown in Figs.(6.1 and 2).

(ii) Determination of Moment of Inertia:

(a) When the neutral axis is below the line x-x, Fig.(6.1).

The moment of inertia of the section can be calculated as follows:-

Let I_{TL} be the total moment of inertia of the section

(ii) contd.

(a) contd.

about the neutral axis and equal to

$$I_{TL} = I_{(AC+HF)} + I_{(ED)} + I_{(CD+FE)} \qquad (A.8)$$

NOW $I_{(AC+HF)}$ may be determined by considering the element dA in Fig.(6.1) and taking its second moment of area about the neutral axis and integrating for the limit of part AC and doubling for part HF which yields the following

$$I_{(AC+HF)} = 2\int_0^{\pi}\int_{r_1}^{r_2} r(r\sin\theta + \bar{y})^2 \, dr \, d\theta$$

Then

$$I_{(AC+HF)} = 2\int_0^{\pi}\int_{r_1}^{r_2} r(r^2\sin^2\theta + 2r\sin\theta\bar{y} + \bar{y}^2)dr\, d\theta$$

Simplify,

$$I_{(AC+HF)} = 2\left[\int_0^{\pi}\int_{r_1}^{r_2} r^3\sin^2\theta\, dr\, d\theta + \int_0^{\pi}\int_{r_1}^{r_2} 2r^2\sin\theta\bar{y}\, dr\, d\theta + \int_0^{\pi}\int_{r_1}^{r_2} r\,\bar{y}^2\, dr\, d\theta\right]$$

by solving the integration values of the above equation:-

$$I_{(AC+HF)} = 2\left[\frac{\pi}{8}rt(4r^2+t^2) + \frac{4}{3}\bar{y}(3r^2t+\tfrac{1}{4}t^3) + \pi rt\,\bar{y}^2\right] \qquad (A.9)$$

Equation (A.9) represents the second moment of area of parts AC and HF about the neutral axis.

$$I_{(ED)} = (b-t)\frac{t^3}{12} + (b-t)t(D-\bar{y})^2 \qquad \text{See Fig.(A.2)}$$

Solving the equation yields,

$$I_{(ED)} = \frac{bt^3}{12} - \frac{t^4}{12} + tbD^2 - 2\bar{y}bDt + tb\bar{y}^2 - t^3D^2 + 2t^2\bar{y}D - t^2\bar{y}^2 \qquad (A.10)$$

Equation (A.10) represents the second moment of area of part ED about the neutral axis.

(ii) contd.

(a) contd.

$$I_{(CD+FE)} = 2\left[\frac{tD'^3}{12} + tD'\left(\frac{D'}{2} - \bar{y}\right)^2\right] \quad \text{, see Fig.(A.2)}$$

where $D' = D + \frac{t}{2}$

then

$$I_{(CD+FE)} = 2\left(\frac{tD'^3}{3} - tD'^2\,\bar{y} + tD'\,\bar{y}^2\right) \qquad \text{(A.11)}$$

Equation (A.11) represents the second moment of area of parts CD and FE about the neutral axis.

$\therefore$ from equation (A.8)

$$I_{TL} = 2\left[\frac{\pi}{8} rt(4r^2+t^2) + \frac{4}{3}\bar{y}t(3r^2+\tfrac{1}{4}t^2)+\pi rt\,\bar{y}^2\right] +$$

$$\frac{bt^3}{12} - \frac{t^4}{12} + tbD^2 - 2t\,\bar{y}bD + tb\bar{y}^2 - t^2D^2 + 2t^2\bar{y}D - t^2\bar{y}^2$$

$$+ 2\left(\frac{tD'^3}{3} - tD'^2\,\bar{y} + tD'\,\bar{y}^2\right)$$

which is equation (6.3).

(b) The same steps as those used in (a) can be used in determining the moment of inertia of the cross-section about the neutral axis when that axis is above the line x-x. Refer to Fig.(6.2) in the calculations.

(iii) Determination of maximum shearing stresses theoretically:

(a) When the neutral axis is below the line x-x, Fig.(6.1). From the simple bending theory, the shearing stresses at any point along the cross-section can be determined by the following equation

$$\tau_{xy} = \frac{F(Ay)}{I\,b_s} \qquad \text{(A.12)}$$

where

τ_{xy} is the shearing stresses at any point in the cross-section,

(iii) contd.

(a) contd.

(Ay) is the first moment of area of either the tension or compression zone about the line passing through the points where shearing stresses are to be calculated.

I is the moment of inertia of the cross-section about the same line.

b_s is the width of the cross-section at the point at shearing stresses is to be calculated.

F is the shearing force in the cross-section.

So in order to determine the maximum shearing stress in the cross section, (Ay) and (I) should be computed about the neutral axis.

Starting with (Ay) which will represent the moment of area of the tension zone (CDEE') about the neutral axis, see Figs.(6.1) and (A.2).

$$\therefore \quad Ay_{(CDE\acute{E})} = Ay_{(C'D+EE')} + Ay_{(ED)} \qquad (A.13)$$

Then

$$Ay_{(C'D+EE')} = 2(D'-\bar{y})\ t\left(\frac{D'-\bar{y}}{2}\right)$$

$$Ay_{(C'D+EE')} = t(D'-\bar{y})^2 \qquad (A.14)$$

Equation (A.14) represents the area moment of part (C'D+EE') about the neutral axis.

$$Ay_{(ED)} = t(b-t)(D-\bar{y}) \qquad (A.15)$$

the above equation represents the area moment of part (ED) about the neutral axis.

From equation (A.13)

(iii) contd.

(a) contd.

$$Ay_{(CDEE')} = t\left[(D'-\bar{y})^2 + (b-t)(D-\bar{y})\right] \qquad (A.16)$$

$\therefore$ Equation (A.16) represents the moment of area of the tension zeon (CDEE') of the cross-section about the neutral axis.

The moment of inertia of the cross-section about the neutral axis can be obtained from equation (6.3), while the width (b_s) of the cross-section is equal to 2t.

Then from equation (A.12) :-

$$\tau_{xy} = \frac{F \times t[(D'-\bar{y})^2+(b-t)(D-\bar{y})]}{2t \times I_{TL}}$$

which then yields equation (6.8) shown below

$$\tau_{xy} = \frac{F[(D'-\bar{y})^2+(b-t)(D-\bar{y})]}{2\ I_{TL}}$$

(b) When the neutral axis is above the line x-x, the maximum shearing stress can be found by the same method as (a) and with reference to Fig.(6.2).

(iv) Determination of shearing stress experimentally:

In determining the shear stress experimentally, 45° strain gauge rosettes were used. The analysis of such rosettes is mentioned in many experimental stress analysis books. Part of the analysis is presented below,

Considering Fig.(A.3B), and from Mohr's Circle geometry,

$$OP = \frac{\varepsilon_A + \varepsilon_C}{2}$$

$$PR = \frac{\varepsilon_A - \varepsilon_C}{2}$$

Now Δ's PAR, PBQ are congruent.

(iv) contd.

Hence $AR = PQ = \varepsilon_B - \frac{\varepsilon_A + \varepsilon_C}{2}$

$$\therefore \tan 2\theta = \frac{AR}{PR} = \frac{2\varepsilon_B - \varepsilon_A - \varepsilon_C}{\varepsilon_A - \varepsilon_C}$$

PA = radius of Mohr's Circle = $\sqrt{PR^2 - AR^2}$

$$PA = \frac{1}{\sqrt{2}} \sqrt{\varepsilon_A^2 + 2\varepsilon_B^2 + \varepsilon_C^2 - 2\varepsilon_B(\varepsilon_A + \varepsilon_C)}$$

$$\therefore \frac{\gamma}{2} = PA \sin 2\theta$$

Then, the shearing strain $\gamma = 2\ PA \sin 2\theta$ (A.17)

and, the shearing stress $\tau_{xy} = 2\ G_{xy}\ PA \sin 2\theta$ (A.18)

The principle strains ε_1 and ε_2 could be obtained from the following

$$\varepsilon_1, \varepsilon_2 = \frac{\varepsilon_A + \varepsilon_C}{2} \pm \frac{1}{2} \sqrt{\varepsilon_A^2 + 2\varepsilon_B^2 + \varepsilon_C^2 - 2\varepsilon_B(\varepsilon_A + \varepsilon_C)}$$

(v) <u>Determination of the maximum deflection of simply supported beams subjected to four point bending:</u>

Referring to Fig.(A.4) and using McCaulay's Method (ref.A-1)

$$EI \frac{d^2y}{dx^2} = -M$$

where M is the maximum bending moment on the beam, then,

$$EI \frac{d^2y}{dx^2} = \frac{Wx}{2} - \frac{W(x-a)}{2} - \frac{W(x-L+a)}{2}$$

$$EI \frac{dy}{dx} = \frac{Wx^2}{4} - \frac{W(x-a)^2}{4} - \frac{W(x-L+a)^2}{4} + A$$

$$\frac{dy}{dx} = 0 \text{ when } x = \frac{L}{2}$$

$$\therefore \quad 0 = \frac{WL^2}{16} - \frac{WL^2}{16} + \frac{WLa}{4} - \frac{Wa^2}{4} + A$$

then

$$A = \frac{Wa(a-L)}{4}$$

(v) contd.

$$EI\,y = \frac{Wx^3}{12} - \frac{W(x-a)^3}{12} - \frac{W(x-L+a)^3}{12} + \frac{Wax(a-L)}{4} + B$$

$y = 0$ when $x = 0$ so $B = 0$

y is maximum when $x = \frac{L}{2}$

$$\therefore\ y_{max} = \frac{W}{12EI}\left[\frac{L^3}{8} - \frac{L^3}{8} + \frac{3L^2}{4}a - \frac{3La^2}{2} - a^3 + \frac{3La^2}{2} - \frac{3aL^2}{2}\right]$$

$$y_{max} = \frac{Wa(3L^2-4a^2)}{48\,EI}$$ which is equation (6.9).

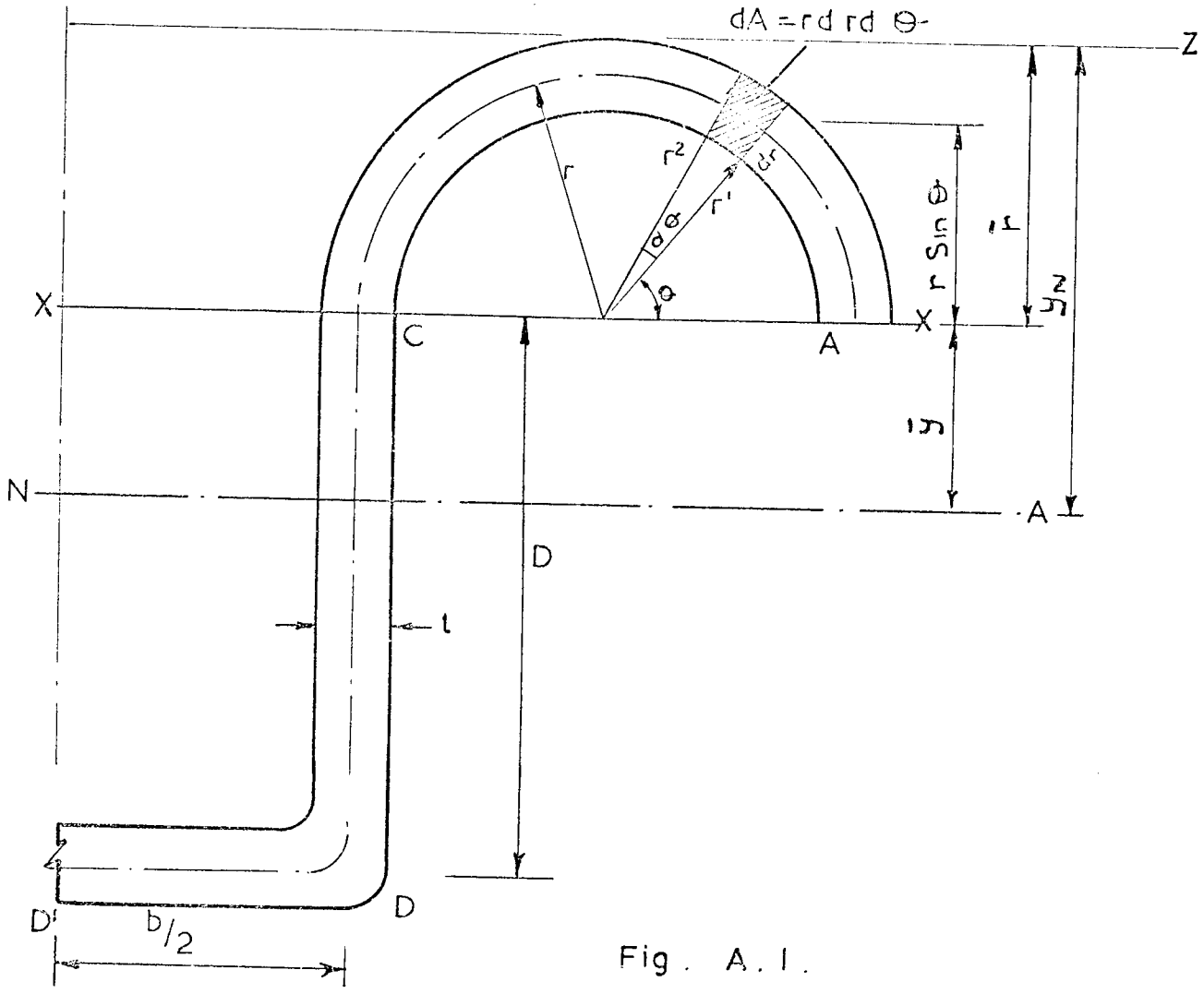

Fig. A.1.

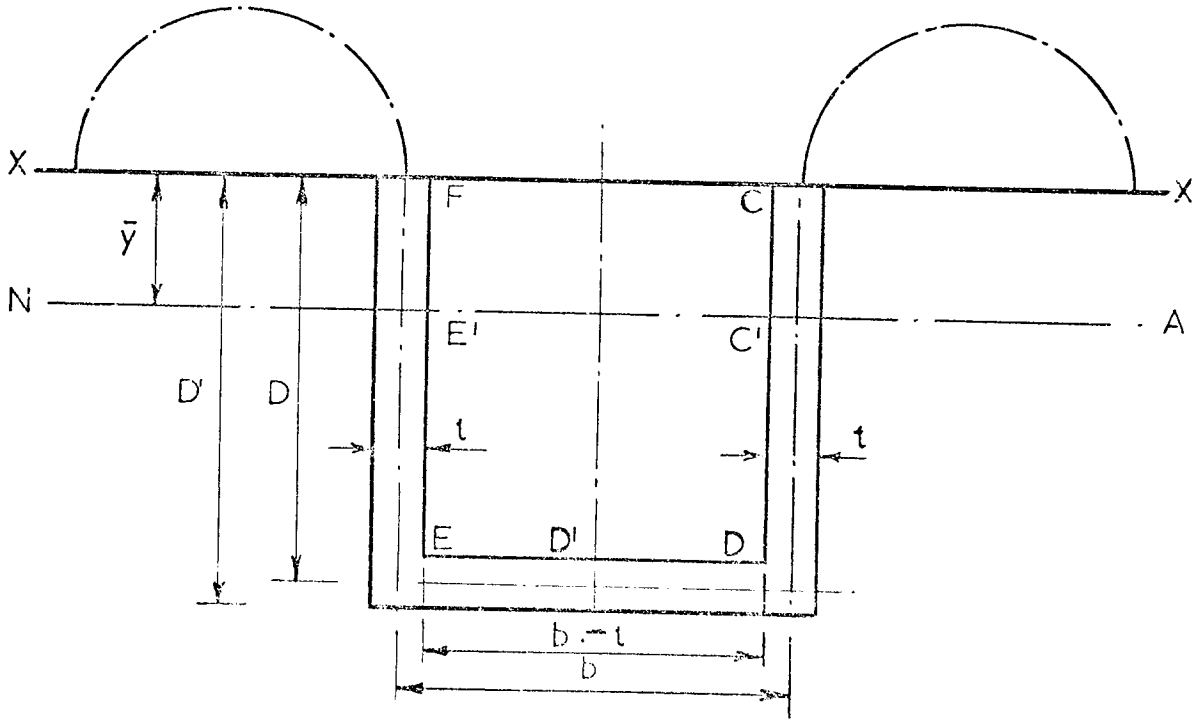

Fig. A.2 The approximation of the lower part of the cross section

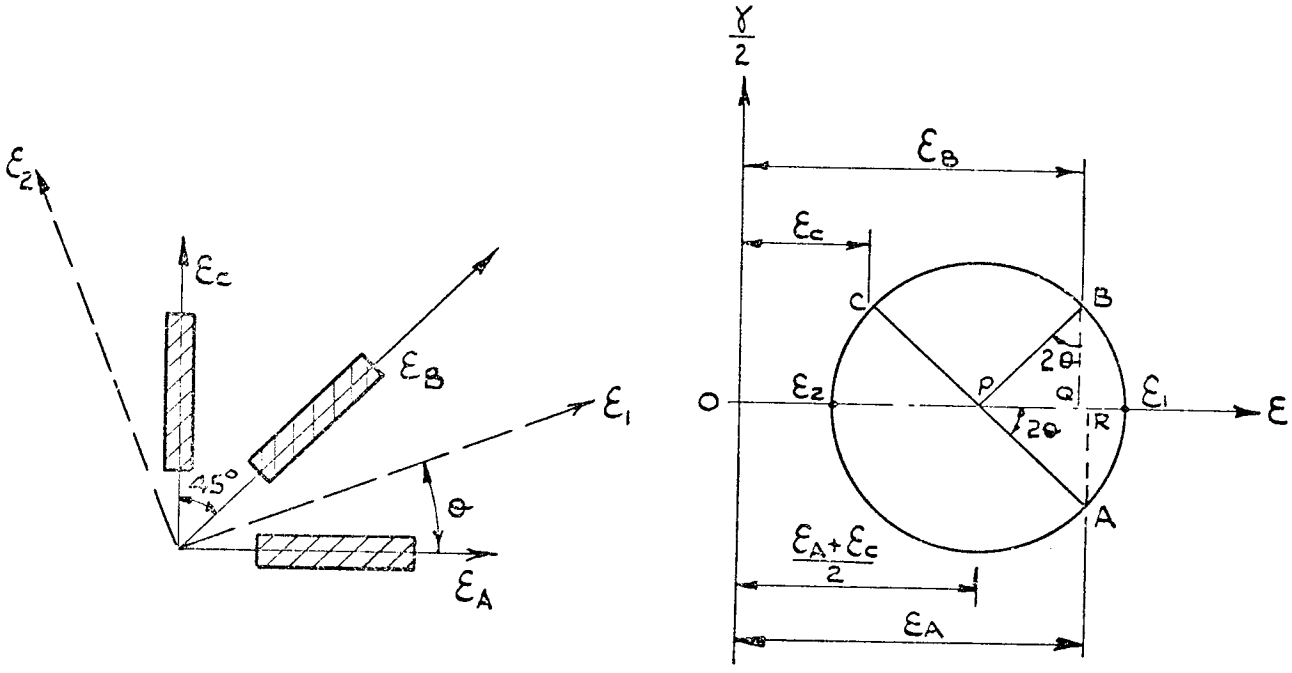

A. 45° Strain rosette

B. Strain Mohr's circle

Fig. A. 3.

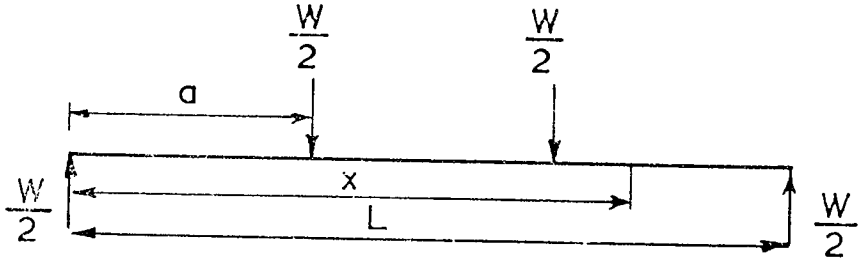

Fig. A. 4.

REFERENCES.

A-1) RYDER,G.H., "Strength of Materials", Macmillin & Co.,Ltd., 1969.